MEASUREMENT AND MODELLING OF COMBUSTION IN A SPARK IGNITION ENGINE

A Thesis submitted for the degree of Doctor of Philosophy

by

Andrew Gavin Brown

Department of Manufacturing and Engineering Systems

BRUNEL UNIVERSITY

March 1991

ABSTRACT

A study has been conducted into the causes of cycle by cycle variations in combustion within a spark ignition engine, the best measured engine parameter to use for its characterization, and the effects that: ignition timing, equivalence ratio, fuel type, throttle position and knock, have upon it.

A Ricardo E6 single cylinder variable compression ratio research engine was instrumented to allow measurement of: cylinder pressure, temperatures, speed, load, fuel flow and air flow. The engine was also fitted with an optical slice that allowed optical access to the combustion chamber and enabled measurement of the early flame speed (up to 10 mm from spark plug gap) using a laser schlieren system. Cylinder pressure data were collected on a dedicated HP1000 computer for every degree of crank angle rotation for up to 300 successive cycles.

A phenomenological model was developed for turbulent combustion that split the combustion process into three phases: early laminar burn, turbulent combustion, and final burn. The model allowed the study of the physical phenomena occurring within the combustion chamber and enabled insights to be gained into their effects on combustion and cyclic variations.

The study showed:

The variation in mixture strength has a far greater effect on the average and Coefficient of Variation (COV) values of all the combustion performance parameters, than does changing the fuel type.

Cycle by cycle variations in combustion are best characterized by COV of imep.

The onset of knock has no discernible effect on the COVs of the measured parameters.

The part throttle results show higher COVs than at Wide Open Throttle (WOT) due to slower burn, supporting the theory that faster initial flame speeds reduce cyclic variations.

The combustion model was used to support the hypothesis that cycle by cycle variations are caused by movement of the flame kernel by turbulence within the combustion chamber.

ACKNOWLEDGEMENTS

I would like to express my grateful thanks to my supervisor Dr. Richard Stone for his help and guidance throughout the project.

I would also like to acknowledge the financial support provided by the SERC, and the valuable contribution from BP Research in providing the CASE award and engine test facility, with special thanks going to Mr. Paul Beckwith and Mr. Peter Hall whose knowledge, interest, and hard work was much appreciated.

Finally I would like to express thanks to my parents for their support and encouragement throughout the project.

CONTENTS

CHAPTER 1

INTRODUCTION AND LITERATURE SURVEY

1.1 INTRODUCTION

One of the most important parameters governing the performance of a spark ignition engine is that of cycle by cycle variations within combustion. The aim of this project is to determine which of the measured engine parameters: imep, maximum pressure and maximum rate of pressure rise best characterizes cyclic variation, then using a laser schlieren system to measure early flame speeds and cylinder pressure analysis, to calculate 0-10, 0-50, 0-90, and 10-90% mass fraction burnt times, and establish a link between the early flame and burn times and cyclic variations.

With the introduction of new legislation on fuel quality and emission standards, plus the phasing out of lead there has been a need to investigate the in-engine combustion characteristics of different pure fuel components that may be used either as straight run alternative fuels (as might be the case with methanol), or as blending agents to boost octane quality (as with methanol and toluene). For this reason a series of tests was carried out on three different fuels at Wide Open Throttle (WOT) and three different equivalence ratios (lambda 0.9, 1.0, and 1.1) over a range of ignition timings (2 - 44 deg.btdc), in order to change

the in cylinder conditions at the point of ignition, and observe the effect on flame times, burn times, measured engine parameters and cyclic variations in combustion.

The fuels chosen were:

1. Iso-octane - (bp. 99 deg.C., density 0.69 kg/m^3, RON 100) which is commonly used as a standard reference fuel.

2. Methanol - (bp. 65 deg.C., density 0.80 kg/m^3, RON 105) which is used as both a straight run fuel or as a supplement to boost octane rating.

3. Toluene - (bp. 111 deg.C., density 0.87 kg/m^3, RON 120) which is used as an octane boost additive.

Similar tests were also carried out using iso-octane as the fuel at WOT with knock present and for further tests at part-throttle.

A phenomenological combustion model for turbulent combustion was developed that split combustion into three phases:

1. Early laminar burning, up to 1% mass fraction burnt.

2. Turbulent combustion.
3. Final burn, in which the mixture within the thermal boundary layer is burnt.

This allowed a study of the physical phenomena occurring within the combustion chamber and their effect on combustion and cyclic variations.

1.2 LITERATURE SURVEY

1.2.1 FUEL AND REFINING TRENDS

With the introduction, in Europe and elsewhere, of new legislation governing the lead and benzene content of petrol, Johnson (1986), plus tighter controls on octane quality and exhaust emissions, the refining industry is going through a transitionary period, where it has to balance its crude supply with product demand both now and in the future.

It is anticipated that the demand for diesel will increase steadily up to the year 2000, with petrol demand increasing up to 1990 then falling back slightly due to increased fuel economy, see figure 1.1, this means that the demand for the lighter fractions of crude oil will increase, whilst the consumption of the heavier fuel oils is expected to decrease. This will lead to petrol and diesel being made up of a greater percentage of converted components (See later).

Volatility is a very important factor in governing the performance of a fuel for spark ignition engines, as the temperature of the fuel increases its constituent hydrocarbons vaporize, with the lower boiling point hydrocarbons vaporizing first, ie. they are more volatile than the higher boiling point ones. A good fuel should evaporate smoothly over the whole range whilst keeping within certain volatility limits, being too volatile or not volatile enough over certain temperature ranges can cause problems in the engine. Figure 1.2 shows volatility curve for gasoline and how it is expected to change in the future. It predicts an increase in front end volatility,giving problems with hot fuel handling in high temperatures, and carburettor icing under low temperature high humidity conditions. The use of aromatics with their lower volatility in the reformate, will extend the volume of fuel not vaporized until the higher temperatures are attained. The lower volatility of the fuel seeping past the pistons during cold starting will lead to increased crankcase oil dilution and engine wear. Furthermore, the reduced tendency for aromatics to resist "cracking", that is the breaking up of the molecule, plus their high carbon/hydrogen ratio will increase combustion deposits in the inlet system and combustion chamber. This will adversely affect the ability of the engine to stay in tune, thus giving bad fuel economy and driveability. So as well as lead, benzene and octane controls, changes in volatility, wider ranges of density, increased aromatic content and stability are also of major concern. These new blends will therefore have to meet specified performance requirements, Van

Passen (1986).

With Current specifications not comprehensive enough, there is a need for future legislation to cover such things as:

1. **Phosphorous content residues.** Phosphorous, in the form of aryl phosphates, is an ignition control additive to change the composition of the lead deposits in the combustion chamber and on the spark plugs to phosphorous containing compounds, with a higher glow temperature and melting point, thus eliminating pre-ignition and spark plug fouling problems. However, with the gradual phasing out of lead and improvements in combustion chamber and spark plug design its use has become less important

2. **End point.** This is the final boiling point of the fuel and shows whether too many of the higher boiling hydrocarbons or aromatics are present. In Britain the end point is specified as being 220 deg.C, British Standards 4040 (1988).

3. **Percent evaporated at 180 degrees C.** This will show the amount of the lighter more volatile hydrocarbons, which make up the majority of gasoline, that are present in the fuel. The value used in Britain is 90 %(V/V), British Standards 4040 (1988).

4. **Specific gravity.** Since petrol is generally bought by volume then the higher the specific gravity the

more miles per gallon, but this is partly offset by the high specific gravity components, such as aromatics, having low calorific values. A typical range for specific gravity of premium gasoline is 0.72-0.78 kg/m^3 at 15 deg.C and 1 atm.

5. **Sulphur**. This is indigenous to all fossil fuels, in amounts that can vary from 0.2 to 6% by mass, Goodger (1975). Most of this is removed during the refining process, but some remains in the form of: corrosive free sulphur, dissolved hydrogen sulphide (H_2S), and mercaptans (thiols, RSH) or non-corrosive sulphides (RSR'), disulphides (RSSR'), and thiophenes. The maximum sulphur content allowed in Britain is 0.2 %(m/m), British Standards 4040 (1988).

6. **Existent gum**. This is caused by unsaturated olefinic materials, produced during the cracking process, which are less stable than the mainly paraffinic straight run product. These consequently form gummy deposits in the engine inlet system, and knock-promoting hydro-peroxides in the combustion chamber. The cause of this is the oxidation of the gasoline via a free radical mechanism, with the formation of a hydro-peroxy radical acting as an initiator for a chain reaction, Hancock (1985).

$$R^{\cdot} + O_2 \rightarrow ROO^{\cdot}$$

free radical hydro-peroxy radical

$$ROO^{-} + RH \rightarrow ROOH + R^{-}$$

hydro-peroxide

In Britain the maximum permissible value is 5 mg/mL, British Standards 4040 (1988).

7. **Copper strip corrosion.** In this test a polished copper strip is immersed in a sample of the fuel, kept at a constant 50 deg. C., for three hours. At the end of this period the strip is removed, washed, and compared with a standard. The significance of this test is to determine the relative degree of corrosivity of the fuel, usually caused by corrosive sulphur compounds remaining in the product after refining (see 5 above), ASTM standards (1980).

These criteria can be dealt with on an international basis, but fuel volatility will have to be at a national level to take account of seasonal and geographical factors in different countries, Johnson (1986).

In many countries the Lead content of petrol is gradually being reduced and eventually phased out altogether, because not only is it a threat to the environment itself, it also affects the catalysts used to decrease harmful exhaust emissions. This stepwise reduction, in the EEC, to 0.4 g/l then 0.15 g/l, with a lead free premium gasoline being available in all countries by 1989, will mean a loss of fuel quality. In each of the above steps the Octane number will fall by 3, with the result of a drop in engine efficiency and

loss in driveability. For each fall of 1 in the octane number, there is a subsequent loss of 1% in engine efficiency, Van Passen (1986).

Lead is not the only constituent of gasoline posing an environmental problem, benzene is also a health risk, since it is a known carcinogen. Moves have already been made in some western European countries to limit the benzene content in gasoline to 5% vol. maximum, with the other countries expected to follow suit soon, Van Passen (1986).

To meet future demands for petrol of the correct quality, the refining industry is going to have to put considerable investment into new processes such as reforming and isomerization, Van Passen (1986). Until recently the majority of the gasoline used was "straight run", that is to say it was obtained by the simple distillation of crude oil. Gasoline was that fraction distilled off between 30 and 200 degrees celsius, Goodger (1975).

The table 1.1 below shows the main product yields from four typical crude oils.

	Arabian light	Nigerian	Brent	Maya	Boiling (deg. C)
LPG	0.7	0.6	2.1	1.0	< 30
Naphtha/ Gas oil	17.8	12.9	17.8	11.8	30- 370
Kerosine	33.1	47.2	35.5	23.1	150-250
Residue	48.4	39.3	45.6	64.2	> 370

Table 1.1: Yield % wt. of main products by distillation Van Passen (1986), Goodger (1975)

Naphtha is the main feedstock for gasoline, with gasoil being the diesel product. The residue is the fraction with a boiling point above 370 degrees celsius, and this is used as industrial fuel oil (although in some cases it needs to be blended with gas oil to meet the required viscosity). Future trends predict an increase in demand for gasoline and diesel, but a fall in the use of industrial fuel oil, particularly in power stations. This is due to an increase in alternative energy sources such as: nuclear power, hydro-electricity, coal and gas. Thus refineries equipped with distillation units only, (called simple refineries) were unable to cope, so new refineries were built that are able to convert the residue to the lighter naphtha and gas oil fractions.

The main methods by which the fuel oil components are converted or upgraded to the lighter product are as follows:

1. **Thermal cracking** - The residue is heated in special furnaces to 450-480 deg.C which causes some of the heavier molecules to crack giving the lighter product, Van Passen (1986).

2. **Catalytic cracking** - Here the residue undergoes a second distillation, under vacuum, with the heavy distillate produced contacted with a catalyst at 470-520 deg. C. causing the conversion to the lighter product, Van Passen (1986). The catalyst used to be silica - alumina clays but more recently zeolite crystals have been used, Hancock (1985).

3. **Visbreaking** - The residue from the vacuum distillation is of very high viscosity and can only be used as fuel oil, if it is blended with gas oil.Instead of using up valuable gas oil, the residue is subjected to a further heat treatment (similar to thermal cracking) that reduces the viscosity by converting the heavier molecules to lighter ones, Van Passen (1986).

4. **Reforming** - This is fast becoming one of the most widely used upgrading processes, as it produces gasoline of a higher octane quality. It employs reactions designed to alter the molecular structure of the molecules by the removal of hydrogen (generally speaking the C-C bonds are left unbroken), so increasing the proportion of aromatics and hence the knock-rating of the gasoline, whilst at the same time not appreciably altering the boiling range of the products compared to the feedstock. The reactions are carried out in a hydrogen atmosphere at high temperature (530 K.), at high pressure (30 bar), and in the presence of a catalyst, normally of platinum, now usually with rhenium, on an alumina base, Hancock (1985).

The principal reactions involved are as follows, with benzene shown as the major product although other reaction products are produced, Goldstein and Waddams (1967):

(a) Dehydrogenation of napthenes

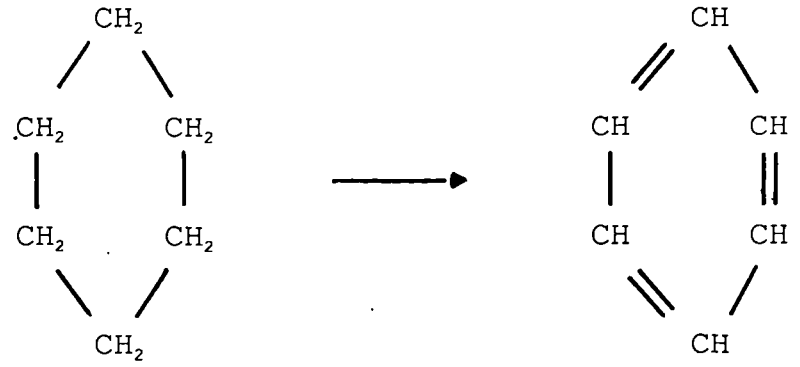

Cyclohexane Benzene

(b) Hydro-dealkylation of higher to lower aromatics with methane as a by-product.

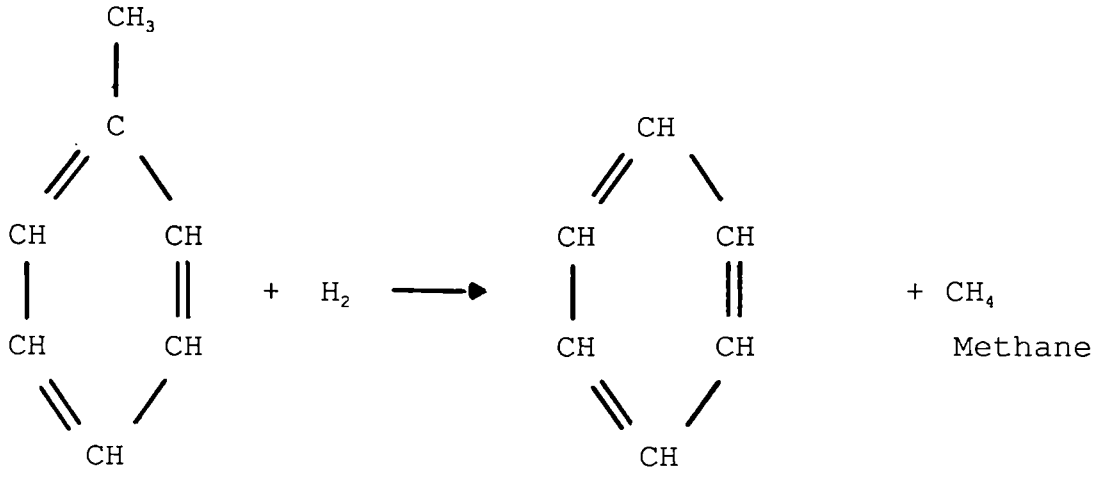

Toluene Benzene Methane

(c) Dehydro-cyclization of n-paraffins to aromatics.

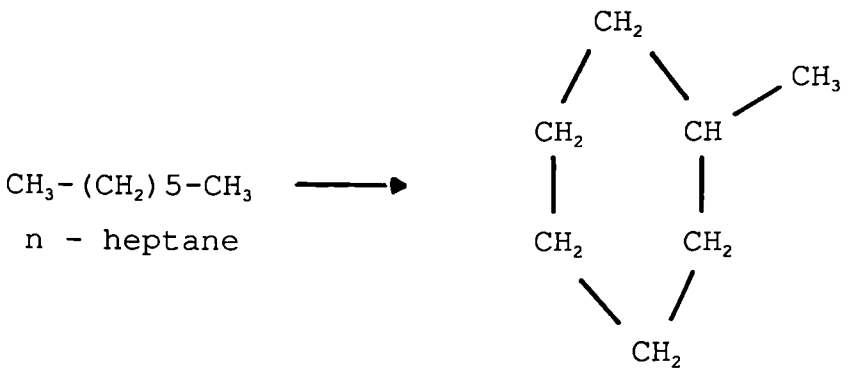

Methylcyclohexane

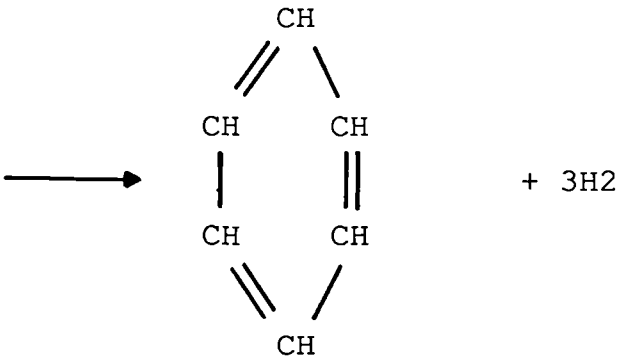

Benzene

(e) Conversion of five ring napthenes to aromatics by dehydro-isomerization

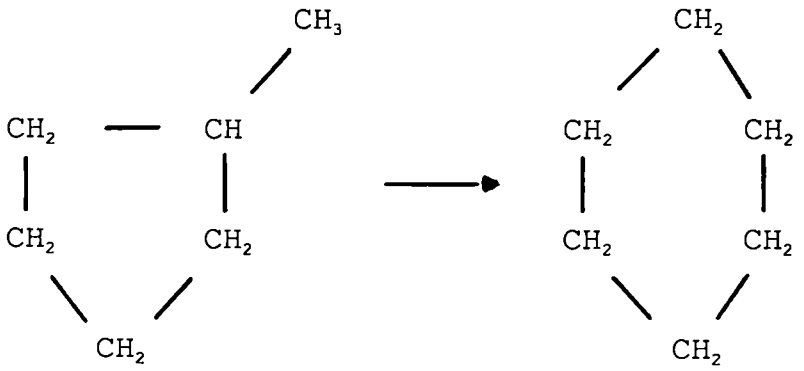

Methyl cyclopentane Cyclohexane

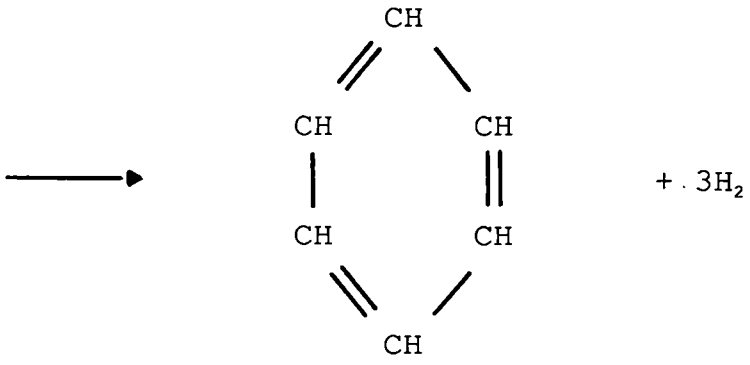

Benzene

(f) Isomerization of n-paraffins

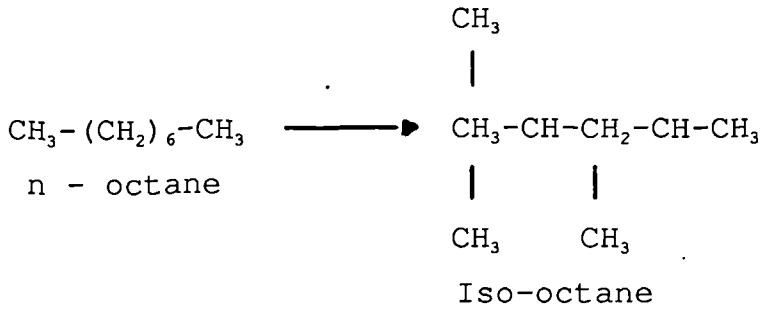

But even with these new refineries, the production of fuel oil still exceeds demand, therefore ways have been found to improve the efficiency of these processes, so reducing the quantity of fuel oil produced whilst increasing the amount of the lighter product. These improvements are as follows:

1. Increased recovery of feedstock for catalytic crackers by increasing the vacuum and improving the distillation equipment.

2. Using better and more resistant catalysts and improving their regeneration.

3. Optimizing the temperature and residence time for thermal cracking and visbreaking.

Even with these improvements it is forecast that demand for diesel and gasoline will outweigh supply, and that fuel oil will remain in surplus, so refiners are looking at new techniques for the conversion of all the

residue to lighter products, Van Passen (1986). These include:

1. **Residue catalytic cracking** - Advances in catalyst technology will allow a mixture of heavy distillate and residue, or even just the light residue on its own, to be used as feedstock.

2. **Flexicoking** - This is a severe thermal process in which the heavy fractions are converted to the light product leaving a solid coke behind , which can be sold as low grade coal. The coke is also gasified during the process, with the gas being burnt in the refinery.

3. **Residue Hydroconversion (HYCON)** - Similar to heavy distillate hydrocracking (oil mixed with hydrogen is passed over a bed of catalyst); however, developments in catalyst and process technology have allowed the use of the residue instead.

1.2.2 FUEL ADDITIVES

Additives are substances blended into a fuel in trace amounts only, up to about 0.2 percent by volume, to carry out a specific function, for example: knock control, ignition control, or as a detergent package. Ideally these additives must not only be effective in what they are meant to do, but must be stable and fuel soluble, with no undesirable side effects on performance, on engine condition, or on fuel storage

stability, and should be non-toxic in storage and in combustion emissions, Goodger (1975).

Perhaps the most important fuel additive has been lead, in the form of the lead alkyls, tetra-ethyl lead (T.E.L) and tetra-methyl lead (T.M.L), these are very effective anti knock additives which can greatly increase the octane rating of a fuel, present day lead content is 0.15g Pb/l and results in increases in pool octane numbers of about 2 to 3 units. The mechanism by which knock occurs has been found to involve free radical formation with the radicals produced being those of hydrogen and oxygen, OH^- and HO_2^-, see later, and its their ability to destroy these radicals that enables TEL and TML to function as anti-knock agents. It has long been known that it is not the TEL or TML themselves that destroy the radicals, but that they decompose in the engine giving lead oxide (PbO), which forms a mist or fog consisting of very finely dispersed particles, and it is this which is the active species in the free radical destruction, Hancock (1985).

But as has been mentioned previously, lead poses a great environmental and health problem and is gradually being phased out completely, so the search is on for new additives, that are environmentally acceptable, to replace lead.

One group of compounds presently undergoing investigation is the oxygenates, these posses a chemically bonded oxygen atom within the molecule, for example: alcohols and ethers, and since they are not

hydrocarbons, they have different blending characteristics when mixed with gasoline. Although they may not be able to completely replace lead as anti- knock agents the oxygenates with their high octane number can fulfill three needs, namely: to extend the total supply of gasoline (the " pool"), increase the octane rating, and add flexibility to meet quality demands. Much has been said about the adverse effects oxygenates have on fuel quality, mainly water tolerance problems leading to phase separation, but much of this can be put down to a lack of knowledge and experience on the part of the blender, Palmer 1986.

Two of the most widely studied groups of oxygenates are the alcohols and ethers, in particular tertiary butyl alcohol (TBA) and methyl tertiary butyl ether (MTBE), with guidelines already laid down to govern their use as gasoline additives, see table 1.2 below.

oxygenate	maximum % volume	Boiling point (deg. C)	Blending RON
Methanol	3	65	115-145
Ethanol	5	78.5	110-125
Iso-propyl alcohol	5	82.4	-----
TBA	7	82.3	108-114
Iso-butyl alcohol	7	88.15	-----
Ethers (5 or more C's per molecule)	10 (MTBE)	55	110-130
Other organic oxygenates	7	-----	-----
Mixture of organic oxygenates	2.5% weight of O_2 not exceeding individual limits set above.		

Table 1.2: Characteristics of oxygenated fuel supplements and their agreed level of addition to commercial gasoline, Van Passen (1986), Hancock (1985), Handbook of Chemistry and Physics .

Tests have been carried out on alcohols and ethers to assess: Material compatibility, anti-knock performance, driveability, exhaust emissions, fuel economy, and inlet system detergency.

1. **Material compatibility.** This includes: Metal corrosion,elastomer attack and effects on tank linings. Metal corrosion tests were carried out using a gasoline containing 20% vol. oxygenates, in 55% vol. aromatic base stock, two reference fuels where used ASTM-C and DIN 51604 plus a "sour" (high peroxides) gasoline. Tests were carried out for 500 hours at 60 and 20 degrees C, with wet (ie 70% of the blend water tolerance at 20 deg. C) and dry fuels. Of the metals tested the descending order of resistance to attack was:

   Brass>Aluminium>Terne>Mazak(zamak)>Zinc>Mild Steel
   most resistant least resistant

   With the descending order of attack severity for the oxygenates being:

   Methanol > Ethanol > TBA > MTBE
   most severe least severe

   It was found that the corrosion rate was increased with increased oxygenate content, temperature, and water content, Palmer (1986).

   A similar test was carried out to determine elastomer attack, but at temperatures of -20, +20,

and +60 deg C, with the results as follows.

Descending order of resistance:

flourosilicone > vito > nitrile > epichlorohydrin
most resistant least resistant

With the descending order of attack severity of the oxygenates being:

Methanol > ethanol > TBA > MTBE
most severe least severe

Again it was found that increasing concentration and temperature increased the attack rate and also a reduction in the aromatic content of the fuel had the same effect, Palmer (1986).

From the above results, it was possible to select the best component materials, with tank linings made from zinc silicate, zinc epoxy, and poly-urethane giving satisfactory results.

2. **Anti-knock performance** of oxygenated fuels is a very important factor, since knock control is the main reason for the addition of oxygenates to the gasoline. There has been increasing uncertainty over the validity of the Motor Octane Number (MON) and Research Octane Number (RON), as indicators of anti-knock performance for hydrocarbon fuels with respect to vehicle/engine conditions. With the

advent of the oxygenates, this controversy has increased, with many researchers finding that the MON and RON of oxygenated fuels does not truly reflect the road anti-knock performance, especially for fuels containing ethanol. But with no other method currently available, the RON and MON can provide a useful yardstick by which to assess fuel anti-knock performance.

All the fuels used in the anti-knock tests, reported by Palmer (1986), were blended to be of about equal RON and MON, (99/88) for leaded and (95/85) unleaded, with the tests being carried out at low speed acceleration and full throttle constant speed. A list of the oxygenate blends and concentrations used are shown in table 1.3 below.

Oxygenate type	blend number and oxygenate concentration level % volume											
	1	2	3	4	5	6	7	8	9	10	11	12
Methanol	3	3	3	5	-	-	-	-	3	-	3	3
Ethanol	-	-	-	-	-	-	-	-	-	5	2	-
TBA	-	2	7	3	7	-	-	-	2	-	-	-
MTBE	-	-	-	-	-	5	10	15	5	-	-	-
Iso-propyl Alcohol	-	-	-	-	-	-	-	-	-	-	-	2

Table 1.3: Test fuel blends - Laboratory data on alcohols and ether compounds assessed, Palmer(1986).

The important trends noted were:

(a) All the oxygenated fuels gave better anti-knock performance compared with just hydrocarbon fuels of the same RON/MON, under low speed acceleration.

(b) All low oxygenate concentration fuels gave comparable anti-knock performance compared with the hydrocarbon fuels, at full throttle constant speed. Any fuel with greater than 5% vol. of ethanol, and to a lesser extent methanol were shown to have a worse performance.

(c) MTBE was by far the best oxygenate additive, with its anti-knock performance increasing with concentration under all conditions.

(d) There is a tendency for the anti-knock properties of the oxygenates to improve in unleaded gasoline.

3. **Driveability**, this includes hot and cold weather performance, and the effect of altitude. Driveability is assessed by awarding demerit points each time the engine runs incorrectly, for example, stumble, hesitation, or surge, with the more demerit points awarded the worse the driveability. It was found that for cold weather driveability, the addition of oxygenates increased the number of demerit points awarded, so decreasing the driveability. This was true for fuels of all

volatilities, but was less marked for the more volatile fuels. The use of a fuel injection system instead of a carburettor made the vehicle more tolerant to lower volatility fuels containing oxygenates. The hot weather performance is defined by the Hot Fuel Handling Parameter (HFHP) :

HFHP = RVP (mbar) + 7 E70 deg.C.% vol.

Where: RVP is the Reed Vapour Pressure E70 deg.C. % vol. is the percent of fuel evaporated at 70 deg. C.

showed that only the fuel containing 5% vol. of methanol made any significant decrease in drive-ability, with the Methanol/TBA and MTBE blends shown to have a slight advantage.

Altitude is known to affect driveability under high temperature conditions. Apart from the 5% methanol blend, the oxygenated fuels gave similar or better performance with respect to the hydrocarbon fuels.

4. **Exhaust emissions.** These are mainly affected by the leaning effects of the oxygenate additives. This is of particular advantage for older vehicles, as they have a tendency to run richer as they get older, Palmer (1986). This is probably due to the fact that these vehicles where generally set to richer mixture settings, and the general trends in engine tune with mileage.

CO emissions were found to decrease, irrespective of the oxygenate, as the oxygen content increased. NOx and hydrocarbon emissions remained unchanged.

Ethanol blends showed an increase in the aldehyde emissions as the blend concentration increased, but all other oxygenates showed only a small increase in these emissions.

5. **Fuel economy**, since the oxygenates have lower calorific values than wholly hydrocarbon fuels, concern has been expressed as to their effect on fuel economy. Tests have been carried out on a range of fuels of constant density, but with varying oxygen content. The results showed a deterioration in fuel economy as the oxygen content increased for TBA, MTBE, and TBA / MTBE / methanol blends. It was found that the deterioration with up to 2.5% wt. oxygen was within acceptable limits, but above this level the fall in fuel economy is quite marked.

   In reality, this deterioration in fuel economy should be offset by the fact that oxygenated fuels have a higher density than the purely hydrocarbon fuels.

6. **Inlet system** detergency is worsened by the oxygenate additives, with increased deposits in the valve and manifold areas. However, there are additives available to counter this. In the area of injector fouling, the oxygenated fuels are thought

to be no worse than the hydrocarbon fuels.

Another group of additives of particular interest are the so called "spark aiders". These are compounds of certain alkali and alkaline earth metals, normally potassium compounds, and are known to improve early flame development and reduce cyclic variation. This effect is thought to be due to the low electron work function of deposits left on the electrode by the spark aider, which leads to a reduction in the loss to the electrode of the electrical energy of the spark, Kalghatgi (1987[1]).

1.2.3 KNOCK

It was first proposed by Ricardo in 1919 that engine knock, as characterized by the well known " pinking " sound, was caused by auto-ignition of the " end gas " prior to the arrival of the flame front, this is distinctly different from the other forms of abnormal combustion such as, pre-ignition and run on, although in the case of pre-ignition the two can be inter-dependent, with one leading to the other or vice-versa.

During a normal combustion cycle the flame front, initiated by the spark, travels uniformly across the cylinder. But during a knocking cycle as the flame front propagates across the cylinder there occurs auto-ignition of the unburned gas ahead of the flame front, giving a sharp increase in pressure and heat transfer to the cylinder wall. To cause auto-ignition

the unburned end gas must be at a high enough temperature and pressure, and have sufficient time for the reaction to occur, therefore knock usually occurs with a high compression ratio and low engine speed where the pressure brought to bear by the piston and advancing flame front raise the temperature of the end gas to a sufficiently high level for spontaneous combustion to occur, Hancock (1985).

The characteristic knocking sound associated with engine knock is caused by relaxation of local pressure imbalances set up by the very high energy release rates observed during knocking cycles, this relaxation initiates a standing shock wave and the gas vibrations associated with knock, Curry (1962).

Other theories have been put forward to account for the " knock " phenomenon, the most notable being the detonation wave theory. This postulates that, due to shock waves or some other disturbance within the combustion chamber, a true detonation wave is established and propagates throughout the unburned portion of the charge at velocities in excess of the sonic velocity. Such a detonation wave has associated with it a sharp pressure discontinuity which could give rise to the characteristic gas vibrations, Curry (1962). This theory has now, largely been discounted by most workers in favour of the autoignition theory, although just recently Maly and Ziegler (1981) showed that detonation waves could develop from a spark ignited flame front. If flame velocities exceed 50 - 100 m/s the mass flux

on the hot side of the flame front rises to sonic or supersonic velocities, Cuttler and Girgis (1988).

Another theory put forward is that of rapid entrainment, in which knock is induced by high rates of energy release associated with rapid flame propagation. Curry (1962) used multiple ionization probes mounted in a split head chamber (see section 1.5), to measure flame propagation. During light knock (that is when less than 100% of the cycles give knock) he observed that flame propagation for the knocking cycles was greater than for non-knocking cycles, but still well below sonic velocities. With no auto-ignition of the unburned charge ahead of the flame front detected, Curry concluded that rapid entrainment of the end gas caused the pressure to rise sharply, resulting in knock. However it is possible that auto-ignition was occurring in the engine, since ionization probes only monitor flame front arrival at a specific point in the chamber and are unable to resolve the source or direction of flame front travel, the estimates of global flame propagation are based on a relatively small amount of temporal and spatial information, Cuttler and Girgis (1988).

When the engine was run in heavy knock, the flame propagation was found to be 10 to 20 times greater than that for normal combustion, with auto-ignition of the charge detected ahead of the flame front. No evidence of a detonation wave was observed since the flame speeds of 93.6 m/s to 374 m/s were well below the sonic velocities of 1248 m/s to 2148 m/s associated with a detonation wave, although they did fall within

the limits set by Maly and Ziegler (1981) for the development of a detonation wave from a spark induced flame front.

This view that flame propagation increases with the onset of knock has recently been challenged, with some workers reporting lower flame speeds during the early part of a knocking cycle compared with a non-knocking cycle, but with a sharp increase in speed during the latter part of the cycle due to the amalgamation of the primary flame front with flame fronts caused by auto-ignition of the end gas, Lightfoot and Negus (1984). Similar results have been reported by Cuttler and Girgis (1988), who observed flame speeds similar to those obtained for non-knocking cycles during the knocking cycles up to the onset of knock. The end gas auto-ignited while the normal flame propagated across the cylinder. Two degrees before auto-ignition became visible, propagation velocities rapidly decreased until the flame front appeared to be stationary relative to the chamber. This is due to the end gas expanding to accommodate the self-induced pressure rise caused by auto-ignition. The subsequent movement of mixture towards the propagating flame front greatly reduces its apparent velocity. Hence flames which decelerate quickly during combustion do not cause auto-ignition but are a consequence of it.

With the engine operating in heavy knock the propagation of the auto-ignited flame fronts has been shown to be seven to eight times faster than that of the normally propagating flame. Roughly 40% of the total

mixture was burnt by auto-ignition with 90% of this being burnt within a very short crank angle period of 7 - 8 degrees of crank angle. It was also found that the earlier auto-ignition occurred (i.e., the closer to top dead centre), then the greater the proportion of the mixture burned, 10% was burned at trace knocking levels as compared to the 40% observed during heavy knock, and at faster combustion rate, 40% consumed within 7 - 8 crank angle degrees for trace knock as opposed to 90% for heavy knock. As a result knock intensity became increasingly stronger, Takagi et al. (1988).

The ignition chemistry of a fuel is a very important factor when considering knock quality, with substances that can form free radicals tending to be pro-knock.

It has been shown that two types of combustion can occur in a spark ignition engine :

1. **Low temperature combustion.** This is a two stage process involving the formation of peroxides and cool flames and is the one commonly observed with most normal fuels.

2. **High temperature combustion.** This is a single stage process, not involving formation of peroxides or cool flames, and is commonly observed with such fuels as benzene, methane and hydrogen.

The passage of the cool flame during low temperature combustion, might produce end gas temperatures that are

much higher than those calculated by thermodynamic analysis of the measured cylinder pressure, due to the significant amount of heat the cool flame releases, Downs et al. (1951). This conclusion was substantiated by Green et al. (1987) who suggested that the main role of cool flames in engine knock is that of heat release, with fuels releasing greater amounts of heat during end gas compression arriving at the point of auto-ignition sooner than other fuels, and so showing a greater tendency to knock.

In Hydrocarbon-oxygen mixtures the cool flames are of a blue colour and are associated with the fluorescence spectrum of formaldehyde. Aldehydes are always present during low temperature combustion with the concentration varying with time but reaching a maximum on the appearance of the cool flame, Benson and Whitehouse (1979). Results published by Downs et al. (1951) showed that addition of formaldehyde and acetaldehyde to a fuel increased the likelihood of knock occurring during low temperature but not high temperature combustion.

The effect of pre-flame reactions or " pre-sensitization " of the fuel ahead of the flame front has a great effect on the combustion properties of a fuel. Investigations have shown that considerable decomposition of the fuel occurs during these reactions, with the main products identified as aldehydes, ketones, peroxides, formaldehyde, and hydrogen peroxide plus free radicals such as H^{-}, OH^{-}, and HO_2^{-}, Lewis and von Elbe (1961). It has already been shown that increasing the concentration of these, with

the exception of the organic peroxides, has a significant affect on the combustion and auto-ignition properties of a fuel.

The mechanism through which combustion and auto-ignition of hydrocarbon fuels is achieved is via free radical reactions. The monovalent free radical, i.e. $OH^{\cdot}$ abstracts a hydrogen atom from the fuel molecule leaving a free valence on one of the constituent carbon atoms of the hydrocarbon fuel chain (i.e. an alkyl radical $R^{\cdot}$). This free valence is capable of capturing an O_2 molecule to form a hydro-peroxy radical ($RCH2\text{-}O\text{-}O^{\cdot}$), which can in turn break up leaving one oxygen attached to the capturing carbon atom in a aldehydic group (RCH=O). The most susceptible hydrogen of the hydrocarbon to attack by the free radical is the tertiary hydrogen atom:

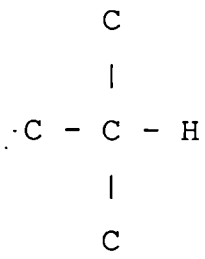

since it is less strongly bound than the secondary hydrogen atom:

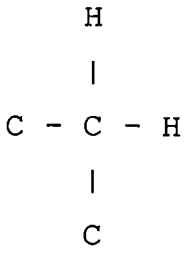

which in turn is preferred over the primary hydrogen atom :

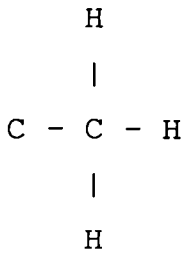

although the tertiary atom is preferred, the greater number of secondary and primary hydrogens means that these react at a faster overall rate. The secondary and primary hydrogens react in the same way as the tertiary atom, but give a ketone as the end product.

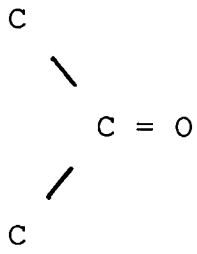

In this way aldehydes and ketones appear as intermediate combustion products, Lewis and von Elbe (1961), Green et al. (1987).

Another path by which the hydro-peroxy radical ($RCH_2-O-O^{\cdot}$), might react is by extraction of a hydrogen atom from another fuel molecule, forming an alkyl hydro-peroxide ($RCH_2-O-O-H$), and an alkyl radical, so setting up a chain reaction.

$$RCH_2^- \xrightarrow{O_2} RCH_2\text{-}O\text{-}O^- \xrightarrow{R.H^-} RCH2\text{-}O\text{-}O\text{-}H + R^-$$

alkyl radical	Hydro-peroxy radical	alkyl hydro-peroxide	alkyl radical

The alkyl hydro-peroxide then decomposes to give a an alkoxy radical (R-CH2-O$^-$) and OH$^-$ with the alkoxy radical forming an alcohol by reaction with another fuel molecule,

$$R\text{-}CH_2\text{-}O^- + RH \longrightarrow R\text{-}CH_2\text{-}OH + R^-$$

or an aldehyde by reaction with oxygen,

$$R\text{-}CH_2\text{-}O^- + O_2 \longrightarrow R\text{-}CH{=}O + HO_2^-$$

the HO_2^- radical then participates in the chain branching sequence:

$$RH + HO_2^- \longrightarrow R^- + H_2O_2$$

the H_2O_2 decomposing to give $2OH^-$, which initiates another reaction.

The majority of the fuel consumption occurs via H abstraction by $OH^{\cdot}$, with the general acceptance that the $HO_2^{\cdot}$ radical was effectively inert, but as has been shown above the HO_2 radical is a crucial branching intermediate, especially at temperatures and pressures associated with knock, Green et al. (1987).

The chain branching mechanism is fairly simple in the case of the lower hydrocarbons, but as the number of carbon atoms is increased, the detailed course of the reaction becomes increasingly complex, and the reaction intermediates or end products becomes increasingly numerous and varied, because the molecules are attacked along their carbon skeletons, also the atomic rearrangements and break-ups become more varied and numerous, and because intermediate products undergo various reactions, Lewis and von Elbe (1961).

There are a number of ways in which knock intensity can be quantified, for example : Maximum cylinder pressure, amplitude of the high frequency pressure oscillations, maximum rate of pressure rise and peak accelerometer output from a knock sensing device. At present their is no universal method of detecting knock and quantifying its intensity. Generally workers choose a criterion best suited to their particular investigation, Cuttler and Girgis (1988), the one adopted for our work is that of the amplitude of the high frequency pressure oscillations (see section 2.5).

1.2.4 FLAME PROPAGATION

Flame propagation is the term used to describe the movement of a burning zone or combustion wave through a combustible gas when ignition is initiated, in the case of a spark ignition engine, by an electric spark. Explosive gases are commonly mixtures of two gases such as oxygen and a fuel gas within the limits of inflammability, Lewis and von Elbe (1961).

It is known that a heat source such as an electric spark (arc) also produces atoms and free radicals which may act as chain carriers in the chemical reaction. The flow of heat and chain carriers from the ignition source initiates chemical reactions in the adjacent layer of the explosive medium , so that the layer itself becomes a source of heat and chain carriers capable of initiating chemical reactions in the next layer, and so on; in this way a zone of burning propagates through the medium, Lewis and von Elbe (1961). Until recently it was thought that the sole purpose of the arc was to provide sufficient energy to initiate a self- sustaining flame kernel and that the arc then had no further influence on the combustion process. It is now thought that the temperature profile of the plasma discharge appears to be imprinted onto the combustion front and remains with the reaction process for a considerable time. This reduces the consequences of adverse effects (such as poor mixture preparation) in determining the burning rate, Hancock et al. (1986).

The flame propagation within an engine has a large amount of turbulence associated with it, so it is this turbulent flame propagation that concerns us most. Laminar flame propagation is achieved in the laboratory using apparatus such as combustion bombs with the value obtained being of great use in engine modelling, since it has the advantage of being less complex and more repeatable than turbulent propagation.

Homogeneous (or pre-mixed) charge combustion is an unsteady process, in which an ignition flame kernel of size 1 mm grows over a time of 1ms into a fully developed flame front with a front to back thickness of 10 mm that propagates through the chamber, Abraham et al. (1985).

The initial phase of combustion, that corresponds to the induction period (sometimes misnamed the ignition delay),involves a relatively smooth laminar flame until the flame kernel has grown to a critical size where it has become self-sustaining, Keck (1982), Borman (1980). Work carried out by Hires et al.(1978), related this period to the time of burning of an individual turbulent eddy. Results published by Kalghatgi (1985) suggest, that initial burning velocity never equals laminar burning velocity, and that even in quiescent or laminar flow conditions it takes a certain time for a spark initiated flame to reach a steady laminar velocity. The flame velocity before this steady state is reached could be higher or lower than the final value, depending on the nature and strength of the spark.

As the flame grows the flame front becomes distorted by the turbulent flow field through which it is propagating and develops a highly wrinkled and multiply connected structure, Keck (1982). The speed of the flame increases to a quasi-steady value of about ten times the laminar velocity, Beretta et al. (1983). This corresponds with results reported by Keck (1982) who observed that the flame speed increased rapidly from a value of about 1m/s (characteristic of a spherical laminar flame) to a steady value of about 10 m/s characteristic of the turbulent intensity in the unburned gas. Similar results have also been reported by, Abraham et al. (1985). The size of the flame kernel at which this steady value is attained is the subject of some disagreement between workers. Kalghatgi (1985), using a laser Schlieren technique to measure flame speed, reported that the flame appeared to be fully developed by the time the flame radius had reached 11 mm. Results published by, Beretta et al. (1983), using a photographic technique showed the flame to be fully developed at a radius of 20 mm, while Abraham et al. (1985), reported that the time required for the fully developed flame front to form had been correlated with the time required for the flame to grow from the ignition kernel to the size of the turbulent length scale, which has been reported to be of the order of 10 mm, Heywood (1980).

Another view of the turbulent flame process is that the flame is a thick zone in which lumps of unburned fuel are entrained and burned, Borman (1980). This contrasts with the wrinkled flame front theory, where the front

is of a definite thickness, although it was suggested that under large scale turbulence the flame front may break up into unconnected islands of burning gas, Lewis and Von Elbe (1961). Entrainment of fuel was also observed by, Beretta et al. (1983), who noted that a significant fraction of the gas entrained behind the flame front was unburned. Such encapsulation becomes increasingly important as the engine speed increases, with no such pockets of unburned reactants being observed at 300 rpm, occurring a few percent of the time at 600 rpm and being present about 30% of the time at 1800rpm. Recent work by Tomita et al. (1988) has concluded that the concept of such a turbulent entrainment model was valid for predicting the combustion in a spark ignition engine. During the early stages of flame propagation, the effect of local turbulent intensity in the vicinity of the spark plug has a large effect on the subsequent combustion event , this is due to convection of the flame kernel which changes the effective location of the spark and the rate of heat loss to the electrodes or to the neighboring walls. The result of this convection is observed as cycle to cycle variations in the pressure history of the engine, see figures 1.3 and 1.4, Abraham et al. (1985). The close correlation between the flow field near the spark gap, the early flame development rates and , the ultimate pressure development has been demonstrated by Swords et al. (1982). Results published by, Curry (1962) showed that variations in the time for complete combustion and in the time of peak pressure could vary by as much as 25% from the average time. This has also been observed by Rashidi (1980), Beretta et. al. (1983), and

Heywood and Vilchis (1984), with the latter showing that the variations are more pronounced in conditions under which the laminar burning velocity is low compared to the turbulence intensity. It is possible that if the laminar burning velocity is large, the time characteristic of the laminar process will be sufficiently small compared to the time associated with the motion of the large scale structures in the flow field that the flame kernel will grow into the fully developed flame front quickly enough not to be affected by the large scale structures, Abraham (1985). It has also been argued that significant combustion variations cannot set in once the flame diameter is larger than the length scales of turbulence, (reported by Heywood (1980), to be of the order of 10 mm). In this stage, the flame front passes through several turbulent eddies and the local fluctuations are averaged out over the flame front, Kalghatgi (1985).

Work by Hancock et al. (1986) has shown that under certain engine conditions both the spark arc and spark duration have a significant effect on the cyclic variations with a longer duration of the spark and larger spark gap producing a greater stability in combustion. This affect is particularly noticeable at an advanced ignition timing and high engine load.

The effect of the advancing flame front on the turbulence intensity ahead of it has been investigated by Lee and lightfoot with results showing enhancement of the turbulence intensity just prior to the flame arrival, but with no difference observed between the

local mean velocities for a motored and fired engine except at flame arrival. This agrees with results published by Witze et. al. (1984) who obtained measurements for turbulence intensity through the flame, these indicated that the turbulence intensity is enhanced in the gas just ahead of the flame, increases through the flame and then decays in the burned gases.

1.2.5 TECHNIQUES FOR FLAME SPEED MEASUREMENT

There are many difficulties associated with the measurement of turbulent burning velocities, due to the fact that under turbulent flow conditions the random gas movements distort (i.e. "wrinkle") the flame front and may even fragment it, (see section 1.4). As the flame is no longer plane, the local burn velocities vary from point to point. However flames in combustion engines are turbulent and there is a need to understand how fast the flame propagates into the turbulent unburned fuel mixture, Gaydon (1979).

The three most commonly used techniques for the measurement of turbulent flame speeds are:

1. Schlieren methods

2. Flame Photography

3. Ionization probes

1. SCHLIEREN METHODS

These methods were first developed to investigate phenomena associated with colourless, transparent or nonluminous substances, for example: the motion of air past an aeroplane wing, the mixing of liquids or gases, or the detection of faults in glass windows - from where the technique derives its name since it was first used in Germany to detect inhomogeneous regions in optical glass which are often in the form of streaks (schliere). In such cases the phenomena that are of interest frequently involve changes of the refractive index across the field to be investigated, which can then be visualized or photographed by using optical methods that depend on the effects of the refractive index changes on the transmission of light, Holder (1963).

The schlieren methods depend on the deflection of a beam of light, from its undisturbed path, when it passes through a medium in which there is a component of the gradient of the refractive index normal to the beam.

The theory of operation is simple, and is based on that given by Liepmann and Roshko (1963), this states that the angle of deflection (θ) in the transverse direction of a beam of light passing through a gaseous medium is given by :

$$\theta = \int_0^L \frac{\alpha}{n} \left(\frac{d\rho}{dx}\right) \cdot dl$$

where α is the Gladstone-Dale constant, n is the refractive index, ρ is the density of the medium and L is the distance over which$(d\rho/dx)$ exists. The co-ordinates l and x are, respectively, in the direction of and normal to the light beam, Lee and Lightfoot.

The development of the schlieren methods for use with internal combustion engines has taken the form of:

a. Schlieren photography,
b. Schlieren shadowography
c. A technique that uses the deflection of a laser beam as a trigger to start or stop a timer.

a). **Schlieren photography.** A typical schlieren apparatus is shown in figure 1.5. A light source is placed at the focal point (f1) of a concave mirror M1, which collimates the light beams from the source and reflects them as parallel beams through the engine cylinder. After passing through the cylinder, the beams strike another concave mirror M2, which focuses the beams at a point f2, (where f2 is the focal length of mirror M2), beyond this point a focusing lens L, is used to produce an image of the working area on a screen or photographic plate Q. It must be remembered that there are two focal planes, one for the image of

the source at f2, and one for the working section at the screen Q. To understand the focusing it is easier to consider pencils of light rather than individual rays,see figure 1.6, for instance point a on the source emits pencil of light adc which focuses at point a* in the source image plane. Other points are focused similarly to form the source image. It should be noted that each of these pencils completely fills the test section. Thus each point in the source image receives light from every portion of the test section.

Now consider light reaching a point g in the test section, this is contained in the pencil abg, it is transmitted in the pencil gb*a* and is focused at the point g* on the screen. This pencil passes through the source image and completely fills it. Other pencils from the test section such as hb*a*, are focused at their image points on the screen, and the image of the test section is formed there.

It should be noted that individual beams passing through the test section may not be parallel, due to the finite size of the source, but the pencils are parallel.

In the absence of any density gradient within the working area, and since the beams are parallel, all the light will be brought to focus at the same point i.e., each point in the source image receives light from every portion of the working area. Now if we consider just two of the beams,A and B, passing through the chamber, see figure 1.7. If a density gradient, such as

is associated with a flame front, passes through the beams they will be deflected by an amount θ, as shown by the dotted lines, and will now be brought to focus at a point f2*, the amount by which the focal point moves is equal to $f2\theta$. This however does not produce any corresponding movement of the image on the screen Q, since the focusing lens L focuses all light from the working region at the same place on the screen, irrespective of its direction or focal point. A method by which this deflection can be detected is described below.

In this (the Toepler) method the deflection of the light beams is detected as a change in the light intensity of that part of the image that corresponds to the beams deflected. This is achieved by placing a knife edge K at the focal plane of the source image, and adjusting it such that in the absence of any density gradient, part of the light from the working area is cut off from the focusing lens L, see figure 1.8, and so the illumination of the image on the screen Q will be uniformly decreased. If now a density gradient is introduced into the working area, the light beams from that part of the area will be displaced as shown in figure 1.8, and so the illumination of the corresponding part of the image on screen Q will either increase or decrease depending on whether the deflection is either up or down with respect to the knife edge. Deflection of the beams along (parallel to) the knife edge produce no change in the illumination of the image, therefore the knife edge has to be placed perpendicular to the direction in which the density grad-

ients are to be observed, Holder (1963), Lewis and von Elbe (1961), Liepmann and Roshko (1963).In the absence of the knife edge the intensity of the light, Io, falling on the screen Q is given by the equation:

$$Io = \frac{Bbh}{m^2.f1^2}$$

where B is the luminance, b the breadth and h the height of the light source, m is the magnification of the image on the screen, and f1 is the focal length of the first mirror.

If a knife edge is now placed at the focal plane and all but a height a of the image is cut off, see figure 1.8, the illumination on the screen falls to a value of I given by the equation:

$$I = \frac{Bba}{m^2.f1.f2}$$

where f2 is the focal length of the second mirror (M2).

If now a density gradient is introduced, that produces an angular deflection of $d\omega$ in the light beams, then the corresponding image of the source is displaced relative to the knife edge by an amount $f2d\omega$, with the change in illumination of the corresponding part of the

image on the screen being equal to :

$$dI = \frac{Bbd\omega}{m^2.f1}$$

This equation will cease to apply if the image of the source at the knife edge, that has a height (f1.f2)h, is completely above or below the knife edge, in which case the image on the screen will either have an illumination equal to Io or be totally dark. The maximum displacement for the image is therefore equal to the height of the image at the knife edge , and the corresponding range of angular deflection $d^*\omega$ is given by :

$$d^*\omega = (h/f1)$$

Holder (1963).

A similar method to the one described above was used by Heywood and Vilchis (1984).

b). **Schlieren shadowography**. This is a much simpler and therefore less expensive method than Schlieren photography, but does not give such good definition of the density gradient. It may often be of advantage where the finer details are not required or need to be suppressed.

It was noted that the positions of the image points on the viewing screen of the schlieren photography system mentioned above where unaffected by deflections in the test section, since the deflected beams where also brought to focus in the focal plane, and that the viewing screen is uniformly illuminated when the knife edge is not inserted into the beam. If however the viewing screen is placed at some point other than the focal plane, the effects of beam deflection will be visible. The ideal position is close to the test section, see figure 1.9.

This shadow effect is illustrated in figure 1.10, which shows parallel light entering the test section, being deflected by a density gradient, then falling upon the viewing screen immediately upon leaving the section. On the screen there are bright regions where the beams crowd together and dark regions where they diverge, Holder and North (1963), Liepmann and Roshko (1963).

Due to its simplicity this method is ideally suited to flame propagation studies in optically accessed engines, with the most usual arrangement being that employed by : Witze (1982), Lightfoot and Negus (1984), Takagi et al. (1988), Witze et al. (1984) and numerous other workers, with most being based on the method developed by Witze and Vilchis (1981).

c). **Technique employing the deflection of a laser beam as a trigger to start or stop a timer.** A typical arrangement for the apparatus used is shown in figure 1.11, this method is the one employed at the BP

research centre. A more detailed description is given in section 2.7.

This technique has also been used by a number of other workers, for example: Swords et al. (1982), Kalghatgi and Swords (1983), Lee and Lightfoot , and Kalghatgi (1985).

2. FLAME PHOTOGRAPHY

As its name suggests this method utilizes a high speed cine camera to photograph the combustion event in an optically accessed engine. This was first achieved with any great success by Rassweiler and Withrow in 1938, who managed to obtain clear pictures of knocking combustion within their engine using a camera that was capable of filming at rates of up to 5000 frames per second. Modern advances in camera design have meant that higher filming rates are now possible, Iwashita and Saito (1983), reported framing rates of 4000 to 10000 pictures per second (pps), using a special high speed shutter TV camera, with Cuttler and Girgis (1988), obtaining rates of 8000 pps. using a rotating prism camera.

A typical experimental set up was developed by Rashidi (1980) and is shown in figure 1.12. This arrangement has subsequently been used by Beretta et al. (1983), and Keck (1982). The engine, a single cylinder over-head valve research engine, was modified by fitting an extension, with a transparent piston containing a quartz window in its crown, to the

original piston. An angled mirror placed beneath the window allowed the combustion chamber to be viewed through a port in the cylinder block. The camera used was a Hycam Model K-2001-R rotating prism camera capable of taking up to 5000 frames per second.

Since the flame photographs where taken with a very short exposure time it was necessary to increase the luminosity of the flame by introducing various chemical additives to the inlet mixture, but selected so as not to affect the combustion rate characteristics. For good intensity over a wide range of the colour spectrum, three salts, namely sodium chloride (yellow), calcium chloride (red), and copper chloride (blue), were used. Sodium chloride was found to be the best, Rashidi (1980).

The problem of luminosity and the possible effect of additives upon the combustion event was overcome by Cuttler and Girgis (1988), using a similar experimental set up to that developed by Rashidi, but employing a Cinemax image intensifier, series coupled to a H10/16 rotating prism camera. The intensifier was able to increase the light intensity levels by 12 stops enabling high speed pictures of the combustion event to be taken without the addition of any additives. Additional lenses were placed between the window in the piston and the front lens of the Cinemax to improve the field of view and the picture magnification.

A similar set up was used by Iwashita and Saito (1983), who used a special high speed shutter TV camera, the

front end of which was an image intensifier, to record flame propagation. The image intensifier increased light levels by 14 stops. The image was focused onto the video screen of a camera tube and finally converted into a television image.

Another method by which photographs of the combustion event may be obtained, is by moving the valves and spark plug to the side of the combustion chamber and placing a quartz window in the top, so allowing optical access from above. This was the method employed by Lightfoot and Negus (1983), who used a Sandia single cylinder research engine, which is modified as above. The advantage of this method is that the whole of the combustion chamber may be viewed and the engine can be run at high speeds. With the engine optically accessed from below, part of the combustion chamber may be obscured by the piston walls, and engine speed is limited by the heavier piston. Another advantage with optical access from above is that by replacing the normal flat top piston with one with a front surfaced mirror bonded to it, light reflecting techniques, such as schlieren shadowography, may also be used.

3. IONISATION PROBES

Apart from visual perception of the fluctuating combustion wave by schlieren methods or high speed cine photography, it is possible to sense the flame front by contact with a probe inserted into the flame. The method is based on the fact that in many pre-mixed

flames the ionization density is several times higher in the immediate vicinity of the flame front than in the hot combustion gas, Lewis and von Elbe (1961).

Ionization gauges consist essentially of a wire in an annulus. The wire is insulated from the body of the gauge, or engine. In this way the fuel-air charge is made an integral part of an electrical circuit, see figure 1.13, The detection of the presence of a flame front is dependant upon a change in the electrical resistance of the gases. When a flame reaches the gap it becomes conducting and completes the electrical circuit, this change in current flow resulting from ionization of the gases when the charge burns is used to detect the presence of the flame front, Curry (1962), Benson and Whitehouse (1979).

This technique has been developed by, Curry (1962), who used 26 "Chromel-P" wires, to serve as the ionization gaps, inserted into the combustion chamber through small passageways drilled into the cylinder head. The passageways were sealed with Sauereisen spark plug cement.

A similar array of 22 ionization gaps were mounted in a modified high compression piston. Because of the high thermal coefficient of expansion of the aluminium piston relative to that of the insulating ceramics, the ionization gaps were made from steel-jacketed thermocouple wire insulated with magnesium oxide.

The problem of maintaining continuous electrical contact with the ionization gaps in the piston head was overcome by fixing two printed circuit boards to the bottom of the piston. The gaps where connected to the boards by PTFE-fluorocarbon (Teflon) coated wires. The 22 electrical circuits were completed by contact with 22 spring-loaded pins mounted in brush assemblies, see figure 1.14.

Eighteen of the piston mounted ion gaps had corresponding gaps directly above them in the cylinder head. The four remaining gaps in the piston were placed opposite the valves, the spark plug and the pressure pickup (areas which were not accessible from the cylinder head), see figure 1.15.

As has been mentioned before, the flame front was detected by the increase in current flow caused by the change in resistance of the gases in the ion gap as the charge burns, this rise in current only becomes of use once it has become sufficiently large to be detected above the noise level of the circuit. This requirement means that there is a definite time interval between the passage of the flame and the time when the signal is of sufficient strength to be detected; this time interval is commonly called the response time. Thus the arrival of the flame front is measured as having occurred later than it actually did.

The response time is affected by many variables, including: fuel type, fuel-air ratio, fuel additives, and other engine conditions. Thus any change in engine

conditions which changes the resistance of the gases in the gap will result in a different response time. In order to maintain a constant response time as engine conditions change, it was necessary to use a variable voltage in the ionization gap circuit. The signals from the ionization gaps were displayed on an oscilloscope and the voltage adjusted to give the desired response time.

CHAPTER 2

ENGINE TEST FACILITY

2.1 ENGINE INSTRUMENTATION

The engine test facility at the BP Research Centre is based around a Ricardo E6 single cylinder variable compression ratio research engine, the specifications for which are shown in table 2.1 below:

Engine specifications of the Ricardo E6

Cylinder bore:	76.2 mm	Flat top piston
Stroke:	111.0 mm	
Connecting rod length:	241.3 mm	
Inlet Valve diameter:	34.6 mm	
Exhaust valve diameter:	30.1 mm	
Compression ratio:	7.5 and 8.5	
Engine speed:	The engine was operated at 1500 rpm	

Valve timings

Inlet:	Valve opens	8 deg. btdc
	Valve closes	36 deg. abdc
Exhaust:	Valve opens	43 deg. bbdc
	Valve closes	6 deg. atdc

Table 2.1: Engine specifications for the Ricardo E6.

The speed and load of the engine are measured and controlled by an electrical dynamometer connected to the crankshaft, this can also be used to motor the engine for starting. The signals from the dynamometer are fed to a central control panel where the values of speed and load are displayed, also displayed here are the temperatures taken from various parts of the engine and the mixture generator assembly. A schematic block diagram of the facility is shown in figure 2.1, The control panel also has the starting switches for the mixture generator, fuel pumps, air heaters and flare igniter as well as for the laser equipment. Warning lights and alarms are also incorporated into the control panel, to warn of problems with: oil pressure and temperature, coolant level and temperature, slow engine speed, high engine speed, excess fuel and fuel leaks, high air heater temperature, coolant failure, whether the engine is being motored, and if the combustion chamber is operational.

2.2 FUEL PREPARATION SYSTEM

There are two separate fuel preparation systems fitted to the engine, a standard carburettor and a mixture generator.

The carburettor can use either an external fuel supply, situated in a dump behind the building, or an internal supply. The fuel flow is measured by timing the uptake of a set volume of fuel. The air flow can be calculated from the inclined manometer reading attached to the

viscous air flow meter, corrections are needed for the air temperature, and these are in the Alcock viscous flowmeter handbook.

The mixture generator uses only the internal fuel supply, which is pressurized by compressed air from the site main. The air can be pre-heated before entering the mixture generator, using electric heaters located just after the air inlet valve. The fuel flow is measured using one of three (rotating) float type flow meters depending on the flow rate required (ie.low, medium or high). The meters are calibrated gravimetrically prior to use to ensure their accuracy, with the correct flow rate read from the calibration graphs produced. The mixture generator works by evaporating the fuel on a hot surface (a series of pipes with hot oil running through them are used), the fuel vapour is then mixed with the air (electrically pre-heated if necessary), and passed along an insulated pipe to the engine. Excess air-fuel mixture is produced to what is required by the engine, with the excess being burnt off at a flare on the roof of the building. The advantages of using the mixture generator over the carburettor are: that less volatile fuels can be used, there is better control over the air-fuel ratio, and it is possible to operate the engine with a leaner fuel-air mixture. The engine is always started on the carburettor (part throttle) with this phased out and the mixture generator phased in when wanted. This is done by shutting off the fuel supply to the carburettor, and waiting until the engine starts to stall then closing the valve to the room air whilst at the same time

opening the valve from the mixture generator, which has already been started and flared off in anticipation.

2.3 PRESSURE AND TEMPERATURE READINGS

The pressure is measured by a Kistler type 6121 piezo-electric pressure transducer flush mounted into the cylinder head, see figure 2.2. The transducer is a rugged air cooled device that works reliably under temperatures of up to 350 degrees C., and can withstand intermittent flash temperatures of up to 2500 degrees C. This is due to a ceramic front plate that forms a double diaphragm, see figure 2.2. The element is a polystable quartz element (Kistler handbook), that is safe against twinning, even under high mechanical loads and high temperatures. The coaxial cable joining the transducer to the charge amplifier must also meet special requirements, it must have extremely high insulation resistance and low capacitance, generating only negligible charge signals when moved. A summary of the technical data for the transducer is shown table 2.2 below.

Specification	Range	Units
Measuring range	0 - 250	bar
Calibrated partial ranges	0 - 25	bar
	0 - 2.5	bar
Overload	350	bar
Sensitivity	≈ -14	pC/bar
Natural frequency	> 55	kHz
Frequency response ±1%	6	kHz

Linearity	< ±1.0	% FSO
Hysteresis	< 1.0	% FSO
Acceleration sensitivity		
axial	< 0.003	bar/g
Transverse	< 0.0002	bar/g
Shock and vibration	2000	g
Thermal sensitivity shift		
20 - 100 deg.C	≈ ± 0.5	%
20 - 350 deg.C	≦ ± 3.0	%
200± 50 deg.C	≈ ± 1.0	%
Calibrated in range	20-350	deg.C
Operating temperature range	-196-350	deg.C
Transient temperature error (Propane flame intermittent on front, 10Hz)	< 0.02	bar
Insulation:		
at 20 deg. c.	10^{13}	ohms
at 350 deg. C.	10^{10}	ohms
Ground insulation:	10^{8}	ohms
Mass	9.5	g

Table 2.2: Technical data for the Kistler type 6121 pressure transducer

The signal from the pressure transducer is amplified using a Kistler 5001 charge amplifier unit, this is a mains operated DC amplifier of very high input impedance, that is designed to convert the electric charge from the transducer into a proportional voltage

on the low impedance amplifier output, (Kistler 5001 instruction manual). The calibration of the amplifier is dependant on the sensitivity of the measuring device fitted, a pressure transducer in this case, which will be given in the literature for that device.

Temperatures are taken at various points around the rig, see figure 2.1, using type K-chromel /alumel thermocouples which are connected directly to the control panel, where the temperature readings are displayed. Type K thermocouples have a temperature range of -200 to +1371 degrees C., with an accuracy over the range 0-277 degrees C. of ±4 degrees C., ASTM STP 470 (1970), although in practice a far better accuracy than this is achieved.

2.4 EXHAUST GAS ANALYSIS

Exhaust gas analysis is carried out using a Micro Oxivision MO-1000 Air Fuel Ratio Meter connected to a NTK Universal Exhaust Gas Oxygen sensor, both of which are supplied by the NGK Spark Plug Co. Ltd.

The sensor, which has a very fast response, is mounted directly onto the exhaust pipe of the engine and gives a direct electrical output signal. The Micro Oxi-vision's high speed processing function gives real time output of the air fuel ratio. The sensors fast response characteristics allow precise measurement of transient engine conditions. As well as air fuel ratio, two other output modes may be selected: percentage oxygen and

lambda. These are selected by means of a switch on the front of the unit, see figure 2.3. A running average of the mode selected over 0.5, 2.0 or 10 seconds may be displayed.

The basic principle of the detecting portion and control circuit of the sensor, which is installed on the exhaust manifold, is shown in figure 2.4.

The detecting portion of the sensor is made up of two zirconium oxide (ZrO_2) substrate elements, one is the O_2 pumping cell (Ip); the other is the O_2 detecting cell (Vs/Icp). Both are heated by ceramic heaters located on the outside of the elements. The sensor operates by utilizing the following properties of ZrO_2:

1. A galvanic potential is caused by different O_2 partial pressures between both sides of a ZrO_2 element.

2. The oxygen ion can be moved by applying the voltage to the ZrO_2 element (the pumping characteristics).

The detection cell employs both properties, whereas the pumping cell only utilizes the pumping characteristic. The detection cell is supplied with a very small constant electric current, and therefore O_2 is moved to the right side of the element, and fills the O_2 reference cavity with a high concentration of oxygen. In the left side of the detector, the detection cell is exposed to the exhaust gas (this area is named the detecting gas cavity). Therefore the detection cell

generates the galvanic potential voltage (Vs).

This galvanic potential voltage is approximately 100mV at lean, and 900mV at rich (from measurements taken with a current ZrO_2oxygen sensor). The pumping cell can control the partial O_2 pressure in the gas detecting cavity by pumping O_2, therefore it can control the output voltage (Vs). As a result, voltage Vs can be kept at 450mV in any gas condition by controlling the pumping current Ip, and simultaneously this value of the Ip corresponds to the air fuel ratio of the exhaust gas. For example with lean mixtures excess O_2 will be present in the exhaust gas therefore O_2 will be removed from the gas detection cavity, by the pumping cell, to maintain the correct galvanic potential whereas for rich mixtures O_2 will be pumped into the cavity until all the excess fuel has been oxidized and the galvanic potential brought back to 450 mV. Figure 2.5 shows the relationship between the value of Ip and the air-fuel ratio of the exhaust gas. The MO-1000 calculates the data for an air-fuel ratio by detecting this pumping current Ip. A summary of the technical data for the sensor and air-fuel ratio meter is shown in table 2.3 below.

MO-1000 AIR-FUEL RATIO METER

1. Sensor Operation System

Icp Current	25 ±3 uA
Vs Voltage	450 mV
Limit Of Pumping Current	-12.5-12.5mA
Heater Supplied Voltage	10.5 ±0.5VDC

2. Data Processing system

Sample Period	10 ms
Measurement for Pumping Current of Sensor	12 Bit A/D

3. Readout

Equipment	4 digit LED
Details	

	Indication Range	Resolution
Lambda	0.500-2.290 λ	0.001 λ
Air-Fuel Ratio	4.00-33.30 A/F	0.01 A/F
O_2%	0.00-22.00 %O_2	0.01 %O_2
Running Average	0.5s; 2s; 10s; and HOLD	

4. Analog Output Voltage

Connector	BNC connector (0-5V)
Display	See 3 above
Function	Real time, running average between 2 and 10 sec. Read out gain of A/F corresponding to 0-5V

5. Range of Usage

Sensor Gain	0.00 - 999
Hydrogen/Carbon Ratio of Fuel	0.00 - 9.99
Oxygen/Carbon Ratio of Fuel	0.00 - 9.99
6. Power Source	AC 90-226V 2A
	(op.AC 180-260V 1A)
	DC 13-16V 5A

7. Environment Operating Conditions

Temperature	5 - 45 deg.C
Humidity	15 - 80 % R.H.

8. Environment Storage Conditions

Temperature	-20 - 70 deg.C
Humidity	5 - 80 % R.H.

9. Physical Size	250mm W X 100mm H
	X 300mm D
10. Weight	4.6 kg

NTK UNIVERSAL EXHAUST GAS OXYGEN SENSOR

1. Measurement Range

- Lambda	0.7 - 2.2
- Air-Fuel Ratio	10 - 30 A/F*
- O_2 Partial Pressure	0 - 22 %

* The measurement range of A/F ratio is shown under normal operating conditions using commonly available gasoline, and indicates the stoichiometric A/F

(lambda=1) times 0.7 to 2.2.

If a fuel using alcohol is used, the measurement range of the air fuel ratio is changed to the following values.

- Methanol	4 - 14 A/F
- Ethanol	6 - 20 A/F

2. Accuracy and Repeatability

	Range	Accuracy	Repeatability
Lambda	$0.9<\lambda<1.1$	$\pm 0.02\ \lambda$	$\pm 0.002\ \lambda$
Other	$\pm 0.03\ \lambda$	$\pm 0.003\ \lambda$	
Air-Fuel Ratio	13<A/F<16	±0.2 A/F	±0.02 A/F
Other	±0.3 A/F	±0.03 A/F	
O_2 Partial Pressure	$0.0<O_2\%<2.0$	$\pm 0.2\ \%O_2$	$\pm 0.02\ \%O_2$
Other	$\pm 0.3\ \%O_2$	$\pm 0.03\ \%O_2$	

Response Time: 0.1 sec. (0-90% of reaction time)

3. Variable Conditions

Exhaust Gas Temperature	0-800	deg.C *
Exhaust Gas Pressure	0.8-1.3	bar *
Max. Operating Temperature (Rubber Seal)	200	deg.C
Tightening Torque	4 $\pm$ 0.5	kg m
Vibration	Up to 30	G
Wiring Temperature	-20-130	deg.C
Wiring Tensile Strength	10	kgf
Thread Size	M18 - p 1.5	

4. Heater Supply Voltage 10.5 ±0.5 V/DC

5. Life Expectancy 1 year or 500 hours (unleaded gasoline).

6. Connector AMP 172192-4

7. Weight 100 g

* Survival gas temperatures and gas pressures are -20 to 950 deg.C and 0.5 to 1.5 bar, but usage outside the above range reduces life expectancy and accuracy.

Table 2.3: Technical data for the Micro Oxivision MO-1000 Air Fuel Ratio Meter and NTK Universal Exhaust Gas Oxygen Sensor.

The installation of the sensor must take place under normal environmental conditions, avoiding strong draughts, with extreme caution being exercised when handling the sensor due to the high temperatures reached by the heating elements. An anti-seize compound is used on the thread for installation on the exhaust manifold, boron nitride is recommended since other pastes or solvents may contain hydrocarbons, which can affect measurement readings.

Calibration of the sensor to the air-fuel ratio meter is via the setting of the sensor gain. This will be covered later in the section.

Once installed on the exhaust manifold the sensor is connected to the air-fuel ratio meter via a six way connector and the meter turned on. All LED indicators are lit during the warm up period of sixty seconds, after which time the status indicator will read READY and the operation mode automatically goes to MEAS, see figure 2.3. The equipment is now ready for use, unless calibration of the sensor is to be carried out or the fuel factor is to be changed in which case a further 10 minutes warm up period is required.

The fuel factor has to be changed each time a different fuel is used and is done by changing the operation mode to CAL, from MEAS, and changing the H/C and O/C ratios to the appropriate values for the particular fuel to be used. The operation mode is then set back to MEAS with the function and output modes selected as needed.

The sensor gain has to be reset each month, or every 200 hours, whichever comes first, and whenever the sensor is replaced (see technical details) and should be carried out under normal environmental conditions since the gain is set to correspond with the oxygen partial pressure under normal atmosphere. In this case normal atmosphere means 20.9% O_2 by volume. To find the exact oxygen partial pressure the temperature, humidity, and atmospheric pressure are measured and the following equation is used:

$$Po = \frac{(P - Ph)}{760} \times 20.9$$

Where:

Po = O_2 pressure (% O_2 by volume)

P = Atmospheric pressure (mmHg)

Ph = Water vapourized pressure (mmHg)

= Pho x Rh

Pho = Saturation water vapourized pressure at dry ambient temperature (mmHg)

Rh = Relative Humidity

and the O_2 pressure corrected accordingly.

2.5 KNOCK BOX

The knock box attached to the engine is manufactured by Cambustion. It works by processing the pressure Vs. crank angle trace obtained from the pressure transducer

and shaft encoder.

A window is taken of the time in which the knock is likely to occur, this is almost always at, or just after, top dead centre, with a knocking cycle showing the customary high frequency spikes caused by cylinder pressure oscillations, see figures 2.6, 2.7, and 2.8. The frequency at which the knock occurs is between 6 and 22 kHz. Most conventional wall vibration type knock sensors are tuned to the 6-8 kHz range, but it has been established that cylinder pressure oscillations from knock occur at a much higher frequency, Nakamura et.al. (1988). The knock box therefore filters out all frequencies below the set level, leaving just the trace caused by knock, plus any background noise from the engine, this is then integrated to produce a voltage that is proportional to the knock. A non-knocking cycle is run, and the same analysis is carried out, with the voltage produced being that due to background noise. This voltage can then be entered into the data processing system, where it is subtracted from the knocking cycle voltage, to leave only the voltage contribution due to knock. By altering this threshold voltage, parts of the knock induced voltage may also be filtered out, so making it possible to detect varying degrees of knock. For example, by increasing the threshold voltage, the oscillations due to light knock may be filtered out, allowing only heavy knocking cycles to be detected.

The signals from the knock box are fed into the HP 1000 data processing computer, see section 2.6, where the

knocking cycles are logged and displayed as a percentage of the total number of cycles recorded.

2.6 DATA PROCESSING

A shaft encoder is attached to the crank shaft of the engine, and this supplies a TDC signal and synchronizing angle signals (one per degree of revolution) to the HP1000 computer situated in the adjacent room see figure 2.1. The HP1000 is a high speed data acquisition system that has a sampling rate of up to 100 kHz. It takes a reading of the cylinder pressure in real time for every degree of crank angle rotation for up to 300 successive cycles, as well as noting the engine speed. The load, temperatures, manometer readings and various other variables are keyed in manually using the BPIN routine. The computer calculates (using the DREDS routine) : the brake horse power (bhp), brake mean effective pressure (bmep), equivalence ratio, brake specific fuel consumption (bsfc), (see figure 2.9). The pressure- time data are converted to mass fraction burnt- time data using a simplified version of the method described by Rassweiler and Withrow (1938). This method assumes that the combustion and expansion processes can be treated as polytropic processes in which PV^k = constant, where k is the polytropic index. In the method used at BP a single averaged value of k is used that has been computed from the pressure - volume data prior to the occurrence of the ignition spark. Since engine geometry and k are now known, the pressure rise due to piston motion can be calculated

and when this is subtracted from the total pressure rise, gives the pressure rise due to combustion. This is then normalized with respect to a datum volume, and assuming combustion is complete the pressure rise due to combustion as a fraction of the overall pressure rise is equivalent to the mass fraction burnt (a more detailed description of the Rassweiler and Withrow method is given in section 3.1.2). A summary of the statistics for the data before and after normalization is shown in figure 2.10.

2.7 LASER FLAME SPEED MEASUREMENT EQUIPMENT

2.7.1 OPTICAL ARRANGEMENT

The position of the flame front is detected either by the attenuation or refraction of a laser beam, that passes through the combustion chamber via two quartz windows. A photograph of the laser beam assembly attached to the rig is shown in figure 2.11. A CR-90-20H He/Ne laser of 2mW power is used as a light source, with the beam divided by a cube beam splitter, to give two parallel beams whose separation can be set between 1 and 12mm (changes made to the laser system are described in section 4.2). The laser and beam splitter may be rotated in their mounts to measure different components of the flame speed. They may also be moved along their horizontal axis, so varying the distance from the spark plug to the first beam. Optical access to the combustion chamber is achieved via two

quartz windows set in a slice placed between the cylinder block and cylinder head, see figure 2.2.

The diagrammatic representation of the optical arrangement is shown in figure 1.11. After passing through the engine, the laser beams are reflected through 90 degrees by a mirror into a dove prism. The dove prism compensates for any rotation in the beam plane, this is achieved by rotating the prism in its holder until the output beams return to the horizontal plane. The beams then fall onto a front mirrored prism which increases the separation of the beams by deflecting them at 90 degrees in opposite directions to each other, with each beam returned to its original path by means of two further mirrors prior to entering the detector box and falling on the surfaces of two position sensitive diodes.

The object of the laser flame speed measurement equipment is to obtain non-invasively, the velocity of a flame front at a certain position within the combustion chamber. This is achieved by using a variation of the schlieren technique. The flame front is an interface between the burnt and unburnt portions of the charge, and as such possesses a temperature and density gradient, so a light beam passing through the front (not normal to it) will be deflected towards the region of highest density. This deflection is picked up by a United Detector Technology SC/10D position sensitive diode, connected to detect horizontal deflection. The signal from the diode is used as a trigger for either starting or stopping a timer, see figure 2.12.

Alternatively, as the flame front passes through the laser beams attenuation of the beams also occurs, this can be detected by the photodiodes, and if marked enough, may be used as the trigger instead of the beam deviation, see figure 2.13. A switch on the back of the main electronics box allows selection of the required trigger. The trigger signal caused by the deflection of the beams leads that due to the attenuation by a few micro-seconds, since deflection is caused by the temperature and density gradient just ahead of the flame front whereas attenuation occurs in the main reaction behind the flame front. For the apparatus used here, attenuation was found to give a better signal to noise ratio.

2.7.2 SIGNAL PROCESSING

The method employed to time the flame front was for two timers to be started simultaneously with the spark, one stopped when the flame front passed through the first beam and the second stopped as it passed through the second beam. By knowing the distance of the first beam away from the spark plug, the beam separation, and the time of arrival of the flame front, then its velocity at that point can be determined. The separation of the beams needs to be as small as possible so that the velocity of the flame front does not alter too much on passing between them, the factors that limit how close the beams may be brought together are: the possibility that one or both of the beams may be deflected into the

path of the other, and the maximum resolution that it is possible to achieve between the beams. The ideal beam separation was found to be 3-4mm, Kalghatgi & Swords (1983).

The initial processing of the signal is carried out in the detector box. Where the current output from each diode is converted to a voltage signal proportional to either intensity or deviation, see figure 2.14. The current output consists of two signals Ia and Ib taken from anode connections at opposite sides of the diodes (only the anode connections that monitor horizontal deflection are used, as the vertical deflection anodes are connected to the 0V line), with the position of the beam being equal to Ia-Ib / Ia+Ib and the intensity equal to Ia+Ib. These calculations are carried out by the divider, and the four signals relating to intensity and deflection for each diode are sent via four coaxial cables to the main electronics box .

Here a switch enables selection of either intensity or deviation signals, with the one selected amplified and converted to a trigger pulse of 25 micro-seconds duration by two monostables. The trigger level is set by means of a potentiometer on the front of the box. When the signal from the photodiodes goes above the trigger level the first monostable is triggered, this prevents re-triggering if the trigger level is exceeded within the next 10ms or so. The second monostable is triggered by the leading edge of the output of the first monostable, and produces the trigger pulse.

If the intensity signal drops below about 2V then there is an unacceptable loss in accuracy in the signal, and too low a bandwidth level. To guard against this, a low intensity monitor is connected to the intensity signals, see figure 2.14, and an LED on the front of the main electronics box is lit continuously if the signals fall too low. If the intensity signals fall too low for only a short period of time, say for example from absorption in the flame, then the LED light will only stay alight for about 1 second.

2.7.3 USE

Fitting of the quartz windows is carried out by first wrapping 0.08mm PTFE tape around the main body of each window (about two layers thick) and placing a gasket over the small stepped section of each. The windows can now be inserted into the holders (stepped section first) and pushed firmly down until their faces are flush with the holder top. Another gasket is then placed around the edge of the window using silicon grease to hold it in place, and the whole assembly is placed on a hotplate to bring it up to the operating temperature of the engine, prior to insertion. Pre-heating the windows slows down the process of fouling of the windows by combustion deposits. When the windows and holders are at the correct temperature, they are inserted into the engine slice, and the window holder screws tightened (with care taken not to over tighten; hand tight plus 1/12th of a turn is recommended). Each

holder is marked to ensure it is inserted into the correct slice opening, with the correct orientation.

The laser may now be switched on by turning the key on the mains supply box and by pressing the laser button on the engine control panel. The engine is started and the beams checked to see that they pass through the engine and are reflected as near as possible onto the centre of the photodiodes (NEVER look directly into the beams as serious eye damage can be sustained, therefore the alignment of the beams must never be checked at eye level or by using a mirror). If the low intensity light comes on, and the windows are clean and the beams are not being interrupted by the piston or valves ,then strong absorption of the beams by the flame front must be occurring, in which case the intensity signal will probably give better results than the deviation signal. Monitoring of the detector signals (A&B), and the final trigger signals can be achieved by connecting an oscilloscope to the appropriate connections at the front of the main electronics box. By monitoring the detector signals (A&B) the height of the intensity (or deviation) signals can be seen, when these fall too low the windows will have become dirty and should be removed and cleaned.

The spark and laser beam trigger signals are fed direct to the HP1000 computer,where they start and stop their respective timers over the 300 cycles recorded for each test. The other variables: beam separation, distance from spark plug to beam 1 and beam alignment, are keyed in manually at the end of the BPIN routine used for

engine testing, mentioned previously. To obtain the laser beam data, the DREDS routine has to be run through as for a normal engine test (see section 2.6) with the PRINT LASER DATA option used at the end, which results in a printout of the times for the flame front to reach beams 1 & 2, the times taken for it to pass between the two beams, plus the average speeds in m /s for it to reach the two beams and pass between them for all 300 cycles, see figure 2.15. Further statistical analysis of the engine and laser data was carried by copying the data onto magnetic tape and transferring it to the University's UNIX mainframe computer, and using the Statistical Package for Social Scientists (SPSS).

CHAPTER 3

THEORY

3.1 COMBUSTION DATA ANALYSIS

3.1.1 INTRODUCTION

Combustion data available from the research engine include: pressure, temperature at inlet, flame propagation, and crank angle (and hence from a knowledge of engine geometry, volume). The flame Propagation is obtained as described in section 2.7 and is used in engine modelling ,see section 3.2, and as a means to determine engine and fuel performance.The pressure and temperature are obtained from a pressure transducer and thermocouple, respectively, set into the cylinder head, with the crank angle (volume) measurements read from a shaft encoder connected to the crank shaft, this also provides a top dead centre (TDC) signal.

The analysis of engine pressure diagrams is important for spark ignition engines. Firstly the original combustion pressure diagrams, see figure 3.1, yield values for parameters such as the maximum rate of pressure rise, and the peak cycle pressure - together with the respective crank angles at which those events occurred,and the indicated mean effective pressure (imep) value for each cycle. Secondly, the normalized

pressure diagrams, see figure 3.2, which form the basis for generating burn-time diagrams, see figure 1.4, which are a convenient way of presenting the results since they show the effects of cyclic dispersion on the initial rate of combustion and on the subsequent combustion processes. Combustion data from different fuels can also be analysed to investigate the differences in burn rate, Rassweiler and Withrow (1938), Stone and Green-Armytage (1987), Dye (1985).

The generation of burn-time diagrams has been achieved by using the method based on work done by Rassweiler and Withrow (1938), described in section 3.1.2 below.

3.1.2 RASSWEILER AND WITHROW METHOD

The burn-time diagrams are produced from normalized pressure diagrams, as mentioned above, assuming that the mass fraction burnt is in proportion to the fraction of total pressure rise due to combustion. These are constructed from incremental elements of pressure rise calculated at constant volume (usually the total combustion chamber volume at top dead centre "Vtdc" is used) and due to combustion only, independant of piston motion and associated with time increments throughout combustion. This is achieved by assuming that the expansion and compression processes can be treated as a polytropic process in which:

$$PV^k = \text{Constant}$$

where P is the pressure, V the volume, and k the polytropic constant, this is the slope of a graph of combustion chamber volume against pressure at that volume, plotted logarithmically. For the analysis carried out at BP, a single averaged value of k is used, that has been evaluated from the compression process prior to the occurrence of the ignition spark. Alteratively, the spark can be suppressed and the polytropic constant can be evaluated over a longer period.

To construct the normalized pressure diagram the pressure card is first split up into incremental elements of pressure rise, as mentioned above, with each of these increments being equal to 1.0 crank angle degree, see figure 3.3, it is then necessary to find the pressure rise due to piston motion. This is done using the equation:

$$Pp = P_1 \left(V_1 / V_2 \right)^k - P_1$$

where Pp is the pressure rise due to piston motion, P_1 is the initial pressure at volume V_1 at the beginning of the increment, and V_2 is the volume of the combustion chamber at the end of the increment.

The pressure rise due to combustion is obtained by subtracting the pressure rise due to piston motion from the total pressure rise over the increment:

$$Pc = \left(P_2 - P_1 \right) - Pp$$

where Pc is the pressure rise due to combustion, and P_2 is the pressure at the end of the increment.

The pressure rise due to combustion as calculated above then has to be normalized to eliminate the effects of volume change due to piston motion. This is achieved by determining what the pressure rise would have been if it had occurred at a constant volume, the volume used is that at top dead centre:

$$Pcn = Pc \cdot (V_2 / Vtdc)$$

where Pcn is the normalized combustion pressure, and Vtdc is the combustion chamber volume at top dead centre. This procedure is then repeated for all the pressure increments to produce the normalized pressure diagram.

To construct the burn-time diagram, the normalized pressure due to combustion for each increment, is found as a percentage of the total normalized pressure rise due to combustion for the whole combustion event, assuming complete combustion, this is then assumed to be equal to the mass fraction burnt. This is repeated for all the normalized pressure increments to produce the diagram.

The assumption, that the mass fraction burnt is proportional to the percentage of the total normalized pressure rise due to combustion, may not be valid because:

a. The total number of species present is varying during combustion.

b. The significance of dissociation varies during combustion, and this influences the energy released per unit mass of fuel burnt and the number of species present at any instant. The assumption that the polytropic constant (k) is constant throughout the combustion event is also not valid because:

(i) The increased heat transfer, as a consequence of the higher temperatures during combustion, will tend to lower the value of k while the pressure is rising and increase the value of k while the pressure is falling.

(ii) The specific heat capacity of the gases will be a function of both the temperature and the varying composition; if the ratio of the specific heat capacities changes then k will also change, Stone and Green-Armytage (1987).

3.2 TURBULENT COMBUSTION MODEL

3.2.1 INTRODUCTION

The reason for developing a phenomenological turbulent combustion model, is to see if it can be used for explaining some of the experimental observations, such as the way ignition timing affects:

(a) The burn times for 0-10%, 0-50%, and 0-90% mass fraction burned.

(b) Cycle by cycle variations in combustion.

The effect that cycle by cycle variations in the mean flow within the combustion chamber, might have upon cycle by cycle variations in combustion, is discussed later in section 3.2.4.

The combustion in a homogeneous charge spark ignition engine is commonly divided into three parts:

(a) **An initial laminar burn**, before the flame kernel is large enough to be influenced by turbulence; this can be considered as corresponding to the first 1% mass fraction burned.

(b) **Turbulent burning**, with a comparatively wide flame front, and pockets of unburned mixture entrained behind the flame front.

(c) **A final burn period**, ("termination period" or "burn-up"), in which the mixture within the thermal boundary layer is burned at a low rate, due to a reduced fluid motion and a lower temperature.

Many different workers have published phenomenological combustion models, including: Keck (1982); Berreta, Rashidi, and Keck (1983); Keck, Heywood, and Noske (1987); Tabaczynski (1976); Tabaczynski, Ferguson, and Radhakrishnam (1977); Tabaczynski, Trinker, and Shannon

(1980); Borgnake (1984); Tomita and Hamamoto (1988); and James (1990).

An overview of much of this work is provided by Heywood (1988), whilst James (1990) provides an overview of his own work, and a discussion of the thin flame and spherical flame front assumptions.

For the majority of cases, the combustion chamber will have a complex geometric shape, in which it will be necessary to define: the enflamed volume, the flame fr nt area, and the area wetted by the enflamed volume. Tw different approaches to this problem are provided by Poulos and Heywood (1987) and Cuttler, Girgis, and Wright (1987). Poulos and Heywood divide the combustion chamber surface into a series of triangular elements, and then check for interception by vectors, of random direction, radiating from the spark plug. Cuttler et. al. fill the combustion with tetrahedra, and employ vector algebra.

However for the purpose of this model, these complications are avoided, since the Ricardo E6 combustion chamber can be treated as a simple disc. Although there are small cavities associated with the: spark plug, pressure transducer and optical windows, these represent only about 2 of the swept volume. Since the standard assumption of a spherical flame front is subject to question (James (1990), it is contended here that modelling the combustion chamber with a disc is not unreasonable. The analytical expressions that define the intersection of a sphere with a disc can be

integrated numerically, to give: the enflamed volume, the flame front area, and the wetted area.

Since the greatest fraction of the charge is burned by turbulent combustion, this will be discussed first.

3.2.2 ENTRAINMENT MODEL FOR TURBULENT COMBUSTION

Before a model for turbulent combustion can be properly constructed it is necessary to assume a specific turbulence structure exists in the combustion chamber. The majority of the turbulence in the cylinder is created during the induction process by the jet like fl w that emerges from the inlet valve. Figure 3.4 sh ws how the shear between the jet and the cylinder contents leads to eddies. The largest eddies are limited by the cylinder boundaries at one extreme, and at the ther by molecular diffusion. These large eddies are unstable and break down into a cascade of smaller eddies.

The characteristic size of these large eddies is defined by the integral length scale, L. Figure 3.5 shows the internal structure of a single turbulent eddy of integral scale.

The Kolmogorov scale (η) defines the dissipation length scale and is assumed to characterize the thickness of the spaghetti-like vortex tubes, with the spacing of the vortex tubes given by the Taylor microscale λ.

The turbulent combustion models used by Keck and co-workers and Tabaczynski and co-workers both seem capable of giving good predictions of turbulent combustion. Since the information published by Tabaczynski and co-workers was more explicit (notably Tabaczynski et. al. (1977) and (1980)), their model has been adopted for this work.

In this model chemical reactions on the Kolmogorov scale is assumed to be instantaneous with the flame assumed to spread by a turbulent entrainment process, with burning occurring in the entrained region at a rate controlled by turbulence parameters. The flame front is assumed to entrain the mixture (ie. spread into the unburned mixture) at a rate that is governed by the turbulence intensity and the local laminar burn speed. The rate at which the mass is entrained into the flame front is given by:

$$\frac{dm_e}{dt} = \rho_u A_f (u' + S_L) \qquad (3.1)$$

where:

m_e = mass entrained into the flame front.

ρ_u = density of the unburned charge.

A_f = flame front area (excluding area in contact with surfaces).

u' = turbulence intensity.

S_L = laminar flame speed.

The turbulence intensity is assumed to be proportional to the mean piston speed. The rate at which the mixture is burned, is assumed to be proportional to the mass of unburned mixture behind the flame front:

$$\frac{dm_b}{dt} = \frac{m_e - m_b}{\tau} \qquad (3.2)$$

where:

m_b = mass burned behind the flame front.

τ = characteristic burn time for an eddy of size λ

λ = the Taylor microscale, that characterizes the eddy spacing.

Since the eddies are assumed to be burned up by laminar flame propagation:

$$\tau = \frac{\lambda}{S_L} \qquad (3.3)$$

This model assumes isotropic and homogenous turbulence throughout the combustion chamber at the time of ignition, with the integral length scale (L_1) at this point assumed to be proportional to the combustion chamber height, Ferguson (1986)

$$L_1 = \frac{0.5\ C_1\ b^2\ h}{b^2 + 2bh} \qquad (3.4)$$

where h = combustion chamber height.

b = combustion chamber bore.

C_1= constant specific to the engine.

and the turbulence intensity (u'_i) calculated from an empirical calculation derived from results obtained by Lancaster (1976).

$$u'_i = 1.26 \left(\frac{\theta_{ig} - \Delta\theta}{\theta_f - \Delta\theta} \right) + 1.30 \qquad (3.5)$$

where θ_g- ignition timing (deg. btdc).

$\Delta\theta$ ignition timing increment (deg.CA).

θ_f- final ignition timing (deg.btdc).

After ignition the integral scale (L) and the turbulence intensity (u') are assumed to be governed by the c nservation of the moment of momentum for coherent eddies.

Thus $$L = L_i \left(\frac{\rho_{ui}}{\rho_u} \right)^{.333} \qquad (3.6)$$

and $$u' = u'_i \left(\frac{\rho_u}{\rho_{ui}} \right)^{.333} \qquad (3.7)$$

For isotropic turbulence:

$$\lambda = \sqrt{\frac{15\ \gamma\ L}{u'}} \qquad (3.8)$$

where:

γ = kinematic viscosity.

By using equations 3.4, 3.5, and 3.6, the eddy burn-up term can be calculated at each time step (equation 3.3). However, this pre-supposes a knowledge of the kinematic viscosity, and the burned and unburned mixture density.

The mass within the combustion chamber (m) can be assumed constant, and this means that the only unknown is the ratio of unburned to burned gas density.

$$m = \rho\ V_0 = \rho_u V_u + \rho_b V_b$$

$$\text{let } D = \frac{\rho_u}{\rho_b}$$

$$\rho_u = \frac{\rho\ V_0}{V - V_b + \frac{V_b}{D}} \qquad (3.9)$$

where:

V = volume.

V_u = volume of unburned mixture.

V_b = volume of burned mixture.

V_0 = volume at ignition.

ρ_0 = unburned mixture density at ignition.

$$mfb = \frac{mb}{m} = \frac{\rho_b V_b}{\rho_0 V_0}$$

where:

mfb = mass fraction burnt

mb = mass burnt

To find V_b:

$$V_b = \frac{mb}{m} \cdot \frac{\rho_0 V_0 D}{\rho_u} \qquad (3.10)$$

Heyw od (1988, p392) acknowledges that the density ratio (D) is a function of the equivalence ratio, the burned gas temperature and pressure, and the level of exhaust residuals in the unburned mixture, but suggests that the value of D≈4 is acceptable for most spark igniti n engine operating conditions. A function could easily be added to the program at a later date to calculate the density ratio more accurately.

A p lytropic process can be used to describe the compression of the unburned mixture (with a user supplied value f the polytropic index). Thus:

$$P \quad P\left(\frac{\rho_u}{\rho_0}\right)^k \qquad (3.11)$$

and $$T_u = \frac{P\ \rho_0\ T_0}{P_0\ \rho_u} \qquad (3.12)$$

where . T_0 = temperature of (unburned) mixture at ignition.

The kinematic viscosity can be calculated from a correlation summarized by Reid et. al. (1977).

$$[(\gamma-\gamma^\circ)\xi+1]^{0.25} = 1.023 + 0.22364\rho_r + 0.5853\rho_r^2 - 0.40758\rho_r^3 + 0.093324\rho_r^4 \qquad (3.13)$$

where: γ = kinematic viscosity.

γ° low pressure gas viscosity = 180μP

ρ_r reduced gas density

$-\frac{PT_c}{T_uP}$ where T_c=critical temperature =132.5K

P_c=critical pressure = 37.6 bar

ξ $\frac{T_c^{1/6}}{M^{1/2}\ P_c^{2/3}}$ where M = molecular weight.

It is also possible to estimate the burned gas temperature (a consequence of assuming D=4):

$$T_b = \frac{P\ V_b\ T_0}{P_0\ V_0\ k_n\ mfb} \qquad (3.14)$$

substituting from 3.8 and 3.10

$$T_b = \frac{D\ P\ \rho_0\ T_0}{P_0\ \rho_u\ k_n} = \frac{D\ T_u}{k_n} \qquad (3.15)$$

where:

k_n = ratio of number of kmols of products to reactants

The final burn period, in which the mixture within the thermal boundary layer is burned is assumed to be an exponential decay and is calculated using the equation:

$$mb = mb(t_w)\ .\ e^{-(t-tw)/\tau b} \qquad (3.16)$$

where:

$mb(t_w)$ = mass burnt at the end of turbulent combustion.

t_w = Time at the end of turbulent combustion.

τ_b = Time constant for final burn.

3.2.3 LAMINAR BURNING VELOCITY

The laminar burning velocity is a function of: the equivalence ratio, pressure, initial temperature of the reactants, and exhaust residuals. The burning velocity can be represented as a parabolic function of equivalence ratio for many substances, and is given by:

$$S_{L,0} = B_m + B_\phi \left(\phi - \phi_m \right)^2 \qquad (3.17)$$

where:

$S_{L,0}$ - burning velocity at datum conditions (298K, 1atm)

B_m = maximum burning velocity occurring at $\phi = \phi_m$

B_ϕ = empirical constant

Values of: B_m, B_ϕ, and ϕ_m are presented in table 3.1 below.

Fuel	ϕ	B_m cm/s	B_ϕ cm/s
Methanol	0.98	41	-140.5
Is - ctane	1. 8	50.4	-84.7
T luene	1. 5	38.6	-205

Table 3.1: Parameters of ϕ_m, B_m and B_ϕ for equation (3.15), methanol and iso-octane data at 1atm and 297K, Gibbs and Calcote 1959, toluene data at the same conditions, Kanury 1975.

The data at higher temperatures and pressures can be fitted to a power law:

$$S_L = S_{L,0} \left(\frac{T_u}{T_0}\right)^{\alpha} \left(\frac{P}{P_0}\right)^{\beta} \qquad (3.18)$$

where:

$$\alpha = 2.18 - 0.8\ (\phi - 1)$$
$$\beta = -0.16 + 0.22\ (\phi - 1)$$

For gasoline, Rhodes and Keck (1985) propose:

$$\alpha_g \quad 2.4 - 0.271\ \phi^{3.15}$$
$$\beta_g - -0.357 + 0.14\ \phi^{2.7} \qquad (3.19)$$

Rhodes and Keck (1985) also found that the proportional reduction in burning velocity caused by the presence of residuals, was essentially independent of: equivalence ratio, pressure, and temperature. They developed the following correlation:

$$S_L(x_b) \quad S_L(x_b = 0)\ (1 - 2.06\ x_b^{0.77}) \qquad (3.20)$$

where x_b = mole fraction of burned gas diluent.

3.2.4 MODELLING OF CYCLE BY CYCLE VARIATIONS IN COMBUSTION

It has been hypothesized that cycle by cycle variation in combustion is caused by convection of the flame kernel during early stages of flame propagation. This changes the effective location of the spark and the rate of heat loss to the electrodes or to the neighbouring walls (see section 1.4). Figure 3.6 shows at typical flame shadow tracing of the flame at a crank angle of 10 deg. after the spark, this was obtained using high speed Schlieren photography in a square piston pre-mixed charge spark ignition engine at 1400rpm, Keck, Heywood and Noske (1987).

To model the effect that this movement has upon combustion the spark gap location was moved to the eight different positions shown in Figure 3.7. The difference between the measured value of the parameter of interest at each of the eight positions and that btained for the E6 position was calculated and an average taken, this was then divided by the E6 position value to obtain the percentage difference. A series of simulations was then carried out varying ignition timing, mixture strength and fuel type so a comparison could be made with the COV of the experimental results (see chapter 5).

CHAPTER 4

EXPERIMENTAL PROCEDURE

4.1 PRELIMINARY EXPERIMENTS

A singular set of preliminary tests was carried out to determine the optimum distance and orientation of the laser beams in relation to the spark plug. These tests are outlined in the table below with the results shown in figure 4.1.

Fuel:	Iso-octane
Ignition Timing:	MBT (26 deg.btdc)
Equivalence ratio:	1.0
Engine speed:	1500 rpm
C mpression ratio:	7.5
Fuel Temperature:	23 deg.C
Air Temperature:	29 deg.C
Atmos. pressure:	1.057 bar
Throttle position:	Wide Open Throttle (WOT)
Beam separation:	3.5 mm
Beam orientation:	Test 1 - vertical Test 2 - in line with spark plug axis.
Distance from plug gap to beam 1:	4.63, 4.74, 5.04, 5.52, 6.12, 6.81, 7.58, 9.24, and 10.12 mm

Table 4.1: Table showing the test carried out to determine laser setup parameters.

From the results it can be seen that very little difference is observed between the flame times for the two beam orientations. However the COV's produce quite different results, with the beams in the vertical orientation giving very little separation of the COV's for flame times to beams 1 and 2, but with the beams placed in line with the spark plug axis a distinct separation is observed with the flames times to beam 2 giving lower COV,s than those for beam 1. It was therefore concluded that using the beams in line with the spark plug axis would give better resolution between the COV's of the flame times.

The distance from the spark plug gap to beam 1 was set at 7.58mm. The closest that the equipment allowed the first beam to be to the spark gap was 4.63mm, due to the size and location of the optical windows. This was achieved using an extended reach spark plug (NGK BE529Y-11) that protruded 3mm into the combustion chamber. At this distance from the spark, the flame speed might still be influenced by the spark event and by the expansion rate of the gas within the flame kernel, and it has already been concluded that the flame front is fully developed by the time the flame radius has reached 10mm, (see section 1.4), so a mid point between these two values was chosen for the experiments.

4.2 CHANGES TO THE LASER SCHLIEREN SYSTEM

The major change to the laser schlieren system was to the beam splitter. It was found that one of the two

parallel beams produced by the splitter was of a significantly lower intensity than the other, which affected the resolution of the trigger signal produced. This was discovered to be due to the way the cubed beam splitter operated, see figure 4.2(a). The incident beam struck the side of the splitter at approximately 45 deg., was then refracted and struck the partially reflective coating running through the centre of the cube, the beam was split and the two beams emerge at the opposite side of the splitter parallel to each other.

The cube beam splitter is in fact designed to split a single beam of light, incident upon it at 90 deg., into two beams at right angles to each other, see figure 4.2(b), with the face of the splitter onto which the incident beam falls having an anti-reflective coating applied to it which gives minimum loss of light only if the beam is incident at 90 deg. and when used with a 45 deg. incident beam resulted in significant loss of light.

This problem was overcome by using the technique shown in figure 4.2(c), for producing the parallel beams. Here the incident beam strikes the anti-reflective coated face of the beam splitter at 90 deg. and then passes onto the partially reflective coated surface. Here it is split, with one beam carrying straight on out of the splitter, the other is reflected at 90 deg. onto a right angle prism, with a mirrored hypotenuse, and is reflected to emerge parallel to the original beam without any significant loss of intensity. This

arrangement also allows accurate control of the spacing between the beams by lateral movement of the prism parallel to the splitter.

4.3 EXPERIMENTAL

The three sets of tests carried out where:

1. WOT - no knock

2. WOT - with knock

3. Part Throttle

the experimental conditions for each set of tests are outlined in the table below.

1. WOT - no knock

Engine speed: 1500 rpm
Compression ratio: 7.5
Room temperature: 25°C.

Fuel	λ	Fuel temp. (°C)	Ignition timing span (°btdc)	atmos. pres. (bar)
Iso-octane	0.9	22	2 - 44	1.02
	1.0	22	2 - 44	1.02
	1.1	22	2 - 44	1.02

Methanol	0.9	23	2 - 32*	1.01
	1.0	23	2 - 40*	1.01
	1.1	23	2 - 44	1.01
Toluene	0.9	23	2 - 44	1.01
	1.0	23	2 - 44	1.01
	1.1	23	2 - 44	1.01

* Ignition advance limited by pre-ignition.

2. WOT - with knock

Engine speed: 1500 rpm,
Compression ratio: 8.5
Room temperature: 25°C.

Fuel	λ	Fuel temp. (°C)	Ignition timing span (°btdc)	atmos. pres. (bar)
Iso-octane	0.9	22	2 - 26*	1.02
	1.0	22	2 - 28*	1.02
	1.1	22	2 - 36*	1.02

* Ignition advance limited by knock intensity

3. Part Throttle

The throttle position was set to give half the torque value of iso-octane at WOT and MBT timing in test 1.

Engine speed: 1500 rpm
Compression ratio: 7.5
Room temperature: 25°C.

Fuel	λ	Fuel temp. (°C)	Ignition timing span (°btdc)	atmos. pres. (bar)
Iso-octane	0.9	20	2 - 44	1.02
	1.0	20	2 - 44	1.02
	1.1	20	2 - 48	1.02

Table 4.2: Table showing the experimental tests carried out.

CHAPTER 5

DISCUSSION OF RESULTS

5.1 THE RESPONSE OF VARIATIONS IN IMEP AND PEAK PRESSURE TO CHANGES IN IGNITION TIMING.

The average values of imep for the three fuels show the customary rise in value with increasing ignition advance, giving a maximum at MBT, then falling off after this point as the ignition timing is advanced further, see figure 5.1. Results for average peak pressure and average maximum rate of pressure rise, figures 5.2 and 5.3 show a steady rise in value with increasing ignition advance, with a slight levelling ut at the more advanced timings.

C mparison of the experimental results for imep, maximum pressure and maximum rate of pressure rise with th se predicted by the combustion model, shows that a very good correlation is observed for the maximum pressure and maximum rate of pressure rise data with not quite as good correlation for imep. At the more advanced ignition timings the model gives higher values for imep and maximum pressure than the experimental results. This is due to the model not making explicit allowance for the effect of dissociation of the fuel, so that the effect of dissociation is under estimated at advanced ignition timings.

It was concluded by Hancock et.al (1986), that cycle by cycle variation within a spark ignition engine could be characterized by the Coefficient Of Variation (COV) of peak pressure as opposed to the COV of other engine criteria, e.g imep. However, results obtained here show that the trends in cyclic variation are heavily dependant upon which criterion is chosen; for example , when the ignition timing is varied the COV of imep and COV of maximum pressure produce different results, see figures 5.4 and 5.5.

The COV of imep shows a steady fall as ignition timing is advanced reaching a minimum around MBT, with a slight increase after this point as the timing is advanced further. This is true for all three fuels at all three mixture strengths.

The combustion model predicts the steady fall in COV of imep but with no distinct minimum around MBT and very little increase at the more advanced timings. This is probably due to the model not accounting for the greater increase in cycle by cycle variations in the mean flow at these timings increasing the movement of the flame kernel around the spark plug gap.

With the weak mixture (lambda 1.1) the COV of maximum pressure, for toluene and iso-octane, shows a distinct fall in value at the most retarded ignition timing, then rises quite quickly as the timing is advanced to give a maximum at around 10 degrees before top dead centre (btdc), before decreasing gradually after this point as the timing is advanced still further, see

figure 5.5. This effect is also noted, albeit to a lesser extent, for toluene at lambda 1.0 . This is due to the ignition timing being so retarded for the initial run that the larger proportion of the peak pressures recorded over the 300 cycles are taken to be that due to piston motion and not combustion, this is only observed at the weak mixture strengths, and toluene at lambda 1.0 (due to the slower burn), since these give the lowest average peak pressures and imep's, see figures 5.1 and 5.2. Both methanol and iso-octane at the weak mixture setting, and all three fuels at a lambda of 0.9 just show a steady decrease in the COV of maximum pressure with advancing ignition timing.

This fall at the most retarded timings is much more evident f r the COV of maximum rate of pressure rise, figure 5.6, with all fuels at all mixture strengths exhibiting the trend, with the exception of methanol at lambda .9 since this gives the highest average maximum pressure and imep, eg. at 20 deg.btdc methanol gives an average imep of 9.37 bar whilst iso-octane and toluene give 9.13 and 9.14 respectively.

These results differ from those of such workers as: Warren and Hinkamp (1956), Karim (1967), and Hirao and Kim (1970) who noted minimum cyclic variations, in terms of the COV of peak pressure at MBT, although the latter noted that the effect of spark timing was influenced by both mixture strength and spark plug location.

The combustion model does not predict the initial fall in COV of maximum pressure for iso-octane and toluene at the weak mixture strengths but does successfully model the trends after this point as well as for the other results. It is shown however, for the modelled results of COV of maximum rate of pressure rise which shows very good correlation between experimental and modelled results.

Although the combustion model predicts the trends for the variation in COV for imep, maximum pressure, and maximum rate of pressure rise the actual values are a lot l wer. This is due to the fact that COV is modelled by m ving the point of ignition to eight points placed symmetrically around the actual position of the spark plug gap in the E6, and these remain constant for all the tests. In real life however, the flame kernel might be m ved to a greater or lesser extent than these values r in one direction more than another, dependant up n in cylinder engine conditions. This is also true f r the COV of burn and flame times.

5.2 THE RESPONSE OF VARIATIONS IN BURN TIMES AND FLAME TIMES TO CHANGES IN IGNITION TIMING

The 10-90% burn times show a steady decrease as ignition timing is advanced,and unlike the 0-10% burn times, there is no increase in the burn time at the more advanced ignition timings, see figures

5.7 and 5.8. This shows that the first 10% of the charge starts off burning quicker than the following 80% and finally ends up burning slower. The point where the two burn durations are the same (ie when both 0-10% and the 10-90% burn times are equal) falls within an ignition advance of 25-35 deg.btdc.

The initial 0-10% burn time is very dependant on the in-cylinder conditions at the point of ignition, the more retarded the ignition timing then the higher the temperature and pressure but the lower the turbulence intensity, Daneshyar and Fuller (1986). The effect of temperature and pressure on laminar burn rate for an iso-octane-air mixture at lambda 1.00 and 1.25 is shown in figure 5.9. Increasing the pressure, ie. retarding the ignition, reduces the burning velocity quite significantly at lower pressures (<10 bar) but at higher pressures (> 10 bar) it has very little effect, with temperature being the much more influential factor. Figure 5.10 sh ws the change in-cylinder pressure at the point of ignition, as the ignition timing is varied. It can be seen that the pressure varies between 4 and 11 bar as the ignition timing is varied fr m 2 to 45 deg.btdc. In other words, as the ignition timing is advanced the pressure decreases, the laminar burning velocity increases, and hence the burn times should decrease. This is observed for the 10-90% burn times and for the 0-10o burn times up to MBT timing. However, when the ignition timing is advanced beyond MBT, the 0-10% burn times increase again. This is due to the decreasing temperature having a greater effect on the flame kernel than the decrease in pressure and

increasing turbulence.

Thus the 0-10% burn time reaches a *minimum* when the in-cylinder conditions are optimum for enhanced burning of the fuel. This is the point of combustion phasing that produces a fast burning cycle, with the majority of the heat release occurring around top centre (TC) when the chamber volume is changing relatively slowly. Thus variations in the measured parameters are mainly due to combustion variations. Either side of this point, the in-cylinder conditions produce slower burning cycles where a significant fraction of the energy release occurs before or after TC, the effect of volume change als bec mes significant and augments the effect of combustion variations. Hence a fast burning combustion process significantly reduces the impact of cyclic combusti n variation *on* engine performance.

The cycle by cycle variation in the 10-90% burn time is much less affected by the turbulence in the cylinder, since by this point the flame kernel has grown beyond a critical size and the effects of turbulence are averaged across the enflamed region. The flame growth is much more influenced by the temperature, and therefore burns faster when the ignition timing is advanced, and the 10-90 burn time ends before TDC.

The 0-50$_0$ and 0-90% burn times, Figure 5.11 and 5.12, show quite a rapid initial fall, up to MBT ignition timing, but then level off or increase slightly at the more advanced ignition timing, due to the slowing of the 0-10% burn rate.

The average flame times to beam 1 and beam 2 are shown in figures 5.13 and 5.14. For iso-octane they show similar trends to the 0-10% burn times with respect to the increase in burn times after MBT, but before MBT timing there is very little change seen with the flame travel times falling only very slightly (or not at all). This is also the case for methanol at lambda 0.9. Toluene and methanol, at lambda 1.0 and 1.1, show a slight increase in flame travel times as ignition timing is advanced. With methanol at lambda 1.0 and toluene at lambda 0.9, there is a quite sharp initial increase in the flame travel times, but the times at the most retarded ignition timing (2 deg.btdc) are significantly faster than the others . Toluene at lambda 0.9 (and to lesser extent at 1.1) gives a much more erratic increase in flame travel times with increasing ignition timing. This was discernible during the testing as "rough" running, with unsteady power output during each run, and is much more apparent in the COV's of the flame times, see figures 5.23 and 5.24, and is probably due to the poorer combustion properties of toluene.

Of the three fuels tested, methanol has the fastest burning rate followed by iso-octane, with toluene being the slowest, as shown in the results for burn times and flame speeds. This is also the case for the laminar burning velocities, see figure 5.15, with comparison of the maximum laminar flame speeds giving a value for methanol of 50.4 cm/sec, iso-octane 41.0 cm/sec and toluene 38.6 cm/sec . From consideration of the

molecular structure of the fuels, see figure 5.16. It can be seen that methanol has a simple alcohol structure, iso-octane is a branch chain alkane, and toluene has an aromatic ring structure. Since the flame front propagates through the combustion chamber, by the creation of reactive radicals (particularly OH^{-}) in the unburnt fuel ahead of it, then the easier it is to create these radicals, and the faster the flame front will travel. Methanol, with its simple structure, will break down the most readily, followed by iso-octane. As toluene has a rigid ring structure, it is the most resistant to the chain breaking mechanisms, it will however quite readily lose a H atom from the CH_3 group giving the stable Benzyl radical which is known to hinder flame propagation.

The varying of the mixture strength has a much greater effect on the parameters measured than does the changing of the fuel type. This tends to suggest that alth ugh fuel structure plays a part in determining the rate of fuel combustion, it is much less important than the air-fuel ratio. This is shown by a comparison of figures 5.17 and 5.18, which show average 0-10% burn times for the three fuels displayed both on a fuel by fuel and lambda by lambda basis, comparison of the ther parameters in the same manner gives similar results.

It has been noted by a number of different workers, Kalghatgi (1985), Soltau (1960-61), Tromans (1982) that cyclic variations are reduced if the flame kernel reaches a critical size more quickly. This theory is

supported by the results obtained for the COV of imep, figure 5.4, and the average 0-10% burn times, figure 5.8. The average 0-10% burn times decrease to a minimum at around MBT, then increase again as the ignition timing is advanced further. This suggests that the cyclic variations should decrease up to MBT then increase again. This pattern is observed for the COV of imep, but not for the COV of peak pressure, suggesting that the COV of imep gives a more correct picture of changes in cyclic variation than the COV of peak pressure.

For all the fuels, the average burn and flame times, figures 5.7, 5.8, and 5.11 to 5.14, increase as the mixture strength decreases, whilst all the COV's for the burn times, figures 5.19-5.22, increase. This supports the hypothesis that for reduced cycle by cycle combustion variations, faster flame propagation is desirable.

The COV of flame times for methanol and iso-octane, figures 5.23 and 5.24, show very little change, staying at around 15-20%. The exceptions are some results for methanol at the most retarded and advanced ignition timings. At the most advanced timings, this was presumably due to the onset of pre-ignition caused by excessive heating of the spark plug electrode whilst at the retarded timings it is probably experimental error.

The reasons for a faster flame speed at a richer mixture setting are that more fuel molecules are present

in the chamber during combustion and hence more radicals are formed ahead of the flame front, and more significantly higher flame temperatures are achieved.

Comparison of modelled and experimental results for 0-10%, 0-50%, 0-90%, and flame times to beams 1 and 2 show very good correlation with the average data. The COV data all show the correct trends.

5.3 THE RESPONSE OF VARIATIONS IN IMEP, PEAK PRESSURE, BURN TIMES, AND FLAME TIMES TO CHANGES IN IGNITION TIMING WITH INCREASING KNOCK INTENSITY

In all cases the onset of knock , see figure 5.25 has no effect upon the averages of the measured parameters, figures 5.26 - 5.28, with the results obtained being almost identical to those for iso-octane without knock present, figures 5.1 to 5.3, 5.7, 5.8, and 5.11 to 5.14. This is as expected, since knock is caused by auto-ignition of the end gas ahead of the flame front and should not affect the early flame propagation. The only results that would possibly show any difference would be the 0-50 , 0-90% and 10-90% burn times, figure 5.27, which should decrease as percentage of knocking cycles increases. However since the burn times are decreasing in any case, due to combustion phasing, the effect of faster combustion due to knock appears to be a less significant factor. The average flame times, also give almost identical results for knocking and non-knocking cycles, compare figures 5.13, 5.14 with

5.28, except for the values at the more retarded ignition timing which show a sudden fall in value for the knock runs.

The results for the COV's of imep, maximum pressure and maximum rate of pressure rise for the runs with knock present, using iso-octane as fuel, figure 5.29, show very little difference to the results obtained for the same fuel but with no knock, figures 5.4 to 5.6. Some differences are to be found in the maximum pressure and the maximum rate of pressure rise at a lambda of 0.9 and ignition timing 2 deg.btdc, where a sudden increase in cycle by cycle variation is observed for the results with knock. This is due to the increase in the compression ratio (from 7.5 to 8.5), used to enable knock to be induced, enhancing combustion through higher temperatures. When this temperature effect is combined with the faster flame speed due to a richer mixture, then the maximum pressure and maximum rate of pressure rise detected, are due to combustion. In other words the higher maximum pressure and maximum rate of pressure rise are not just that to piston motion, as was the case for the other two mixture strengths, see section 5.1. Since very little knock is present at this retarded timing this is unlikely to have any effect, see figure 5.25.

The COV of burn times show very little difference between the non-knocking and knocking tests, compare figures 5.19 - 5.22 with 5.30.

The COV of flame times for the knocking results show similar trends to the non-knocking results except for the values at the most retarded ignition timing which show a significant increase, see figure 5.31. This is observed at all three mixture strengths and coincides with a sudden decrease in the average flame times, see figure 5.28. This is not observed for the average and COV burn times values for the knocking results, see figures 5.27 and 5.30, or for the flame times of the non-knocking iso-octane tests, see figures 5.13, 5.14, 5.23, and 5.24, and is due to errors in the flame speed measurements caused by the retarded ignition timing at the higher compression ratio.

5.4 THE RESPONSE OF IMEP, PEAK PRESSURE, BURN TIMES, AND FLAME TIMES TO CHANGES IN IGNITION TIMING AT PART THROTTLE.

The results for the average values of imep, maximum pressure, and maximum rate of pressure rise for the part throttle tests are shown in figure 5.32. These show identical trends to those at wide open throttle (WOT) for the same fuel (iso-octane), see figures 5.1 to 5.3, but with lower values. The value of MBT at part throttle is much higher, particularly at the weaker mixture strength, (45 deg.btdc as opposed to 22 deg.btdc at WOT).

The average 0-10%, 10-90%, 0-50%, and 0-90% burn times, figure 5.33 and 5.34, also show identical

trends to the WOT results (figures 5.7, 5.8 and 5.11 and 5.12) but with higher values, showing that combustion is slower at part throttle, eg. average 0-10% burn time, lambda 1.0, ignition timing 22 deg.btdc, the WOT result is 2.13 ms, whilst at part throttle it is 2.38 ms . This is due partly to the lower pressures during combustion but more significantly the lower temperatures both at ignition and during combustion within the chamber, caused by the reduction in charge inducted per cycle.

The slower combustion observed at part throttle, is also apparent in the results for the average flame times to beams 1 and 2, figure 5.35, when compared with the results obtained at WOT, figures 5.13 and 5.14, eg. beam 1, lambda 1.0, ignition timing 22 deg.btdc the WOT result is 1.2 ms whilst at part throttle it is 1.62 ms. It is also seen that varying the mixture strength has a significantly greater effect on the average flame times, particularly for lambda 0.9 and 1.1, at the part throttle setting. This is also the case for the average burn times, but not to any great extent for average imep, maximum pressure, and maximum rate of pressure rise.

The COV of imep, like the average values, show identical trends for the two throttle settings. However the part throttle tests, figure 5.36, give significantly higher results than those at WOT, figure 5.4, confirming the hypothesis that the faster the initial flame speed then the lower the COV. The effect of

residuals will also have a much greater effect at part throttle.

Comparison of the COV's of maximum pressure at part throttle, figure 5.36 and WOT, figure 5.5 is similar to that for imep, with the exception of results at very retarded ignition timing which give very much lower results at part throttle, especially at lambda 1.0 and 1.1. This is due to the vast majority of the peak pressures, for the 300 cycles, being due to piston motion and not combustion, see section 5.1.

The COV's of maximum rate of pressure rise are only slightly higher at part throttle, compared to the WOT results, eg. lambda 1.0, ignition timing 22 deg.btdc part throttle result is 26.64, figure 5.35, WOT result is 23.55, figure 5.6, although they are a lot more erratic.

The results for the COV's of 0-10% burn time show very little difference between part throttle, figure 5.37, and WOT, figure 5.19, at a lambda of 0.9, but the part throttle results give higher values for lambda 1.0 and 1.1 at the more retarded ignition timing, with the difference decreasing as ignition timing is advanced, this is illustrated in the table below.

Ignition Timing (deg.btdc)	Lambda	Part throttle (%)	WOT (%)
2	0.9	9.24	9.18
2	1.0	9.68	14.21
2	1.1	12.81	18.72
22	0.9	8.15	7.14
22	1.0	7.99	8.17
22	1.1	9.06	10.54

Table 5.1: Comparison of variation in COV of 0-10% burn times with ignition timing and mixture strength at WOT and part throttle.

A similar result is seen for the COV of 10-90%, 0-50%, and 0-90 burn times, with the exception of the lambda 1.1 part throttle results, see figure 5.37 and 5.38. These show an initial increase in COV at the more retarded ignition timings before falling off with further ignition advance, but with the values always significantly higher than those at WOT, see figure 5.18. This is in keeping with the larger increase in the average values for lambda 1.0 and 1.1 observed for the part throttle results compared with those at WOT..

The COV's of flame times to beam 1 and beam 2 show no difference between part throttle, figure 5.39, and WOT, figures 5.23 and 5.24. The average flame times, are however, significantly higher at part throttle, see

above, giving a slower burn rate, and hence the COV's should be higher for part throttle than for WOT.

As with the average values the COV's of burn times and flame times show greater variation with changes in mixture strength at part throttle than at WOT, but unlike the average values this is also reflected in the COV's of imep, maximum pressure, and maximum rate of pressure rise.

The modelled results for the average values show good correlation with the experimental data with the COV results all showing the correct trends. The over estimation of the average imep and maximum pressure by the combustion model at the more advanced ignition timings is reduced considerably at part throttle. This supports the theory that the over estimation is due to the model n t allowing fully for the effect of dissociation of the fuel since, it would be expected that dissociation w uld be less at the lower temperatures and pressures encountered at part throttle.

CHAPTER 6

CONCLUSIONS AND FUTURE WORK

6.1 SUMMARY

A series of tests has been carried out using three different fuels:

iso-octane, methanol, and toluene

with varying ignition timing:

2 - 44 deg. btdc

at three different equivalence ratios:

lambda 0.9 (rich), 1.0, and 1.1 (weak).

Tw sets of tests with iso-octane were carried out at W T with and without knock present. Tests were also c nducted at part load with iso-octane, again with varying ignition timing:

2 - 48 deg.btdc

and at three equivalence ratios:

lambda 0.9 (rich), 1.0, and 1.1 (weak).

A phenomenological combustion model has been developed that divides the combustion event into three phases:

(a) **An initial laminar burn,** before the flame kernel is large enough to be influenced by turbulence; this

can be considered as corresponding to the first 1% mass fraction burnt.

(b) **Turbulent burning**, with a comparatively wide flame front, and pockets of unburned mixture entrained behind the flame front. The greatest fraction of the charge is burnt during this phase.

(c) **A final burn period**, in which the mixture within the thermal boundary layer is burned at low rate, due to the reduced fluid motion and a lower temperature.

This has been used to:

(a). Predict turbulent combustion in the Ricardo E6.

(b). Model the experimental results and gain insights into cycle by cycle variations in combustion. The measured engine parameters were: imep, maximum pressure, maximum rate of pressure rise, early flame times and 0-10, 0-50, and 0-90% burn times.

6.2 CONCLUSIONS

The following conclusions can be drawn:

1. The variation in mixture strength has a far greater effect on the average and COV values of all the combustion performance parameters than does changing the fuel type, (see chapter 5).

2. Cycle by cycle variations in combustion are best characterized by the COV of imep and not the COV of maximum pressure, (see section 5.1).

3. The onset of knock has no discernible effect on the COV's of the measured parameters, (see section 5.3).

4. The part throttle results show higher COVs than at WOT due to the slower burn, supporting the theory that faster the initial flame speeds the lower the cyclic variations, (see section 5.4).

5. The combustion model was used to support the hypothesis that cycle by cycle variations in combustion are caused by movement of the flame kernel by turbulence within the combustion chamber, (see chapter 5).

6.3 FUTURE WORK

This concerns the further development of the combustion model:

1. Replace the empirical method of deducing the density ratio with a thermodynamic method.

2. Extend the model to make allowance for the greater dissociation of the fuel at the more advanced ignition timings.

3. Develop a relationship between distance and direction of flame kernel movement and the turbulence within the combustion chamber.

4. Obtain the laminar burning velocity of toluene for a range of equivalence ratios at standard temperature and pressure.

BIBLIOGRAPHY

1. **ABRAHAM, J.; FORMAN, A. AND BRACCO, F.V. 1985,** A Discussion of Turbulent Flame Structure in Pre-mixed Charges, SAE Paper No. 850354.

2. **ASTM STANDARDS, 1980,** Part 23 D130 - 80.

3. **ASTM SPECIAL TECHNICAL PUBLICATION. 1970,** Manual On the Use of Thermocouples in Temperature Measurement, ASTM Philadelphia.

4. **BARR,P.K. AND WITZE, P.O. 1988,** Some Limitations to the Spherical Flame Front Assumption Used in Phenomenological Engine Models, SAE Paper No. 880129.

5. **BENJAMIN, S.F.; HAYNES, C.D. AND TIDMARSH, D.H. 1986,** Lean Burn Engines for Low Exhaust Emissions, Pr c. Instn Mech. Engnrs, Vol. C320/86

6. **BENSON, R.S. AND WHITEHOUSE, N.D. 1979,** Internal C mbustion Engines, Permagon Press, 1979.

7. **BERETTA, G.P.; RASHIDI, M. AND KECK, J. 1983,** Turbulent Flame Pr pagation and Combustion in Spark Ignition Engines, C mbustion and Flame, Vol. 52, pp. 217-245.

8. **BORGNAKKE, C. 1984,** Flame Propagation and Heat Transfer Effects in a Spark Ignition Engines, Fuel Economy in Road Vehicles Powered by Spark Ignition Engines, Edited by Hilliard, J.C. and Springer, G.S., Plenum Press 1984.

9. **BORMAN, G.L. 1980,** Modelling Flame Propagation and Heat Release in Engines - An Introductory Overview, Combustion Modeling in Reciprocating Engines, Edited by Mattavi, J.J. and Amann, C.A. Plenum Press 1980.

10. **BRITISH STANDARDS 4040, 1988,** Leaded Petrol (Gasoline) For Motor Vehicles.

11. **COLLIS, D.C. AND WILLIAMS, M.J. 1959,** Two Dimensional Convection from Heated Wires at Low Reynolds Numbers, Fundamentals of Fluid Mechanics, Vol. 6, pp. 357-384, 1959

12. **CURRY, S. 1962,** Three Dimensional Study of Flame Pr pagation in a Spark Ignition Engine, SAE Paper N . 452B.

13. **CUTTLER, D.H. AND GIRGIS, N.S. 1988,** Photography f c mbustion During Knocking Cycles in Disc and C mpact Chambers, SAE Paper No. 880195.

14. **CUTTLER, D.H. ; GIRGIS, N.S. AND WRIGHT, C.C. 1987,** Reduction and Analysis of Combustion Data Using Linear and N n-linear Regression Techniques, Proc. Instn. Mech. Engnrs., Paper C17/87, pp. 219-230.

15. **DANESHYAR, H. AND FULLER, D.E. 1986,** Definition and Measurement of Turbulence Parameters in Reciprocating I.C. Engines, SAE Paper No. 861529.

16. **DOWNS, D, ; WALSH, A.D. AND WHEELER, R.W. 1951,** A Study of Reactions That Lead to Knock in a Spark Ignition Engine, Phil. Trans. of the Royal Society of London. Ser A, Vol 243, pp. 462.

17. **DYE , A. 1985,** New Approach to Combustion Analysis, Automotive Engineer, Feb/Mar, pp. 32-35, 1985.

18. **FERGUSON, C.R. 1986,** Internal Combustion Engines, Applied Thermosciences, Wiley, New York.

19. **GAYDON, A.G. AND WOLFHARD, H.G. 1979,** Flames; Their Structure, Radiation and Temperature, 4th Edition, Chapman and Hall, London.

20. **GIBBS, G.J. AND CALCOTE, H.F. 1959,** Effect of Molecular Structure on Burning Velocity, Journal of Chemical and Engineering Data, Vol 4, No.3, pp 226-237, July 1959.

21. **GOLDSTEIN, R.F. AND WADDAMS, A.L. 1967,** The Petroleum Chemicals Industry, 3rd Edition, E. and F. Sp n Ltd, London.

22. **GOODGER, E.M. 1975,** Hydrocarbon Fuels, The Macmillan Press Ltd., London.

23. **GOODGER, E.M. 1980,** Alternative Fuels - Chemical Energy Resources, The Macmillan Press Ltd, London.

24. **GREEN,R.M.; PARKER, C.D.; PITZ, W.J. AND WESTBROOK, C.K. 1987,** The Autoignition of Iso-butane in a Spark Ignition Engine, SAE Paper No. 870169.

25. **HALL, J.A. 1966,** The Measurement of Temperature, Chapman and Hall Ltd.

26. **HANCOCK, E . G. 1985,** The Technology of Gasoline, Blackwell Scientific Publications.

27. **HANCOCK, M.S.; BUCKINGHAM, D.J. AND BELMONT M.R. 1986,** The Influence of Arc Parameters on Combustion in a Spark Ignition Engine, SAE Paper No. 860321.

28. **HEYWOOD, J.B. 1980,** Engine Combustion Modeling - An Overview, Combustion Modeling in Reciprocating Engines, Edited by Mattavi, J.N. and Amann C.A, Plenum Press.

29. **HEYWOOD, J.B. 1988,** Internal Combustion Engine Fundamentals, McGraw-Hill.

30. **HEYWOOD, J.B. AND VILCHIS, F.R. 1984,** Comparison of Flame *Development* in a Spark Ignition Engine Fueled with Propane and Hydrogen, Comb. Sci. and Tech., Vol 38, pp. 313-324.

31. **HIRO, O. AND KIM, Y. 1970,** Combustion Variation Analysis on Flame Propagation in Four Cycle Gas line Engines, Special Issue of JARI Technical Mem randum: Intermediate Reports of Combustion and Emission Researches, pp. 30-42, Japan Automobile Research Institute, Inc., March 1970.

32. **HIRES, S.D.; TABACYNSKI, R.J. AND NOVAK, J.M. 1978,** The Prediction of Ignition Delay and Combustion Intervals for a Homogeneous Charge, Spark Ignition Engine, SAE Paper No. 780232.

33. **HOLDER, D.W. AND NORTH, R.J. 1963,** Schlieren Methods, Department of Scientific and Industrial Research - National Physical Laboratory, Her Majesty's Stationary Office, London.

34. **IWASHITA, Y. AND SAITO, A. 1983,** Observations of Knock Using a High Speed Shutter TV Camera System, SAE Paper No. 831696.

35. **JAMES, E.H. 1987,** Laminar Burning Velocities of Iso-octane Air Mixtures - A Literature Review, SAE Paper No. 870170.

36. **JAMES, E.H. 1990,** Further Aspects of Combustion Modelling in Spark Ignition Engines, SAE Paper No. 900684.

37. **JOHNSON, E.W. 1986,** The Importance of Diesel and Gasoline Fuel Quality Now and in the Future, Proc. Instn. Mech Engnrs, 1986-11, pp. 17.

38. **KALGHATGI, G.T. 1987[1],** Improvements in Early Flame Development in a Spark Ignition Engine Brought About by "Spark Aider" Fuel Additives, Comb. Sci. Tech. , 1987, Vol. 52, pp. 427-446.

39. **KALGHATGI, G.T. 1985,** Early Flame Development in a Spark Ignition Engine, Combustion and Flame, Vol. 60, pp. 299-308.

4 . **KALGHATGI, G.T. 1987,** Spark Ignition, Early Flame Development and Cyclic Variation in Internal C mbustion Engines, SAE Paper No. 870163.

41. **KALGHATGI, G.T. AND SWORDS, D. 1983,** Flame Speed Measurements in an Internal Combustion Engine, Combustion and Flame, 1983, Vol. 49, pp. 163-169.

42. **KANURY, A.M. 1975,** Introduction to Combustion Phenomena, Table 4.3, Gordon and Breach Science Publishers, New York 1975.

43. **KARIM, G.A. 1967,** An Examination of the Nature of the Random Cyclic Pressure Variations in a Spark Ignition Engine, J. of the Institute of Petroleum, Vol. 53, No. 519, March 1967.

44. **KECK, J. 1982,** Turbulent Flame Structure and Speed in Spark Ignition Engines, 19th Int. Symp. on Combustion / The Combustion Institute 1982, pp. 1415-1466.

45. **KECK, J. ; HEYWOOD, J.B. AND NOSKE, G. 1987,** Early Flame Development and Burning Rates in Spark Ignition *Engines and Their* Cyclic Variability, SAE Paper No. 870164.

46. **LANCASTER, D.R. 1976,** Effects of Engine Variables on Turbulence in a Spark Ignition Engine, SAE Paper N . 760159.

47. **LANCASTER,D.R.; KRIEGER, R.B.; SORENSON, S.C. AND HULL, W.L. 1976,** Effects of Turbulence on Spark Ignition Engine Combustion, SAE Paper No. 760160.

48. **LEE, O.K. AND LIGHTFOOT, N.S.,** Conditional Measurements of Turbulent Burning Velocities in a Spark Ignition Engine, The American Society of Mechanical Engineers, Heat Transfer in Fire and Combustion Systems HTD-Vol.45 pp. 323-329.

49. **LEWIS B. AND VON ELBE, G. 1961,** Combustion, Flames and Explosions of Gases, 2nd Ed., Academic Press, New York, 1961

50. **LIEPMANN, H.W. AND ROSHKO, A. 1963,** Elements of Gas Dynamics, J.Wiley and Sons Inc., New York.

51. **LIGHTFOOT, N.S. AND NEGUS, C.R. 1984,** Investigation of the Knock Phenomenon in an Optically-accessed Engine, 20th Int. Symp. on Combustion 1984, Paper No. 12.

52. **LYON, D. 1986,** Knock and Cyclic Dispersion in a Spark Ignition Engine, Proc. Instn. Mech Engnrs., 1986-11, p.105.

53. **MALE, T.,** Photographs at 500,000 Frames per Second of Combustion and Detonation in a Reciprocating Engine, Combustion in Engines and Rockets, 3rd Symp. on Combustion, Flame and Explosion Phenomena, pp.721-726

54. **MALEY, R. AND ZIEGLER, G. 1981,** Theoretical and Experimental Investigation of the Knocking Process, Int. Symp. on Knocking of Combustion Engines, d-3180, Wolfsburg, Germany, 26/27 November 1981.

55. **MILLER, C.D. 1947,** Roles of Detonation Waves *and* Aut ignition in Spark Ignition Knock as Shown by Ph tographs Taken at 40,000 and 20,000 Frames Per Second, SAE Part. Trans. 1947, Vol.1 No.1.

56. **NAKAMURA, N.; OHNO, E.; KANAMARU, M. AND FUNAYAMA, F. 1988,** Control of Knock Improved, Automotive Engineer, Jan.1988, Vol.96, No.1, pp. 65-69.

57. **NACA REPORT 1300 1959,** Basic Considerations in the Combustion of Hydrocarbon Fuels with Air.

58. **PALMER, F.H. 1986,** Vehicle Performance of Gasoline Containing Oxygenates, Proc. Instn. Mech Engnrs., 1980-11, pp.33.

59. **POULOS, S.G. AND HEYWOOD, J.B. 1983,** The Effect of Chamber Geometry on Spark Ignition Engine Combustion, SAE Paper No. 830334.

60. **RASHIDI, M. 1980,** Measurements of Flame Velocity and Entrained Velocity from High Speed Photographs in the Spark Ignition Engine, Proc. Instn. Mech Engnrs., Vol.194, pp. 231-238.

61. **RASSWEILER, G.M. AND WITHROW, L. 1938,** Motion Pictures of Engine Flames Correlated with Pressure Cards, SAE Paper No. 800131, Originally presented 14th Jan. 1938.

62. **REID, R.C.; PRAUSNITZ, J.M. AND SHERWOOD, T.W. 1977,** The Properties of Gases and Liquids, 3rd Ed., New York Press, Mcgraw-Hill, 1977.

63. **RHODES, D.B. AND KECK, J.C. 1985,** Laminar Burning Speed Measurements of Indolene-Air-Diluent Mixtures at High Pressures and Temperatures, SAE Paper No. 850047.

64. **RICARDO, H.R. AND HEMPSON, J.G.G.,** The high Speed Internal Combustion Engine, 5th Edition, Blackie and Son, London.

65. **SOLTAU, J.P. 1960-61,** Cylinder Pressure Variations in Petrol Engines, Proc. Instn. Mech. Engrs. No.2, pp. 99-117, 1960-61.

66. **STONE, C.R. AND GREEN-ARMYTAGE, D.I. 1987,** Comparison of Methods for the Calculation of Mass Fraction Burnt from Engine Pressure-Time Diagrams, Proc. Instn. Mech Engnrs. 1987, Vol. 201, No. D1.

67. **SWORDS, M.D. ; KALGHATGI, G.T. AND WATTS, S. 1982,** An Experimental Study of Ignition and Flame Development in a Spark Ignition Engine, SAE Paper No. 821220.

68. **TABACZYNSKI, R.J. 1976,** Turbulence and Turbulent Combustion in Spark Ignition Engines, Prog. Energy Combust. Sci., Vol. 2, pp. 143-165, 1976.

69. **TABACZYNSKI, R.J. ; FERGUSON, C.R. AND RADHAKRISHNAN, K. 1977,** A Turbulent Entrainment Model for Spark Ignition Engine Combustion, SAE Paper No. 770647.

70. **TABACZYNSKI, R.J. ; *TRINKER, F.H.* AND SHANNON, B.A.S. 1980,** Further Refinement and Validation of a Turbulent Flame Propagation Model for Spark Igniti n Engines, Combustion and Flame, 1980, Vol. 39, pp. 111-121.

71. **TAKAGI, Y. ; ITOH, T. AND IIJIMA, T. 1988,** An Analytical Study on Knocking Heat Release and its Control in a Spark Ignition Engine, SAE Paper No. 880196.

72. **TOMITA, E. AND HAMAMOTO Y. 1988,** The Effect of Turbulence on Combustion in the Cylinder of a Spark Ignition Engine - Evaluation of an Entrainment Model, SAE Paper No. 880128.

73. **TROMANS, P.S. 1982,** The Interaction Between Strain Fields and Flames - A Possible Source of Combustion Variations in Spark Ignition Engines, ASME, Proc. Fluid Mechanics of Combustion Systems, 1982.

74. **VAN PASSEN, C.W.C. 1986,** Changing Refining Practice to Meet Gasoline and Diesel Demands and Specification Requirements, Proc. Instn. Mech. Engnrs., 1986-11, pp.25.

75. **WARREN, J.A. AND HINKAMP, J.B. 1956,** New Instrumentation for Engine Combustion Studies, SAE Transactions, Vol. 64, pp. 665-677, 1956.

76. **WITZE, P.O. 1982,** The Effect of Spark Location on Combustion in a Variable Swirl Engine, SAE Paper No. 820044.

77. **WITZE, P.O. ; MARTIN, J.K. AND BORNAKKE, C. 1984,** C nditionally-Sampled *Velocity and* Turbulence Measurements in a Spark Ignition Engine, Comb. Sci. and Tech., Vol. 36, pp. 301.

78. **WITZE, P.O. AND VILCHIS, F.R. 1981,** Stroboscopic Laser Shadowgraph Study of the Effect of Swirl on H mogeneous Combustion in a Spark Ignition Engine, SAE Paper No. 810226.

79. **ZAWADZKI, A. AND JAROSINSKI, J. 1983,** Laminarization of Flames in a Rotating Flow, Comb. Sci. and Tech., Vol. 35, pp. 1-13.

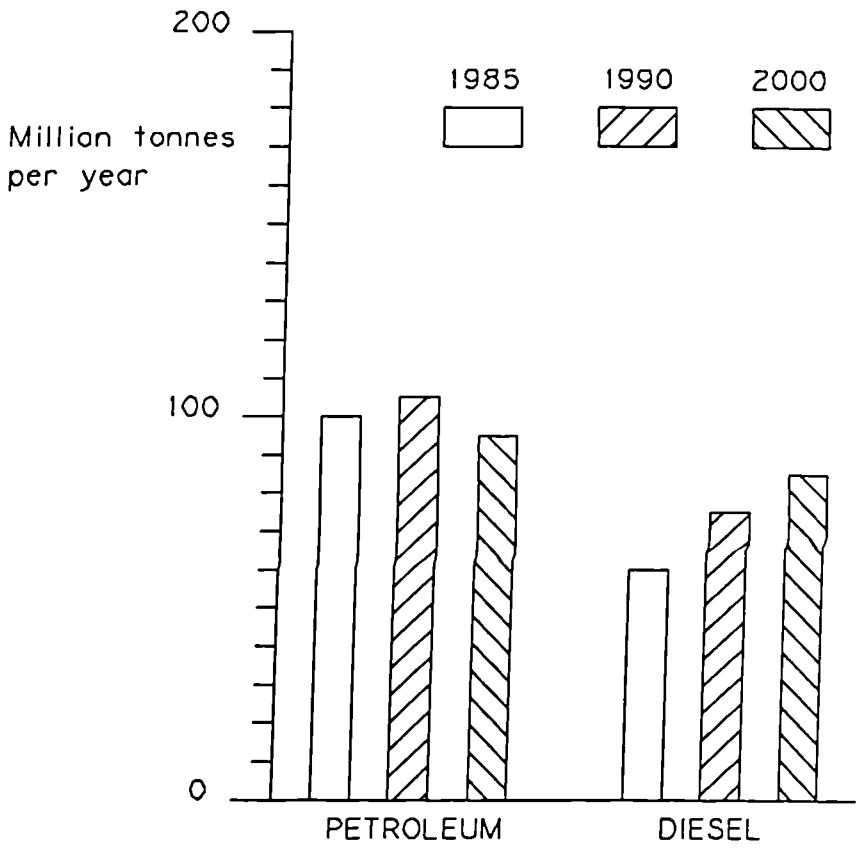

Figure 1.1: Expected European fuel demand, Johnson(1986).

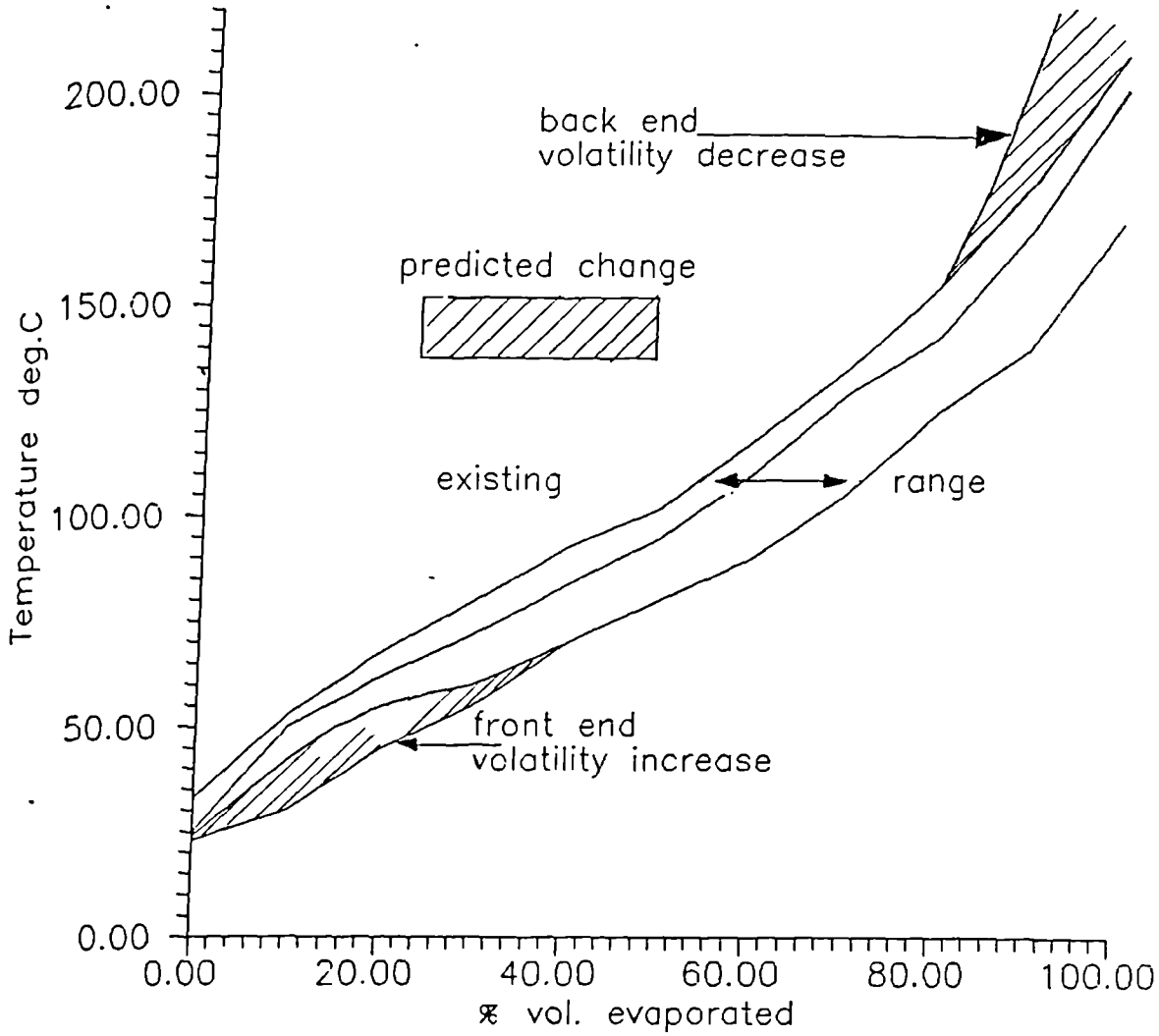

Figure 1.2: Distillation characteristics of gasoline and predicted changes, Johnson (1986).

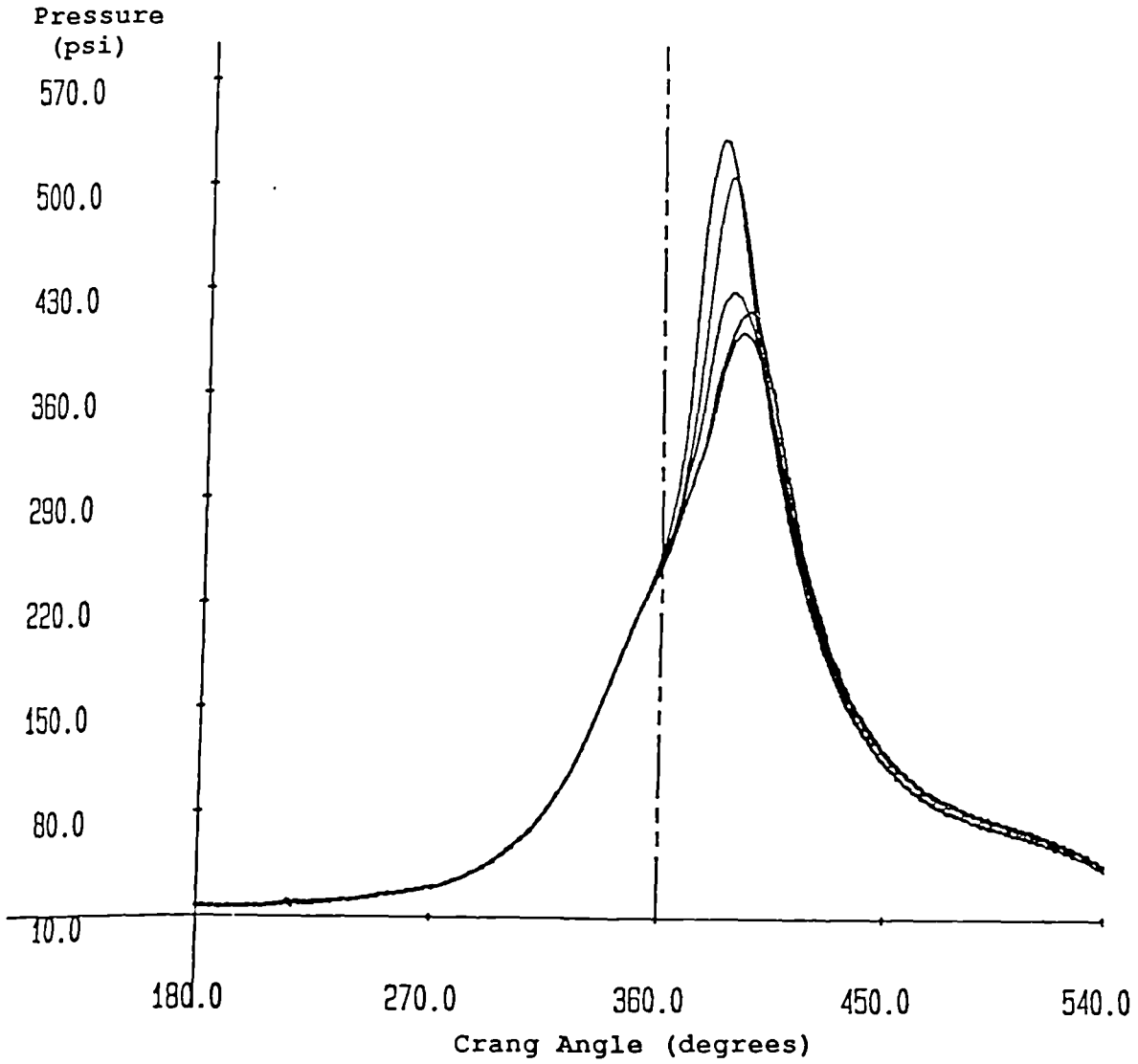

Figure 1.3: Pressure-Time diagram of pre-normalized pressure showing cyclic variation for five consecutive cycles, courtesy of BP research.

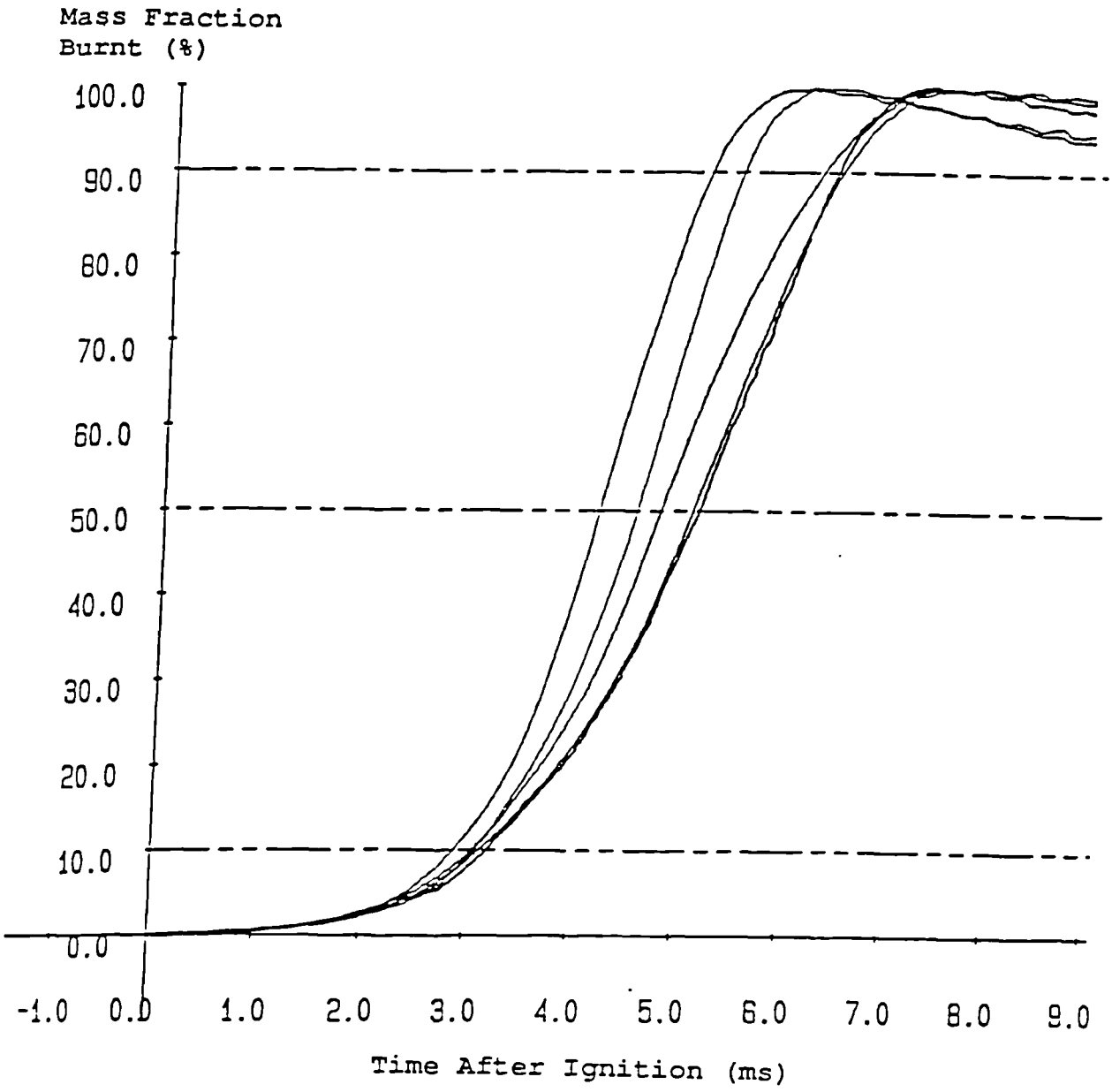

Figure 1.4: Mass fraction burnt as a function of time for five consecutive cycles, courtesy of BP research.

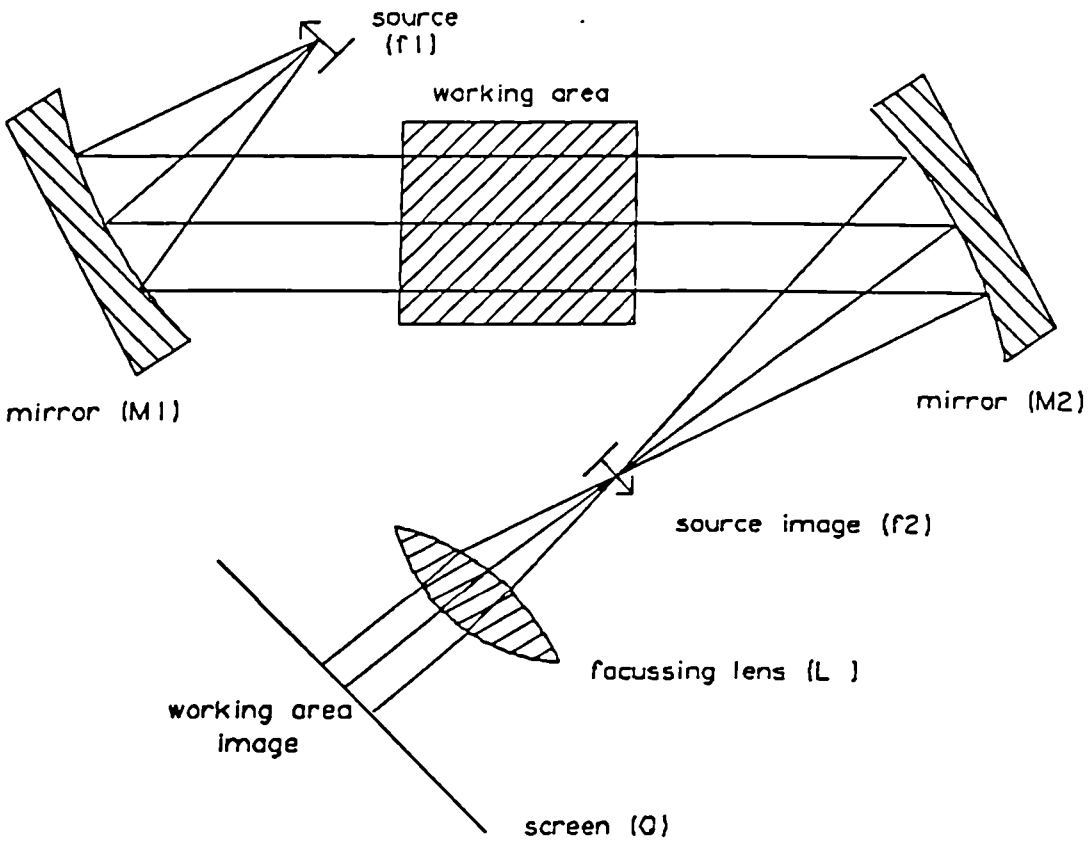

Figure 1.5: Arrangement of apparatus for schlieren photography, Holder and North (1963).

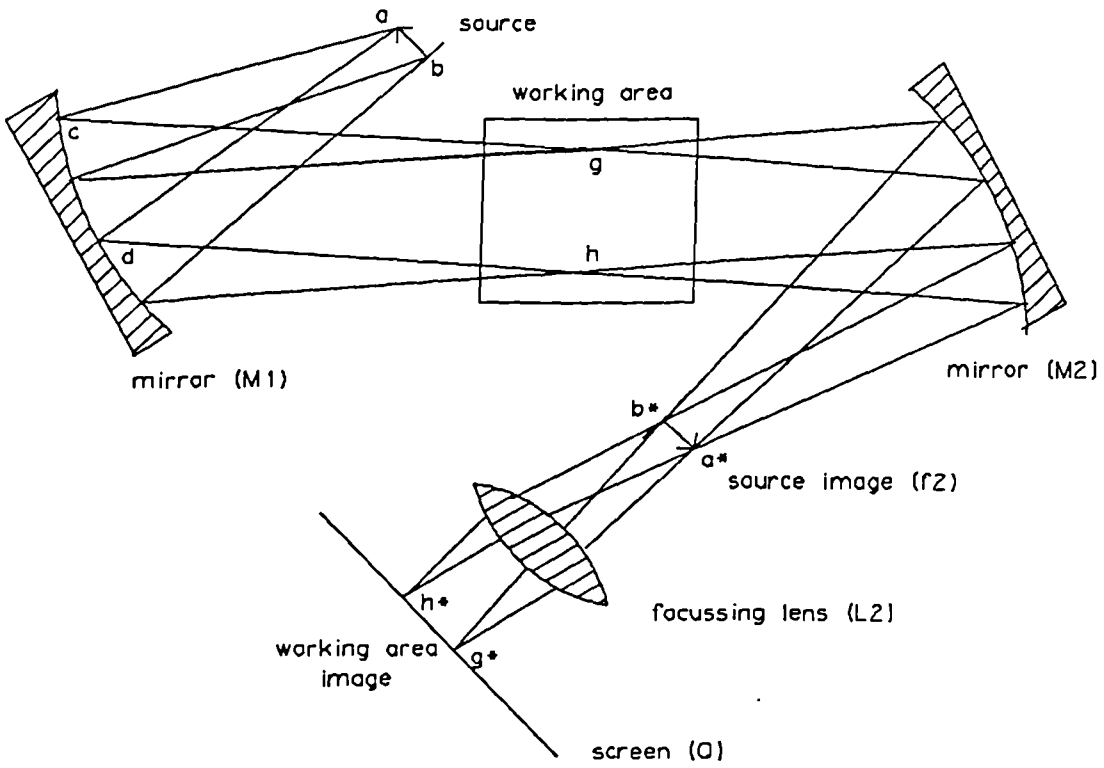

Figure 1.6: Arrangement of apparatus for schlieren photography, showing pencils of light, Holder and North (1963), Liepmann and Roshko (1963).

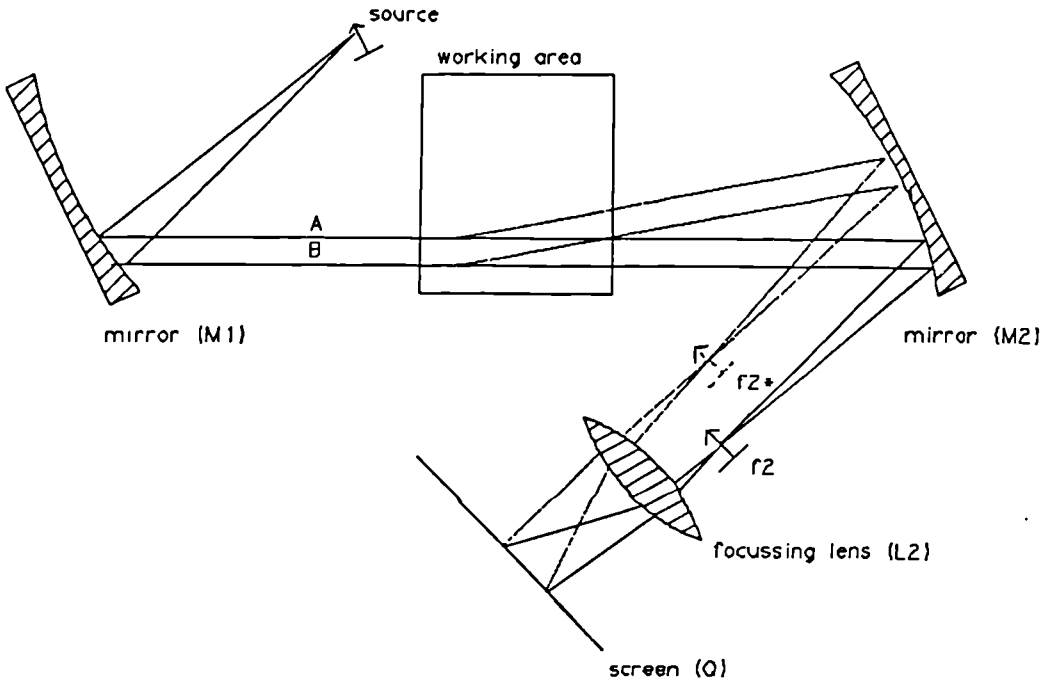

Figure 1.7: Effect of deflection of beams by a density gradient, (flow is perpendicular to paper), Holder and North (1963).

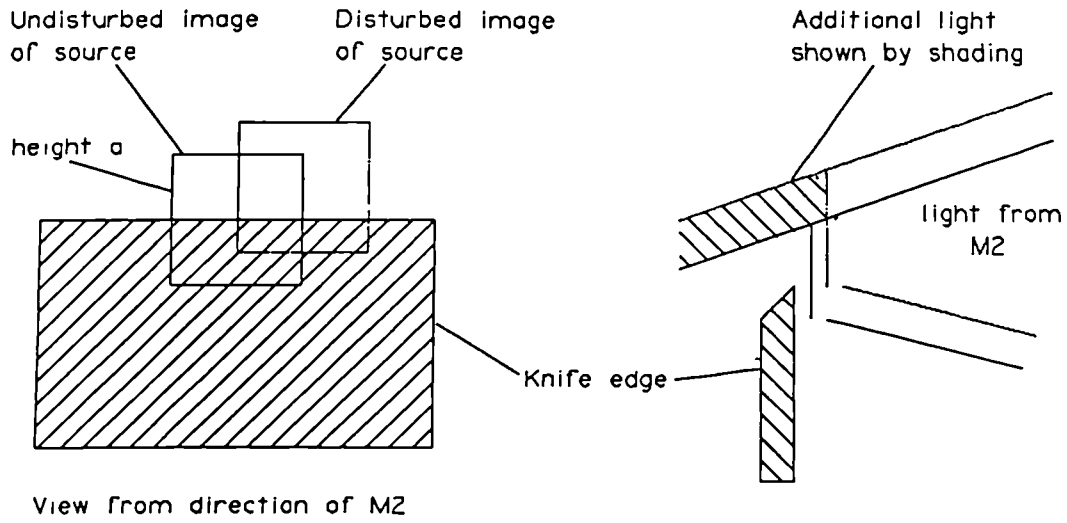

Figure 1.8: The arrangement of the knife edge, Holder and North (1963).

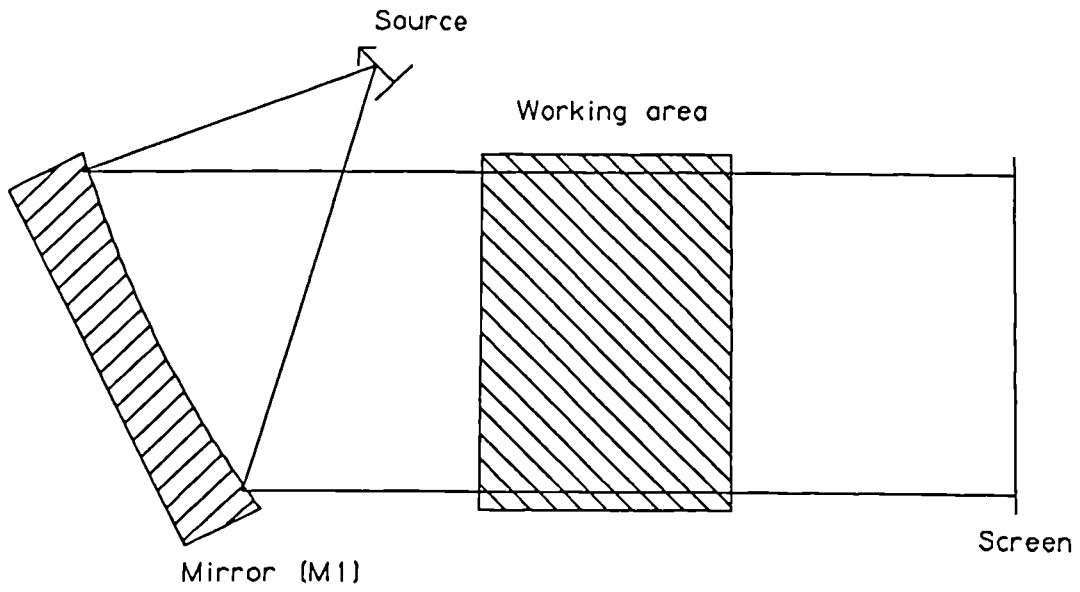

Figure 1.9: Arrangement of the apparatus for the direct shadow method, Holder and North (1962).

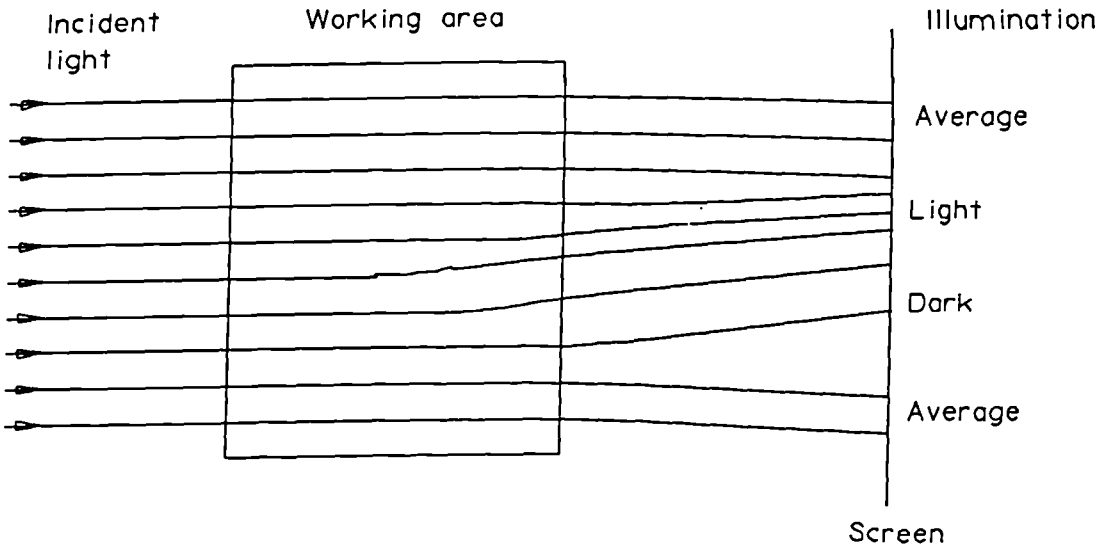

Figure 1.10: The shadow effect, Liepmann and Roshko (1963).

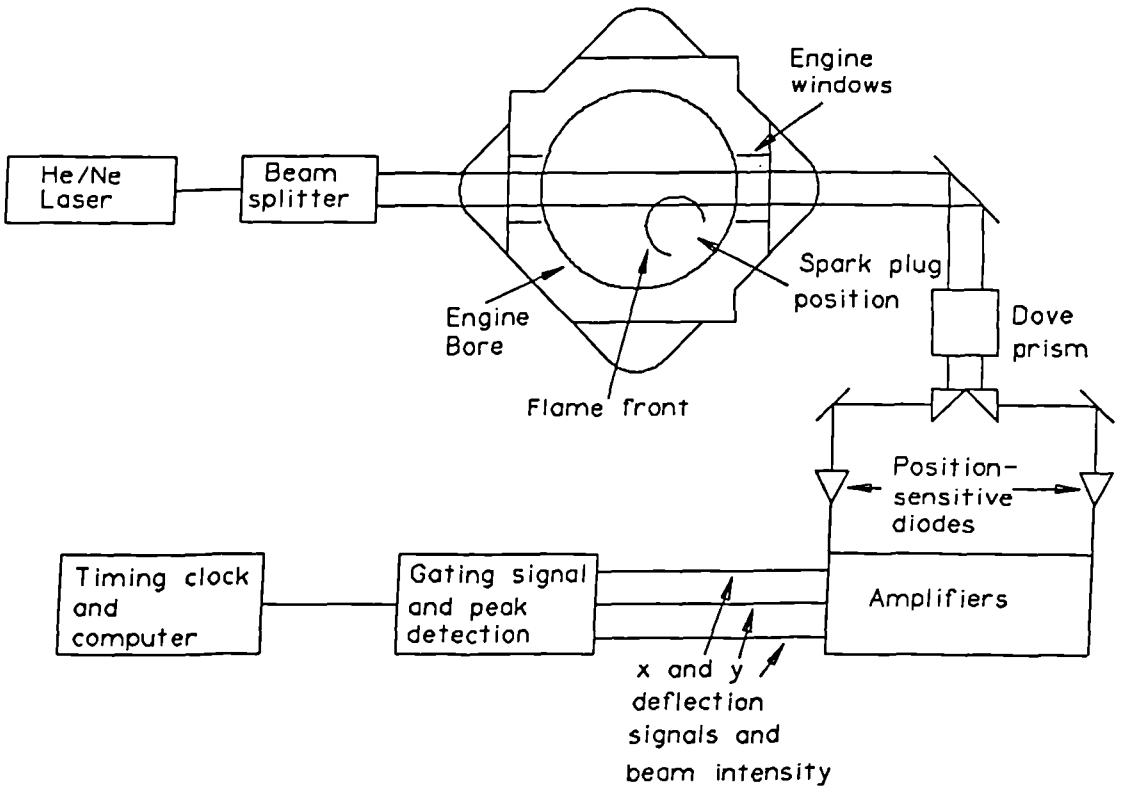

Figure 1.11: Beam deflection geometry and signal processing, Kalghatgi and Swords (1983).

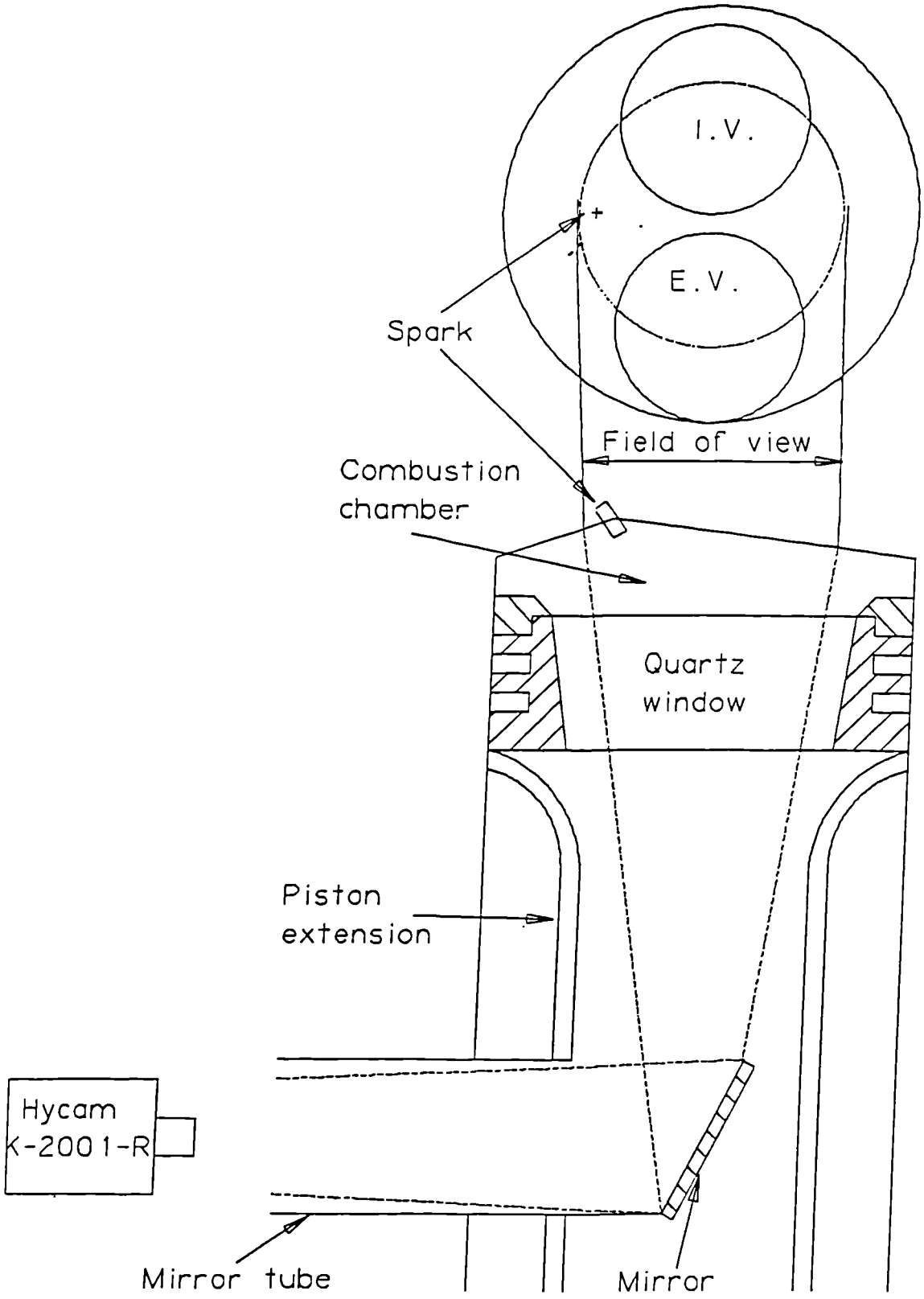

Figure 1.12: Schematic arrangement of the transparent piston engine, Rashidi (1980).

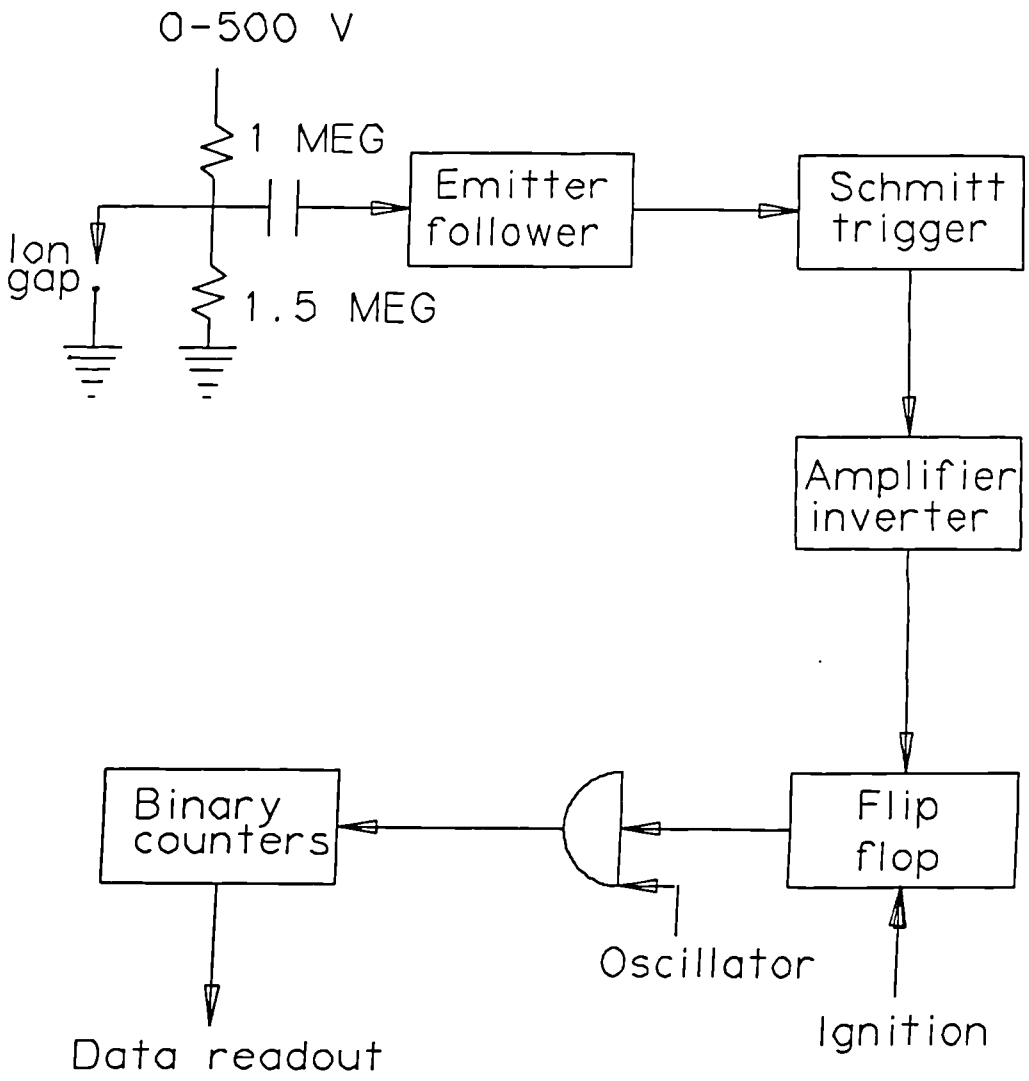

Figure 1.13: A schematic of one of the 28 data collection channels, Curry (1982).

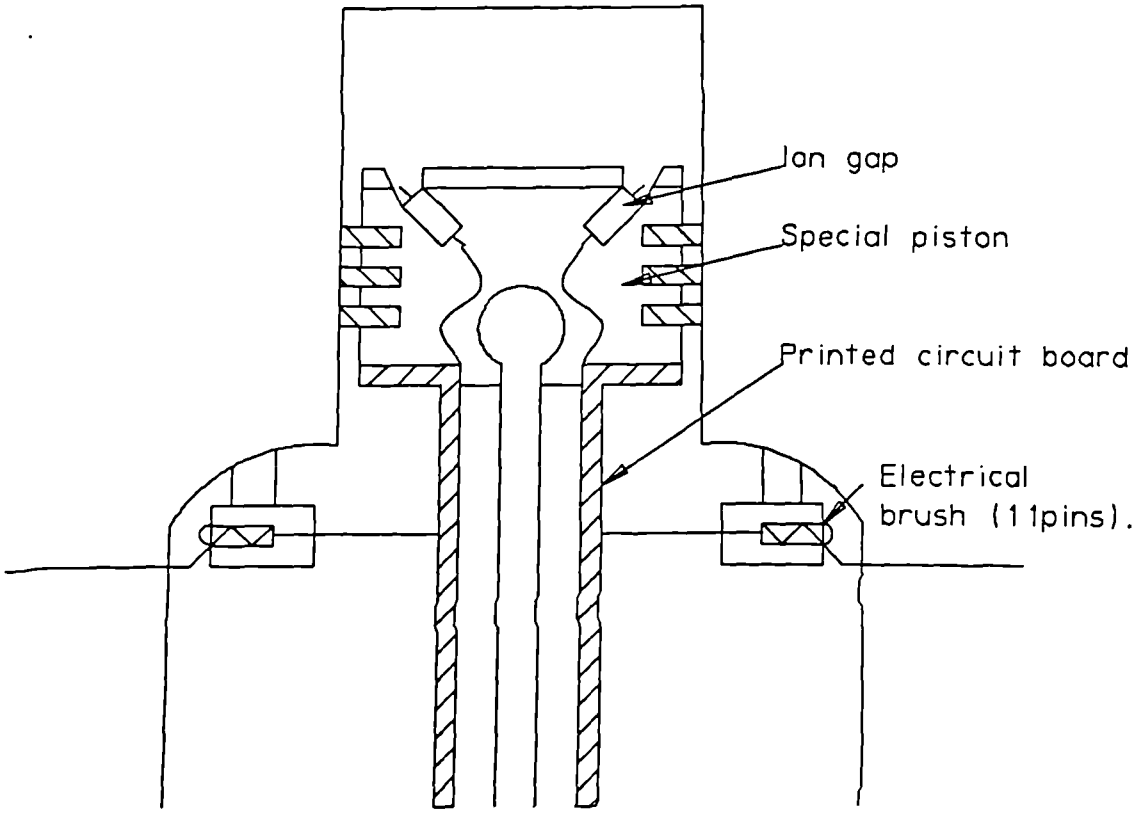

Figure 1.14: Special piston and electrical brush assembly, Curry (1963).

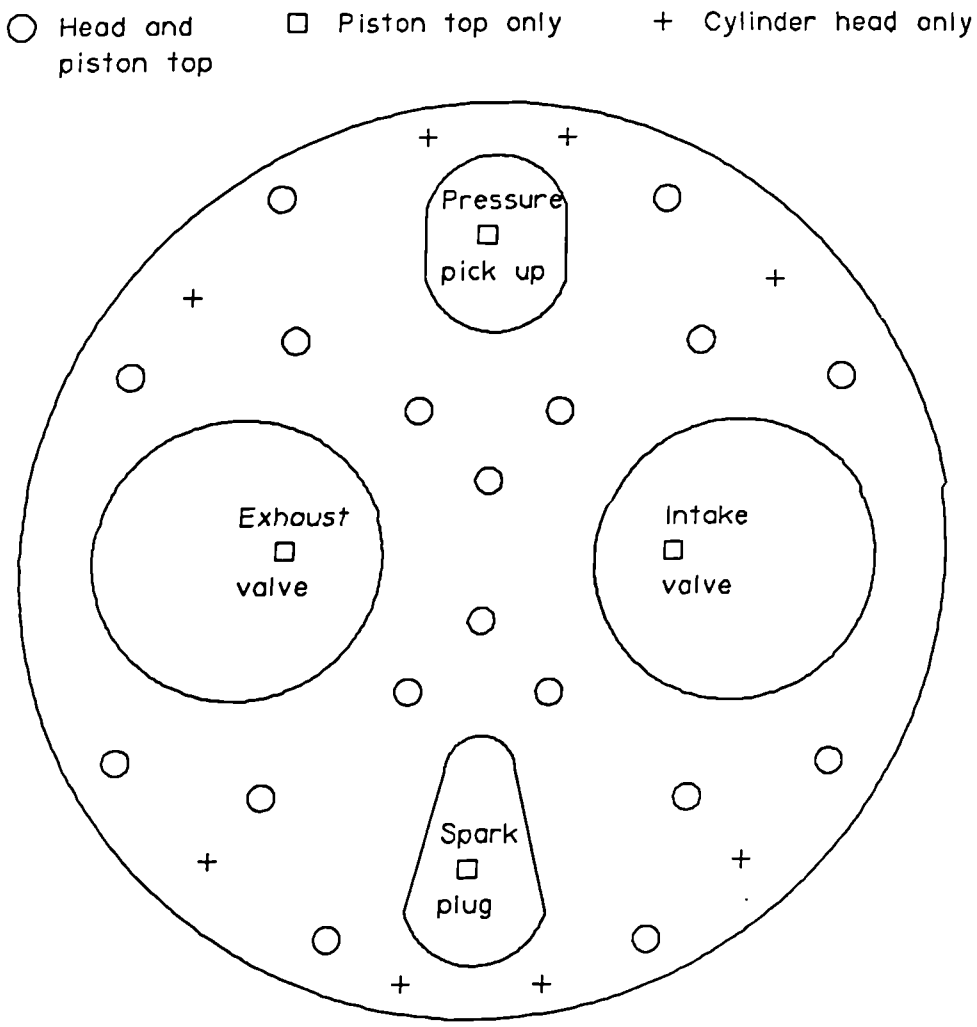

Figure 1.15: Installation of ion gaps on piston and cylinder head surfaces, Curry (1963).

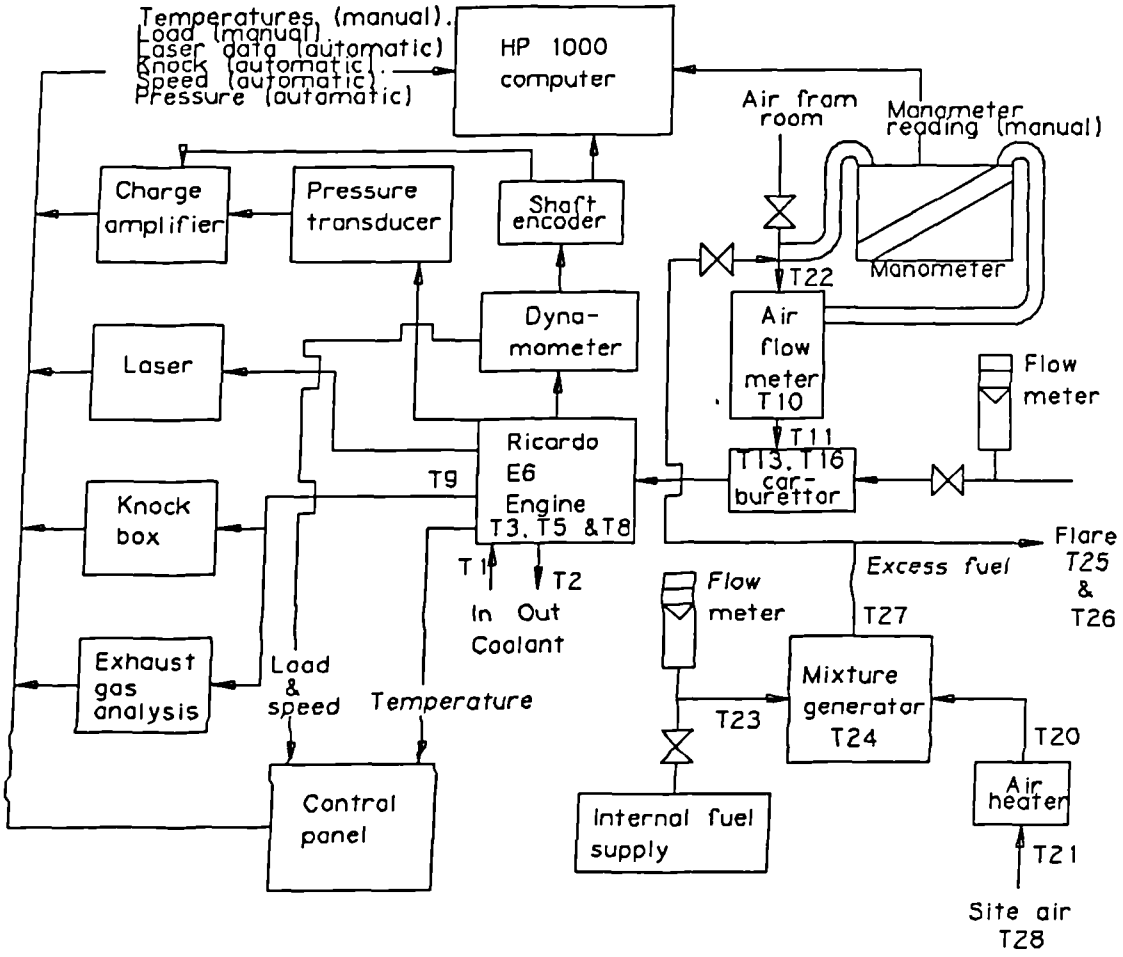

Figure 2.1: Engine test facility at the BP Research Centre.

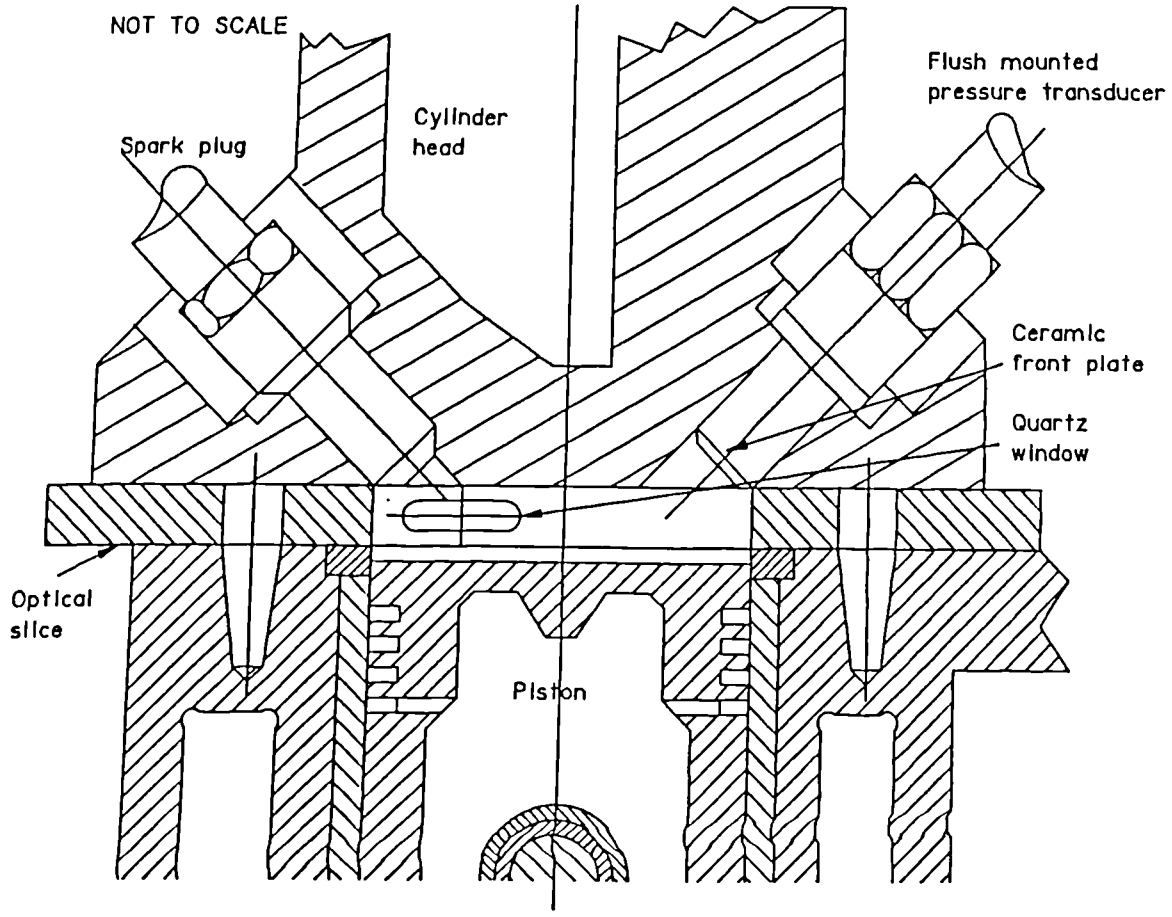

Figure 2.2: Ricardo E6 with optical slice.

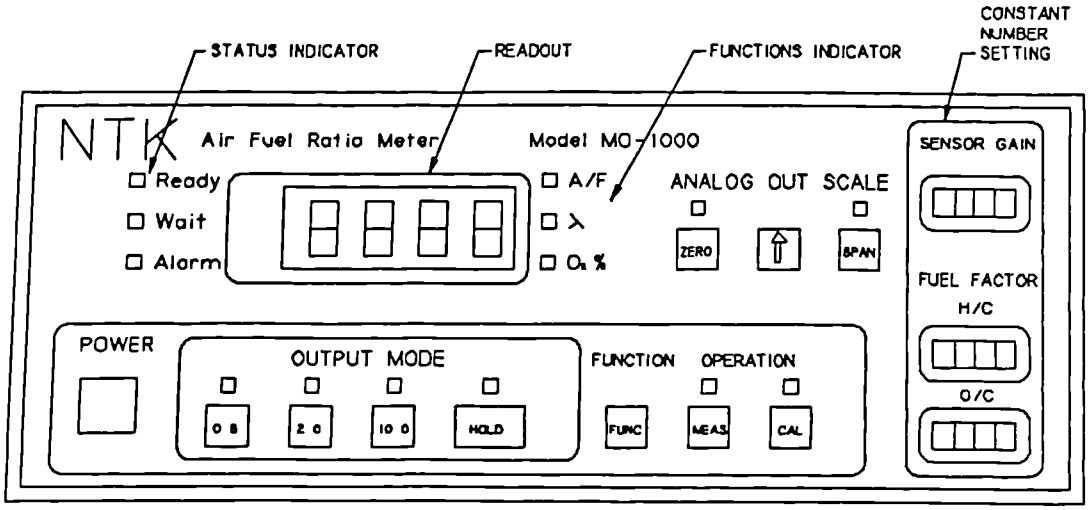

Figure 2.3: Front panel of air fuel ratio meter.

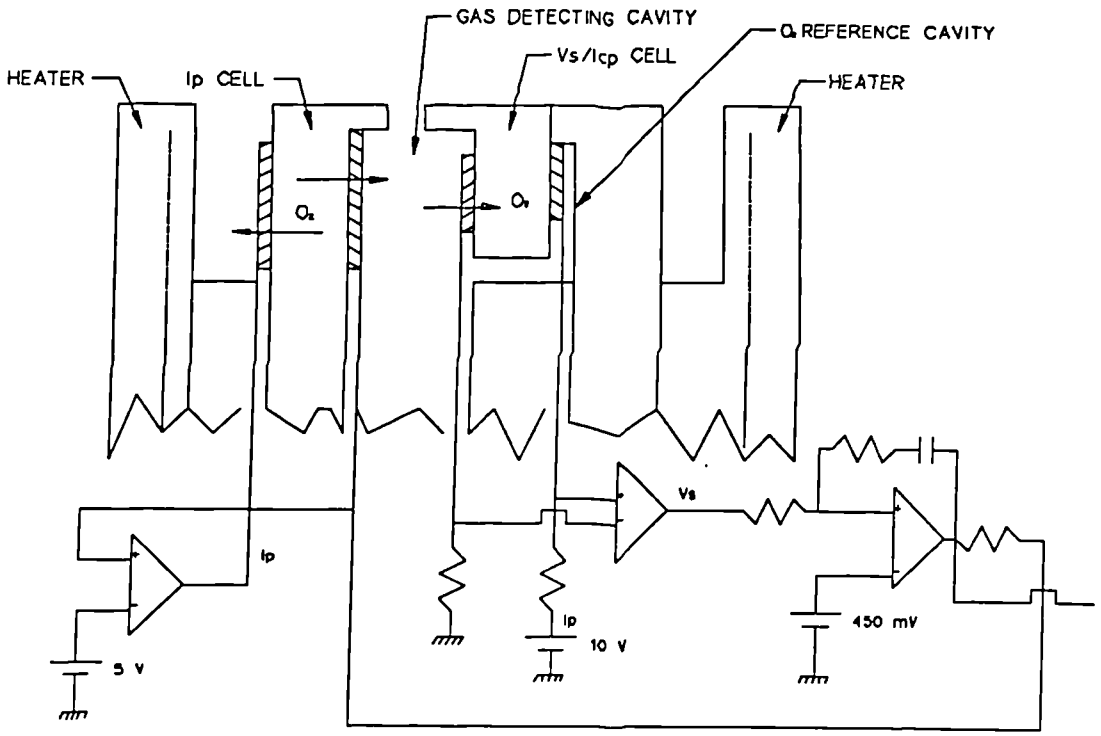

Figure 2.4: Basic principle and control circuit of the detecting portion of the sensor.

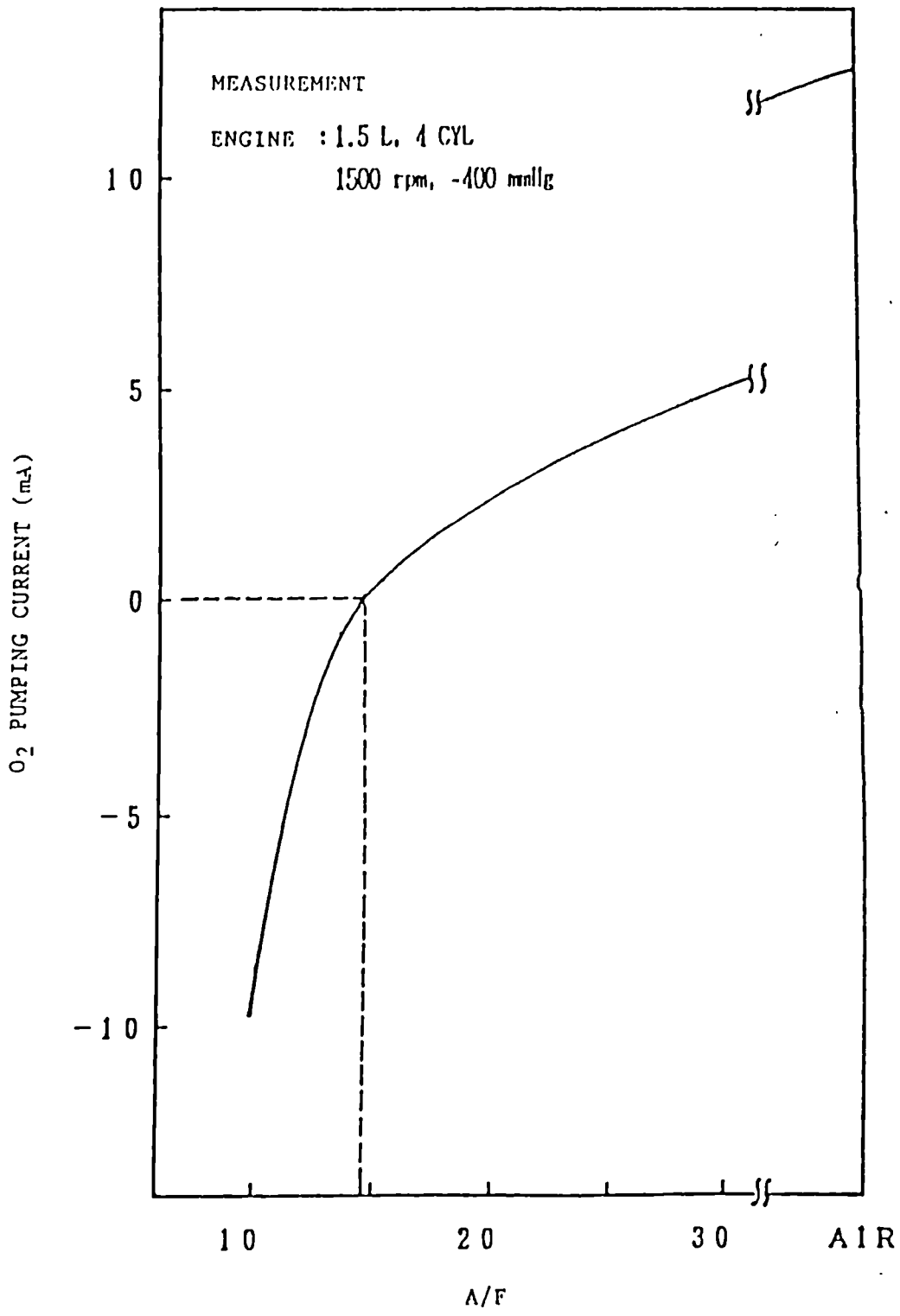

Figure 2.5: Relation between air fuel ratio and sensor output.

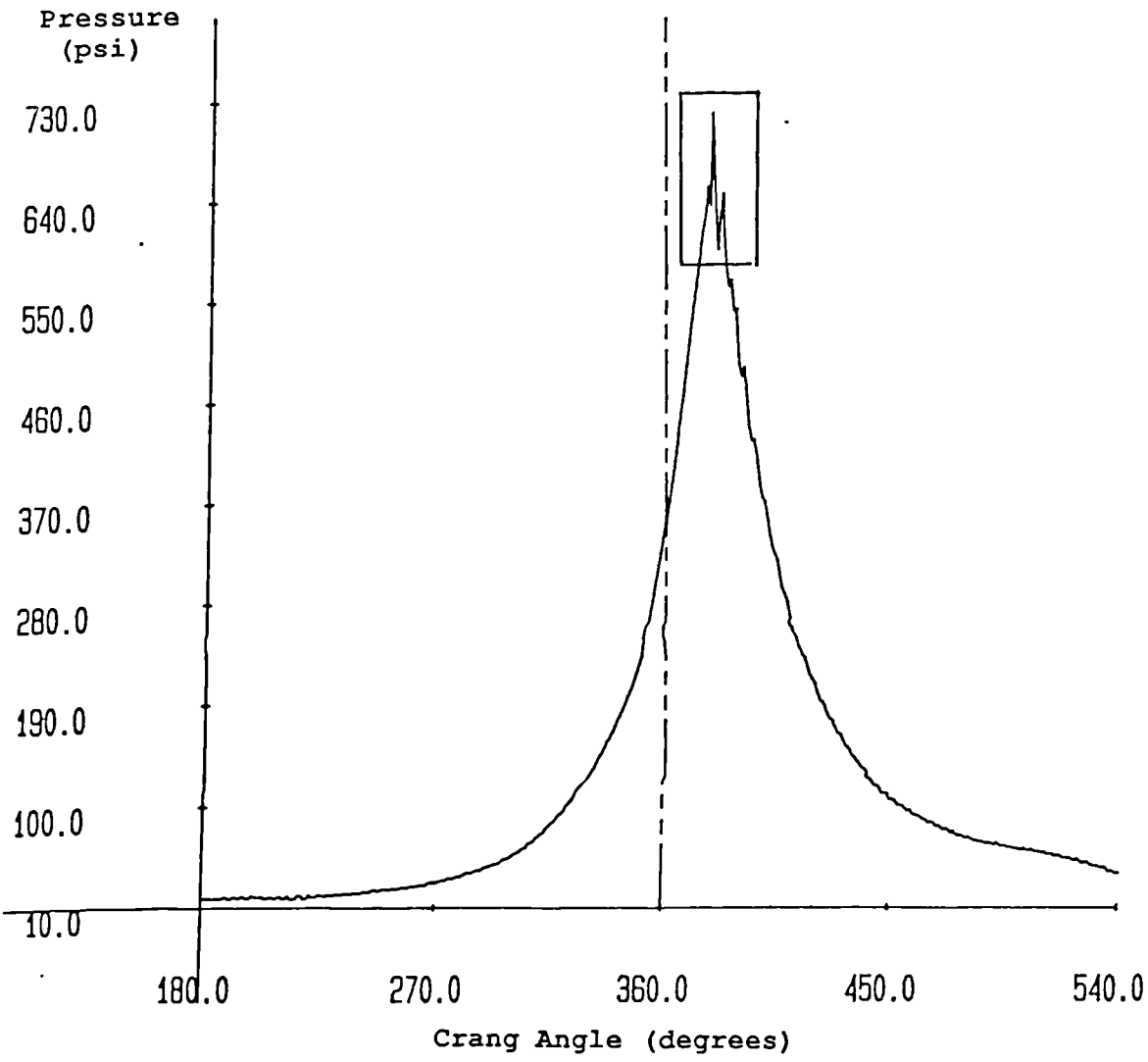

Figure 2.6: Pressure-Time diagram of pre-normalized pressure for a knocking cycle showing the customary high frequency spikes and the window taken by the knock box.

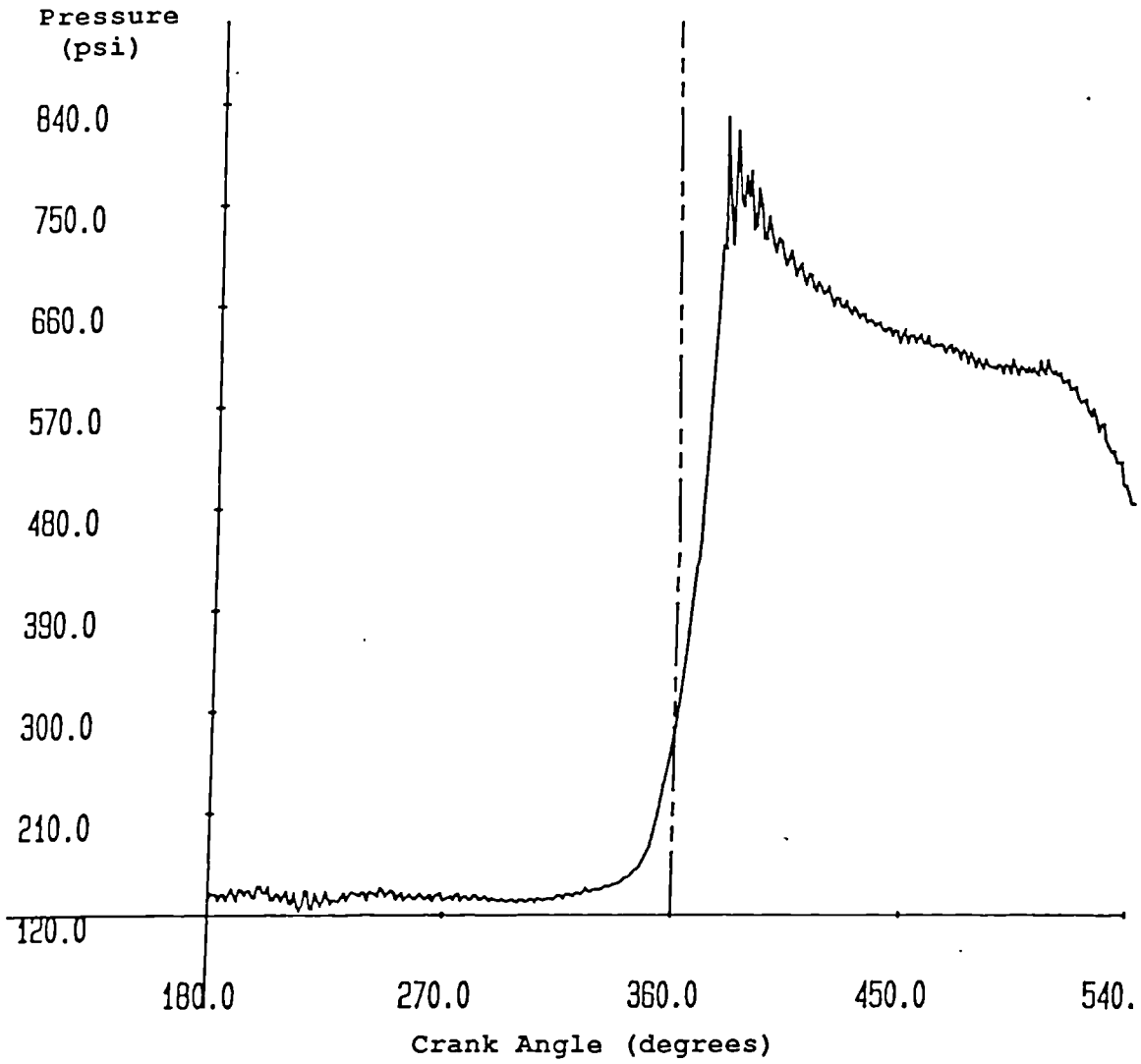

Figure 2.7: Pressure-Time diagram of normalized pressure showing the effect of knock.

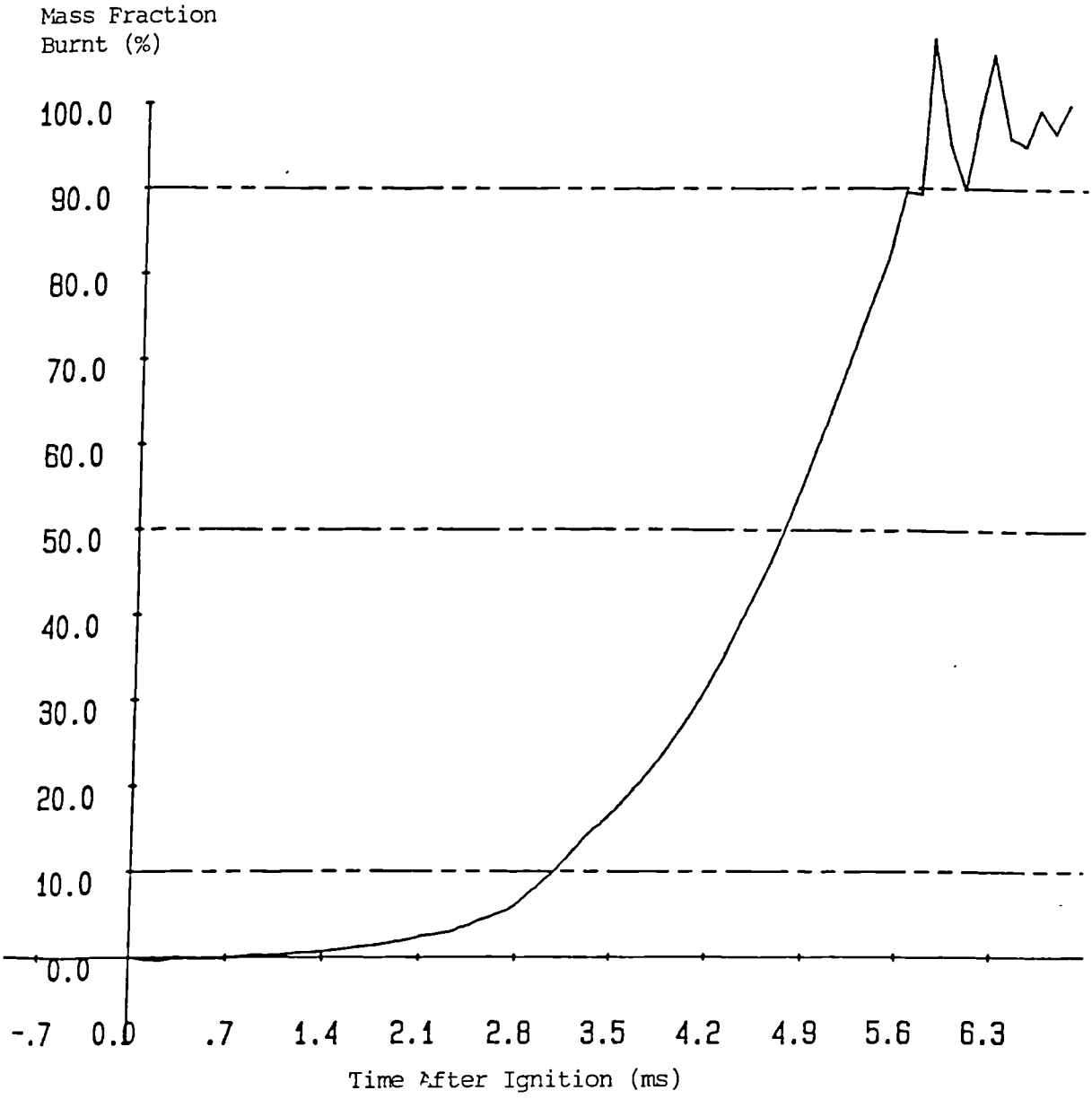

Figure 2.8: Effect of knock on mass fraction burnt as a function of time.

RUN NUMBER - A1274

KEYED IN DATA -

DATE	29 5 90	COMPRESSION RATIO	7.50	SPARK PLUG POSN.	1	COMB. CHAMBER TYPE	1
THROTTLE POSN.	2.0	ACTUAL SPEED	1500	FUEL CODE	ISO-OCT		
FUEL S.G.	.6919	STOICH AIR/FUEL RAT.	15.0				
NO. OF STROKES	4	ANALYSIS	FO	ALCOCK MAN. SLP.	3		
BARO PRESS.	30.12	TDUCER SCALE	5.0	STABILITY	2	KNOCK LEVEL	0
IGN. ADVANCE	14.0	HTG. OIL TEMP	23.0	CYL.PRESS.CORR.	-5.16	TORQUE	12.70
WATER TEMPERATURE	84.0	INTAKE AIR TEMP	40.0	FUEL TEMPERATURE	20.0		
ORIFICE AIR TEMP	29.0	ORIFICE AIR PRESS	.9				
FUEL FLOW METER	50.0	ALCOCK FLOWMETER	12.3	ALCOCK F/M. D/S.	-3.5		
FLOW METER ID	ME						
CALIB.GRADIENT	1.4140						
CALIB.INTERCEPT	-9.0000						

RESULTS DERIVED FROM KEYED IN DATA -

BHP1	3.626	BHP2	2.704	BMEP1	61.925	BMEP2	426.974
AFLO	107.872	CFMR	61.700	CSG	.69574	FFLO	5.581
AFR	19.330	EQR	.779	AFCCF	.971	MDCF	1.163
MMC	.700125	FCON	2.066274	BSFC1	.569860	BSFC2	.347
VOL. EFF	51.685	ISFC1	.4198				

Figure 2.9: Keyed in data and derived results for the BPIN routine.

ALL 300. CYCLES --- KNOCK LIMIT 175.96 VOLTS
RUN NUMBER --- A1274

SHORT SUMMARY - STATISTICS OF DATA BEFORE NORMALIZATION

MAXIMUM PRESSURE -	MAX =	352.11	C.A. OF MAX PRESS-	MAX =	404.00
	MIN =	106.08		MIN =	384.00
	MEAN=	249.44		MEAN=	393.35
	SD =	28.96		SD =	3.40
MAX PRESS RATE -	MAX =	12.04	C.A. OF MAX RATE -	MAX =	387.00
	MIN =	2.83		MIN =	1.00
	MEAN=	6.44		MEAN=	230.90
	SD =	1.51		SD =	145.71
SPARK ANGLE -	MAX =	346.00	GAMMA -	MAX =	1.1405
	MIN =	346.00		MIN =	1.1042
	MEAN=	346.00		MEAN=	1.1211
	SD =	0.00		SD =	.0070
IMEP -	MAX =	87.78	PMEP -	MAX =	4.87
	MIN =	78.24		MIN =	2.34
	MEAN=	84.06		MEAN=	4.22
	SD =	1.82		SD =	.35

COEFF. OF VARATION OF PEAK PRESSURE - 11.61

SHORT SUMMARY - STATISTICS OF DATA AFTER NORMALIZATION - FO METHOD USED

MAXIMUM PRESSURE -	MAX =	472.92	C.A. OF MAX PRESS-	MAX =	427.00
	MIN =	441.44		MIN =	388.00
	MEAN=	458.54		MEAN=	405.50
	SD =	5.73		SD =	6.27
MAX PRESS RATE -	MAX =	65.81	C.A. OF MAX RATE -	MAX =	401.00
	MIN =	10.46		MIN =	208.00
	MEAN=	35.14		MEAN=	213.34
	SD =	13.49		SD =	26.85
0-10% BURN TIME -	MAX =	3.00 ms	10%-90% BURN TIME	MAX =	4.45 ms
	MIN =	1.89		MIN =	2.00
	MEAN=	2.47		MEAN=	3.16
	SD =	.20		SD =	.44
0-50% BURN TIME -	MAX =	5.34 ms	0%-90% BURN TIME	MAX =	7.34 ms
	MIN =	3.33		MIN =	4.11
	MEAN=	4.29		MEAN=	5.63
	SD =	.35		SD =	.54

COEFF. OF VARATION OF PEAK PRESSURE - 1.25

Figure 2.10: Statistics for the data before and after normalization.

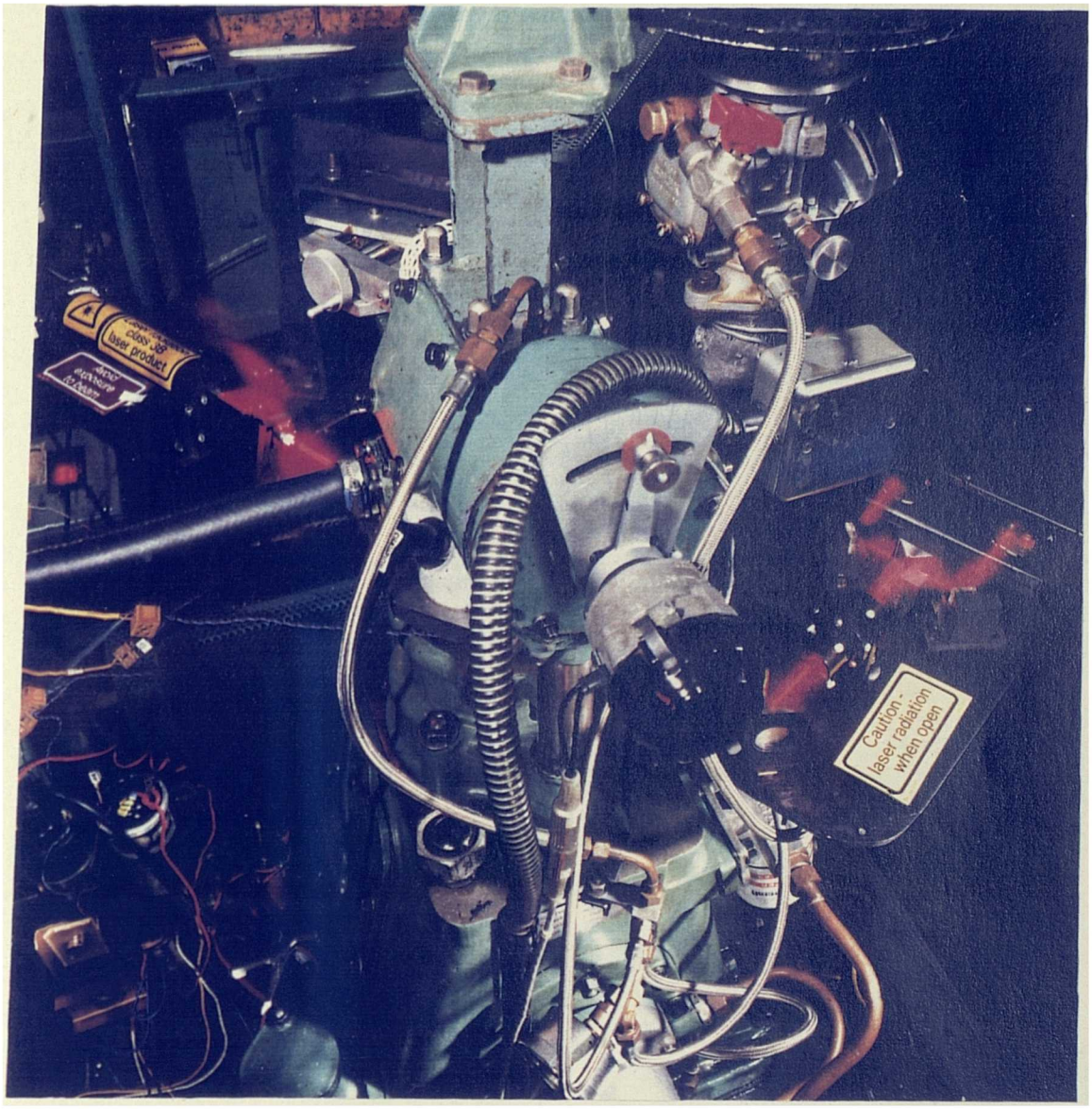

Figure 2.11: Photograph showing laser schlieren equipment in place on the engine.

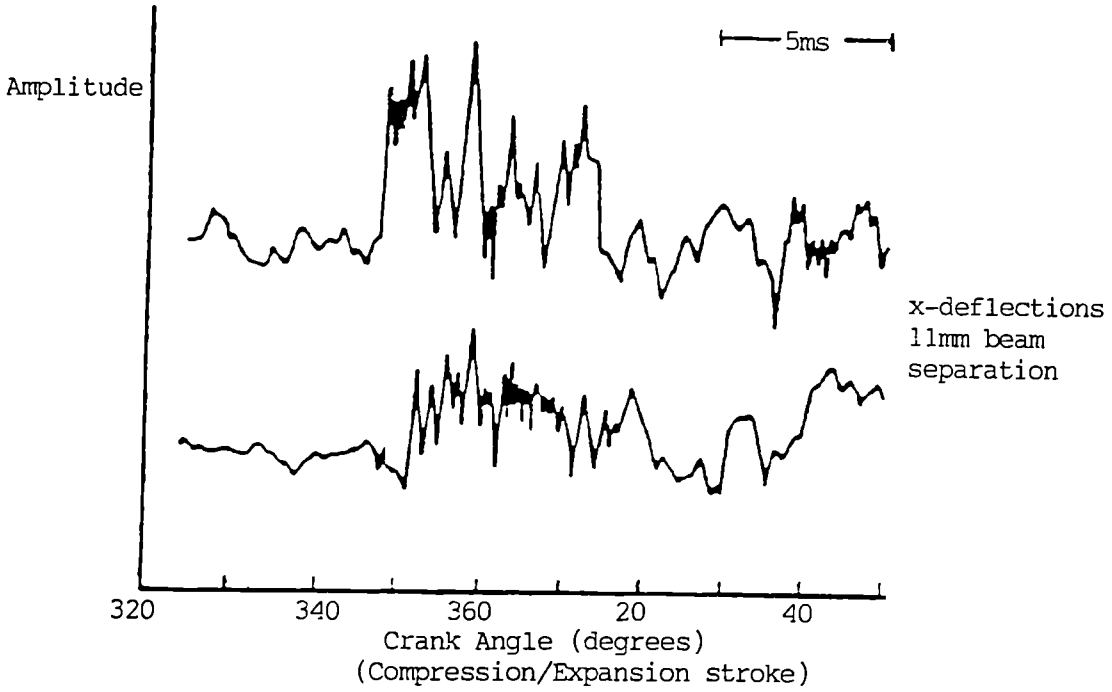

Figure 2.12: Laser (x) deviation for two laser beams passing through the engine cylinder, Kalghatgi and Swords (1983).

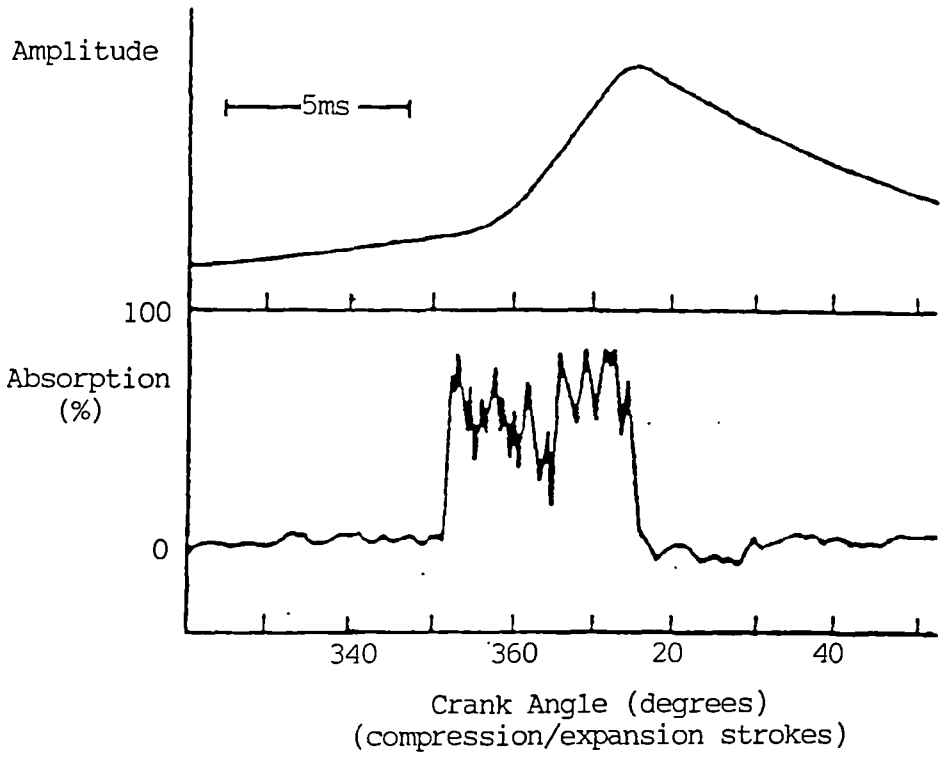

Figure 2.13: Laser absorption signal with corresponding pressure trace.

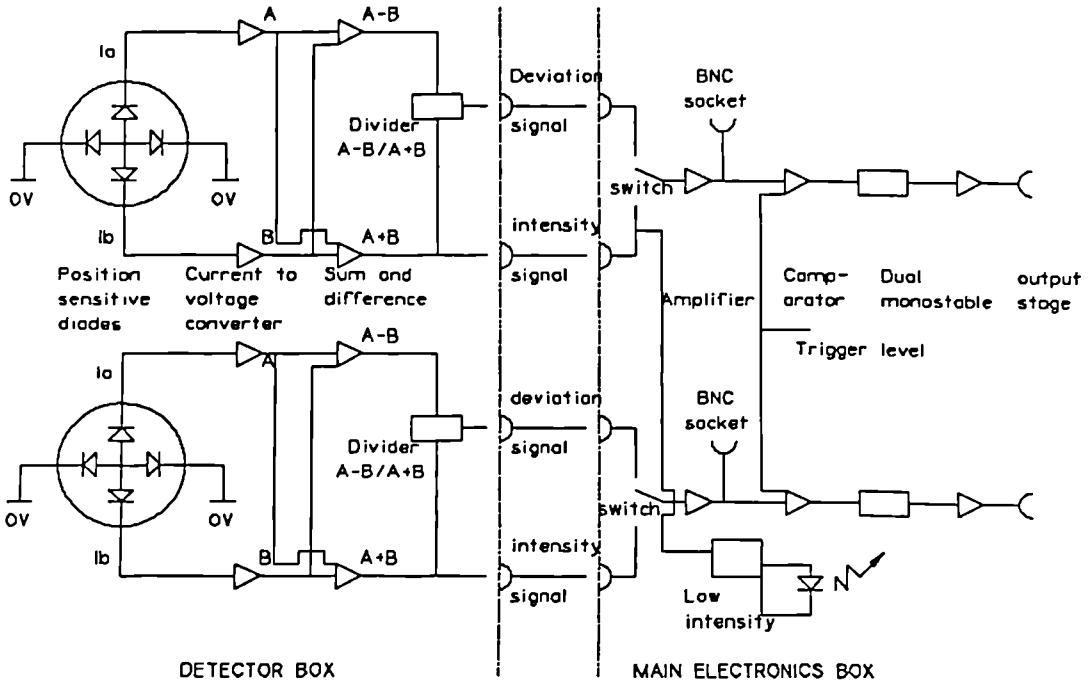

Figure 2.14: Layout of electronics for laser assembly, Harwell Instruction Manual.

RUN NUMBER [illegible] DATE [illegible]
ACTUAL RPM [illegible] Microseconds per Degree [illegible]
NOM SP ADV [illegible] Nom Time SP to TDC [illegible]

DISTANCE BETWEEN BEAMS .....) 3.500m.m.
DISTANCE OF BEAM 1 FROM SPARK PLUG ...) 7.458m.m.
BEAM ALLIGNMENT .....) YES

CYCLE	TIMES in microSec TO BEAM1	TO BEAM2	BETWEEN BEAMS	AVERAGE SPEEDS in M/SEC BETWEEN BEAMS	TO BEAM1	TO BEAM2	CYCLE	TIMES in microSec TO BEAM1	TO BEAM2	BETWEEN BEAMS	AVERAGE SPEEDS in M/SEC BETWEEN BEAMS	TO BEAM1	TO BEAM2
1	1235	1349	114	30 7	6.03	8.12	151	1432	1709	357	9.80	5.20	6.12
2	1334	1623	289	12.1	5 50	6.75	152	1035	1349	314	11.1	7.20	8.12
3	1354	1620	266	13 2	5.50	6.76	153	1371	1569	198	17.7	5.43	6.98
4	1315	1645	330	10.6	5.67	6.66	154	1655	1915	260	13.5	4 50	5.72
5	1398	1718	320	10.9	5.33	6.37	155	1310	1613	295	11.9	5.65	6.79
6	1418	1743	325	10.8	5.25	6.28	156	1549	1992	443	7.90	4.81	5.50
7	1415	1574	159	22 0	5.27	6.96	157	1083	1425	342	10.2	6.88	7.68
8	1689	2002	313	11.2	4.41	5.47	158	1508	1912	324	10.8	4.69	5.73
9	1131	1336	205	17 1	6.59	8.28	159	1232	1646	414	8.45	6.05	6.65
10	1455	1574	119	29 4	5.12	6.96	160	1581	1804	223	15.7	4.71	6.07
11	1160	1417	257	13.6	6 42	7.73	161	1295	1567	272	12.9	5.75	6.99
12	1043	1422	379	9 23	7.14	7.78	162	1586	1769	183	19.1	4.70	6.19
13	1325	1588	263	13 3	5.62	6.90	163	975	1083	100	32.4	7.64	10.1
14	1218	1577	359	9 75	6 12	6 74	164	1234	1610	376	9.31	6.04	6.80
15	1020	1369	349	10 0	7.30	8 00	165	963	1312	349	10.0	7.74	8.35
16	1394	1691	297	11 8	5 34	6.48	166	1277	1593	316	11.1	5.83	6.87
17	1474	1637	163	19.1	5.12	6.69	167	1593	1848	255	13.7	4.68	5.93
18	1906	2186	280	12.5	3 91	5.01	168	1491	1851	360	9.72	5.00	5.92
19	1243	1626	383	9 14	5.99	6 73	169	1516	1864	348	10.1	4.91	5.87
20	1420	1594	174	20 1	5.25	6.87	170	1418	1660	242	14.5	5.25	6.60
21	1528	1926	496	8 62	4 90	5.69	171	1409	1656	167	21.0	5 00	6.61
22	1645	2069	424	8.25	4.53	5.29	172	1418	1522	104	33.7	5.25	7.19
23	1169	1399	230	15 2	6.37	7.83	173	1090	1325	235	14.9	6.83	8.26
24	1255	1425	170	20 6	5.94	7.68	174	1495	1531	36	97.2	4.98	7.15
25	1230	1613	383	9 14	6.06	6.79	175	1159	1394	235	14.9	6.43	7.06
26	1344	1689	345	10 1	5.54	6 48	176	1419	1842	423	8.27	5.25	5.94
2	1210	1418	208	16 8	6 16	7.72	177	1586	1809	223	15.7	4.70	6.05
28	1498	1751	253	13 8	4 97	6.25	178	1719	1996	277	12.6	4.33	5.49
29	1482	1782	300	11.7	5 03	6.14	179	1048	1259	211	16.6	7.11	8.70
30	1281	1694	413	8 47	5 82	6 46	180	1475	1725	250	14.0	5.05	6.35
31	1287	1492	285	12.3	6.17	7.34	181	1343	1713	370	9.46	5 55	6.39
32	1386	1674	288	12 2	5 38	6 54	182	1599	1894	295	11.9	4.66	5.78
33	1640	2012	372	9 41	4 54	5 44	183	1211	1530	319	11.0	6.15	7.16
34	1373	1629	256	13 7	5 43	6.72	184	1451	1635	184	19.0	5.13	6.70
35	1772	1057	305	11 5	4 90	5 90	185	807	1134	327	10.7	9.23	9.66
36	1807	2088	281	12 5	4.12	5.24	186	889	1178	281	12.5	8.38	9.36
37	1166	1633	467	7.49	6.39	6.71	187	1313	1696	383	9.14	5.67	6.46
38	1632	1764	132	26 5	4 56	6 21	188	1324	1556	232	15.1	5.63	7.04
39	1337	1628	291	12 8	5 57	6.73	189	1520	1918	398	8.79	4.90	5.71
40	1761	1684	123	28 5	4 77	6 58	190	1361	1974	613	5.71	5.47	5.55
41	1178	1516	346	10.1	6 37	7.22	191	1039	1373	334	10.5	7.17	7.98
42	1718	1898	380	9 21	4 91	5 77	192	1487	1750	261	13.4	5.00	6.26
43	1186	1497	391	8 95	6 74	7 31	193	1456	1744	288	12.2	5.12	6.28
44	1344	1778	434	8 06	5 54	6 16	194	1484	1797	313	11.2	5.02	6.09
45	1602	1715	313	11 2	4 65	5 72	195	1186	1559	373	9.38	6.28	7.02
46	830	1065	235	14.9	8 90	10.3	196	1402	1984	422	8.29	5.03	5.75
47	1078	1404	326	9 77	6 96	7.71	197	1234	1560	326	10.7	6.04	7.02
48	1194	1615	421	8 31	6 24	6 78	198	1358	1653	295	11.9	5.49	6.62
49	13 3	1692	319	11 8	5 43	6 47	199	1338	1585	247	14.2	5.57	6.91
50	1172	1530	366	9 56	6.36	7 12	200	951	1264	313	11.2	7.83	8.66
51	1772	1877	2 5	1 3	4 74	5 90	201	1535	1782	247	14.2	4.85	6.14
52	1168	1409	241	14 5	6 38	7 77	202	1803	1553	330	10.6	3.96	7.85
53	1493	1813	320	10 9	4 99	6 04	203	1406	1766	360	9.72	5.30	6.20
54	1397	1762	365	9 59	5 33	6.21	204	1248	1455	215	16.3	6.01	7.53
55	10 2	1306	3 4	11 5	7 44	8 38	205	1762	2235	473	7.40	4.23	4.90
56	1314	1671	347	10 1	5 63	6 55	206	1172	1476	304	11.5	6.36	7.42
57	1288	1713	2 5	17 6	5 78	7.24	207	1471	1635	164	21.3	5.06	6.70
58	1218	1547	319	11 0	6 07	7 88	208	1315	1637	322	10.9	5.67	6.69
59	1555	1872	315	11 1	4 78	5 85	209	1210	1567	357	9.80	6.16	6.99
60	1064	1355	2 3	11 9	7 02	8.08	210	1096	1194	98	35.7	6.80	9.17
61	1546	1 21	195	17 9	4 88	6 36	211	1437	1808	371	9.43	5.18	6.06
62	1671	1409	242	14 5	4 51	7 77	212	1494	1578	84	41.7	4.99	6.94
63	1719	1704	185	18 9	4 90	6 43	213	1506	1850	344	10.2	4.95	5.92
64	1092	1498	406	8 62	6 82	7 31	214	1124	1295	171	20.5	6.63	8.46
65	1468	1698	230	15 2	5 18	6 48	215	1137	1198	61	57.4	6.55	9.14
66	1378	1707	337	10 4	5 44	6 41	216	1215	1516	301	11.6	6.13	7.22
67	884	1190	306	11 4	8 43	9 20	217	936	1256	320	10.9	7.96	8.72
68	1045	1343	298	11 7	7 13	8 15	218	1358	1714	356	9.83	5 49	6.39
69	989	1222	233	15 0	7 53	8 96	219	1352	1654	302	11.6	5.51	6.62
70	1415	1659	244	14 3	5 27	6.60	220	1446	1800	354	9.89	5.15	6.08
71	1676	1989	333	10 5	4 58	5.51	221	1409	1751	262	13.4	5 00	6.25
72	1142	1339	197	17 8	6 52	8 18	222	1326	1682	356	9.83	5.62	6.51
73	1149	1404	255	13 7	6 48	7 88	223	1411	1620	209	16.7	5.28	6.76
74	1488	1738	250	14 5	5.01	6 33	224	920	1205	277	12.6	8.03	9.09
75	1755	1058	303	11 6	4 77	5 07	225	1270	1498	228	15.4	5.87	7.31
76	1489	1717	380	11 4	5 29	6 38	226	1350	1546	196	17.9	5.52	7.08
77	1858	2208	350	10 0	4 03	4 98	227	909	1305	396	11.1	7 53	8.59
78	1483	1812	329	10 6	5 82	6 84	228	1452	1729	277	12.6	5.13	6.33
79	1440	1736	296	11 8	5 17	6 31	229	1529	1876	347	10.1	4.87	5.84
80	1233	1442	209	16 7	6 04	7 59	230	1290	1663	365	9.59	5.74	6.58
81	1099	1351	252	13 7	6 78	8.11	231	1361	1460	99	35 4	5.47	7.50
82	1229	1472	243	14 4	6 06	7 44	232	1669	1878	201	17.4	4.46	5.86
83	1576	1810	234	15 0	4 73	6 05	233	1335	1672	337	10 4	5.58	6.55
84	1438	1716	286	12 2	5 21	6 30	234	1715	2047	332	10.5	4 34	5.35
85	1092	1428	328	10 7	6 82	7.71	235	1539	1831	292	12.0	4.84	5.98
86	1105	1429	324	10 8	6 74	7 66	236	1442	1028	378	9.26	5.17	6.02
87	1325	1479	154	22 7	5 62	7 40	237	1389	1636	247	14.2	5.36	6.69
88	1558	1759	201	17 4	4 78	6.23	238	1216	1490	282	12.4	6.13	7.31
89	1375	1513	138	25 4	5 42	7 24	239	1177	1574	377	9.28	6.22	6.96
90	1389	1791	282	12 4	5 69	6 88	240	1382	1630	256	13.7	5.39	6.68
91	1406	1804	398	8 79	5 30	6 07	241	1568	1791	231	15.2	4.78	6.11
92	1494	1853	359	9.75	4 99	5.91	242	1246	1657	411	8.52	5.98	6.61

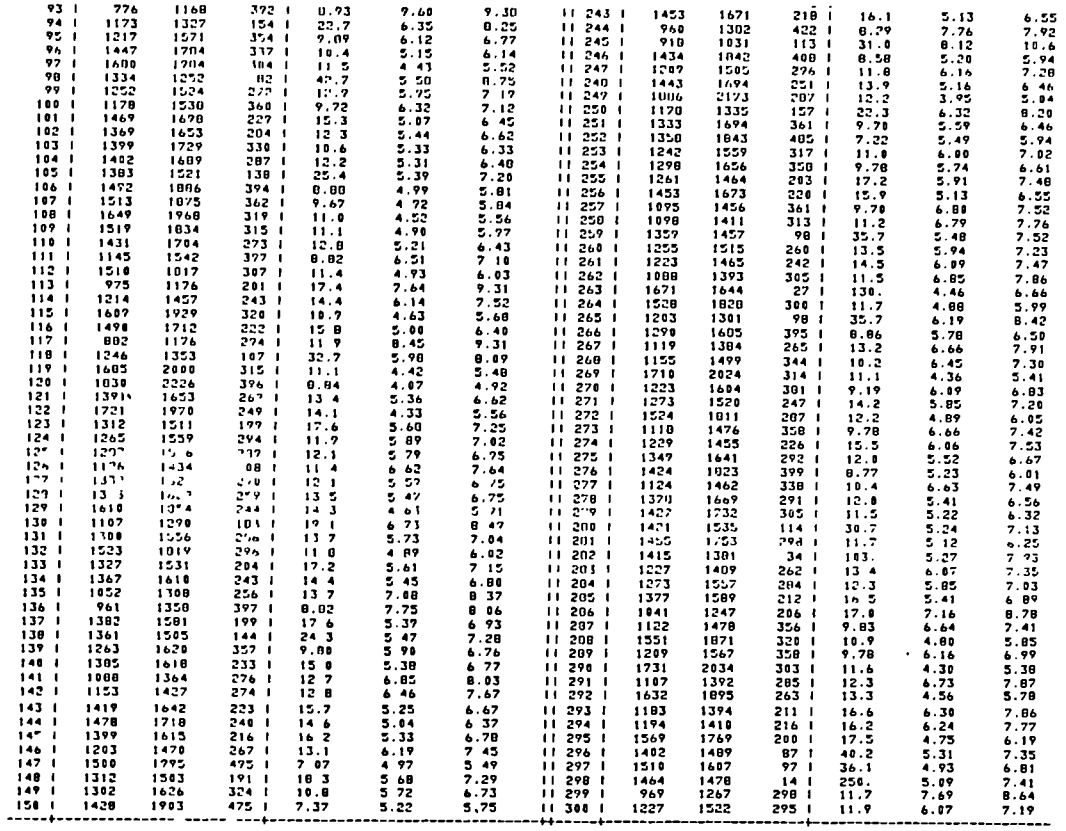

93	776	1168	392	0.93	9.60	9.30	243	1453	1671	218	16.1	5.13	6.55
94	1173	1327	154	23.7	6.35	8.25	244	960	1302	422	8.79	7.76	7.92
95	1217	1571	354	9.09	6.12	6.77	245	910	1031	113	31.0	8.12	10.6
96	1447	1784	337	10.4	5.15	6.14	246	1434	1842	408	8.58	5.20	5.94
97	1680	1784	104	11.5	4.43	5.52	247	1089	1585	296	11.8	6.16	7.28
98	1334	1252	82	48.7	5.50	8.75	248	1443	1694	251	13.9	5.16	6.46
99	1252	1524	272	10.9	5.95	7.17	249	1006	2173	207	12.2	3.95	5.84
100	1178	1538	360	9.72	6.32	7.12	250	1170	1335	157	22.3	6.32	8.20
101	1469	1696	227	15.3	5.07	6.45	251	1333	1694	361	9.70	5.59	6.46
102	1369	1653	284	12.3	5.44	6.62	252	1358	1843	485	7.22	5.49	5.94
103	1399	1729	330	10.6	5.33	6.33	253	1242	1559	317	11.8	6.00	7.02
104	1402	1689	287	12.2	5.31	6.40	254	1298	1656	358	9.78	5.74	6.61
105	1383	1521	138	25.4	5.39	7.20	255	1261	1464	203	17.2	5.91	7.48
106	1492	1886	394	8.80	4.99	5.81	256	1453	1673	220	15.9	5.13	6.55
107	1513	1875	362	9.67	4.72	5.84	257	1095	1456	361	9.70	6.88	7.52
108	1649	1968	319	11.0	4.52	5.56	258	1098	1411	313	11.2	6.79	7.76
109	1519	1834	315	11.1	4.90	5.97	259	1359	1457	98	35.7	5.48	7.52
110	1431	1704	273	12.8	5.21	6.43	260	1255	1515	260	13.5	5.94	7.23
111	1145	1542	397	8.82	6.51	7.18	261	1223	1465	242	14.5	6.09	7.47
112	1510	1817	307	11.4	4.93	6.03	262	1088	1393	305	11.5	6.85	7.86
113	975	1176	201	17.4	7.64	9.31	263	1671	1644	27	130.	4.46	6.66
114	1214	1457	243	14.4	6.14	7.52	264	1528	1828	300	11.7	4.88	5.99
115	1609	1929	320	10.9	4.63	5.68	265	1203	1301	98	35.7	6.19	8.42
116	1498	1712	222	15.8	5.00	6.40	266	1298	1605	395	8.86	5.78	6.50
117	882	1176	294	11.9	8.45	9.31	267	1119	1384	265	13.2	6.66	7.91
118	1246	1353	107	32.7	5.98	8.09	268	1155	1499	344	10.2	6.45	7.30
119	1605	2000	315	11.1	4.42	5.48	269	1710	2024	314	11.1	4.36	5.41
120	1830	2226	396	8.84	4.07	4.92	270	1223	1684	301	9.19	6.09	6.83
121	1391	1653	262	13.4	5.36	6.62	271	1273	1520	247	14.2	5.85	7.20
122	1721	1970	249	14.1	4.33	5.56	272	1524	1811	287	12.2	4.89	6.05
123	1312	1511	199	17.6	5.60	7.25	273	1118	1476	358	9.78	6.66	7.42
124	1265	1559	294	11.9	5.89	7.02	274	1229	1455	226	15.5	6.06	7.53
125	1207	1536	329	12.1	5.79	6.75	275	1349	1641	292	12.8	5.52	6.67
126	1176	1434	88	11.4	6.62	7.64	276	1424	1823	399	8.77	5.23	6.81
127	1377	1552	175	12.1	5.59	6.75	277	1124	1462	338	10.4	6.63	7.49
128	13.5	1643	279	13.5	5.47	6.75	278	1370	1669	291	12.8	5.41	6.56
129	1610	1854	244	14.3	4.61	5.71	279	1427	1732	305	11.5	5.22	6.32
130	1107	1290	183	19.1	6.73	8.47	280	1421	1535	114	30.7	5.24	7.13
131	1308	1556	248	13.7	5.73	7.04	281	1455	1753	298	11.7	5.12	6.25
132	1523	1819	296	11.8	4.89	6.02	282	1415	1381	34	183.	5.27	7.93
133	1327	1531	204	17.2	5.61	7.15	283	1227	1489	262	13.4	6.07	7.35
134	1367	1610	243	14.4	5.45	6.88	284	1273	1557	284	12.3	5.85	7.03
135	1052	1308	256	13.7	7.68	8.37	285	1377	1589	212	16.5	5.41	6.89
136	961	1358	397	8.82	7.75	8.06	286	1841	1247	206	17.8	7.16	8.78
137	1382	1581	199	17.6	5.39	6.93	287	1122	1478	356	9.83	6.64	7.41
138	1361	1505	144	24.3	5.47	7.28	288	1551	1871	320	10.9	4.80	5.85
139	1263	1620	357	9.88	5.98	6.76	289	1209	1567	358	9.78	6.16	6.99
140	1385	1618	233	15.8	5.38	6.77	290	1731	2034	303	11.6	4.30	5.38
141	1088	1364	276	12.7	6.85	8.03	291	1107	1392	285	12.3	6.73	7.87
142	1153	1427	274	12.8	6.46	7.67	292	1632	1895	263	13.3	4.56	5.78
143	1419	1642	223	15.7	5.25	6.67	293	1183	1394	211	16.6	6.30	7.86
144	1478	1718	240	14.6	5.04	6.37	294	1194	1418	216	16.2	6.24	7.77
145	1399	1615	216	16.2	5.33	6.78	295	1569	1769	200	17.5	4.75	6.19
146	1203	1470	267	13.1	6.19	7.45	296	1402	1489	87	40.2	5.31	7.35
147	1500	1995	495	7.07	4.97	5.49	297	1510	1607	97	36.1	4.93	6.81
148	1312	1503	191	18.3	5.68	7.29	298	1464	1478	14	256.	5.09	7.41
149	1302	1626	324	10.8	5.72	6.73	299	969	1267	298	11.7	7.69	8.64
150	1428	1903	475	7.37	5.22	5.75	300	1227	1522	295	11.9	6.07	7.19

Summary of cycles 1 to 300 is as follows

Time to beam 1		Time to beam 2		Time between beams	
Min =	776 microSec	Min =	1831 microSec	Min =	14 microSec
Max =	1986 microSec	Max =	2235 microSec	Max =	613 microSec
Mean =	1341.71 microSec	Mean =	1618.52 microSec	Mean =	281.58 microSec
SD =	207.340	SD =	221.487	SD =	89.142

Speeds calculated from the above summary

Speed to beam 1		Speed to beam 2		Speed between beams	
Min =	3.91 M Sec	Min =	4.90 M/Sec	Min =	5.71 M/Sec
MAX =	9.60 M Sec	MAX =	10.6 M/Sec	MAX =	256. M/Sec
Mean =	5.55 M Sec	Mean =	6.77 M/Sec	Mean =	12.4 M/Sec

Figure 2.15: Printout of laser flame speeds and times for all 300 cycles and a summary of statistics.

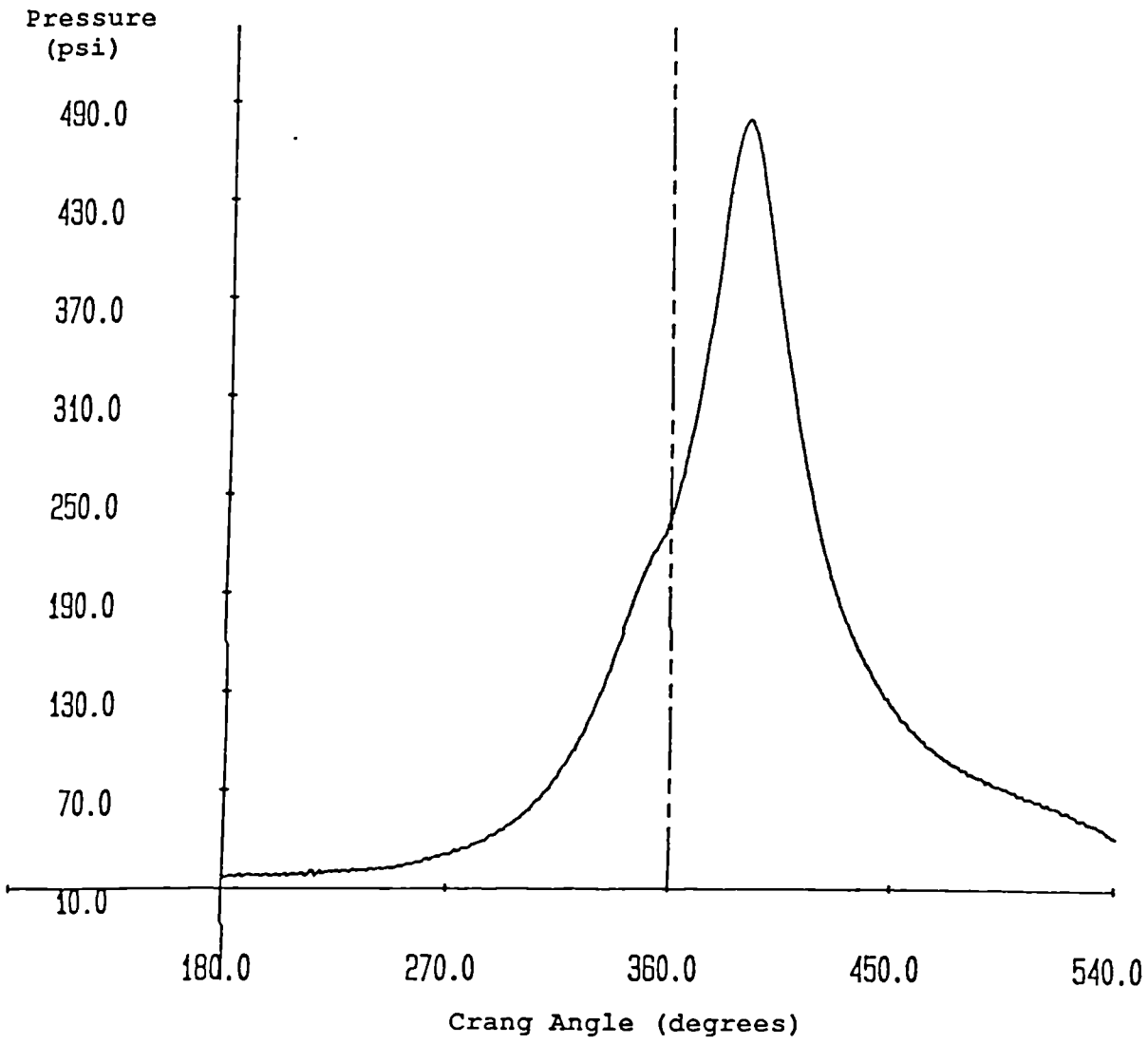

Figure 3.1: Original pressure-time diagram of pre-normalized pressure, courtesy of BP research.

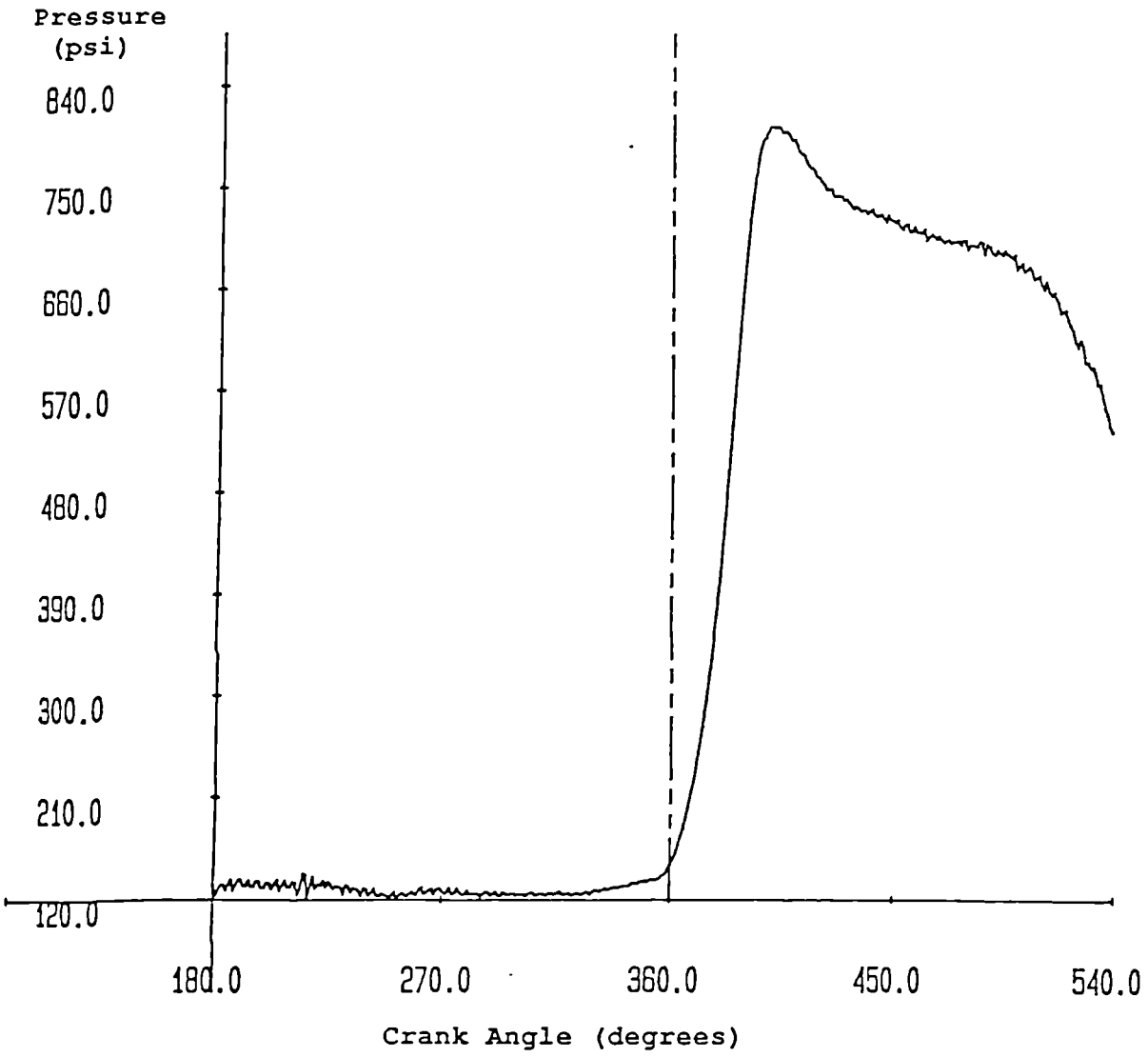

Figure 3.2: Pressure-time diagram of normalized pressure, courtesy of BP research.

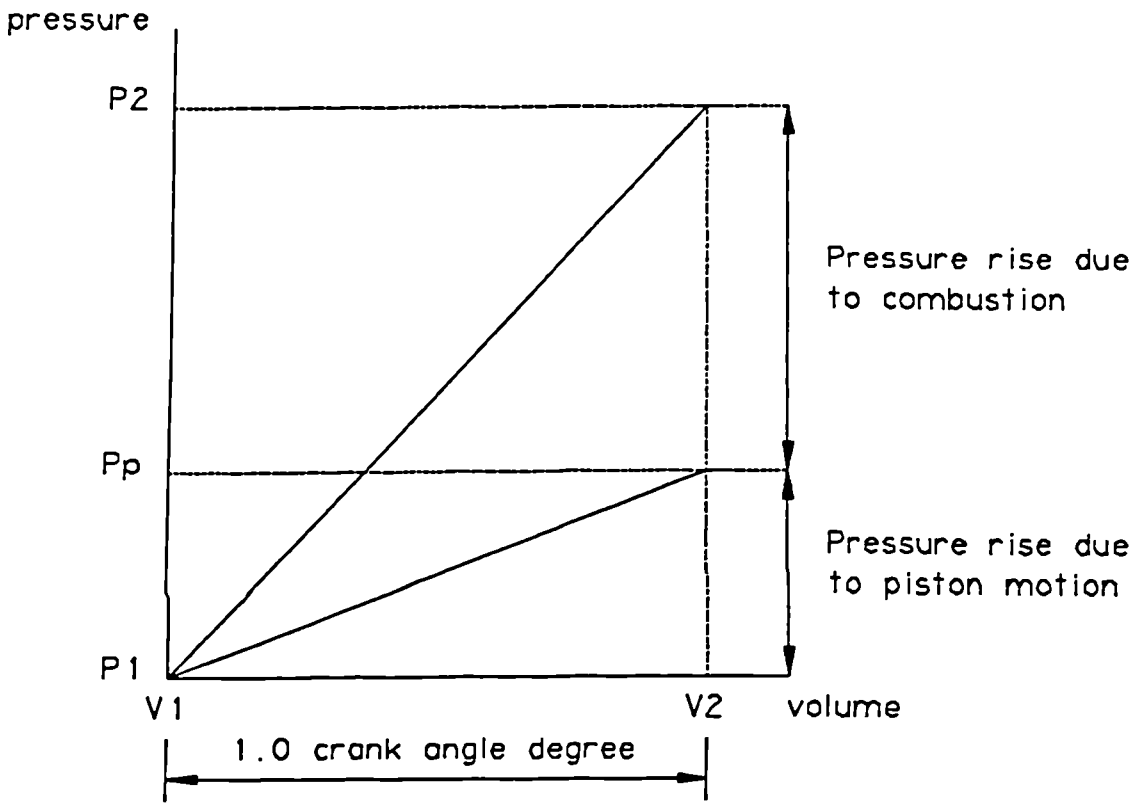

Figure 3.3: Single pressure increment showing pressure rise due to combustion and piston motion, Rassweiler and Withrow (1938).

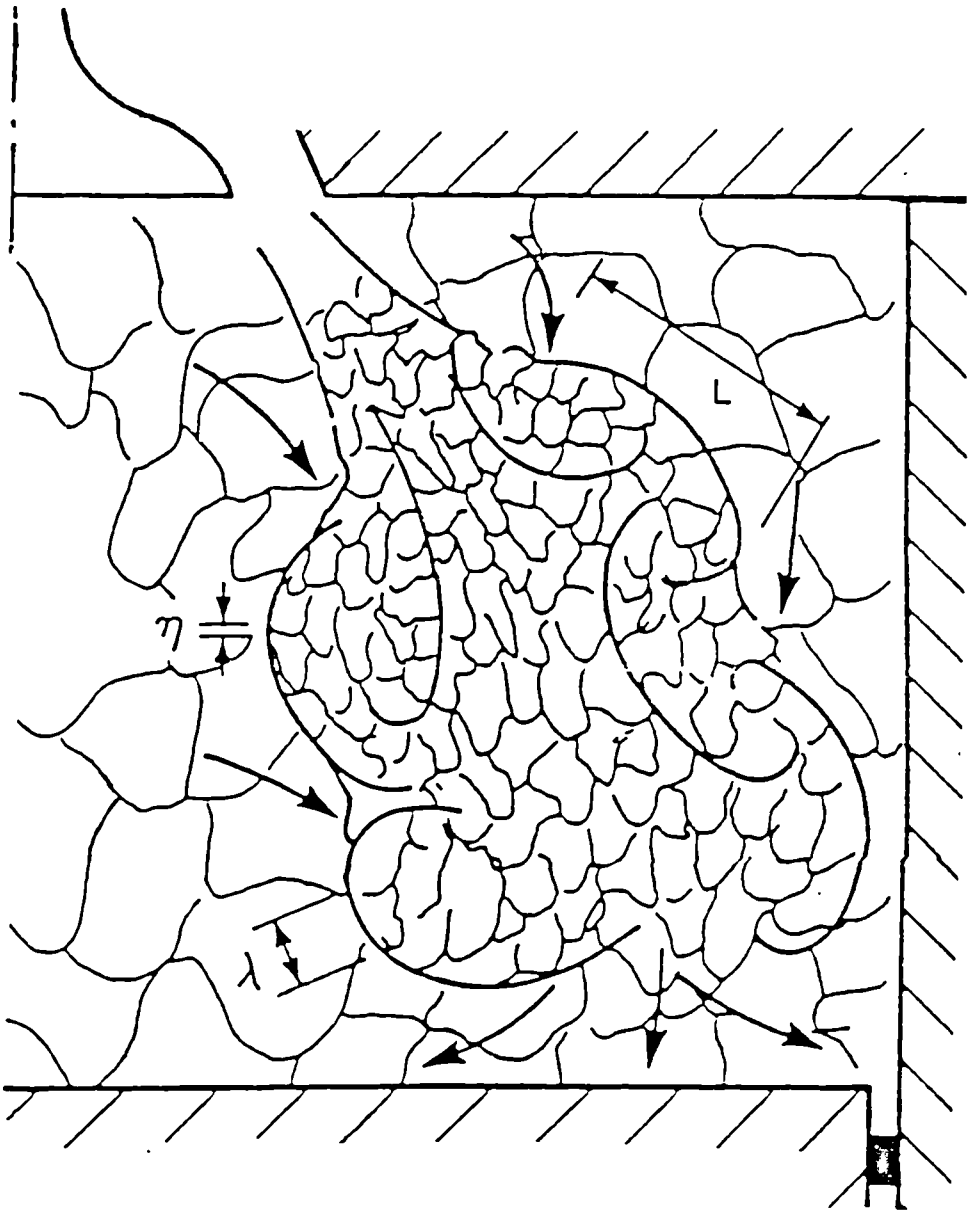

Figure 3.4: A representation of the induction process, to show the generation of eddies by shear action, and the characteristic length scales of turbulence.

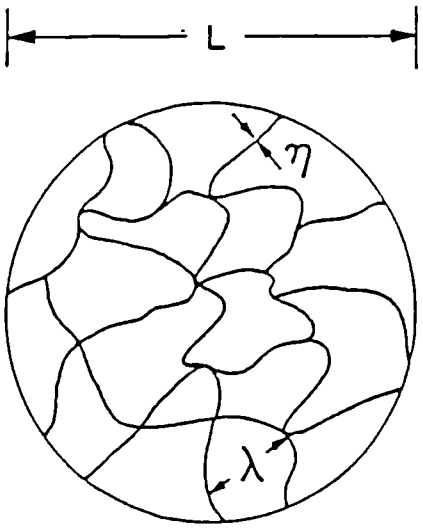

Figure 3.5: A schematic of the internal structure of a single turbulent eddy of integral scale L, Tabaczynski et. al. (1977).

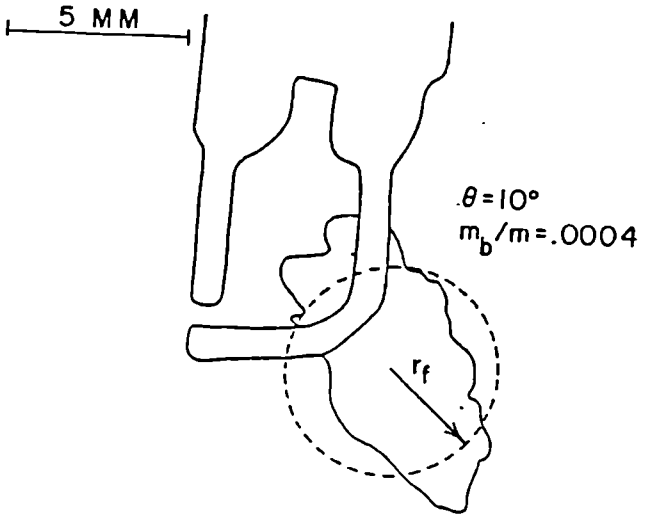

Figure 3.6: Typical flame shadow tracing showing convection and distortion of early flame kernel "shadow". Dashed circle has same area and centre as "shadow". Keck et. al. (1987).

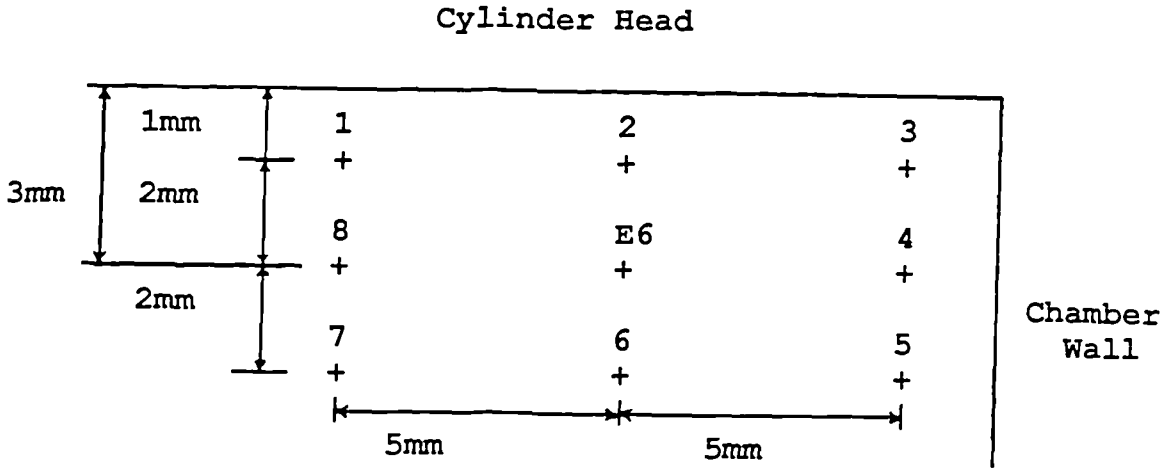

Figure 3.7: Schematic showing the positioning of the spark plug gap used in the modelling of cyclic variability.

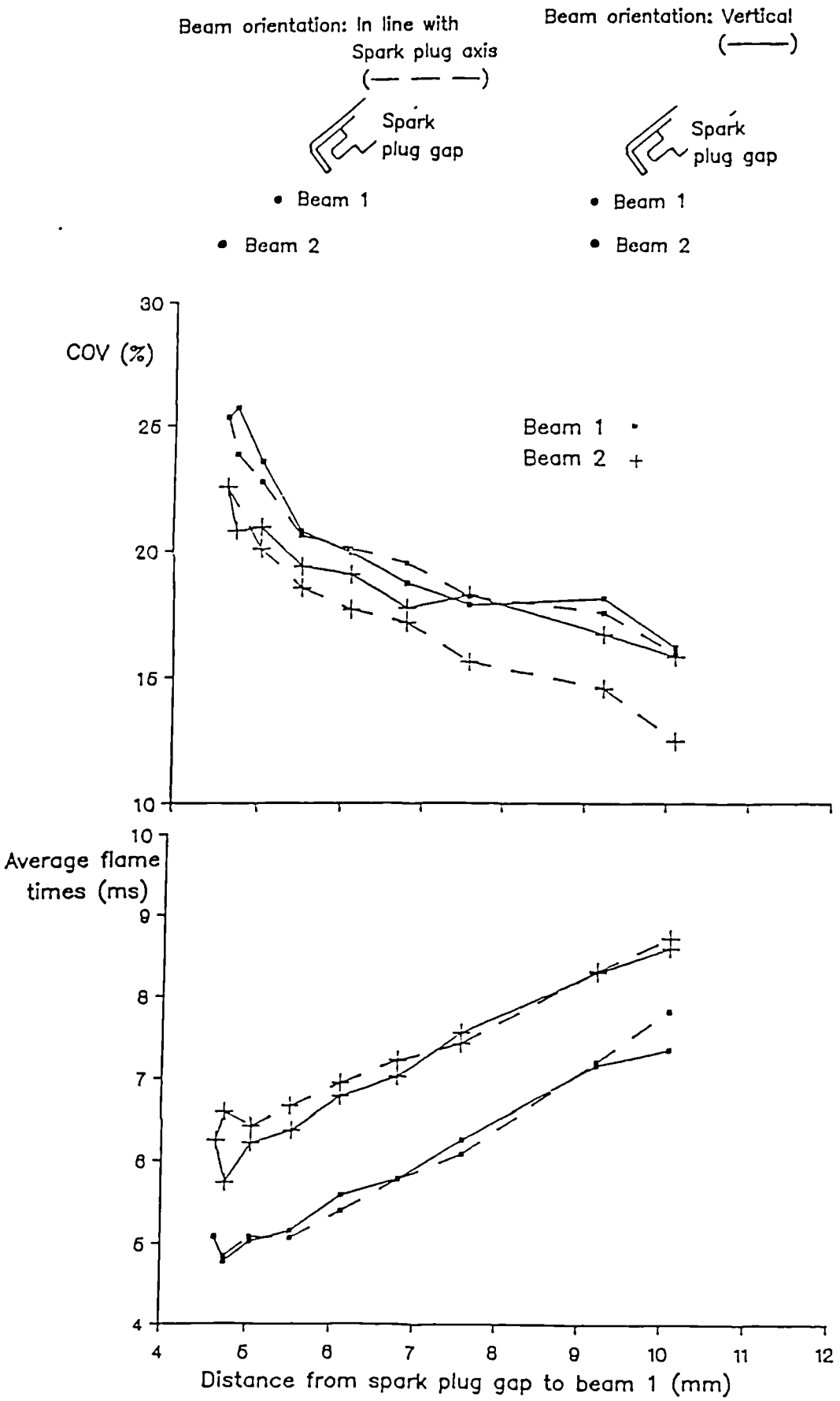

Figure 4.1: Variation in average and COV of flame times to beams 1 and 2 with distance from spark plug gap and beam orientation.

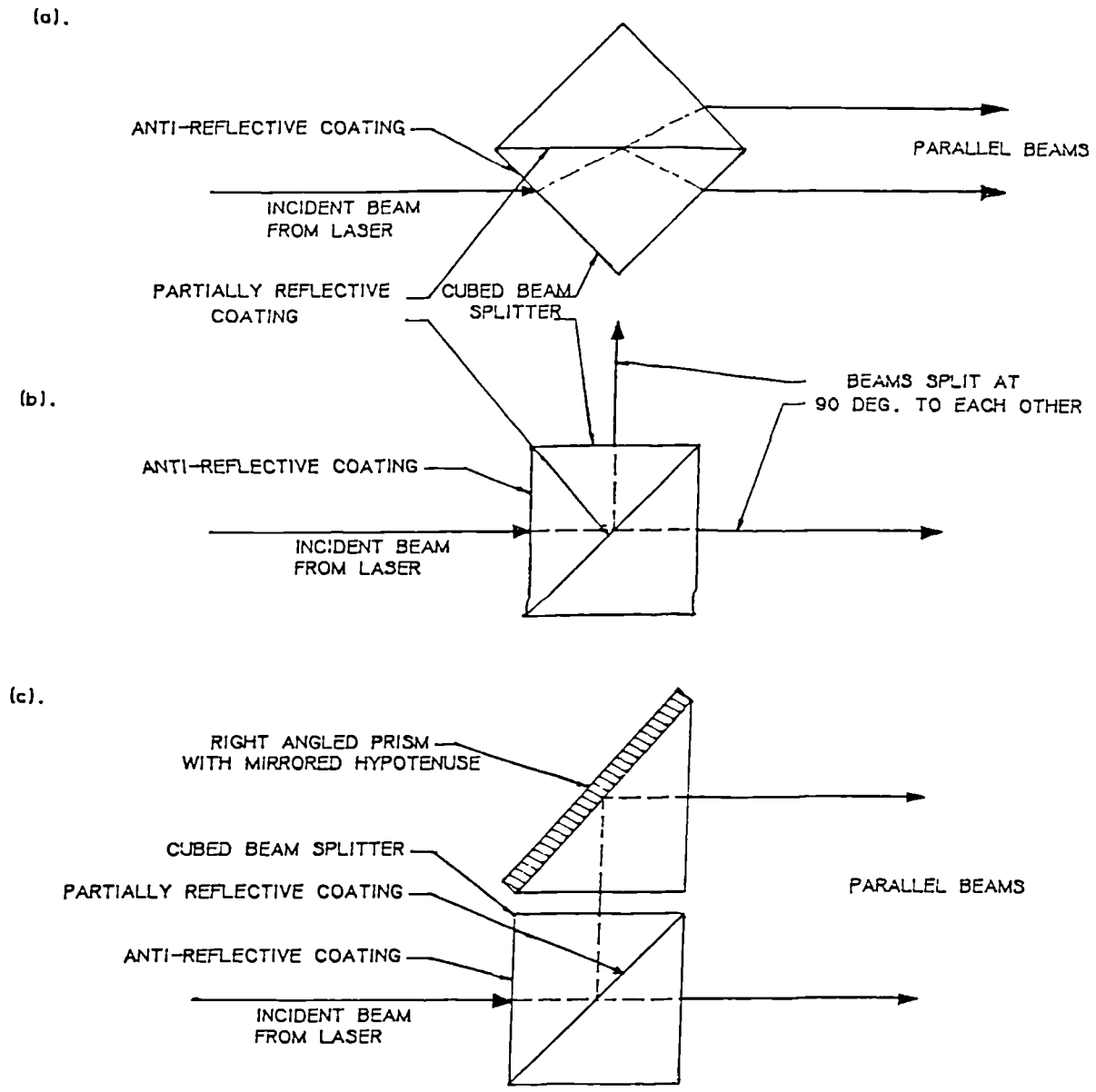

Figure 4.2: (a). Original method used to obtain parallel beams.
(b). Correct orientation for beam splitter use.
(c). Technique developed to obtain parallel beams.

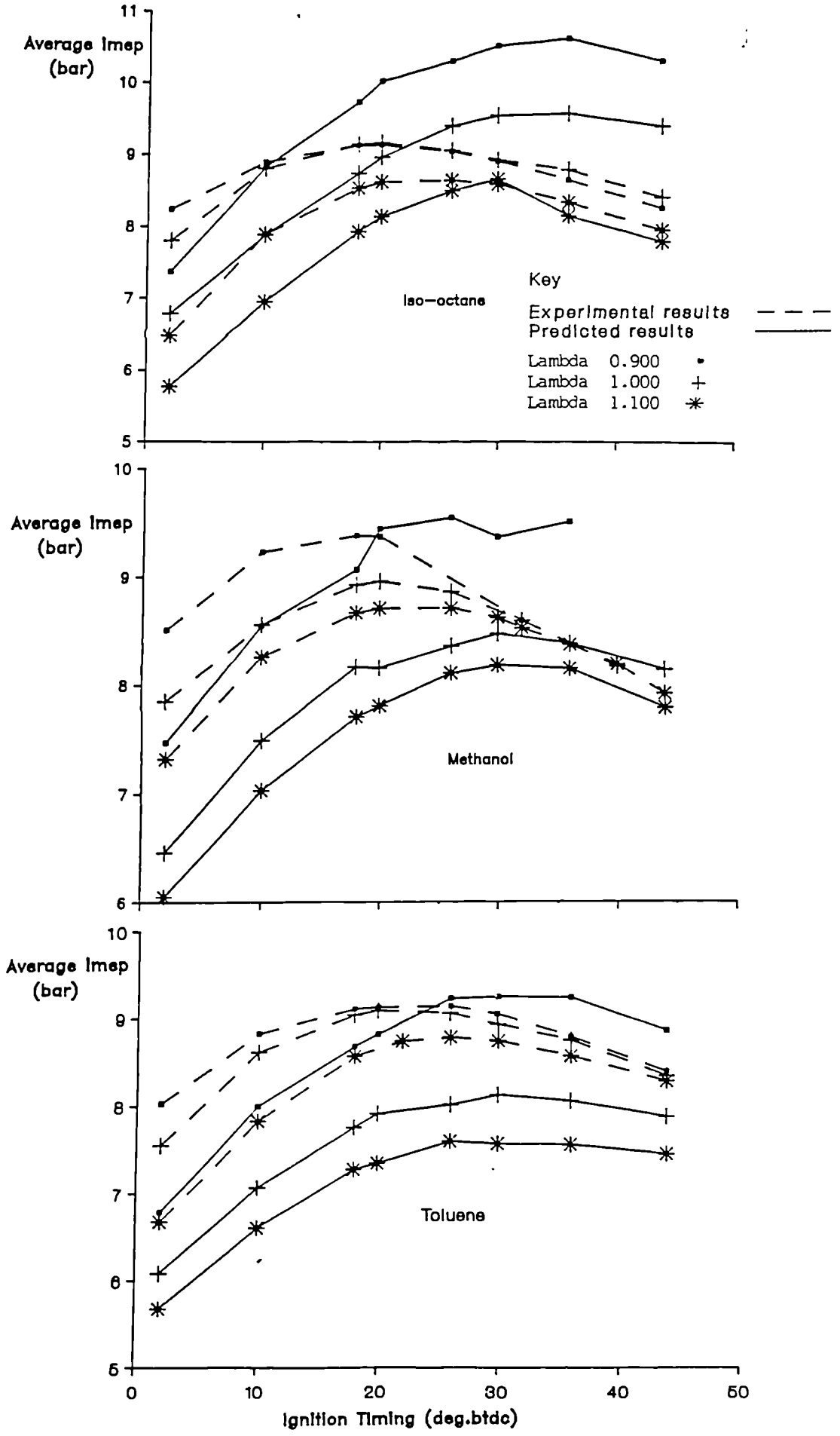

Figure 5.1: Comparison of experimental and predicted values for the variation of average imep with ignition timing and mixture strength for the fuels tested.

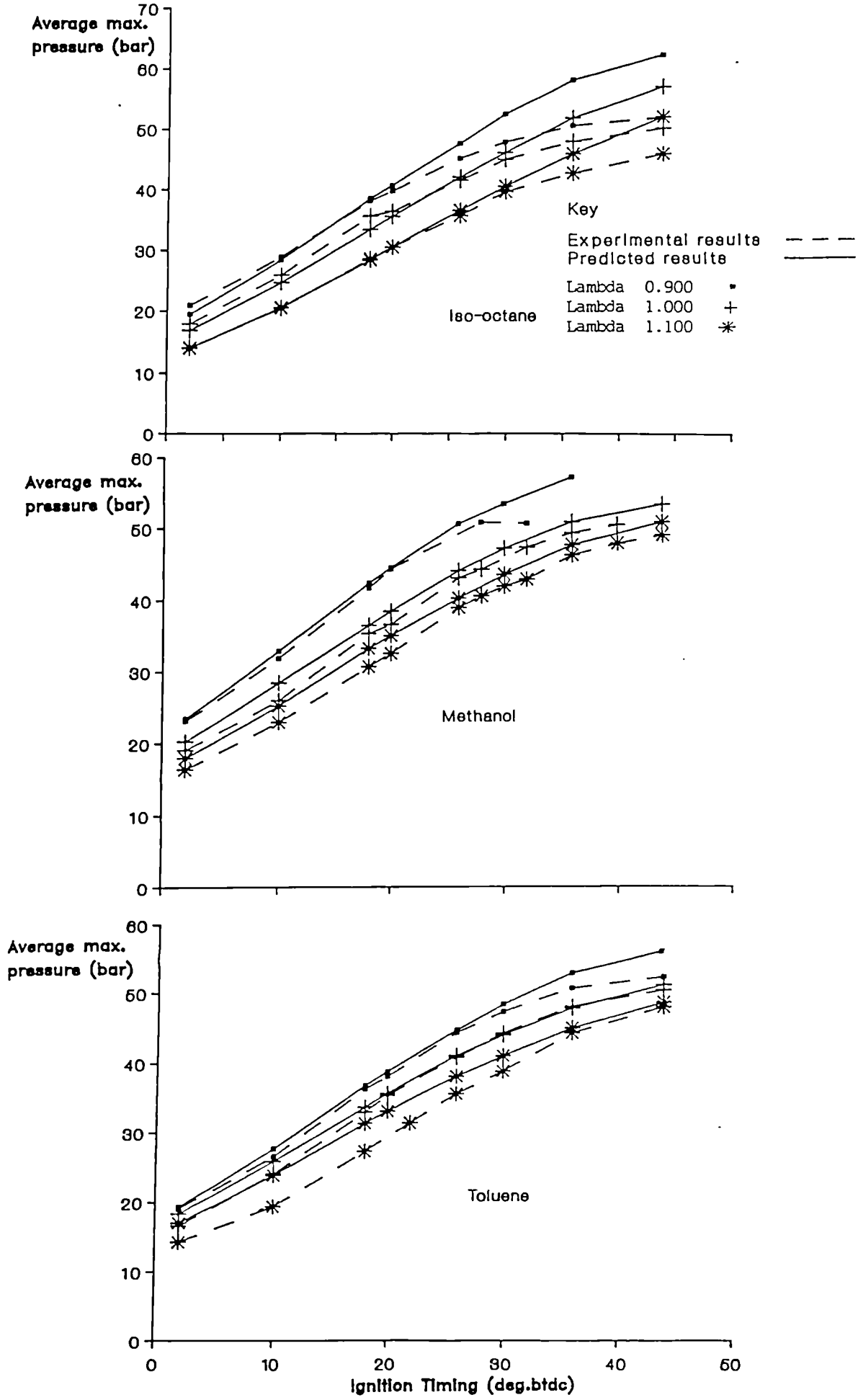

Figure 5.2: Comparison of experimental and predicted values for the variation of average maximum pressure with ignition timing and mixture strength for the fuels tested.

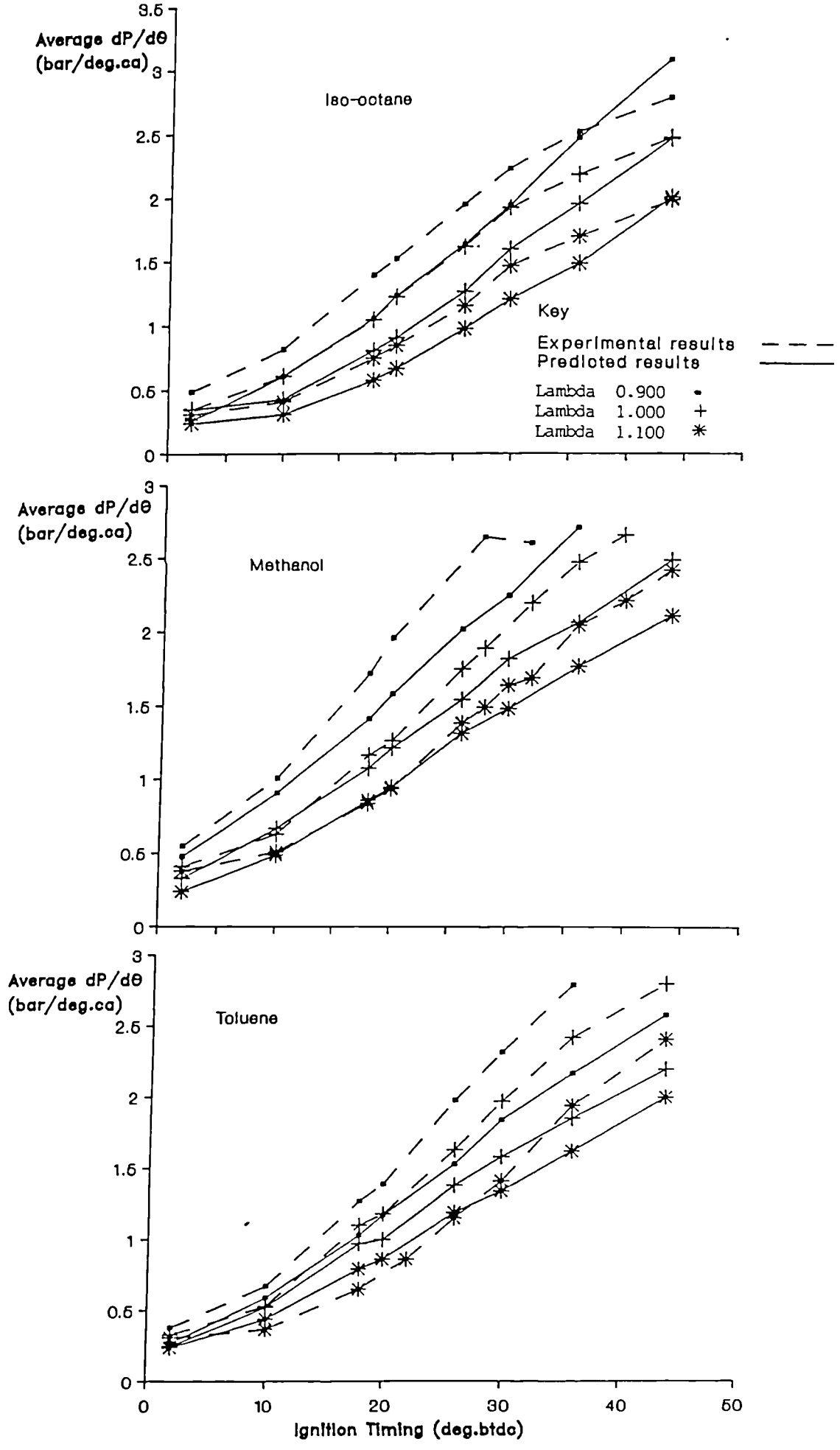

Figure 5.3: Comparison of experimental and predicted values for the variation of average maximum rate of pressure rise with ignition timing and mixture strength for the fuels tested.

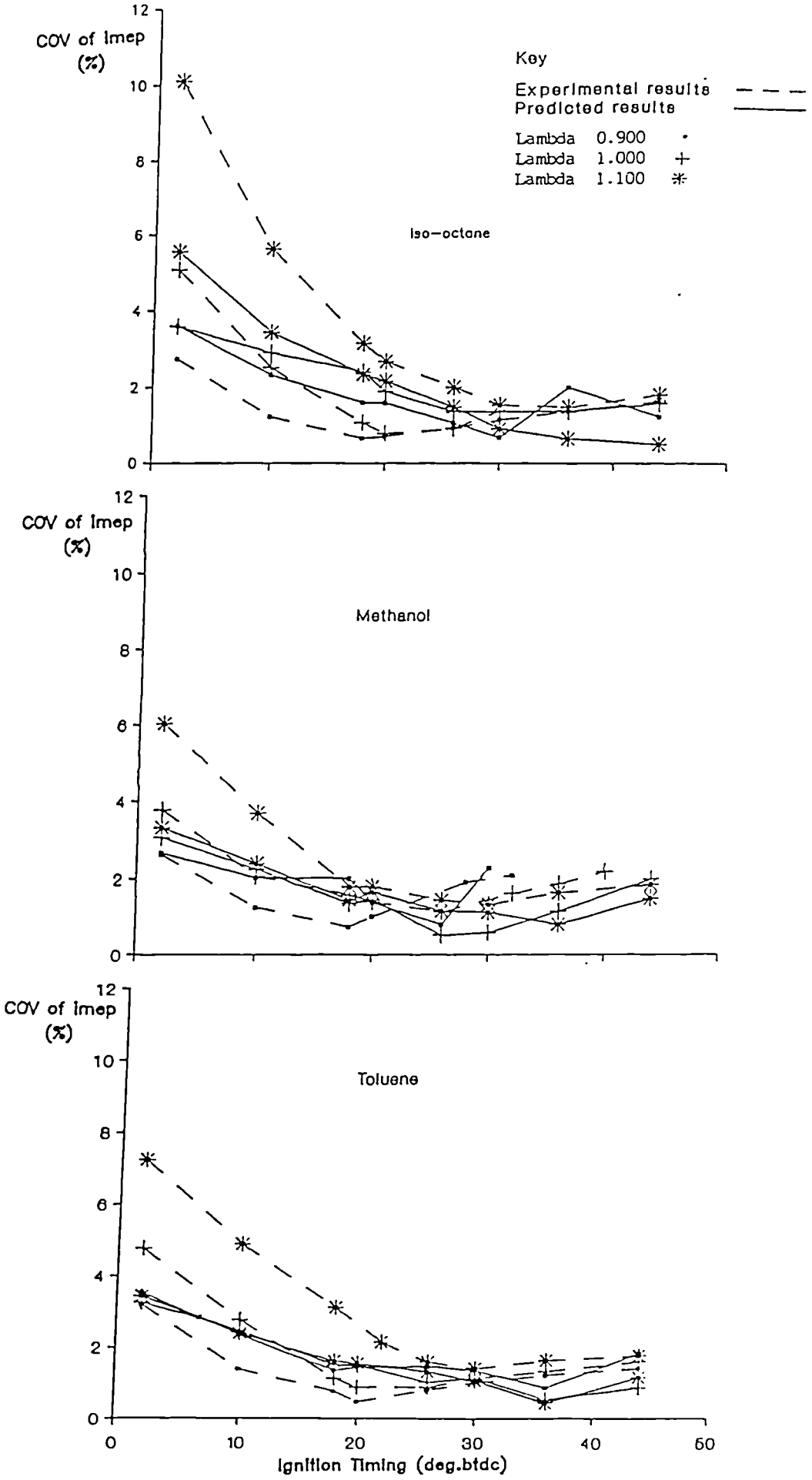

Figure 5.4: Comparison of experimental and predicted values for the variation in COV of imep with ignition timing and mixture strength for the fuels tested.

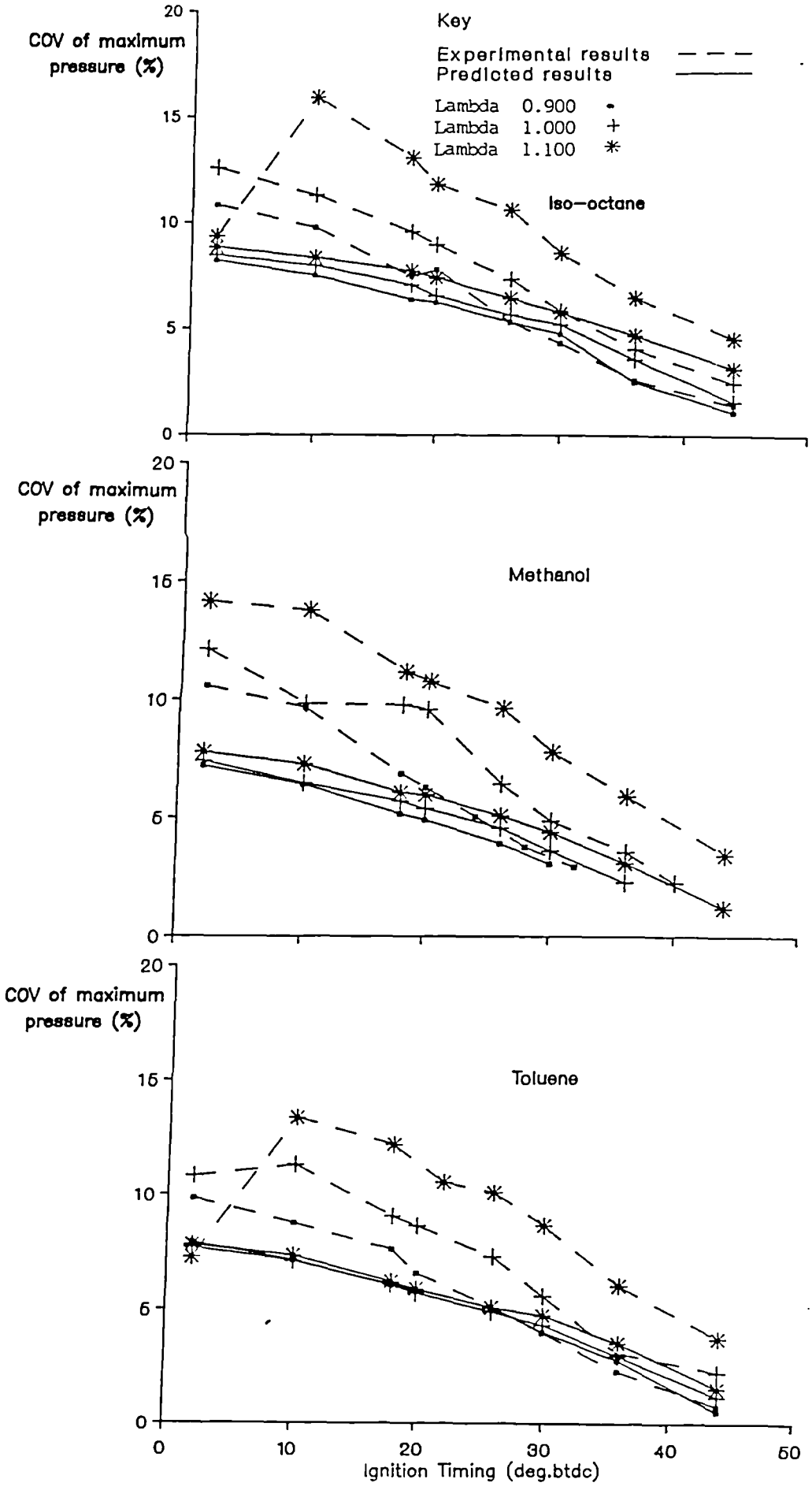

Figure 5.5: Comparison of experimental and predicted values for the variation in COV of maximum pressure with ignition timing and mixture strength for the fuels tested.

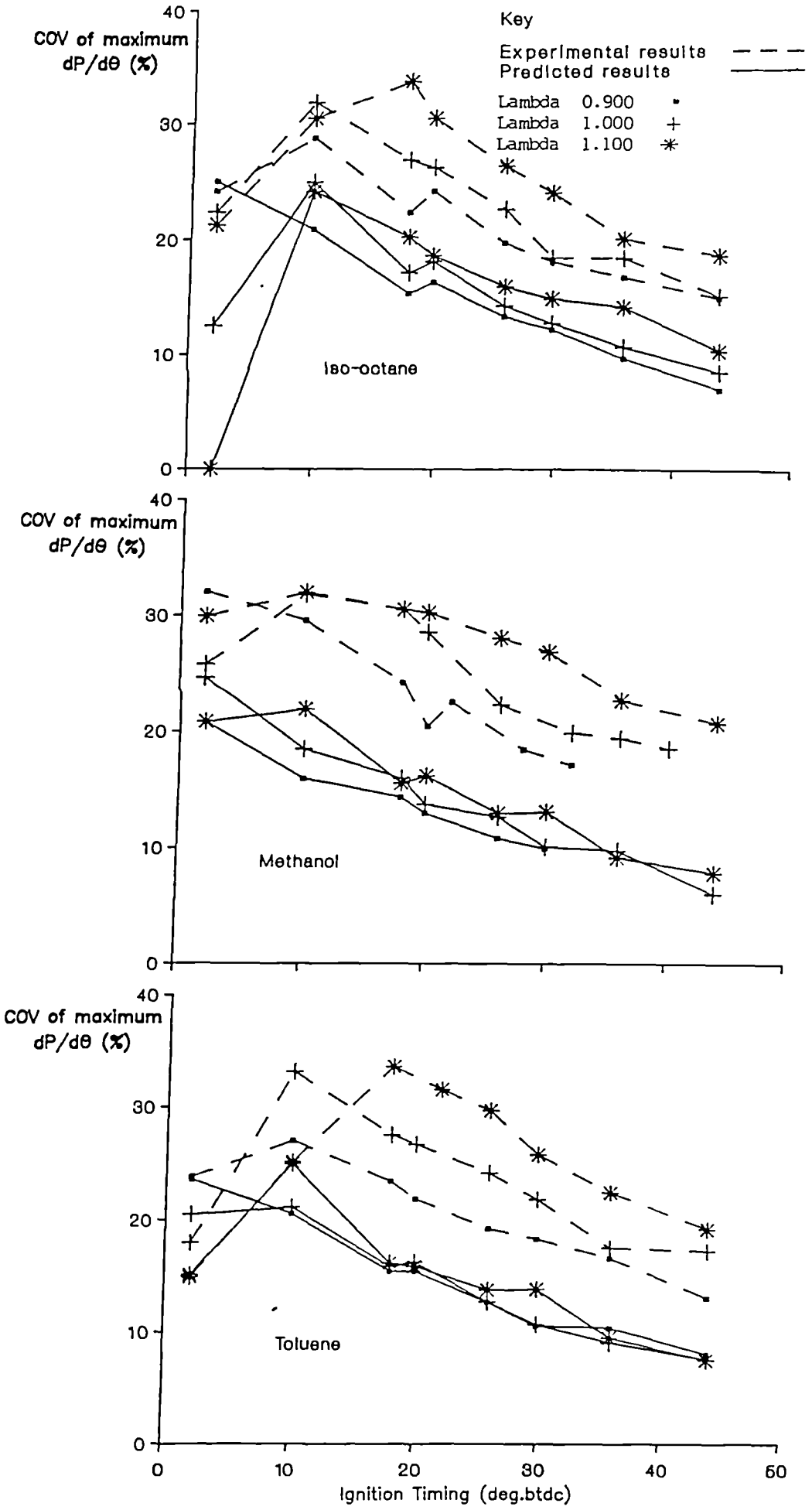

Figure 5.6: Comparison of experimental and predicted values for the variation in COV of maximum rate of pressure rise with ignition timing and mixture strength for the fuels tested.

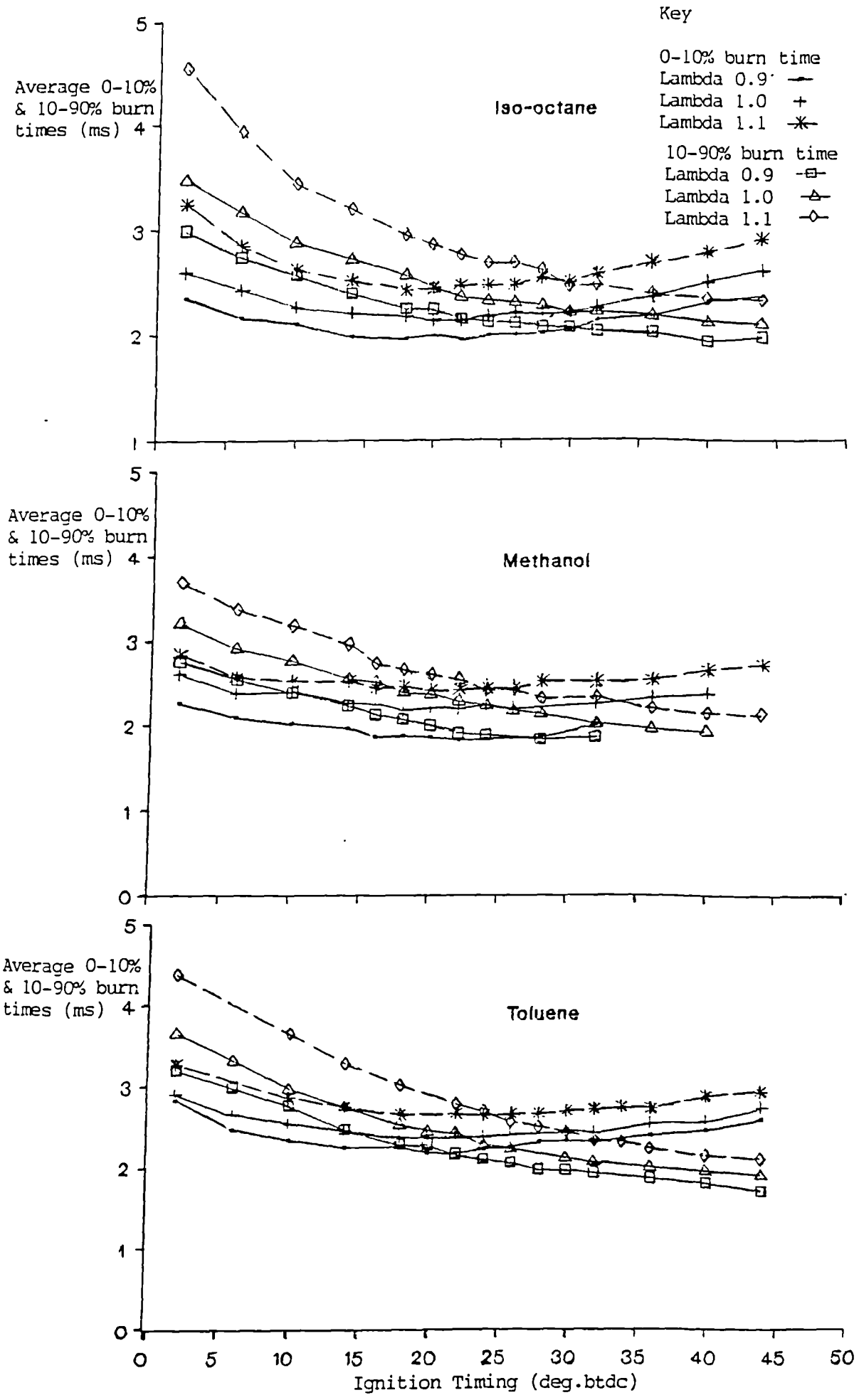

Figure 5.7: Variation of average 0-10% and 10-90% burn times with ignition timing and mixture strength for the fuels tested.

PAGE
MISSING

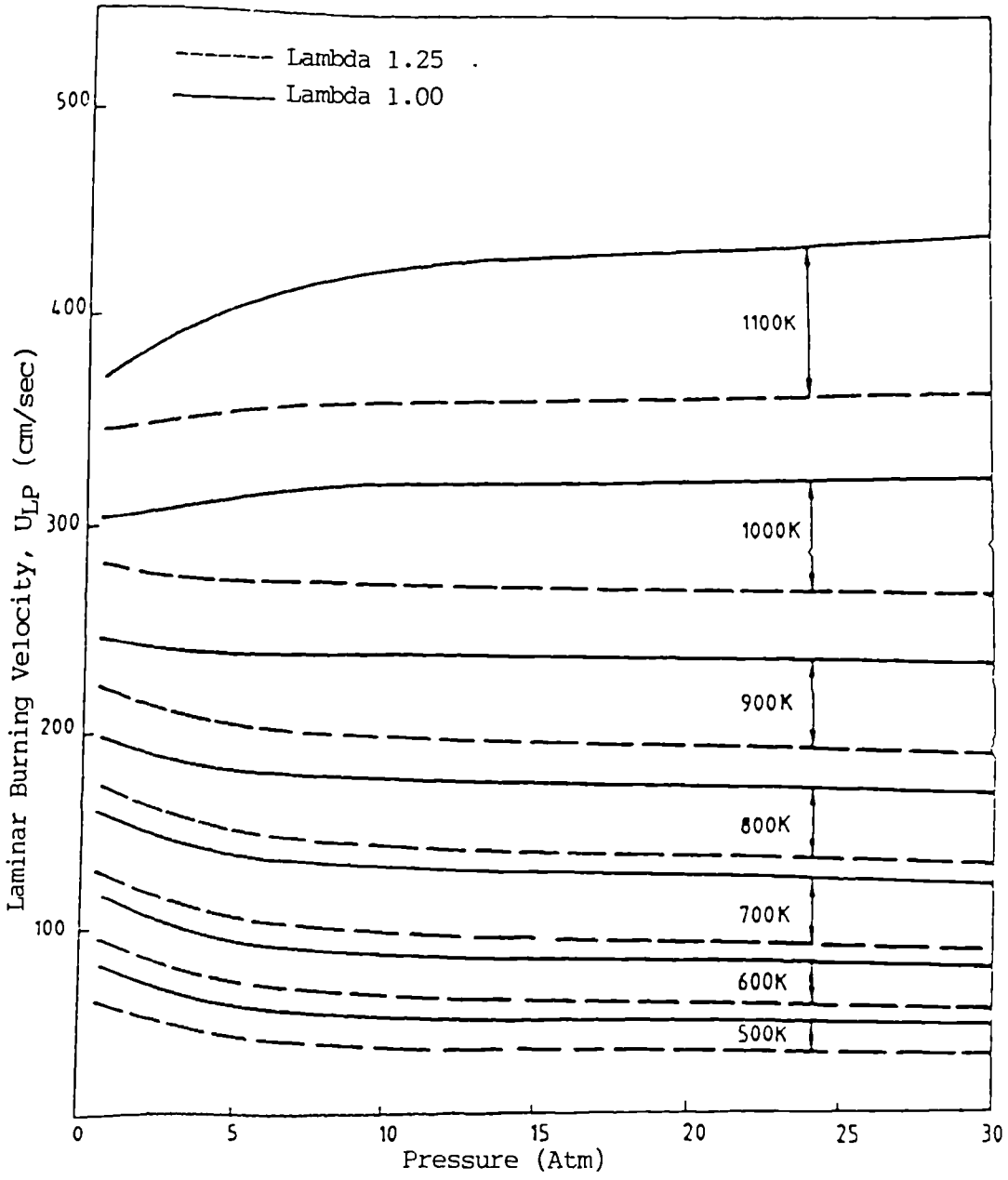

Figure 5.9: Predicted laminar burning velocities for iso-octane/air mixtures, James (1987).

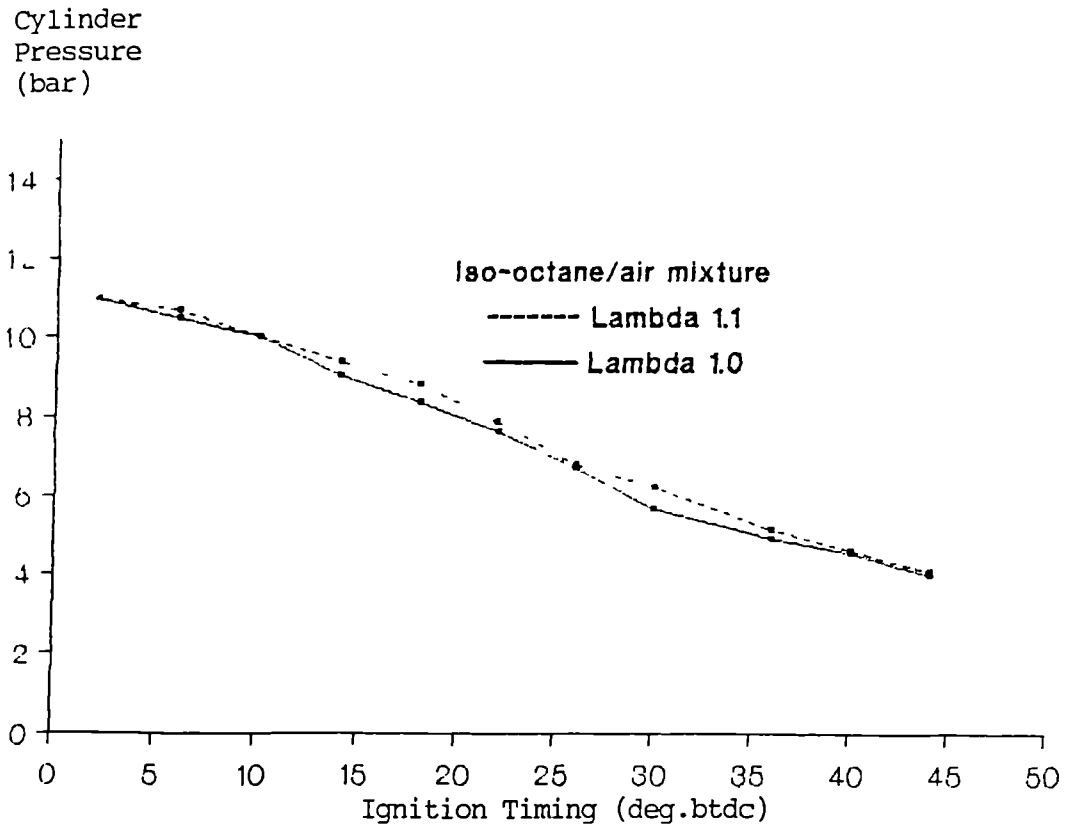

Figure 5.10: Variations in cylinder pressure at the point of ignition with changes in ignition timing.

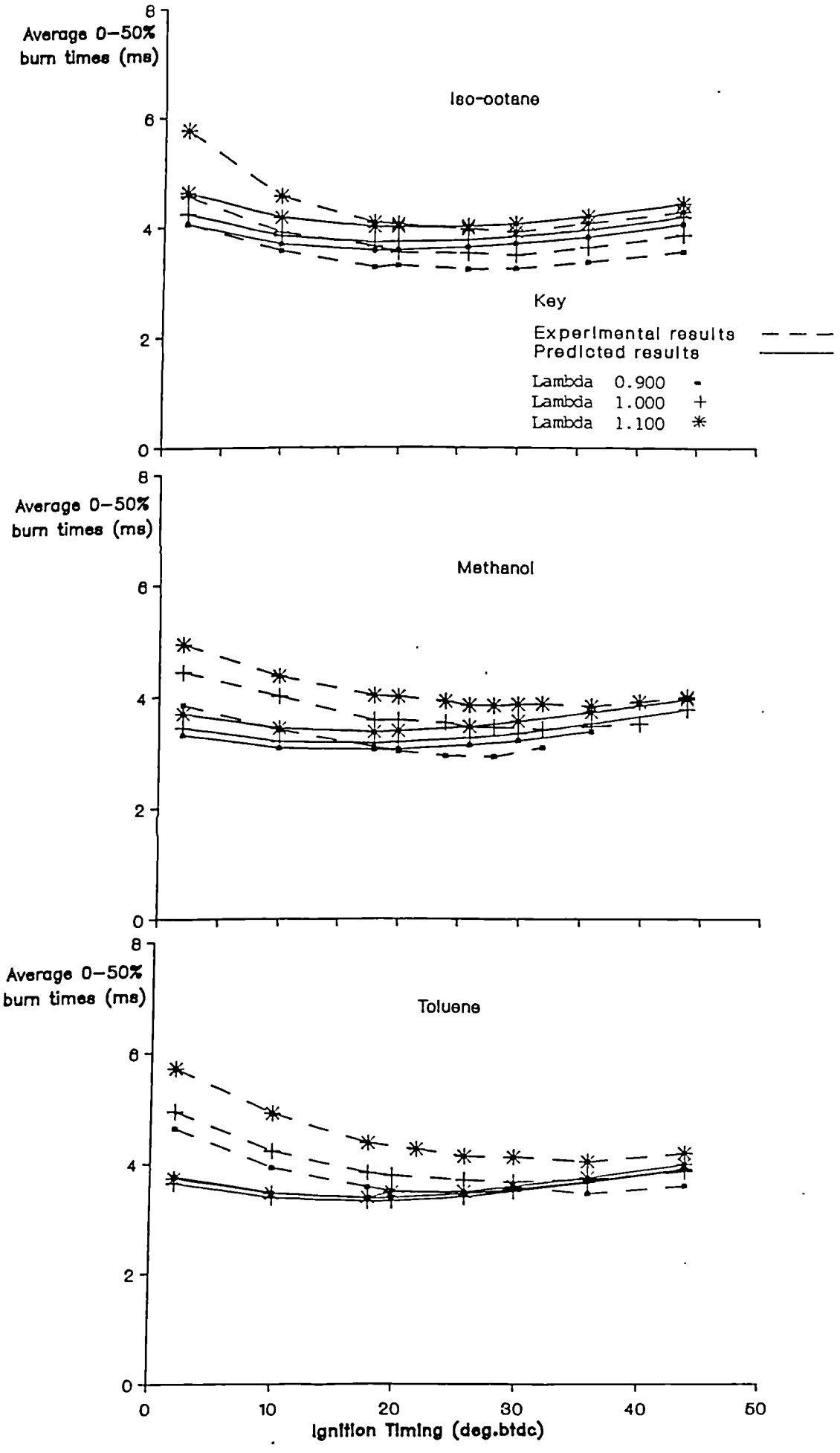

Figure 5.11: Comparison of experimental and predicted values for the variation in average 0-50% burn times with ignition timing and mixture strength for the fuels tested.

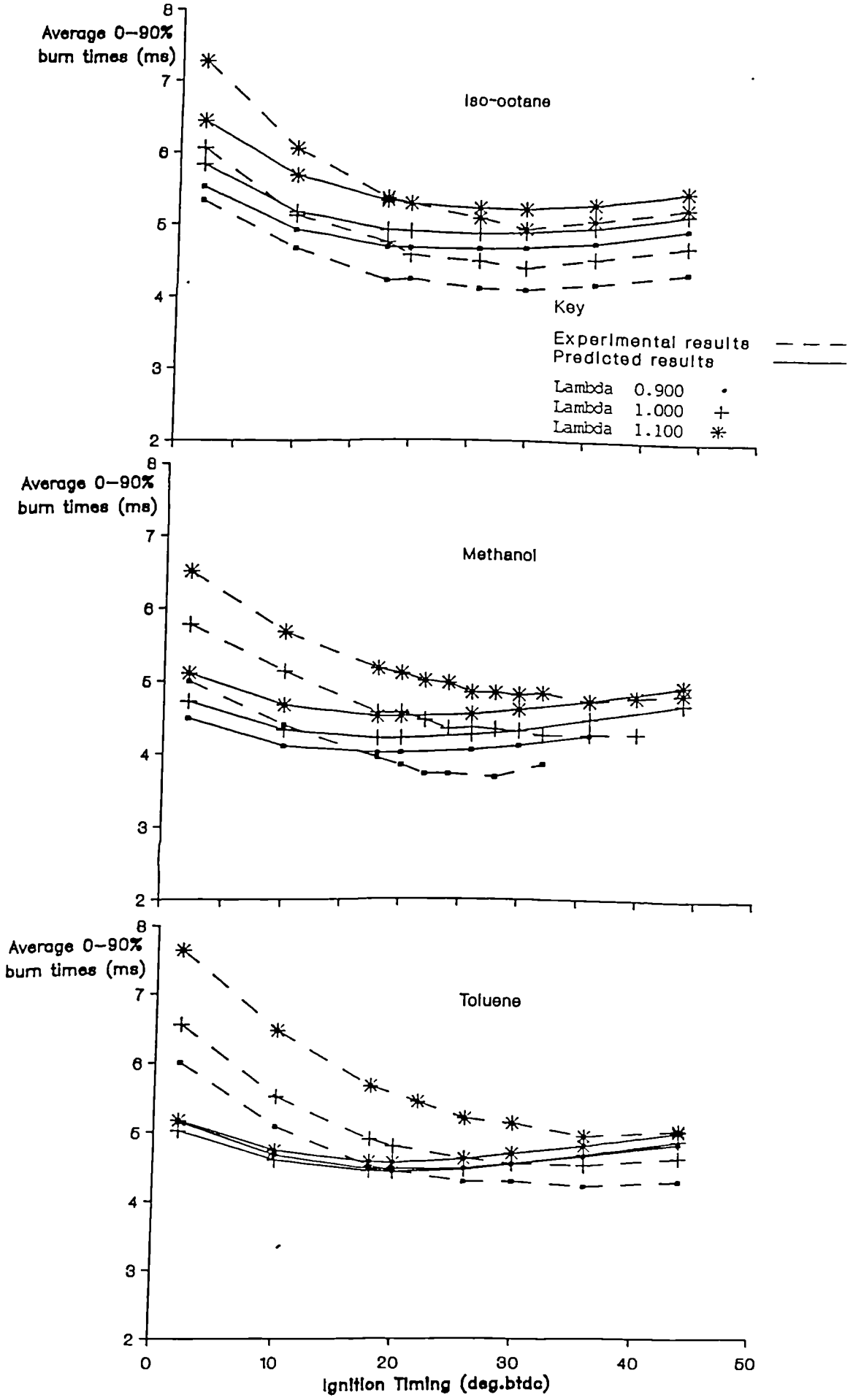

Figure 5.12: Comparison of experimental and predicted values for the variation in average 0-90% burn times with ignition timing and mixture strength for the fuels tested.

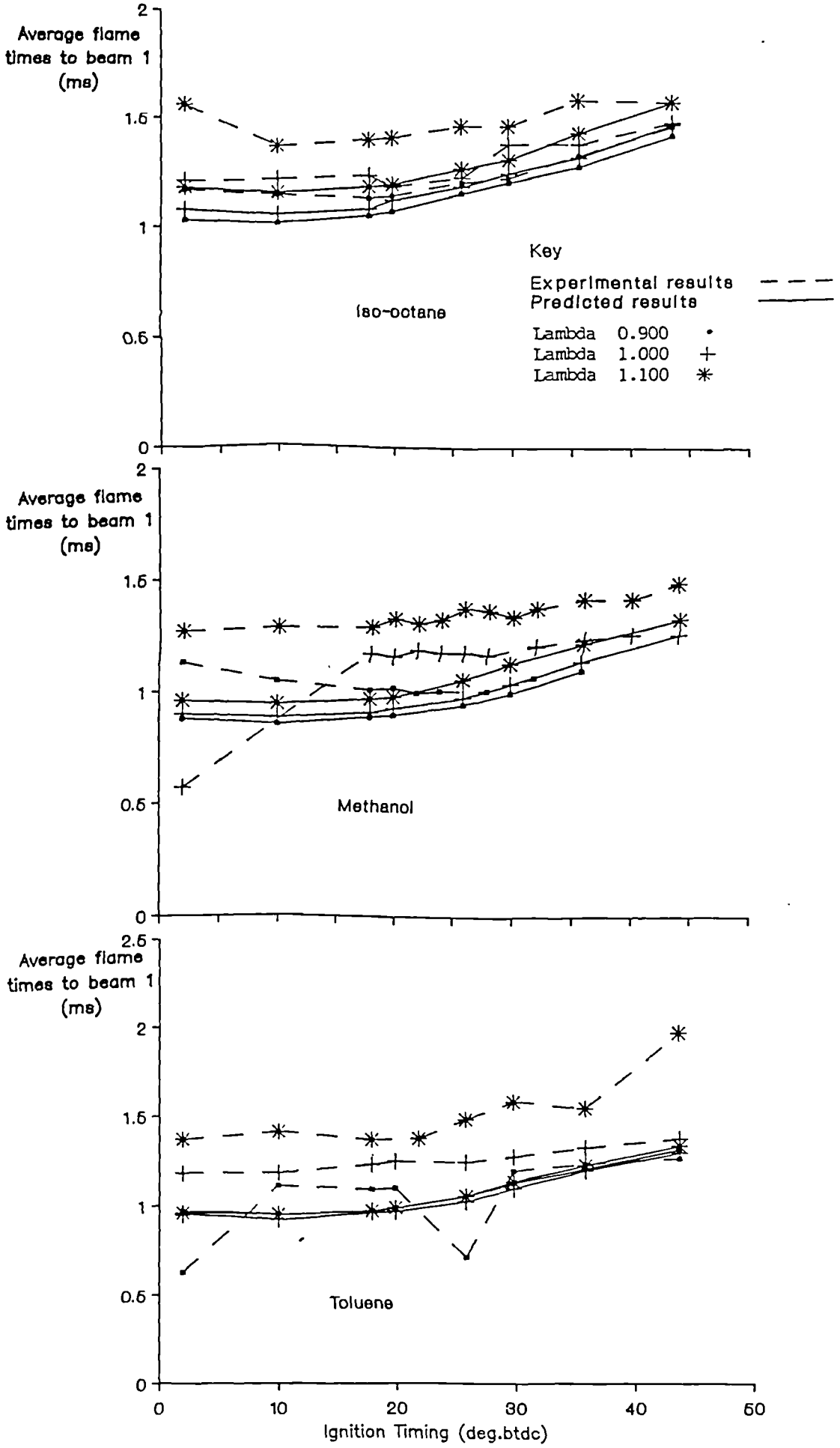

Figure 5.13: Comparison of experimental and predicted values for the variation in average flame times to beam 1 with ignition timing and mixture strength for the fuels tested.

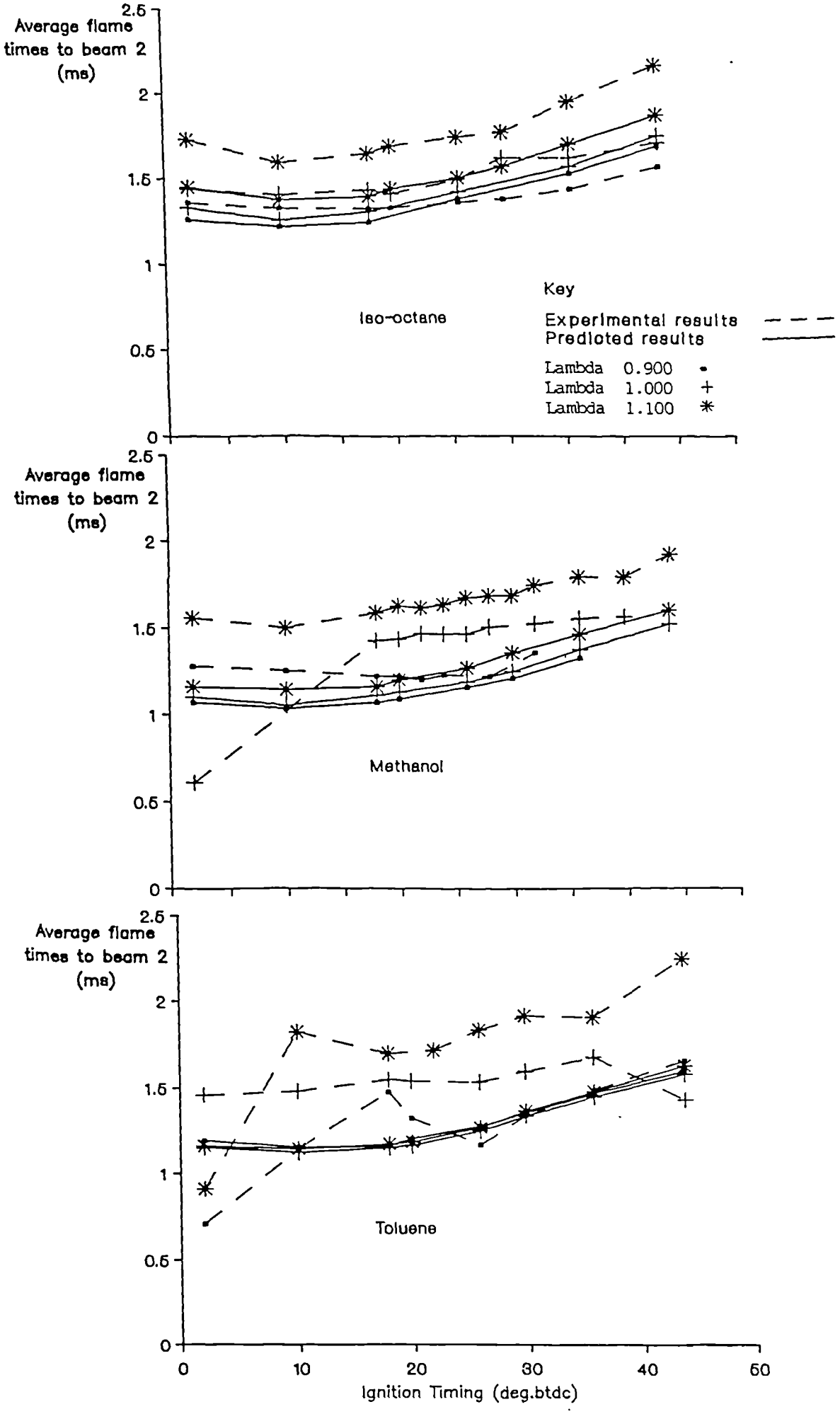

Figure 5.14: Comparison of experimental and predicted values for the variation in average flame times to beam 2 with ignition timing and mixture strength for the fuels tested.

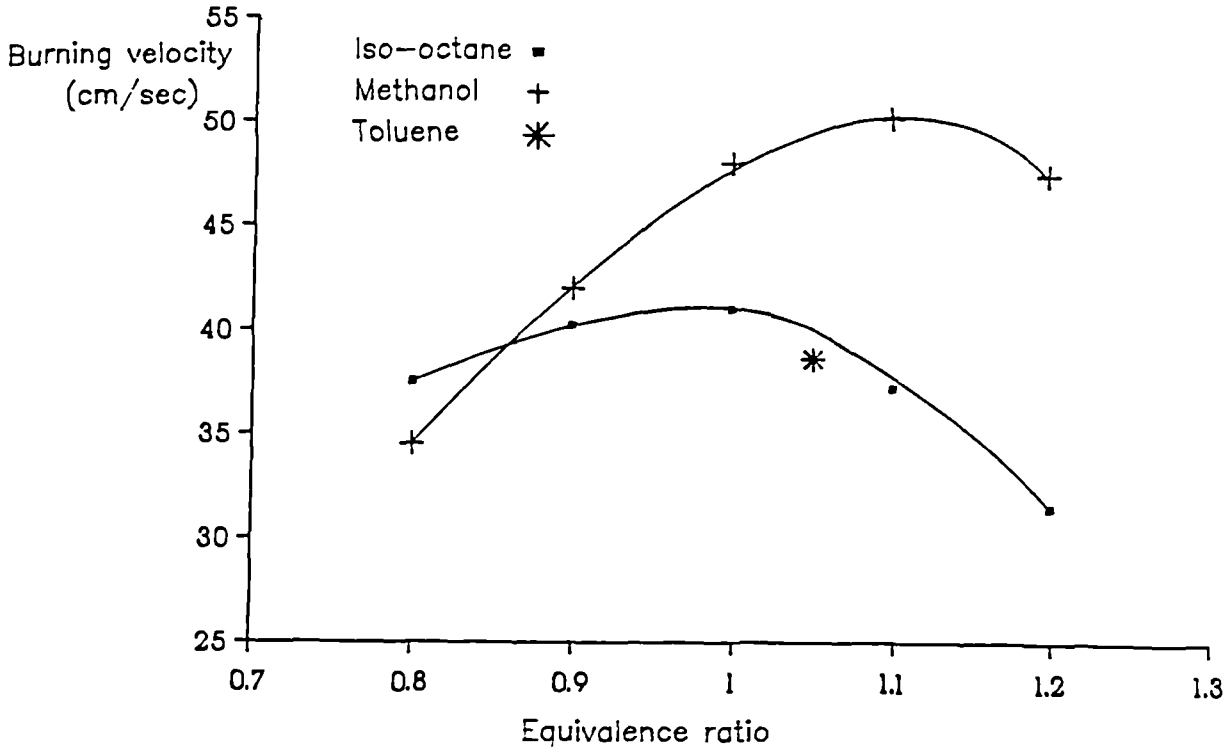

Figure 5.15: Laminar burning velocity for iso-octane and methanol as a function of equivalence ratio, at 1 atm. and 297K, Gibbs and Calcote 1959, and the maximum burning velocity of toluene at the same conditions, Kanury 1975.

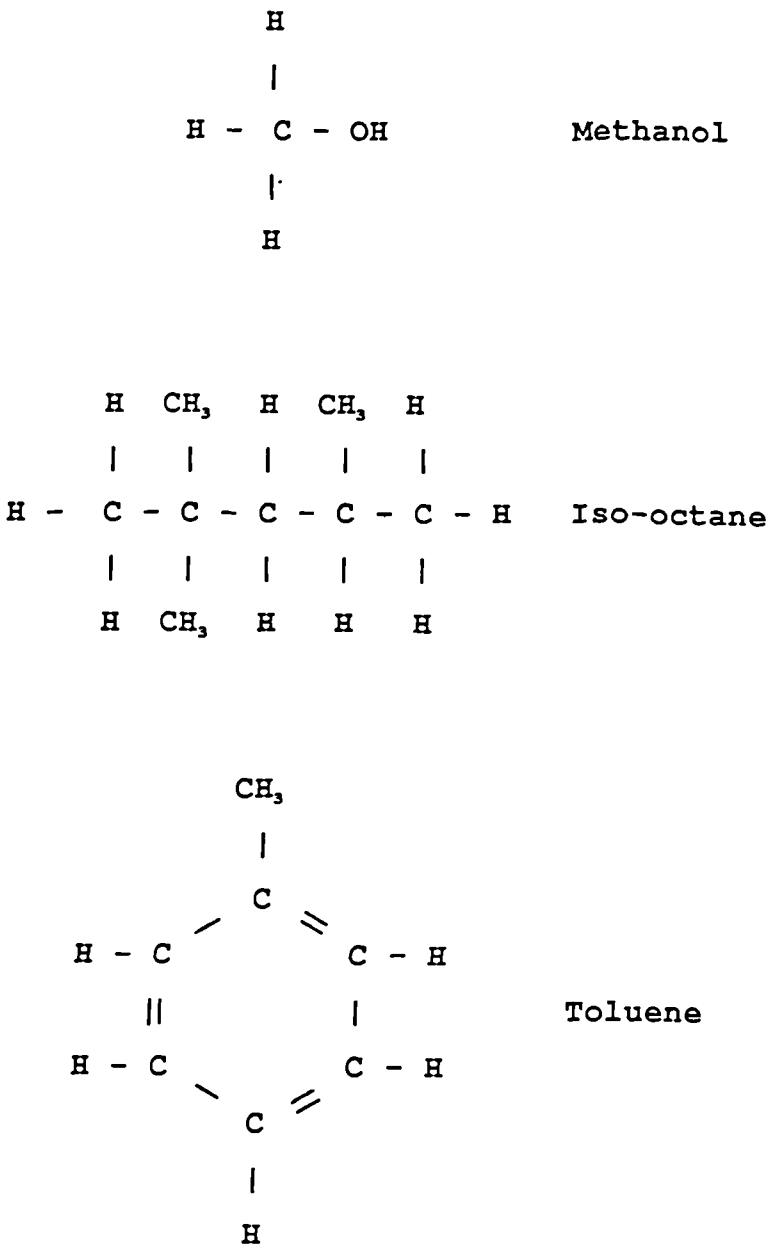

Figure 5.16: Diagram showing the different molecular structure of the three fuels tested.

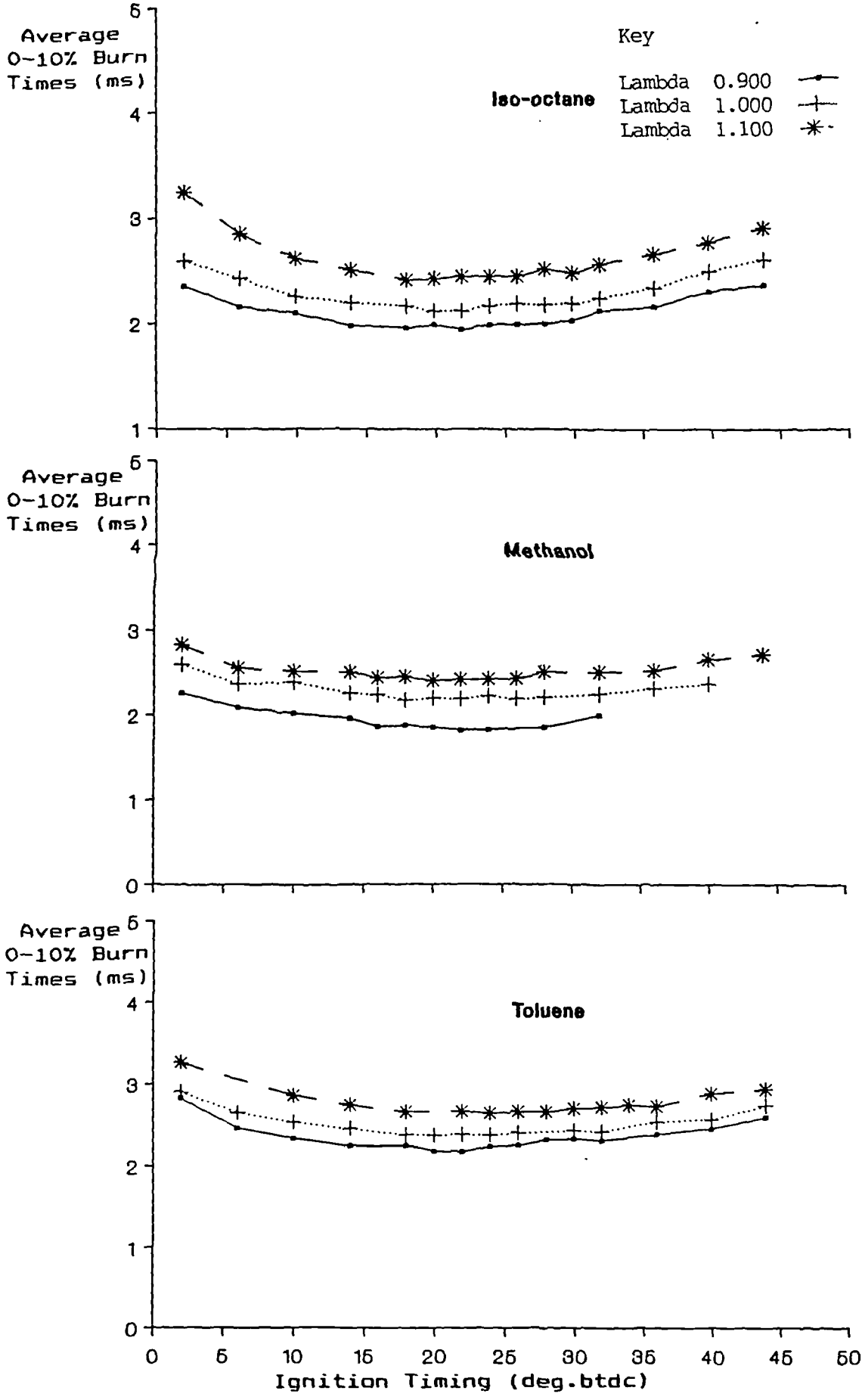

Figure 5.17: Average 0-10% burn times plotted on a fuel by fuel basis.

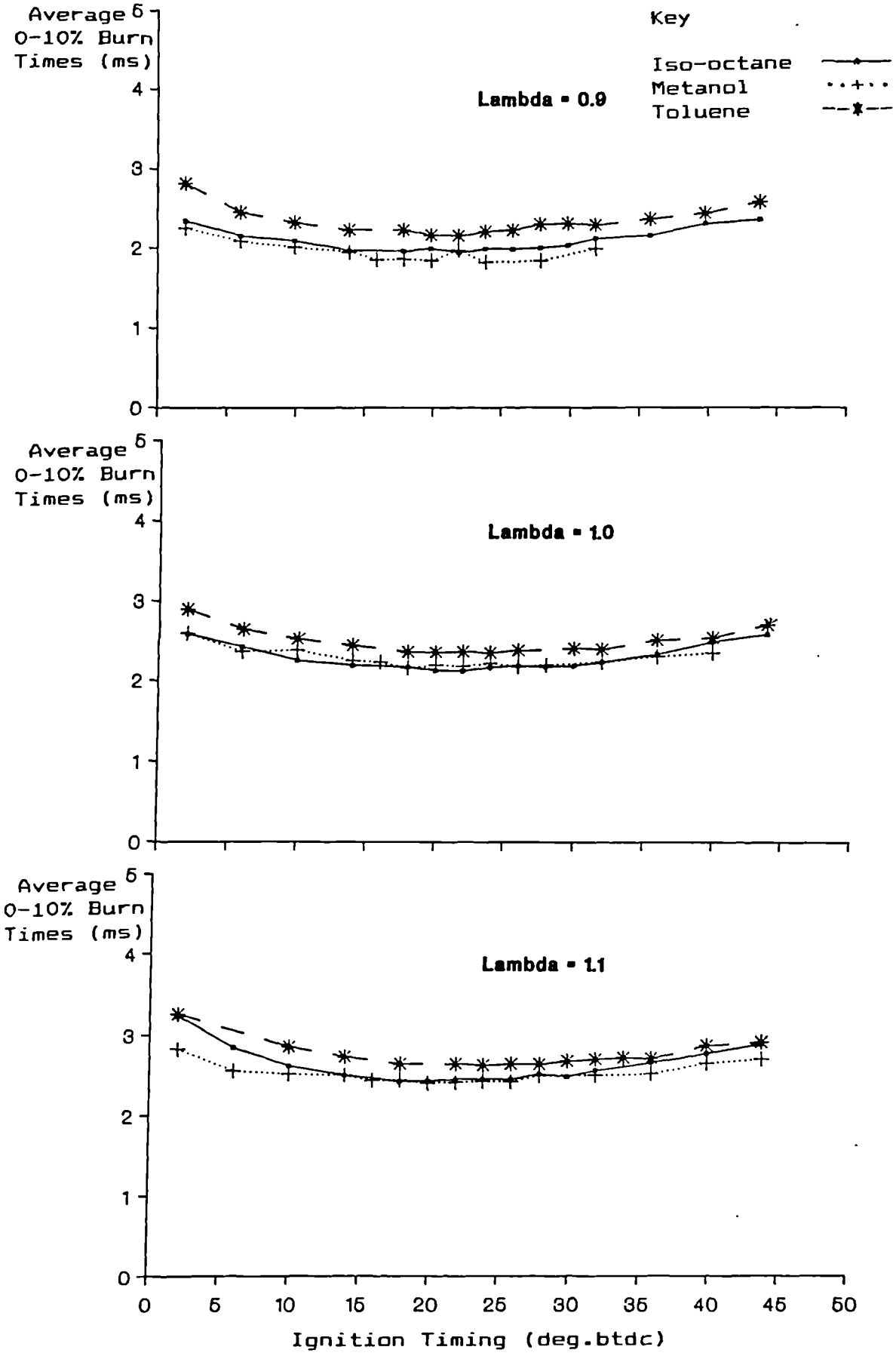

Figure 5.18: Average 0-10% burn times plotted on a lambda by lambda basis.

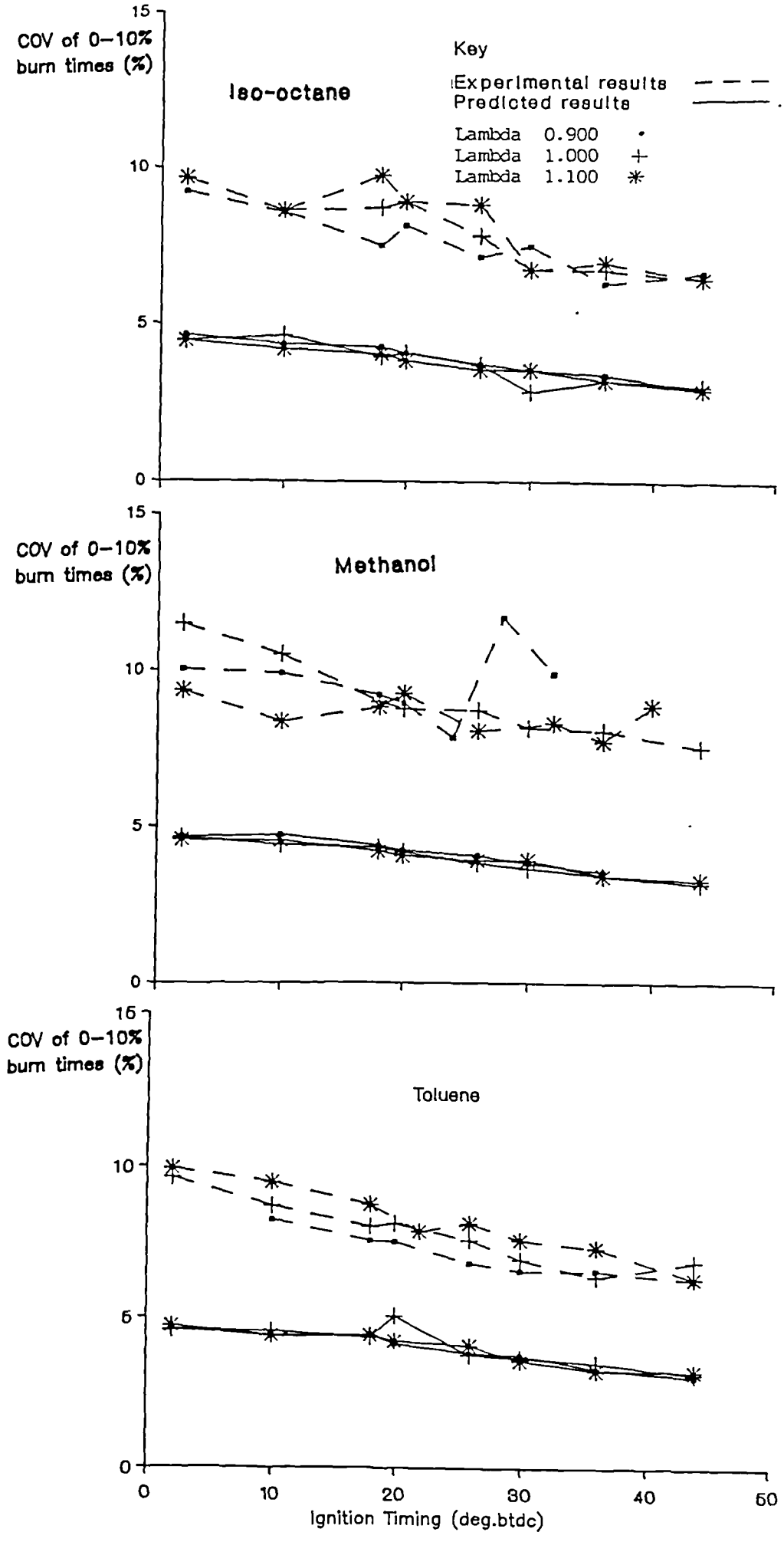

Figure 5.19: Comparison of experimental and predicted values for the variation in COV of 0-10% burn times with ignition timing and mixture strength for the fuels tested.

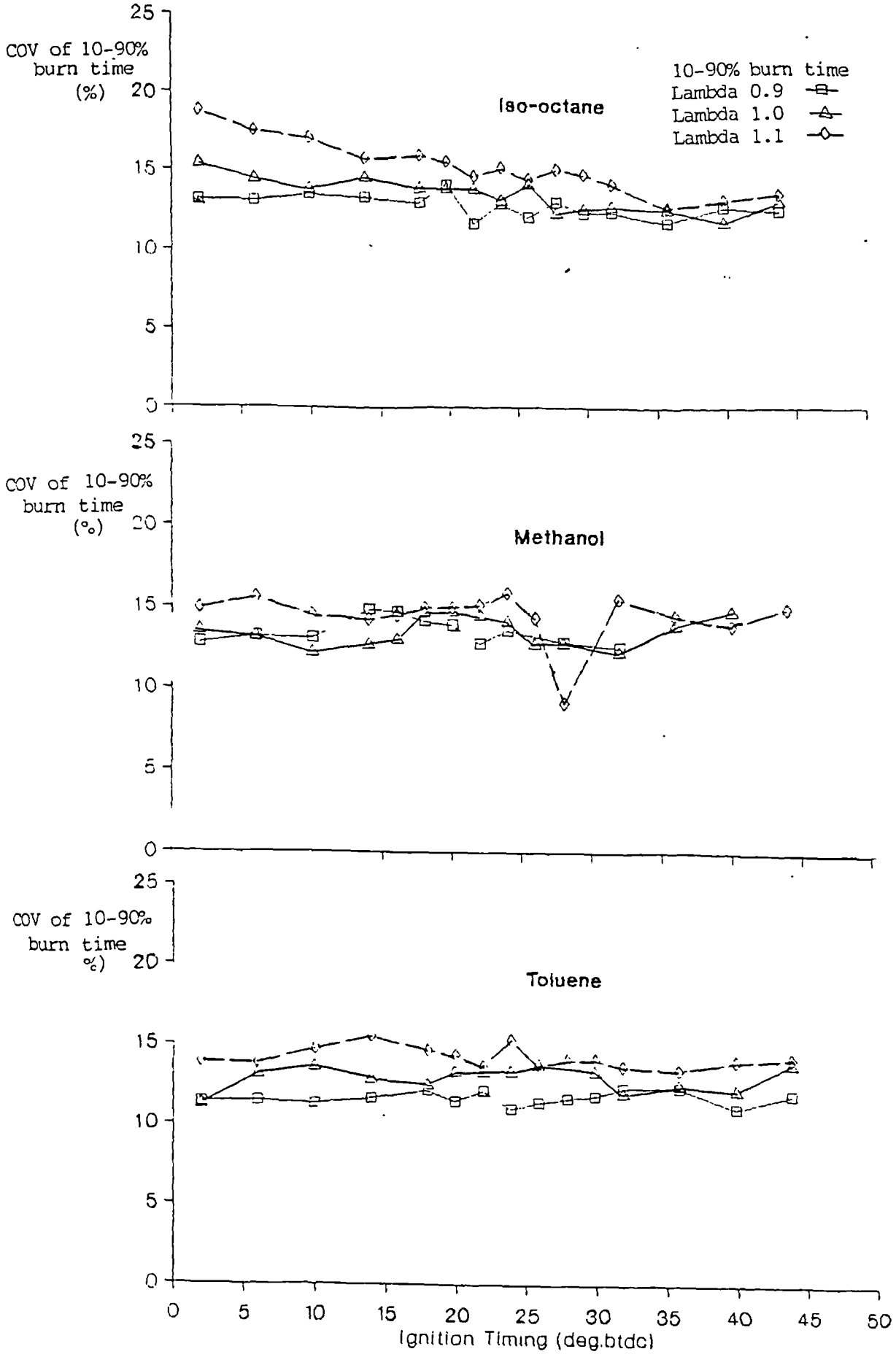

Figure 5.20: Variation in COV of 10-90% burn times with ignition timing and mixture strength for the fuels tested.

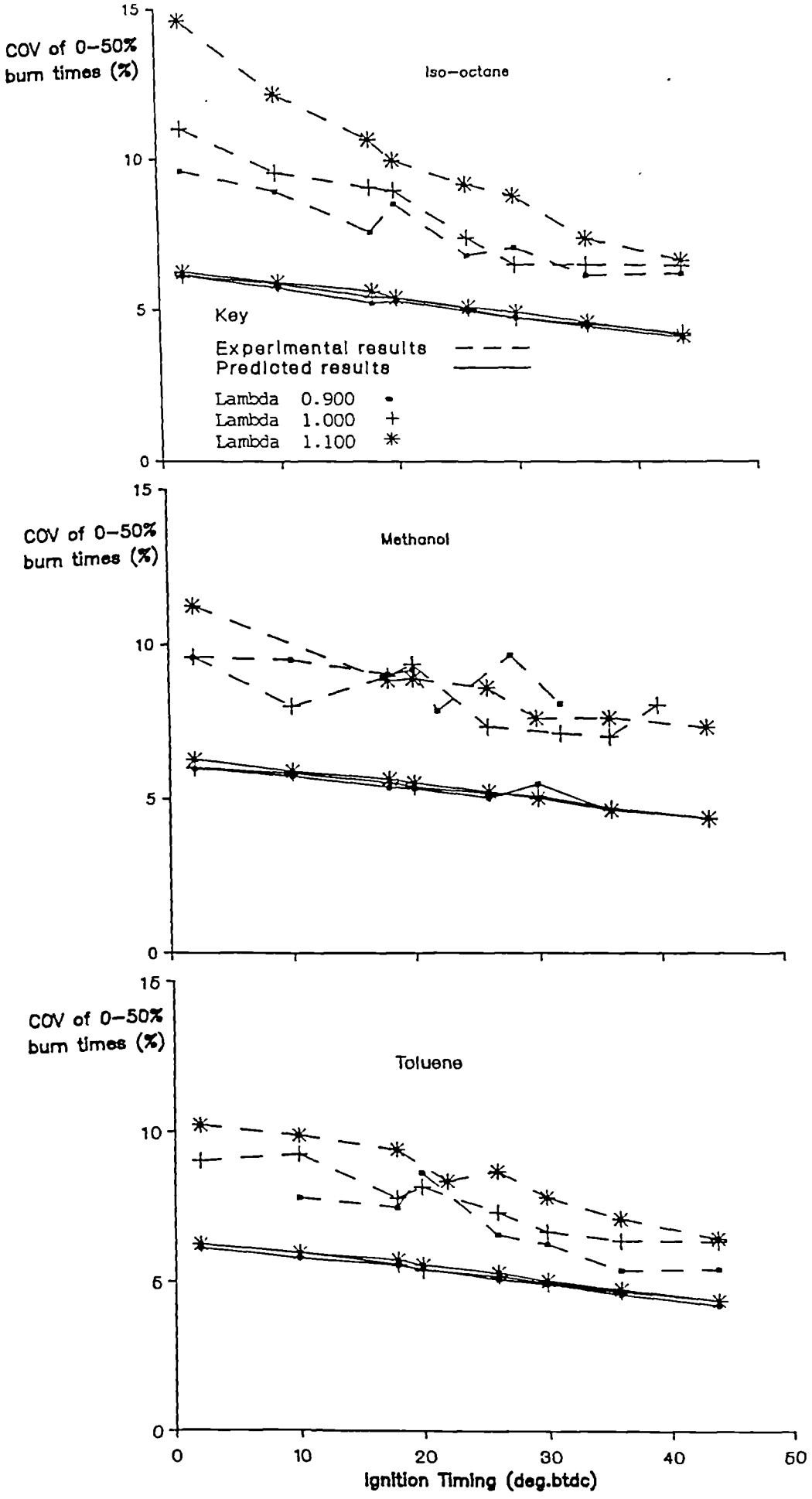

Figure 5.21: Comparison of experimental and predicted values for the variation in COV of 0-50% burn times with ignition timing and mixture strength for the fuels tested.

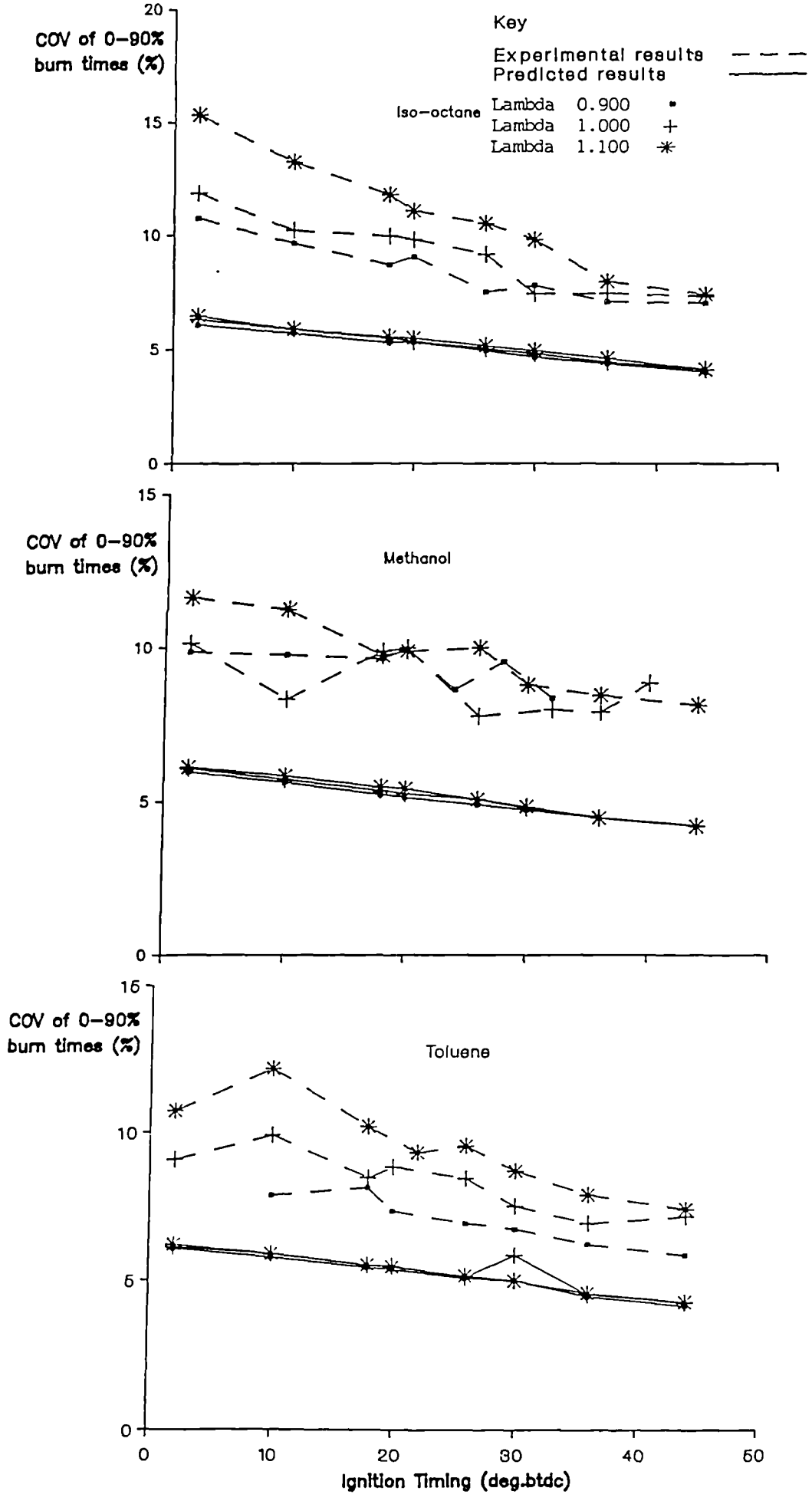

Figure 5.22: Comparison of experimental and predicted values for the variation in COV of 0-90% burn times with ignition timing and mixture strength for the fuels tested.

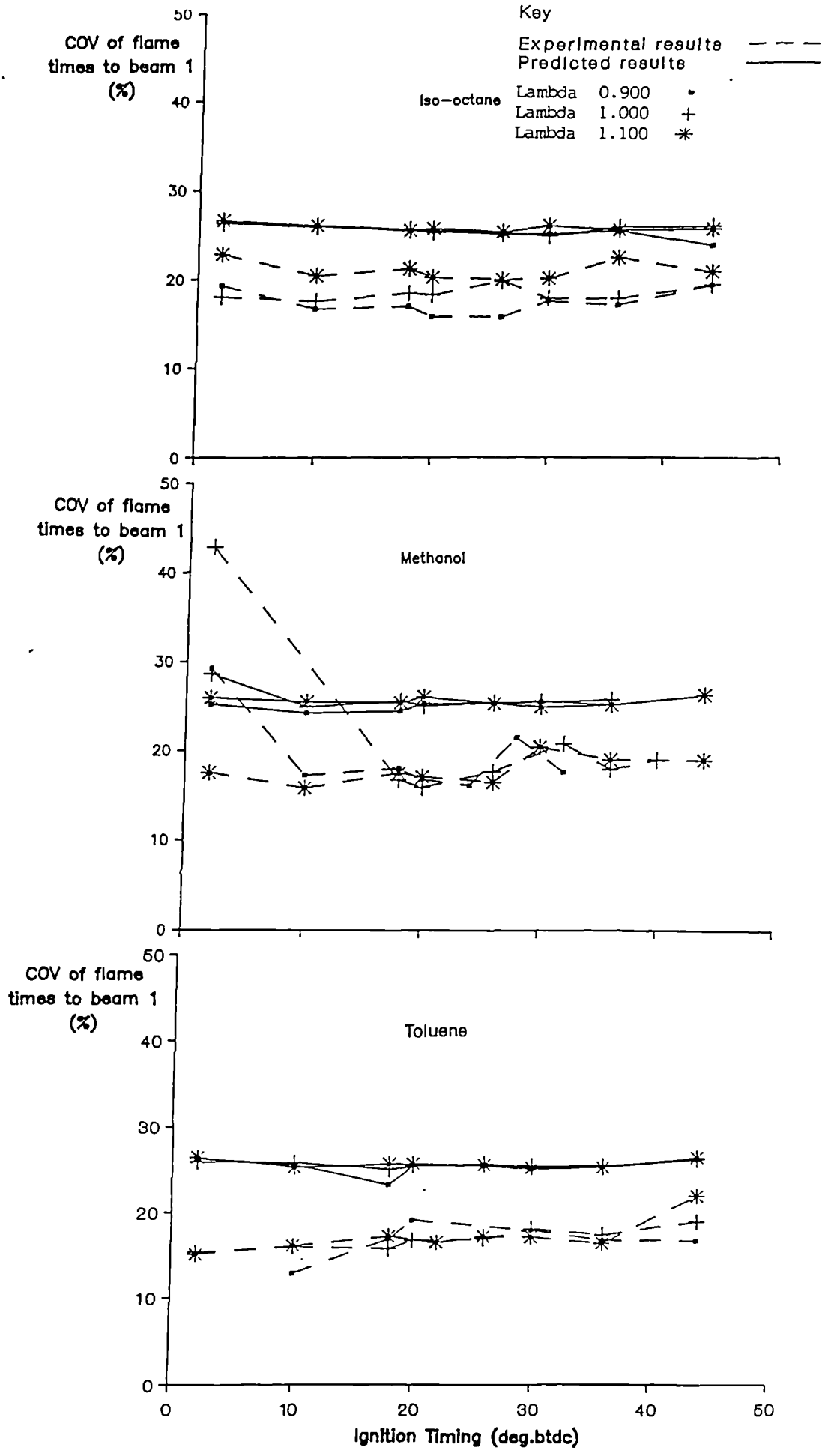

Figure 5.23: Comparison of experimental and predicted values for the variation in COV of flame times to beam 1 with ignition timing and mixture strength for the fuels tested.

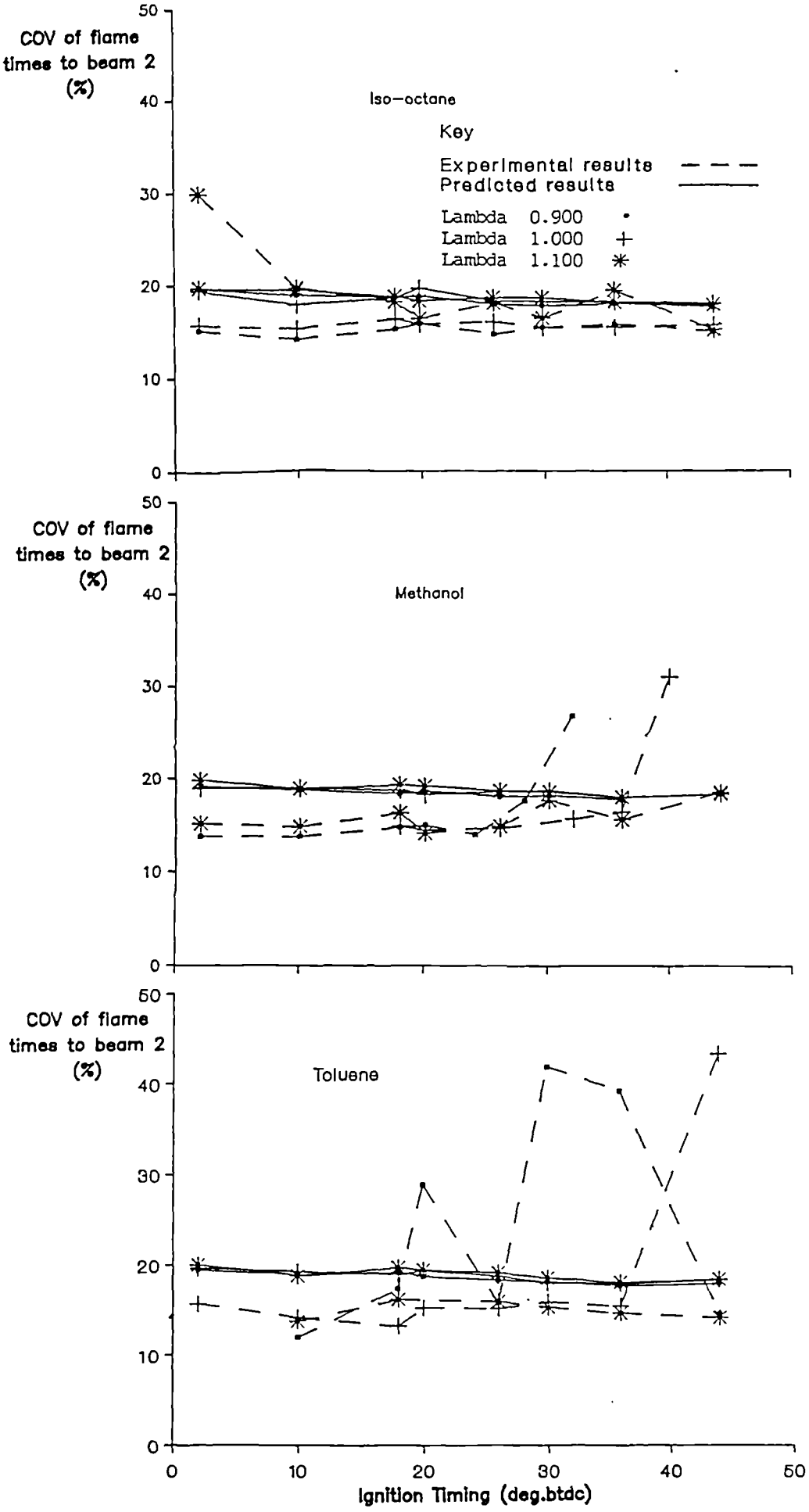

Figure 5.24: Comparison of experimental and predicted values for the variation in COV of flame times to beam 2 with ignition timing and mixture strength for the fuels tested.

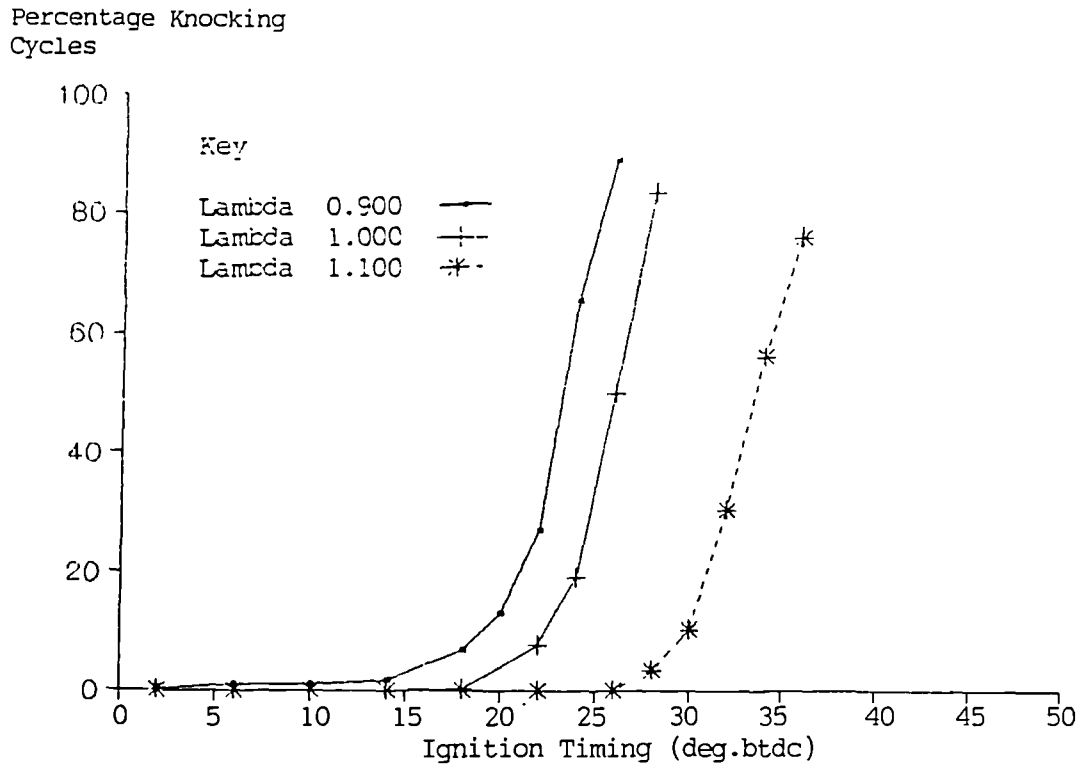

Figure 5.25: Variation in percentage knocking cycles with ignition timing and mixture strength.

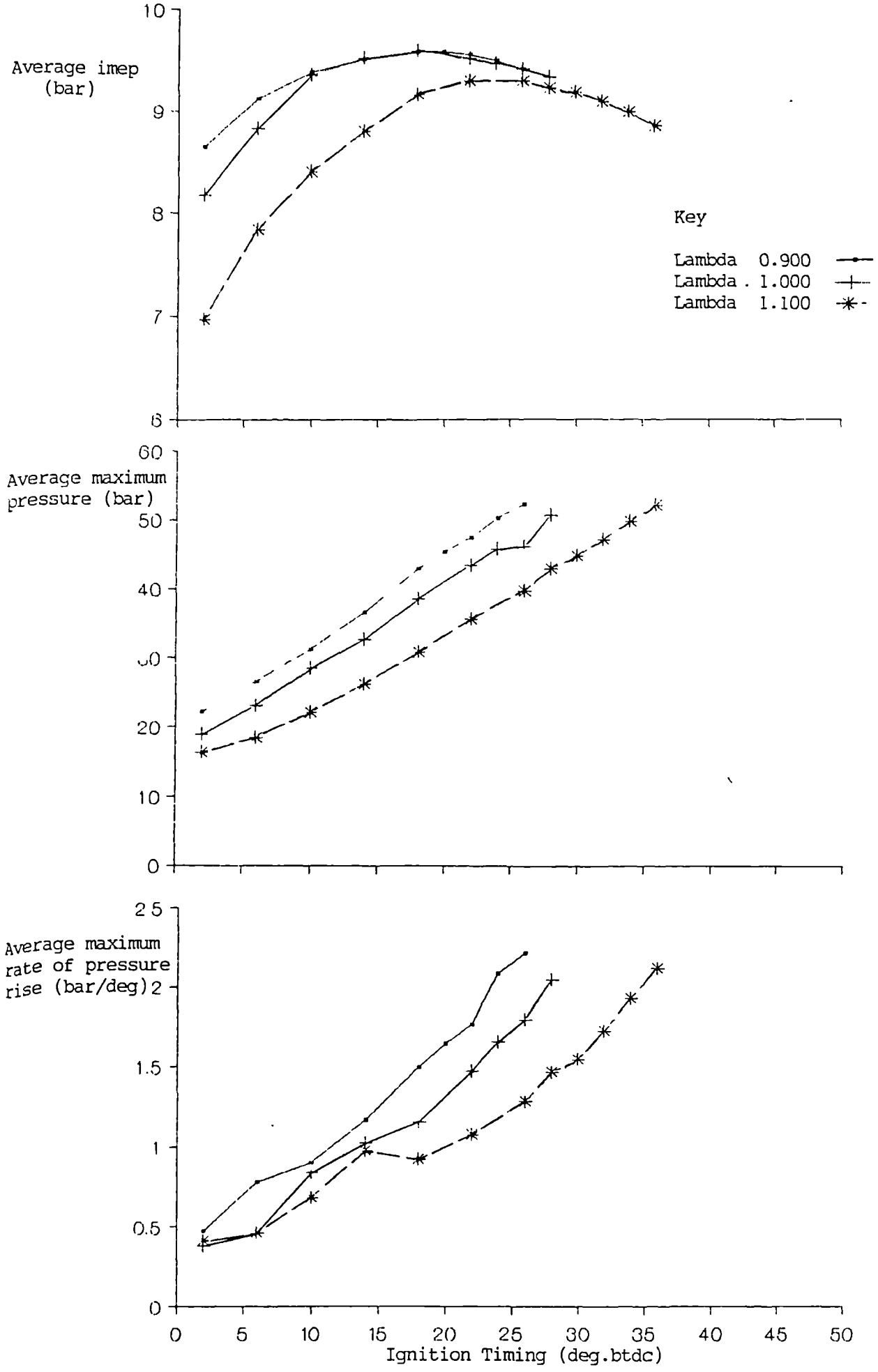

Figure 5.26: Variation in average measured engine parameters with ignition timing and mixture strength for the tests with knock present.

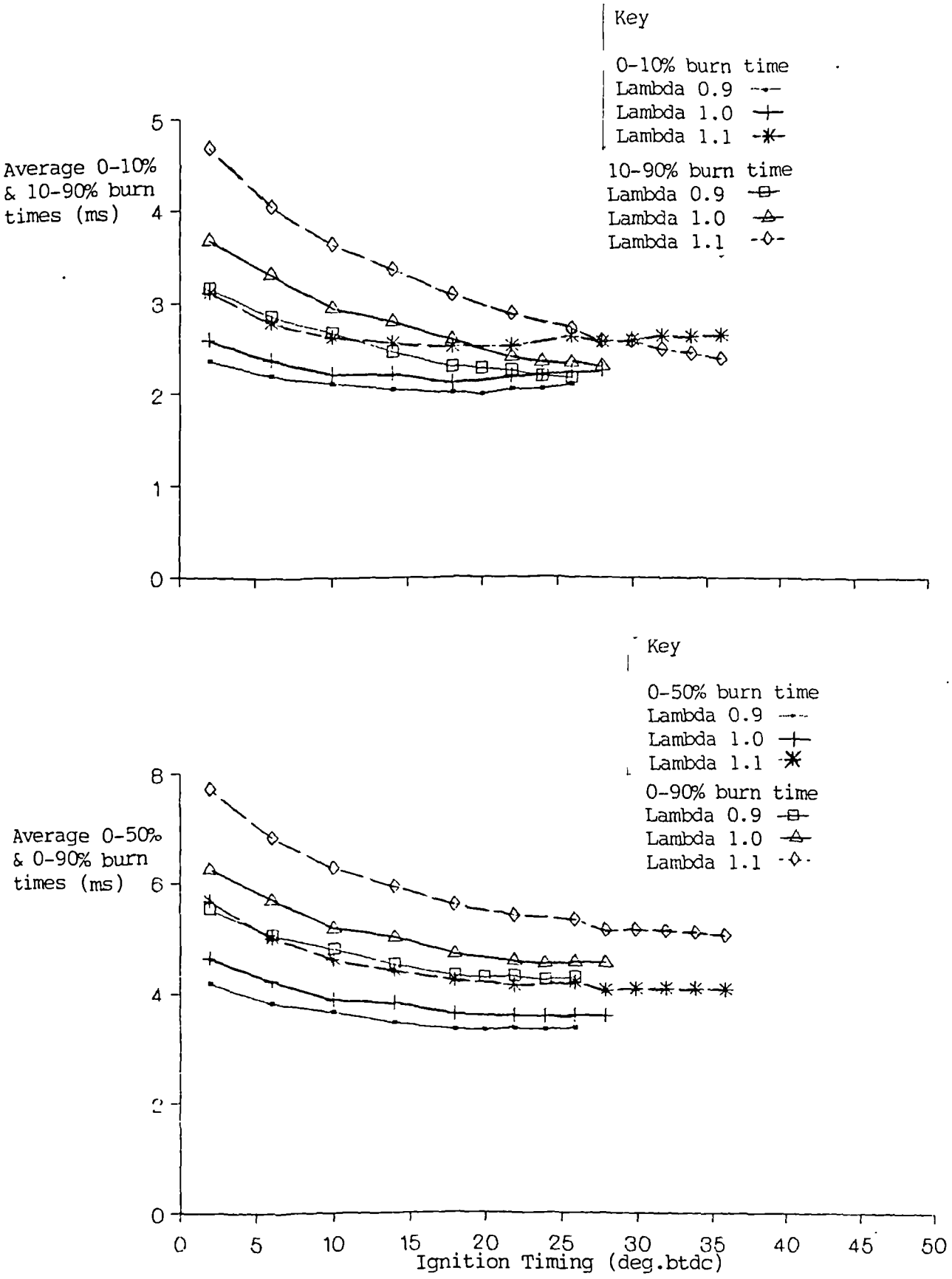

Figure 5.27: Variation in average burn times with ignition timing and mixture strength for the test with knock present.

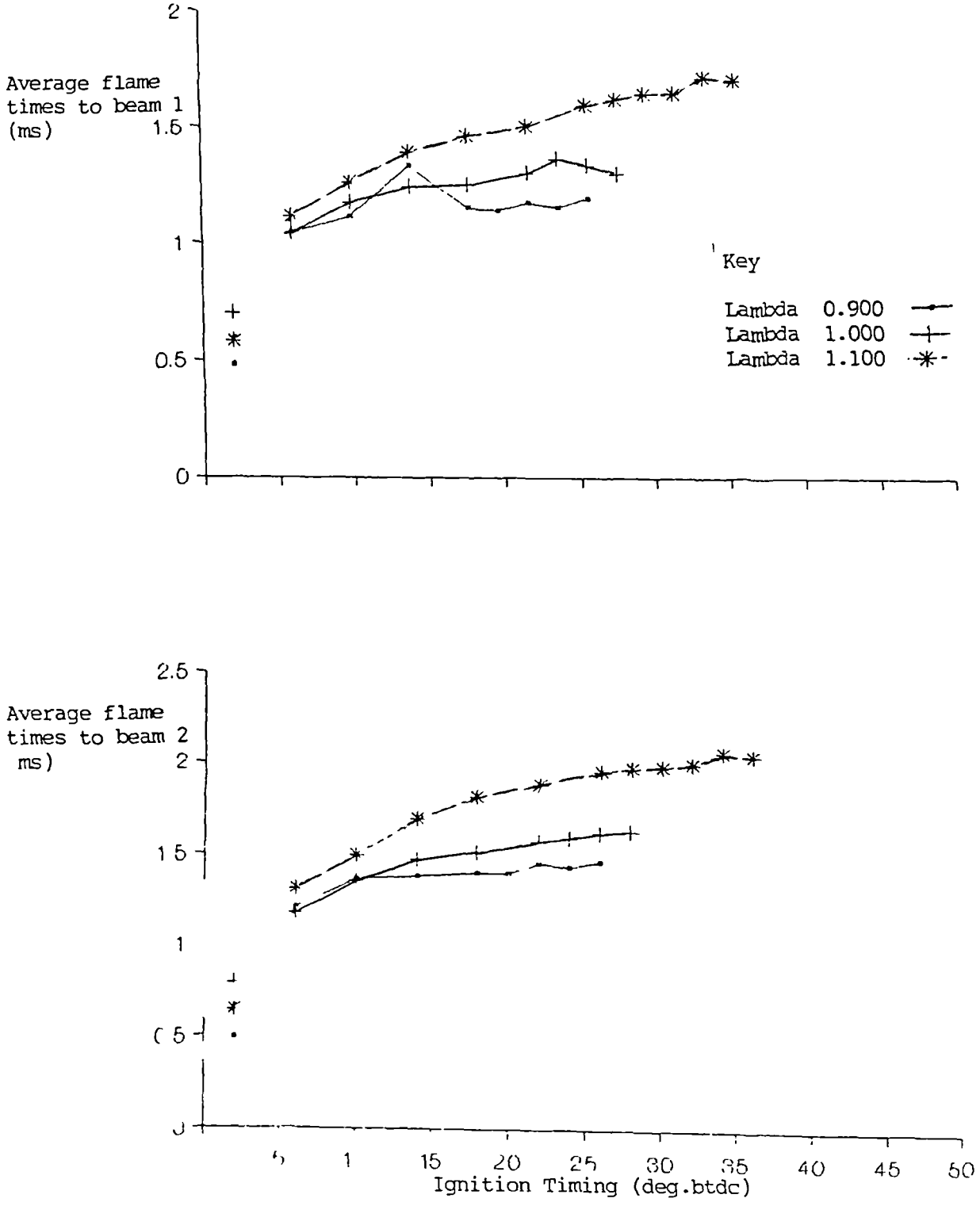

Figure 5.28: Variation in average flame times with ignition timing and mixture strength for the tests with knock present.

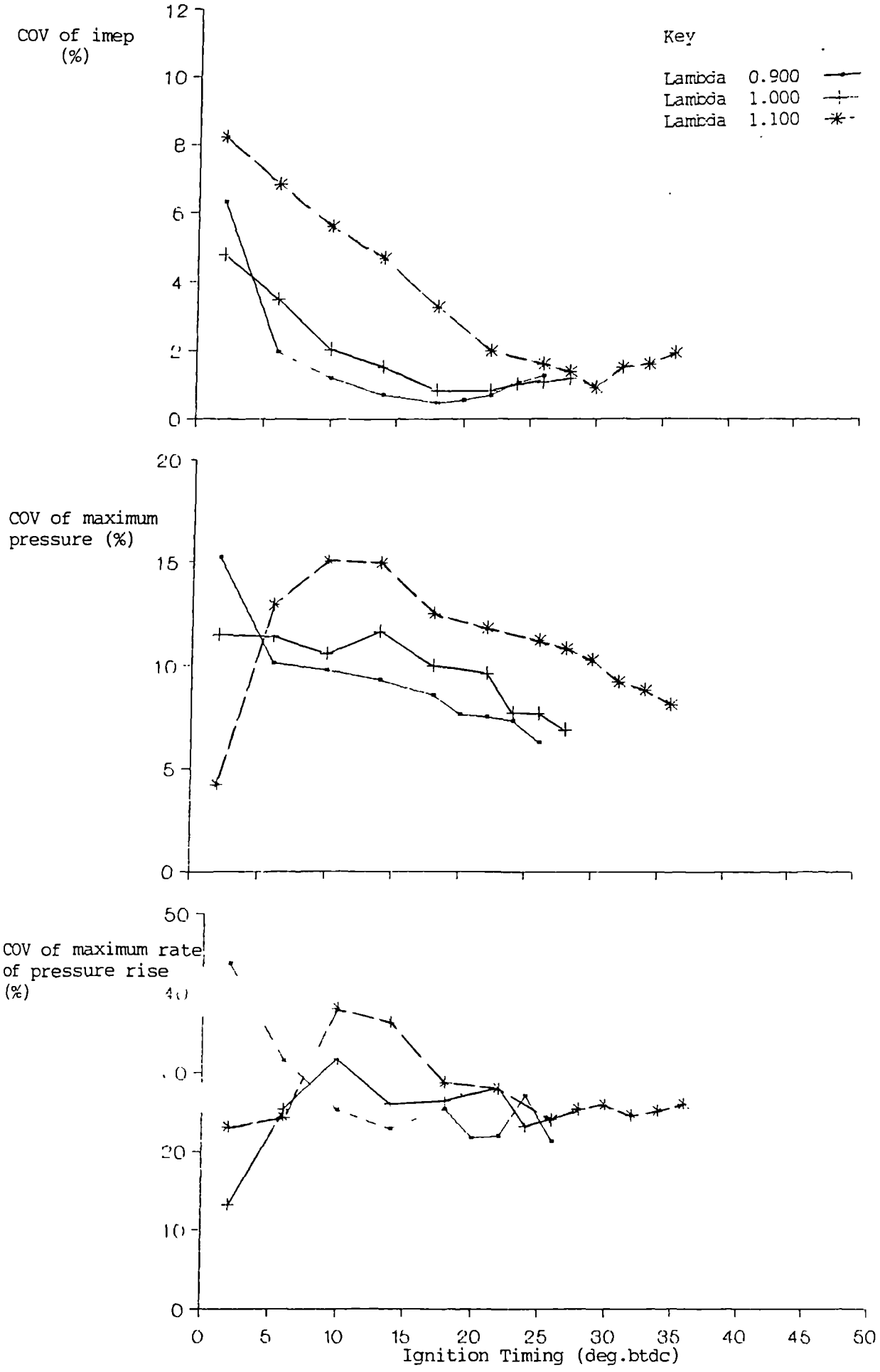

Figure 5.29: Variation in COV of measured engine parameters with ignition timing and mixture strength for the tests with knock present.

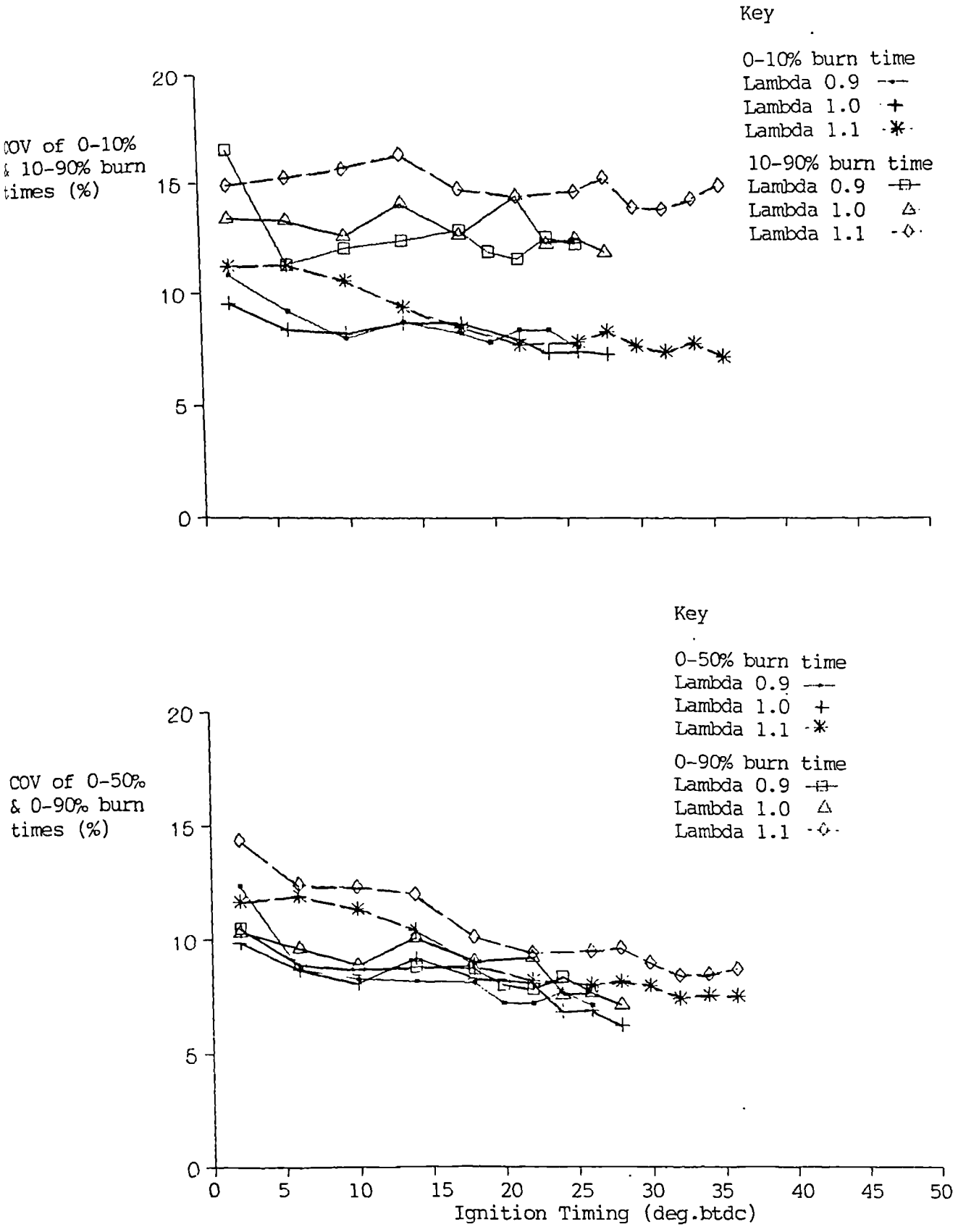

Figure 5.30: Variation in COV of burn times with ignition timing and mixture strength for the tests with knock present.

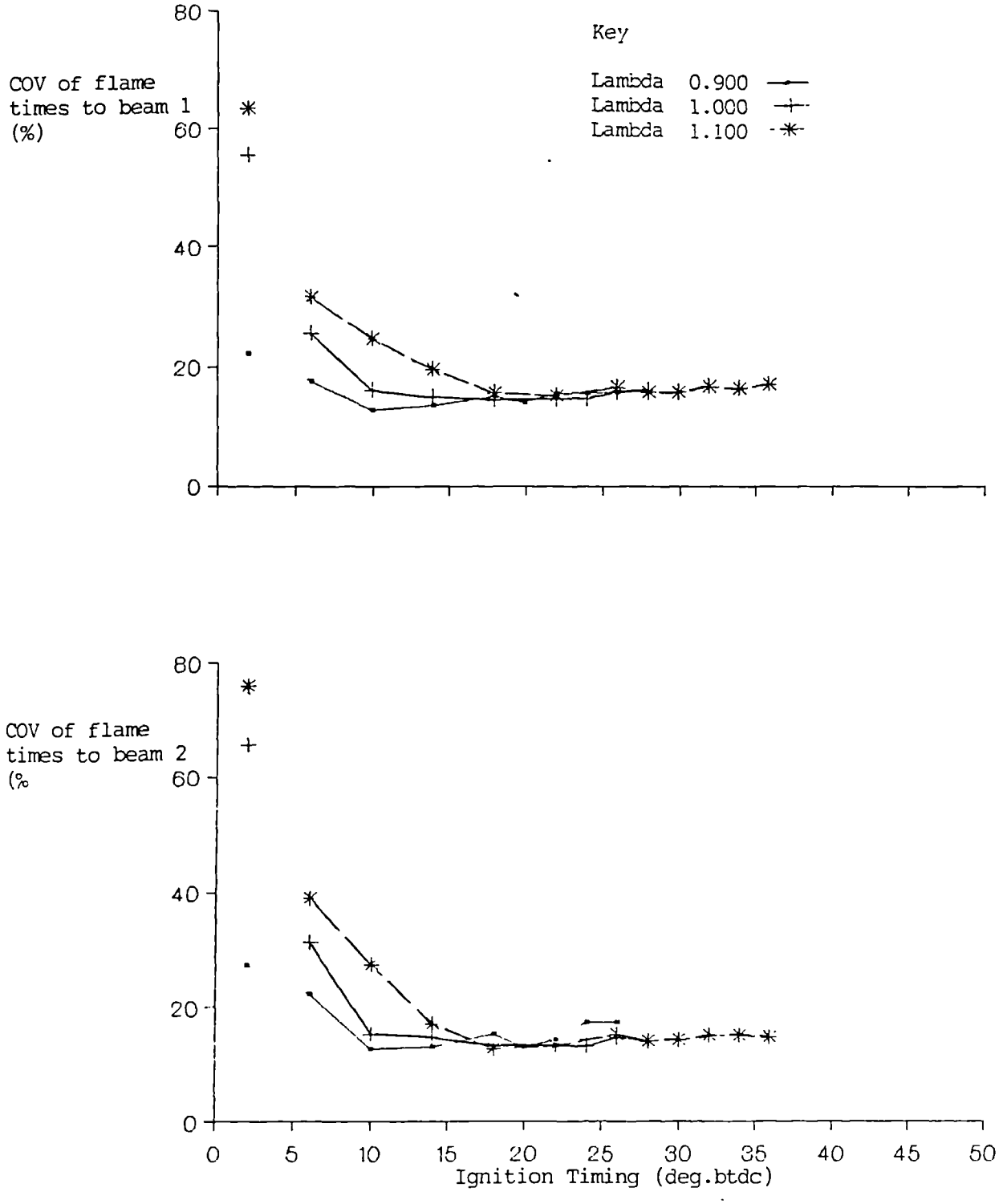

Figure 5.31: Variation in COV of flame times with ignition timing and mixture strength for the tests with knock present.

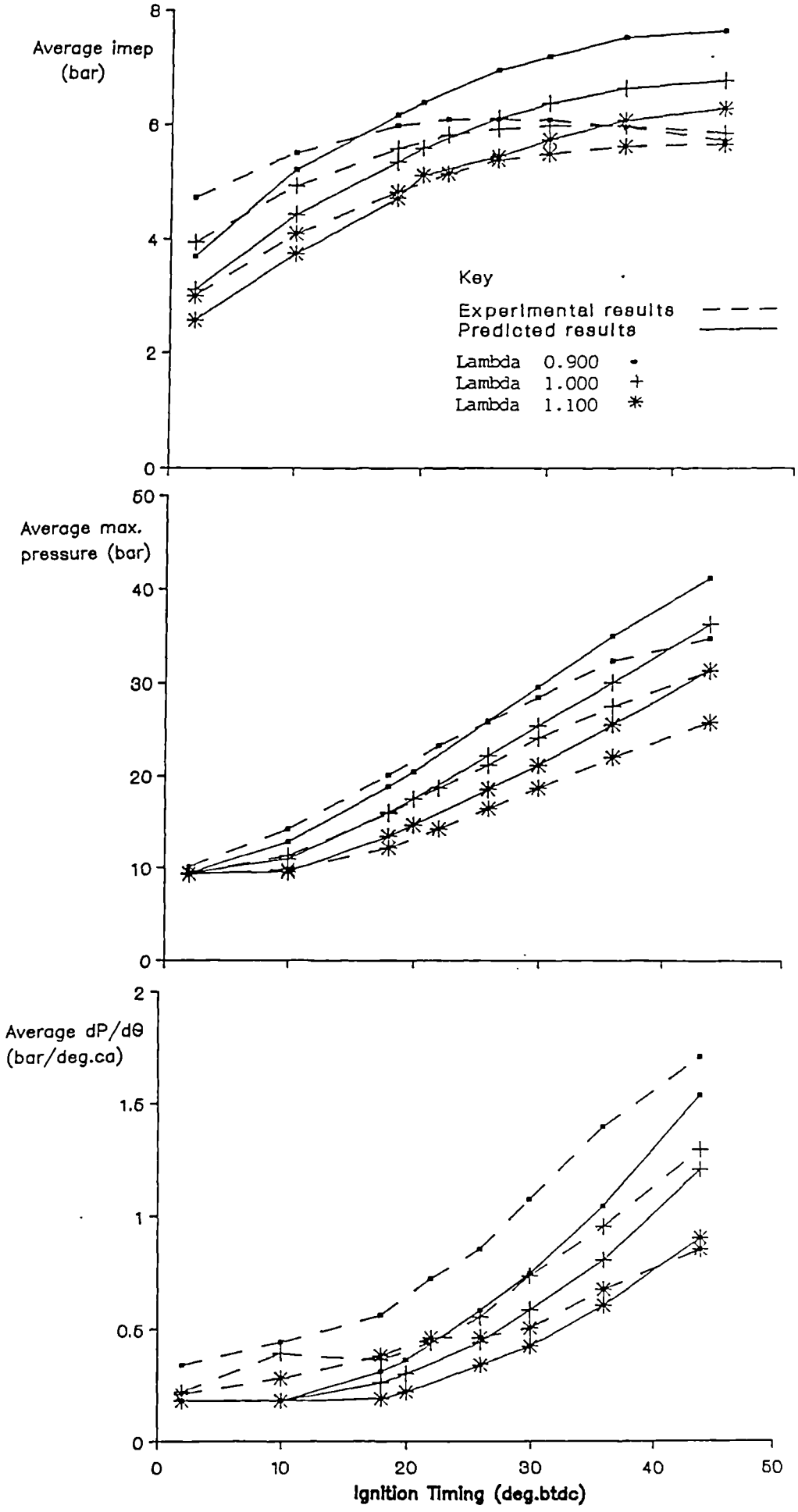

Figure 5.32: Comparison of experimental and predicted values for the variation of average measured engine parameters with ignition timing and mixture strength at part throttle.

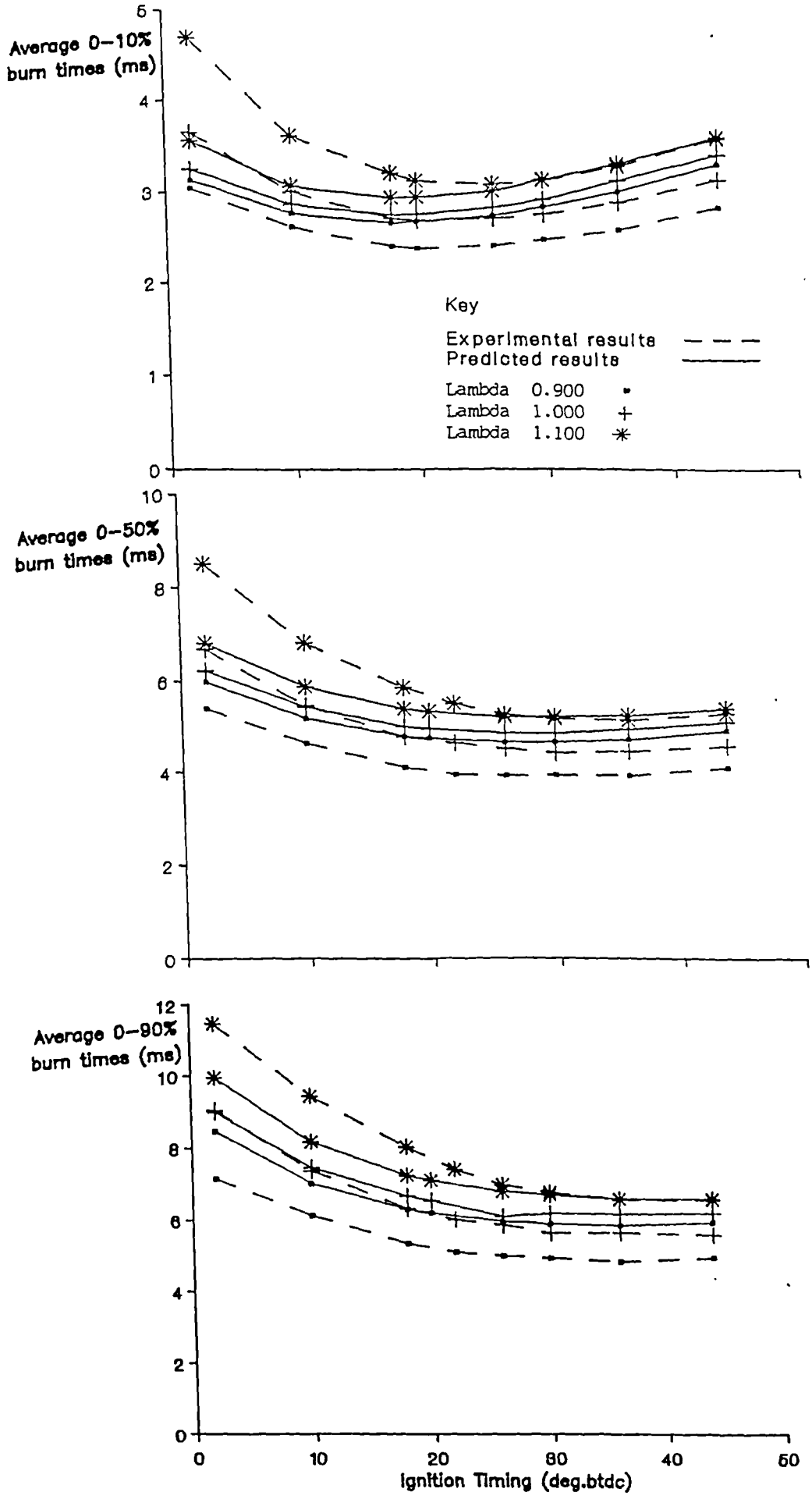

Figure 5.33: Comparison of experimental and predicted values for the variation of average burn times with ignition timing and mixture strength at part throttle.

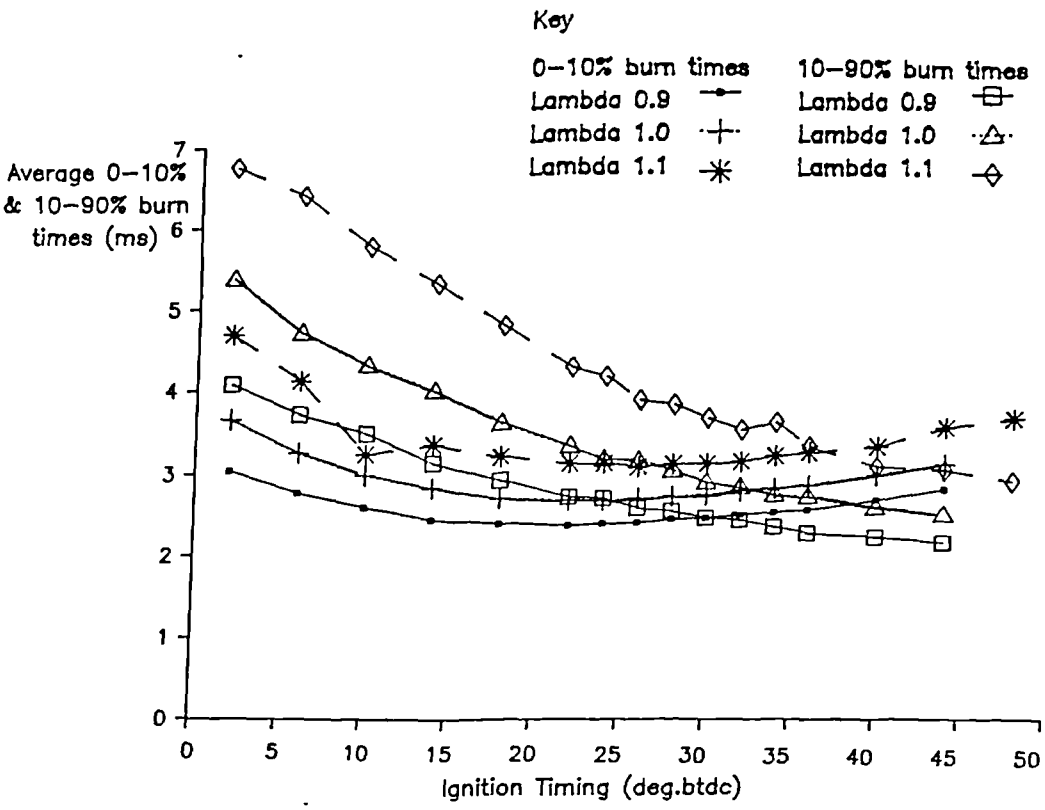

Figure 5.34: Variation in average 0-10% and 10-90% burn times with ignition timing and mixture strength at part throttle.

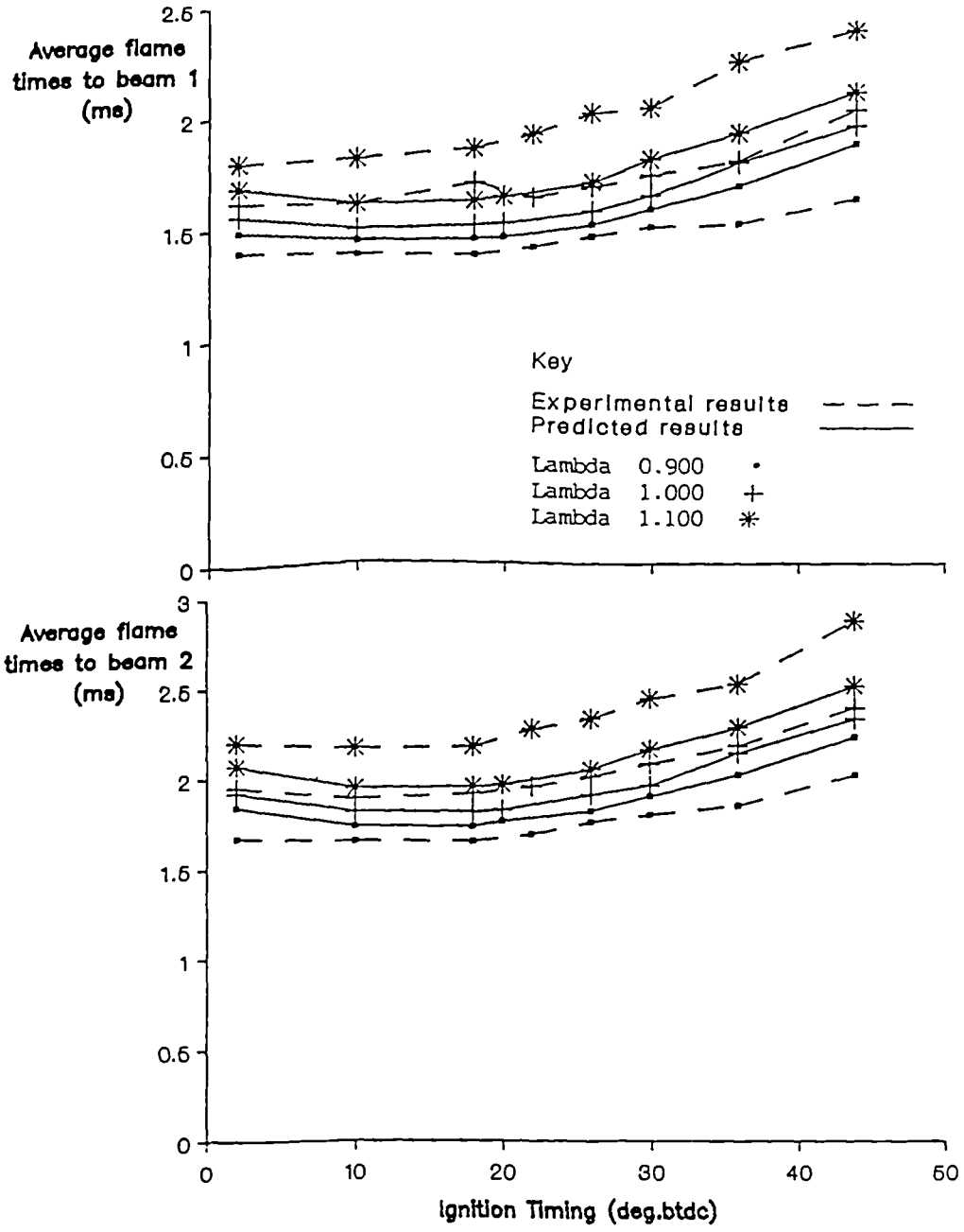

Figure 5.35: Comparison of experimental and predicted values for the variation of average flame times with ignition timing and mixture strength at part throttle.

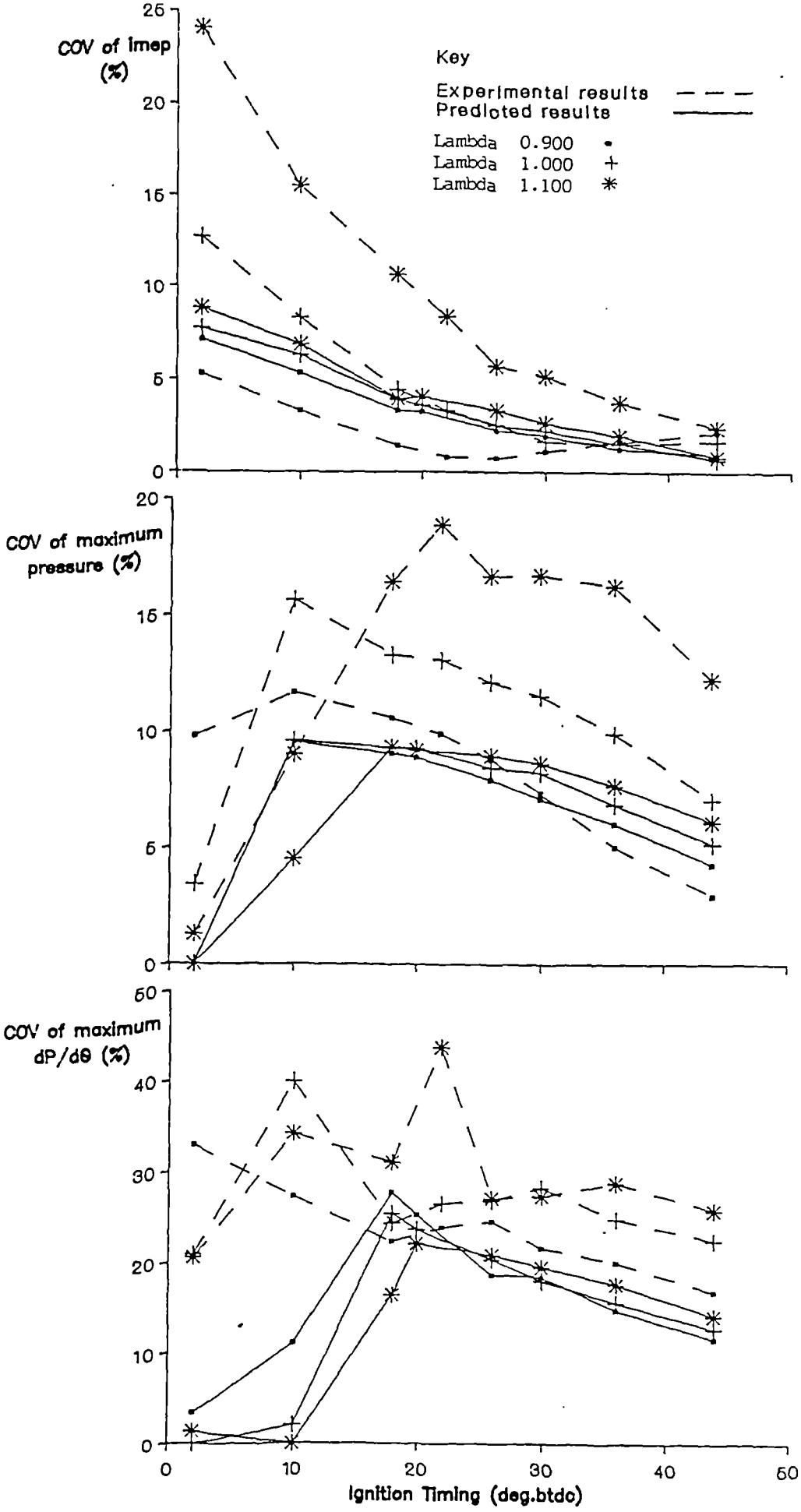

Figure 5.36: Comparison of experimental and predicted values for the variation in COV of measured engine parameters with ignition timing and mixture strength at part throttle.

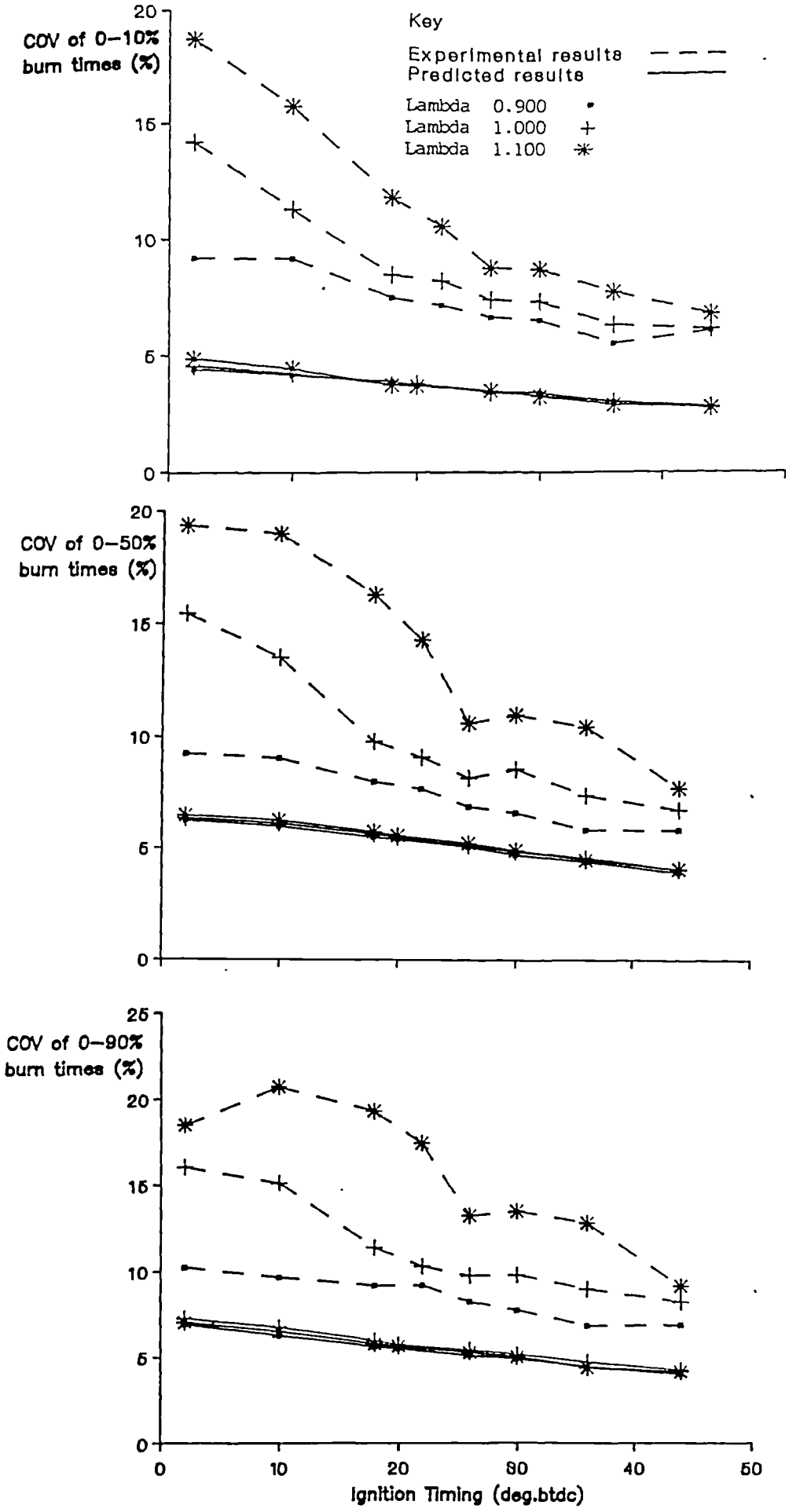

Figure 5.37: Comparison of experimental and predicted values for the variation in COV of burn times with ignition timing and mixture strength at part throttle.

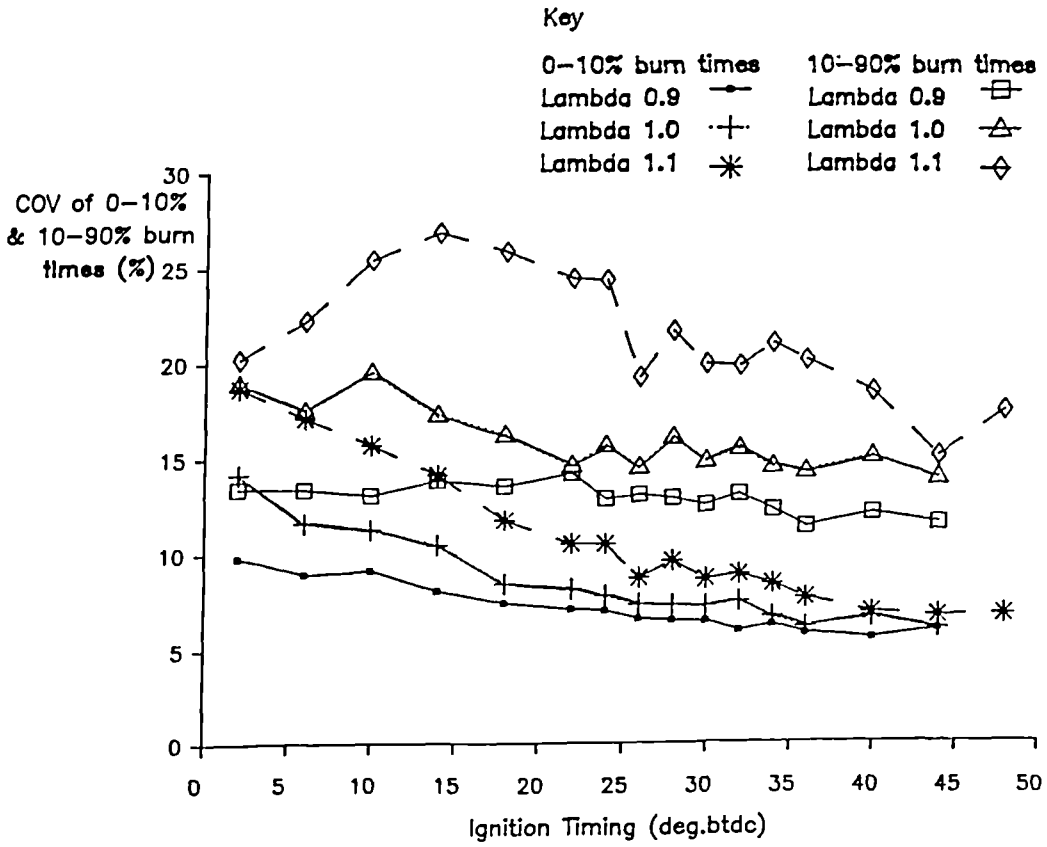

Figure 5.38: Variation in COV of 0-10% and 10-90% burn times with ignition timing and mixture strength at part throttle.

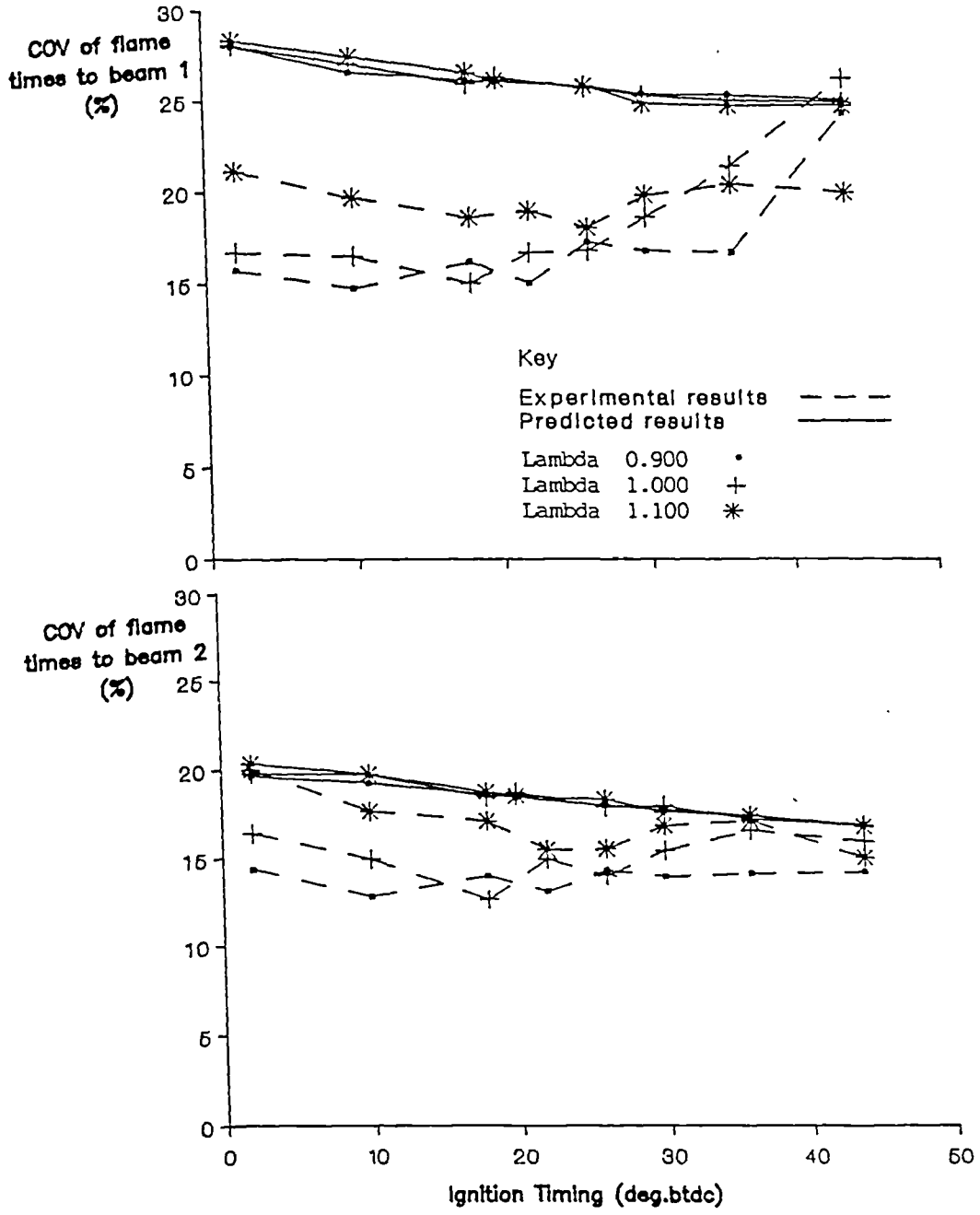

Figure 5.39: Comparison of experimental and predicted values for the variation in COV of flame times with ignition timing and mixture strength at part throttle.

APPENDIX 1

```
/*****************************************************************/
/*****************************************************************/
/************************  MASTER.H  *****************************/
/*****************************************************************/
/*****************************************************************/
/*************       HEADER FILE FOR MASTER.C        ************/
/*************  Written by Andrew Brown, April 1990  ************/
/*****************************************************************/
/*****************************************************************/
/*****************************************************************/

#include <stdio.h>
#include <stdlib.h>
#include <malloc.h>
#include <math.h>
#include <string.h>

#define PI 3.141592654
#define MAXVALS 361
#define C2              0.42      /* constant for intergral
                                     length scale                 /*
#define rad             0.0175    /* conversion factor degrees
                                     to radians                   /*
#define printflag       0.00      /* flag for printing marker
                                     statements                   /*
#define mfbendt         0.9       /* mfb for end of turbulent
                                     combustion                   /*
#define taub1           1.6       /* time constant for final
                                     pressure decay               /*
#define vol_eff         0.917     /* volumetric efficiency of
                                     E6 @ 1500rpm & WOT           /*

FILE *fp;                         /* file for engine data         /*
FILE *mb1;                        /* file for results             /*
FILE *maxr;                       /* file for max. rate of
                                     pressure rise                /*
FILE *bat1;                       /* file for input data          /*

       double press_ivc;          /* pressure at inlet valve
                                     closure (dyn/cm2)            /*
       double dtheta;             /* crank angle increments       /*
       double denra;              /* density ratio unburnt:burnt  /*
       double turbi;              /* initial turbulence intensity
                                     (cm/s)                       /*
       double taub;               /* time constant for final burn/*
       double rc;                 /* cylinder radius (cm)         /*
       double rt;                 /* crank throw (cm)             /*
       double l;                  /* conrod length (cm)           /*
       double sl;                 /* laminar flame speed (cm/s)   /*
       double rs;                 /* distance from centre of
                                     chamber to spark gap (cm)    /*
       double zs;                 /* height of cylinder head
                                     above spark gap (cm)         /*
       double zs1;                /* height of cylinder head
                                     above beam 1 (cm)            /*
       double zs2;                /* height of cylinder head
                                     above beam 2 (cm)            /*
       double rs1;                /* distance from centre of
                                     chamber to beam 1 (cm)       /*
       double rs2;                /* distance from centre of
                                     chamber to beam 2 (cm)       /*
       double lp1;                /* distance from sprak plug
                                     gap to beam 1 (cm)           /*
       double lp2;                /* distance from sprak plug
                                     gap to beam 2 (cm)           /*
```

```
 double rv;              /* compression ratio              /*
 double k1;              /* polytropic index for
                            compression                    /*
 double k2;              /* polytropic index for
                            expansion                      /*
 double drf;             /* guess for change in
                            flame radius                   /*
 double nu;              /* dynamic viscisity
                            (dyn s/cm2)                    /*
 double nu1;             /* intermediate step in
                            vicosity calc.                 /*
 double rd;              /* reduced gas density            /*
 double rpm;             /* engine speed                   /*
 double volsw;           /* swept volume                   /*
 double denui;           /* initial density of
                            unburnt gas (g/cm3)            /*
 double linti;           /* initial integral
                            length scale (cm)              /*
 double  ivc;            /* inlet valve closure
                            (degrees abdc)                 /*
 double  evo;            /* exhaust valve open
                            (degrees abdc)                 /*
 double  ign;            /* ignition timing
                            (degrees abdc)                 /*
double r;                /* flame radius                   /*
 double rg;              /* gas constant                   /*
 double sli;             /* laminar flame speed
                            (cm/s) at 298k and 1atm        /*
 double zp;              /* piston pos below spark         /*
 double oldzp;           /* old piston pos below spark     /*
 double zpivc;           /* piston pos at ivc              /*
 double zpevo;           /* piston pos at evo              /*
 double theta;           /* crank angle increments         /*
 double theta_max;       /* theta for maximum pressure     /*
 double theta_rise;      /* theta for max. rate of
                            pressure rise                  /*
 double vol,volfl;       /* cylinder volume                /*
 double volfl;           /* enflamed volume                /*
 double bore_area;       /* cylinder bore area             /*
 double af;              /* flame front area               /*
 double as;              /* flame wetted area excluding
                            piston                         /*
 double ap;              /* piston wetted area             /*
 double dt;              /* time increment                 /*
 double tminustw;        /* time spent in final burn       /*
 double mfb;             /* mass frac burnt                /*
 double xb;              /* mole fraction diluent          /*
 double volivc;          /* vol at inlet valve closure     /*
 double alp,bet;         /* fuel constants                 /*
 double press_eoc;       /* pres. at end of
                            combustion loop                /*
 double vol_eoc;         /* vol at end of
                            combustion loop                /*

 double crank[MAXVALS];     /* array for crank angle
                               counter                     /*
 double volume[MAXVALS];    /* array for cylinder
                               volume                      /*
 double massfrac[MAXVALS];  /* array for mass
                               fraction burnt              /*
 double flamrad[MAXVALS];   /* array for flame radius      /*
 double atheta[MAXVALS];    /* array for crank angle
                               increments                  /*
 double pressure[MAXVALS];  /* array for pressure          /*
 double rate[MAXVALS];      /* array for max rate of
                               pressure rise data          /*
 double volsum[MAXVALS];    /* array for sum of volumes
                               array                       /*
```

```
double presum[MAXVALS];  /* array for sum of pressure
                            array                        /*
double wa[MAXVALS];      /* intermediate array in
                            calc of imep                 /*
double pres;           /* cylinder pressure              /*
double pres_evo;       /* cylinder pressure at evo       /*
   double dpres;       /* cylinder pressure
                            increment                    /*
doubledpresum;         /*  intermediate in exponential
                            decay of pressure            /*
double wat;            /* intermediatein cal of
                            imep                         /*
double pimep;          /* pumping imep                   /*
double dv;             /* change in burnt gas
                            volume                       /*
double oldvolfl;       /* old enflamed volume            /*
double oldaf;          /* old flame front area           /*
double oldas;          /* old flame wetted area          /*
double oldap;          /* old piston wetted area         /*
double denu;           /* density of unburnt gas         /*
double tempu;          /* temp of unburnt gas            /*
double tempui;         /* initial unburnt gas temp.      /*
double temp_ivc;       /* temperature at ivc             /*
double  turb;          /* turbulence intensity (cm/s)    /*
double  lint;          /* integral length scale (cm)     /*
double  lmicr;         /* Taylor microscale (cm)         /*
double dme,me;         /* mass entrained (gm)            /*
double mb;             /* mass burned (g)                /*
double newmb;          /* new mass burned (g)            /*
double oldmb;          /* old mass burned (g)            /*
double dmb;            /* mass burned increment          /*
double lastdmb;        /* mass burn increment at end
                            of turb combustion           /*
double frinc;          /* linear interpolation for
                            mass burned                  /*
double tau;            /* burn-up time of vortex         /*
double mass;           /* mass trapped in cyl @ ivc      /*
double dpdt;           /* maximum rate of
                            pressure rise                /*
double beamdiff;       /*  diff  in  theta  for  first
                            increment and next increment
                            for flame cutting beams      /*
double beaminc;        /* linear interpolation for
                            flame cutting beams          /*
double beam1;          /* theta for flame cutting
                            beam 1                       /*
double beam2;          /* theta for flame cutting
                            beam 2                       /*
double dpdtmax;        /* max rate of pressure
                            rise                         /*
double phi;            /* equivalence ratio              /*
double mfbinc;         /* linear interpolation for
                            mass frac burned             /*
double thetadiff;      /* diff in theta for first
                            increment and next increment
                            for desired mass frac burnt
double theta10;        /* theta for 10% mass frac
                            burnt                        /*
double theta50;        /* theta for 50% mass frac
                            burnt                        /*
double theta90;        /* theta for 90% mass frac
                            burnt                        /*
double theta1;         /* theta in canal module          /*
double max_pres;       /* max cylinder pressure          /*
double max_rise;       /* max rate press rise            /*
double stop;           /* bdc after end of
                            combustion                   /*
```

```
        double fuel;            /* 1=methanol, 2=iso-oct,
                                   3=toluene, 4=phenol,
                                   5=methane                    /*
        int i;                  /* crank angle increment
                                   counter                      /*
        int k;                  /* combustion loop increment
                                    counter                     /*
        int tag;                /* marker to print slow burn
                                    warning                     /*
        char slow_burn;         /* exit marker for slow
                                   burning cycles               /*
        char full_burn;         /* exit marker for fully
                                   burnt cycles*/
        char prnt;              /* option to print results      /*
```

```
/*****************************************************************/
/*****************************************************************/
/************************    MASTER.C  ***************************/
/*****************************************************************/
/*****************************************************************/
/******  This program is for predicting the turbulent  ********/
/****** combustion in a spark ignition engine for disc ********/
/******          shaped combustion chambers.           ********/
/*****************************************************************/
/*****************************************************************/
/*******      Written by Andrew Brown, April 1990 **************/
/*****************************************************************/
/*****************************************************************/
/*****************************************************************/


#include "master.h"


/*****************************************************************/
/*****************************************************************/
/*****************************************************************/
/************ function to evaluate piston position **************/
/*****************************************************************/
/*****************************************************************/
/*****************************************************************/

void piston_pos(void)
{
zp=(2*rt)/(rv-1)-zs+(rt*(1+cos(theta)))+l-sqrt(l*l-(rt*rt*sin(
theta)*sin(theta)));
}

/*****************************************************************/
/*****************************************************************/
/*****************************************************************/

void main(void)
{
   i=0;                         /* crank angle increment counter*/

   k=0.00;
   tag=0.00;
   newmb=0.0;
   af=0.0;
   as=0.0;
   zp=0.0;
   volfl=0.0;
   dpdt=0.0;
   dpdtmax=0.0;
   tminustw=0;
```

```
      ap=0.0;
      wat=0.0;
      dpresum=0.0;

      input();                          /* calling module for user inputs*/


      theta=theta*rad;
      dtheta=dtheta*rad;
      ivc=ivc*rad;
      evo=evo*rad;
      ign=(180-ign)*rad;

      fuels ();                          /* calling module to calculate
                                           initial laminar flame speed */

      fp=fopen("data.res","w");             /* opening a data file */
      mb1=fopen("stats.res","w");           /* opening a stats file*/


     bore_area=PI*rc*rc;
     rg=0.287+0.02*phi/(1+0.0676*phi);
     volsw=(PI*rc*rc)*2*rt/(1000000);
     dt=60*dtheta/(rpm*2.0*PI);
     zpivc=(2*rt)/(rv-1)-zs+(rt*(1+cos(ivc)))
           +1-sqrt(1*1-(rt*rt*sin(ivc)*sin(ivc)));
    volivc =bore_area*(zpivc+zs);
    temp_ivc=(press_ivc*volivc*298)/(vol_eff*(volsw*1000000)*0.1);
    denui=press_ivc/(rg*temp_ivc);
    mass=denui*volivc;
    stop=360*rad;

     /*determining distance from plug gap to laser beams*/

          lp1=sqrt(((rs-rs1)*(rs-rs1)+(zs1-zs)*(zs1-zs)));
          lp2=sqrt(((rs-rs2)*(rs-rs2)+(zs2-zs)*(zs2-zs)));

   for (theta=0.00;theta<=stop;theta=theta+dtheta)
       {
       oldzp=zp;
       piston_pos();
       vol=bore_area*(zp+zs);
         if (theta<ivc)
            {
             i++;
             pres=press_ivc;
             vol=bore_area*(zp+zs);
             fprintf(fp,"%lf %lf %lf %lf %lf %lf %lf
                     %lf\n",theta/rad,pres*10,r,mfb,
                     vol,af,denu,volfl);
            }
        if (theta>=ivc && theta<=ign)
           {

/*************************************************************/
/****** start of loop for compression prior to ignition *******/
/*************************************************************/

            i++;              /*crank angle increment counter*/
            pres=press_ivc*pow((volivc/vol),k1);
            volume[i]=vol;           /*creating volume array*/
            fprintf(fp,"%lf %lf %lf %lf %lf %lf %lf %lf\n"
                    ,theta/rad,pres*10,r,
            mfb,vol,af,denu,volfl);

/*************************************************************/
/****** end of loop for compression prior to ignition *********/
/*************************************************************/
```

```
            } else if (theta>ign && mfb<1.00){

/*************************************************************/
/***************** start of combustion loop ******************/
/*************************************************************/

          if (theta<ign+dtheta) /* calculation of temperature
                                   at ignition*/
             {
              tempui=(pres*vol)/(mass*rg);
             }
       i++;                    /*crank angle increment counter*/


       system ("cls");         /*writting continuous display to
                                  screen*/
       printf(" Mass fraction burnt\n");
       printf(" %lf %%  \n",mfb*100);


       volfl=volfl*vol/volume[i-1];

       denu=(denui*volivc)/(volfl/denra + (vol-volfl));
       /*equ. 3.9*/

       if (mfb<0.01||mfb==0.0)

 /*calc of integral length scales for initial combustion*/

          {
           linti=0.5*C2*(4*rc*rc)*(zp+zs)/(4*rc*rc
                 +(2*rc)*(zp+zs));
           /*equ. 3.4*/
           lint=linti;
           }
           if (mfb==0.010)

 /* calc of initial integral length scale for turbulent
                      combustion*/

             {
              linti=0.5*C2*(4*rc*rc)*(zp+zs)/(4*rc*rc
                    +(2*rc)*(zp+zs));
              lint=linti;
              }
              if (mfb>0.010)

  /*calc of integral length scale for turbulent combustion*/

                  {
                  lint=linti*(pow((denui/denu),0.3333));
                  /*equ. 3.6*/
                  }

     turb=turbi*(pow((denu/denui),0.3333));
     /*equ. 3.7*/

     dme=dt*denu*af*(turb+sl);
     /*equ. 3.1*/

     pres=press_ivc*pow((denu/denui),k1);
     /*equ. 3.11*/

     tempu=(pres*denui*tempui)/(press_ivc*denu);
     /*equ. 3.12*/

     rd=(pres*132.5)/(tempu*37.6);
```

```
        nu1=1.023+0.23364*rd+0.58533*rd*rd-0.40758*rd*rd*rd
             +0.093324*rd*rd*rd*rd;
        nu=nu1*nu1*nu1*nu1-1.038+0.18;
        /*equ. 3.13*/

        lmicr=sqrt(15*lint*nu/turb);
        /*equ. 3.8*/

        sl=sli*pow((tempu/298),alp)*pow((pres/0.10),bet);
        /*equ. 3.18*/

        sl=sl*(1-2.06*pow((xb),0.77));
        /*equ. 3.20*/

        me = dme+me;

        tau= lmicr/sl;
        /*equ. 3.3*/

        mass=denui*volivc;
        if (mfb<mfbendt)
           {

            dmb=(dt/tau)*(me-mb);
            /*equ. 3.2*/

            lastdmb=dmb;

           }else{      /* calc. for exponential decay of final
                          boundry layer*/
              tminustw=tminustw+dt;

              dmb=lastdmb*exp(-tminustw/taub);
              /*equ. 3.16*/

              }
              mb = mb+dmb;
              r=r-drf;
              while (newmb<mb||newmb==0)

        /*loop to determine new mass burnt*/

              {
              ++k;                              /*counter for loop*/
              r=r+drf;
              geometry();

              denu=(denui*volivc)/(volfl/denra + (vol-volfl));
              /*equ. 3.9*/

              oldmb=newmb;
              oldaf=af;
              oldas=as;
              oldap=ap;
              oldvolfl=volfl;
              newmb=volfl*denu/denra;
              vol=bore_area*(zp+zs);
              if (volfl==vol || k>200)   /*loop to exit for full
                                            burn*/
                 {
                 newmb=mass;
                 goto full_burn;
                 }
           }
      k=0.00;

/*linear interpolation to find correct values
  of af,as,ap,r and volfl*/
```

```
        frinc=(pow(mb,0.3333)-pow(oldmb,0.3333))
                /(pow(newmb,0.3333)-pow(oldmb,0.3333));

        af=(sqrt(oldaf)+frinc*(sqrt(af)-sqrt(oldaf)))
            *(sqrt(oldaf)+frinc*(sqrt(af)-sqrt(oldaf)));

        as=(sqrt(oldas)+frinc*(sqrt(as)-sqrt(oldas)))
            *(sqrt(oldas)+frinc*(sqrt(as)-sqrt(oldas)));

        ap=(sqrt(oldap)+frinc*(sqrt(ap)-sqrt(oldap)))
            *(sqrt(oldap)+frinc*(sqrt(ap)-sqrt(oldap)));

        r=r-drf+frinc*drf;
        frinc=(mb-oldmb)/(newmb-oldmb);
        volfl=oldvolfl + frinc*(volfl-oldvolfl);

         full_burn:
         newmb=mb;
         mfb=mb/mass;


         volume[i]=vol;                /* creating volume array*/


         fprintf(fp,"%lf %lf %lf %lf %lf %lf %lf %lf \n"
                 ,theta/rad,pres*10,r,mfb,vol,af,denu,volfl);

        press_eoc=pres;
        vol_eoc=vol;

/*****************************************************************/
/*************** end of combustion loop **************************/
/*****************************************************************/


        } else if (theta<=evo && mfb>1.00){

/*****************************************************************/
/****************** start of expansion loop **********************/
/*****************************************************************/

         i++;                    /*crank angle increment counter*/

          pres=press_eoc*pow((vol_eoc/vol),k2);
          pres_evo=pres;
          dpdt=0.0;
          fprintf(fp,"%lf %lf %lf %lf %lf %lf %lf %lf \n"
                    ,theta/rad,pres*10,r,
          mfb,vol,af,denu,volfl);

/*****************************************************************/
/******************** end of expansion loop **********************/
/*****************************************************************/

       } else if (theta>evo && theta<=stop) {
            i++;

          if (pres>0.11)
             {
               dpres=pres_evo*exp(-(theta/taub1));

               dpresum=dpres+dpresum;
               pres=pres_evo-dpresum;
               vol=bore_area*(zp+zs);
               fprintf(fp,"%lf %lf %lf %lf %lf %lf %lf %lf \n"
                         ,theta/rad,pres*10,r,
              mfb,vol,af,denu,volfl);
```

```
                    }else{
                     pres=0.1000000;
                     vol=bore_area*(zp+zs);
                     fprintf(fp,"%lf %lf %lf %lf %lf %lf %lf %lf
                              \n",theta/rad,pres*10,r,
                     mfb,vol,af,denu,volfl);
                     }
                }
    }
          fclose(fp);

          printf("           Data analysis in progress\n");

          canal();    /*module to calculate engine parameters */

          fclose(fp);
          fclose(mb1);
          fclose(maxr);

          printf("\n");
          printf("\n");
          printf("Do you want a print out of the results
            (Y/N)\n");
          printf("Then press RETURN \n");

          scanf("%s",&prnt);
           if (prnt=='Y'||prnt=='y')
              {
              system ("print stats.res");
              }
             if (prnt=='N'||prnt=='n')
                {
          printf("End of program\n");
                }

}
```